Doctoral Thesis:

Organizing dimetal subunits: From structure to nanodevices

By

Mohammad-Reza Azani

Supervised by

Dr. Félix Zamora

Dr. Rubén Mas-Ballesté

Department of Inorganic Chemistry, Faculty of Science, Autonoma University of Madrid

Madrid, 2014

Organizing dimetal subunits:

From structure to nanodevices

By

Mohammad-Reza Azani

Supervised by

Félix Zamora

Department of Inorganic Chemistry, Faculty of Science, Autonoma University of Madrid

Rubén Mas-Ballesté

Department of Inorganic Chemistry, Faculty of Science, Autonoma University of Madrid

This dissertation is submitted for the degree of Doctor of Philosophy in Science of **Chemistry**

Faculty of Science Madrid, 2014

I would like to dedicate this thesis to my best classmate, my best friend and my loving wife, **Azin**, for her unbelievable love, encouragement and assistance

I also would like to dedicate this thesis to my kind parents and my wife's parents for their unending support and encouragement

“Don't aim for success if you want it; just do what you love and believe in, and it will come naturally.”

David Frost

Acknowlegements

I would like to thank all of my family, friends, and collaborators who have been a part of my life. You have not only made it possible for me to complete graduate school and my dissertation, but also made it a personally and professionally rewarding part of my life.

My advisors, Professor Felix Zamora and Doctor Ruben Mas-Balleste, have dedicated enormous energy and countless hours to helping me through every step of my dissertation. Their advices and encouragement have been unending and invaluable, guiding me to define the direction of my research. Their attentions to detail have helped me hone my ideas and improve the quality of my dissertation.

I also would like to thank Professor Salome Delgado, Dr. Pilar Amo-ocho, Dr. Gonzalo Givaja, Dr. Alejandro Guijarro, Miguel-Angel Fernandez and all the staff in the Department of Inorganic Chemistry has also been invaluable during my time at Autonoma University of Madrid. I consider each of them my friends and colleagues; their support and help has kept me grounded and focused during my work.

I also would like to thank Professor Tomas Torres for his unbelievable cooperation and support.

Special thanks to my colleagues Cristina, Marta, Khaled, David, Eva and Isadora and Azin for their support to complete my work.

I would like to thank Professor Santiago Alvarez and Dr. Gabriel Aullon from University of Barcelona, Professor Angel Rubio, Dr. Oscar Castillo, Dr. Alejandro Perez Paz and Leonardo A. Espinosa Leal from university of Pais Vasco, Dr. Teodor Parella from Autonoma University of Barcelona, Professor Antonio Laguna and Olga Crespo from University of Zaragoza, Professor Massimiliano Cavallini, Dr. Denis Gentili, Arian Shehu and Francesca Leonardi from Institute for Nanostructured Materials of CNR of Bologna (CNR-ISMN), Dr. Eva Mateo-Marti from Astrobiology Center (CSIC-INTA) of Madrid, Professor Julio Gomez-Herrero from Department of Condensed Matter Physics of Autonoma University of Madrid for their time and professionalism that has always shown remarkable contributing to the development and quality of the manner of this thesis.

Lastly, and most importantly, I wish to thank my wonderful family, the completion of this work would not have been possible without their encouragement, love and support. Thanks for provided me with so many great memories, opportunities and experiences.

Also a special thank you to the rest of the people who have been important in my life throughout my education.

Abstract

In this thesis the phenomena are discussed that results on supramolecular aggregations of bimetallic $[Pt_2L_4]$ and $[AuL_2]$. Experimental data was shown that variables such as temperature, concentration, solvent and the nature of the ligand L have a critical effect on the reversible self-assembly of supramolecular bimetallic units. These experimental results were approved by computational and theoretical studies. The supramolecular assemblies of $[AuL_2]_n$ (n=2, 3) were observed in some cases in solution as a result of Au(I)···Au(I) aurophilic interactions, which can direct the assembly of oligomeric structures in crystal phase. Analogously, Pt(II)···Pt(II) attraction and interaction account for the assembly of $[Pt_2L_4]_n$ supramolecules which can result on 1D semiconductive arrangements in crystal phase and direct the formation of 1D nanofibres on surfaces. Oxidation of $[Pt_2L_4]$ to $[Pt_2L_4I]_n$ produces highly conductive polymers that can reversibly assemble/disassemble into $[Pt_2L_4]$ and $[Pt_2L_4I_2]$. Such outstanding ability results on an unprecedented process ability that enables MMX polymers for technological applications as molecular wires.

Resumen

En esta tesis se analizan los fenómenos que se traduce en agregaciones supramoleculares de bimetálica [Pt_2L_4] y [AuL_2]. Los datos experimentales se demostró que variables como la temperatura, la concentración, el disolvente y la naturaleza del ligando L tienen un efecto crítico sobre el auto-ensamblaje reversible de unidades bimetálicas supramoleculares. Estos resultados experimentales fueron aprobados por estudios computacionales y teóricos. Se observaron los agregados supramoleculares de $[AuL_2]_n$ (n=2, 3) en algunos casos en solución como resultado de Au(I)**…**Au(I) interacciones aurophilic , que pueden dirigir el conjunto de las estructuras oligoméricas en cristal fase . Análogamente, Pt(II)**…**Pt(II) la atracción y la cuenta de la interacción para el montaje de $[Pt_2L_4]_n$ supramoléculas lo cual puede resultar en 1D arreglos semiconductoras en fase de cristal y dirigir la formación de nanofibras de 1D en las superficies. La oxidación de [Pt_2L_4] a $[Pt_2L_4I]_n$ produce polímeros altamente conductores que forma reversible puede montar / desmontar en [Pt_2L_4] y [$Pt_2L_4I_2$]. Esta extraordinaria capacidad resulta en una capacidad de proceso sin precedentes que permite a los polímeros MMX para aplicaciones tecnológicas como cables moleculares.

Table of Contents

Chapter 1

I. Introduction

1. General Introduction

Nowadays, a main topic in material science is the isolation and characterization of low-dimensional materials that could generate complex structures at nanometer scale showing unique physical properties that significantly differ from analogous bulk samples.[1]

In general, we can found two main strategies to obtain nanomaterials: top-down and bottom-up techniques. The top-down approach refers to miniaturization of bulk samples to get nano-sized materials. In contrast, the bottom-up approach consists in building up nano materials from their structural basic units (atoms or molecules).[2]

Supramolecular chemistry plays a leading role to the rational design of the bottom-up strategies. Supramolecular chemistry is understood as the area of chemistry that studies the assembly processes to obtain entities beyond molecules held together through weak interactions.[3] Supramolecular chemistry studies the spontaneous and reversible self-assembly of organic or inorganic molecules by different types of weak interactions. The resulting supramolecular structures can show new properties that do not present the individual components.[4] Typical weak interactions are hydrogen bonding, van der Waals forces, electrostatic forces, Metal-Ligand interactions or weak Metal-Metal bonding. While hydrogen-bonding-based structures have been widely studied, other types of intermolecular interactions such as weak Metal-Metal or Metal-Ligand bonding remain less explored.[5] On this line, supramolecular coordination chemistry describes systems in which the building blocks are held together by weak coordination bonds. Following this concept, recently, the assembly of metal ions and organic ligands has been very useful in the design of new structures with regular shapes and sizes at the nanometer scale.[1] In addition, compounds containing Metal-Metal interactions have recently attracted much attention because such interaction can act as a driving force to form one dimensional structures with unusual electrical and magnetic properties.[5] Some selected examples of linear structures presenting weak Metal-Metal and Metal-Ligand interactions are shown below.

---

[1] S. Logothetidis, *Nanostructured Material and their Applications,* Springer, **2012**.
[2] B. C. Crandall and J. Lewis, *Nanotechnology:Reserch and perspectives*, MIT press, **1992**.
[3] J. M. Lehn, *Supramolecular Chemistry: Concepts and Perspectives*, VCH. Weinheim, **1995**.
[4] J. M. Lehn, *Proc. Nat. Acad. Sci. USA.,* **2002**, *99*, 4763-4768.
[5] a) J. K. Bera and K. R. Dunbar, *Angew. Chem. Int. Ed.,* **2002**, *41*, 4453-4458. b) F. A. Cotton, C. A. Murillo and R. A. Walton, *Multiple Bonds Between Metal Atoms*, Springer Science and Business Media Inc., New York, **2005**.

1.1. One-dimensional materials based on Metal-Metal interaction

1.1.1. Metal-Metal Bonding: from multiple bonds to weak interactions

Metal-Metal interactions can be rationalized by considering the overlapping of different d orbitals of metal centers, which result on diverse bonding schemes.[6] Figure 1.1 shows the possible symmetries in which d orbital can overlap. From an energy point of view the strongest covalent bond is the established in a σ symmetry arising from combination of d_z^2 orbitals from each atom. In addition, two π bonds can be formed from the overlap of two d_{zx} or two d_{yz} orbitals from each metal center. Finally, the weakest orbital interaction is the one in δ symmetry which is the result of overlapping of two d_{xy} or two $d_{x^2-y^2}$ orbitals.[6]

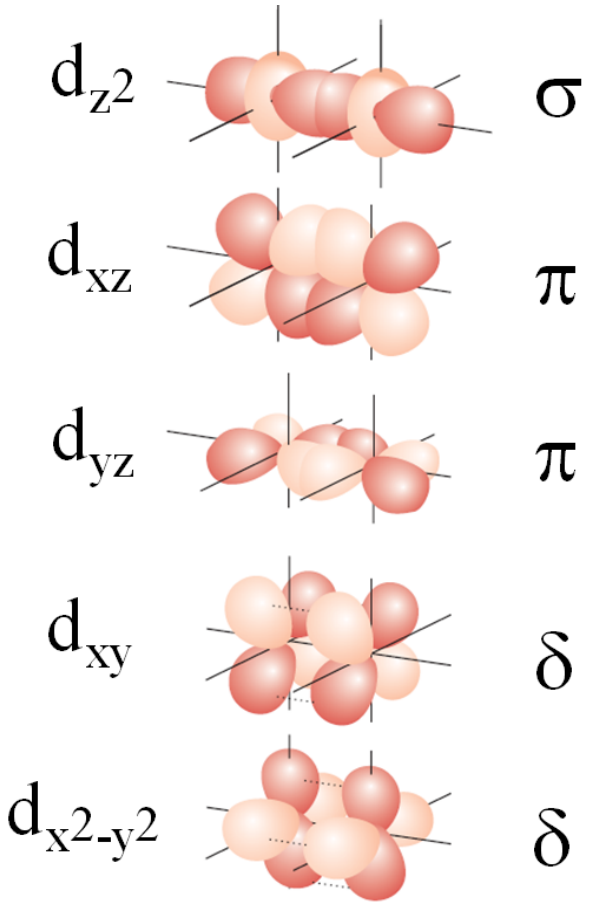

Figure 1.1. Overlap of d orbitals that result in metal-metal bonding as shown in reference 6.

[6] P. Atkins, T. Overton, J. Rourke, M. Weller and F. Armstrong, *Inorganic Chemistry*, Oxford University press, fifth Edition, **2010.**

As an example, molecular orbital diagram resulting from Metal-Metal interactions between two metal centers with square planar geometry is shown in Scheme 1.1. In this diagram the empty $d_{x^2-y^2}$ orbitals are not shown because they act as the electron acceptor sites to establish Metal-Ligand bonding, and thus do not participate in Metal-Metal bonding. The bond strength depends on the electron count. For this molecular obital diagram, the maximum bonding interaction is reached when 8 electrons occupy the 4 bonding molecular orbitals. Thus, formally, a quadruple bond is found between two metal centers with a d^4 electronic configuration. Once more than 8 electrons are added, the anti bonding orbitals begin to fill up and start to cancel out Metal-Metal bonds. Thus, formally, the bond order between two square planar metal centers with d^8 electronic configuration is zero.[6] Coordination geometries other than square planar uses different orbitals for Metal-Ligand bonding. Thus, in some highly coordinatively unsaturated compounds the five d orbitals can participate in Metal-Metal interactions and bond order can reach to five. In quintuple bond, ten electrons participate in bonding between the two metal centers as found in the structure of $[Cr(Terphenyl)]_2$ with molecular orbital configuration $\sigma^2\pi^4\delta^4$.[7]

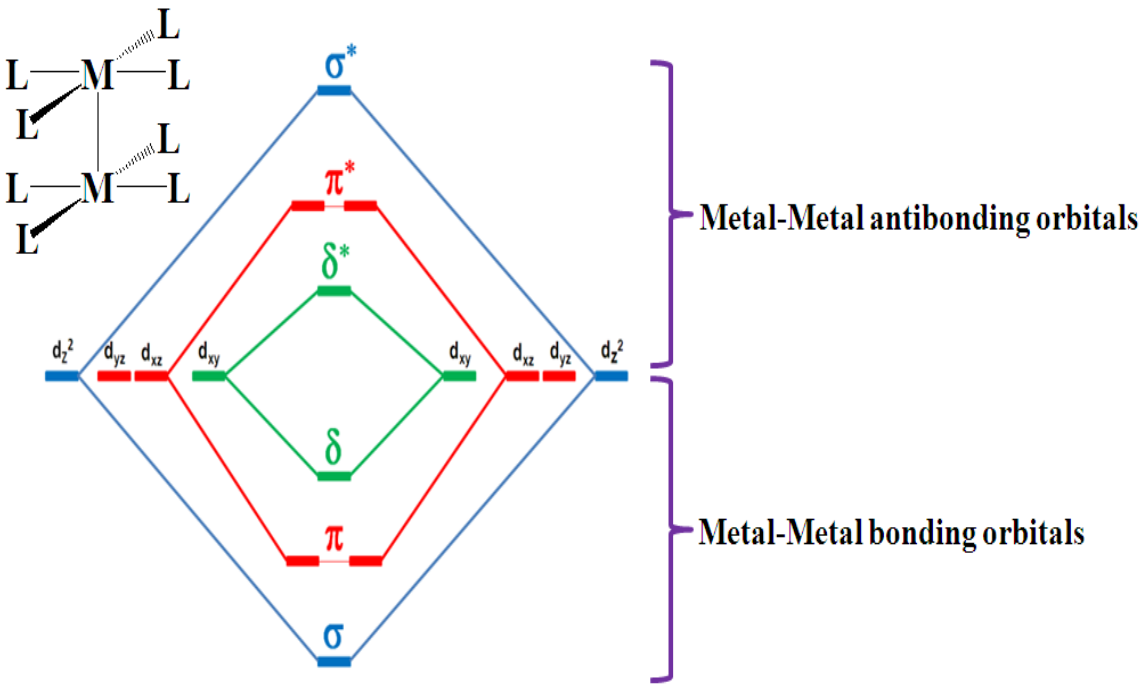

Scheme 1.1. Molecular orbital diagram for the interaction of two square planar metal centers.

[7] T. Nguyen, A. D. Sutton, M. Brynda, J. C. Fettinger, G. J. Long and P. Power, *Science*, **2005**, *310*, 844-847.

Table 1.1 shows the relationship between the numbers of electrons in d orbitals of each atom with the Metal-Metal bond order in homobimetallic fragments with square planar coordination geometry.

Electron Count	Number of Covalent Metal-Metal Bond
$(d^1\text{-}d^1)$	Single bond
$(d^2\text{-}d^2)$	Double bond
$(d^3\text{-}d^3)$	Triple bond
$(d^4\text{-}d^4)$	Quadruple bond
$(d^5\text{-}d^5)$	Triple bond
$(d^6\text{-}d^6)$	Double bond
$(d^7\text{-}d^7)$	Single bond
$(d^8\text{-}d^8)$	No bond

Table 1.1. Relationship between the numbers of electrons in d orbitals of metal atoms with the number of covalent Metal-Metal bonds.

Table 1.2 shows some examples of Metal-Metal bonded complexes. As shown in table 1.2 the different bond order for complexes with same metal centers and ligands and how it is related with the experimentally found Metal-Metal distance.[6]

Complex	Configuration	Bond order	M-M bond length / pm
$[Mo_2(SO_4)_4]^{4-}$	$\sigma^2\pi^4\delta^2$	4	211
$[Mo_2(SO_4)_4]^{3-}$	$\sigma^2\pi^4\delta^1$	3.5	217
$[Mo_2(PO_3OH)_4]^{2-}$	$\sigma^2\pi^4$	3	222
$[Ru_2(CO_2Cl)_4Cl_2]^{-}$	$\sigma^2\pi^4\delta^2\delta^{*1}\pi^{*2}$	2.5	227
$[Ru_2(CO_2Cl)_4(COCH_3)_2]$	$\sigma^2\pi^4\delta^2\delta^{*2}\pi^{*2}$	2	238
$[Ru_2(CO_2CH_3)_4(H_2O)_2]^{+}$	$\sigma^2\pi^4\delta^2\delta^{*1}\pi^{*4}$	1.5	232
$[Ru_2(CO_2CH_3)_4(H_2O)_2]$	$\sigma^2\pi^4\delta^2\delta^{*2}\pi^{*4}$	1	239

Table 1.2. Examples of Metal-Metal bonded complexes as shown in reference 6.

In addition to the covalent sharing of electrons by symmetry allowed d orbital overlapping presented above, there is another type of relatively strong Metal-Metal interaction. This second type of bonding between two metal centers occur when one metal act as electron donor towards an electron acceptor metal center. In that case, generally, an electron lone pair in a full d orbital interacts with an empty orbital of another metal. Such bonding scheme (known as dative bonding) can proceed between an electron rich metal and an electron poor metal. Dative bonding interactions appear between same metals with different geometries or oxidation state[8] (scheme 1.2 (a)) or when different metals with different oxidation state[9] are used (scheme 1.2 (b)). It is usually indicated by using an arrow instead of a line between metal centers in the schematic structure.

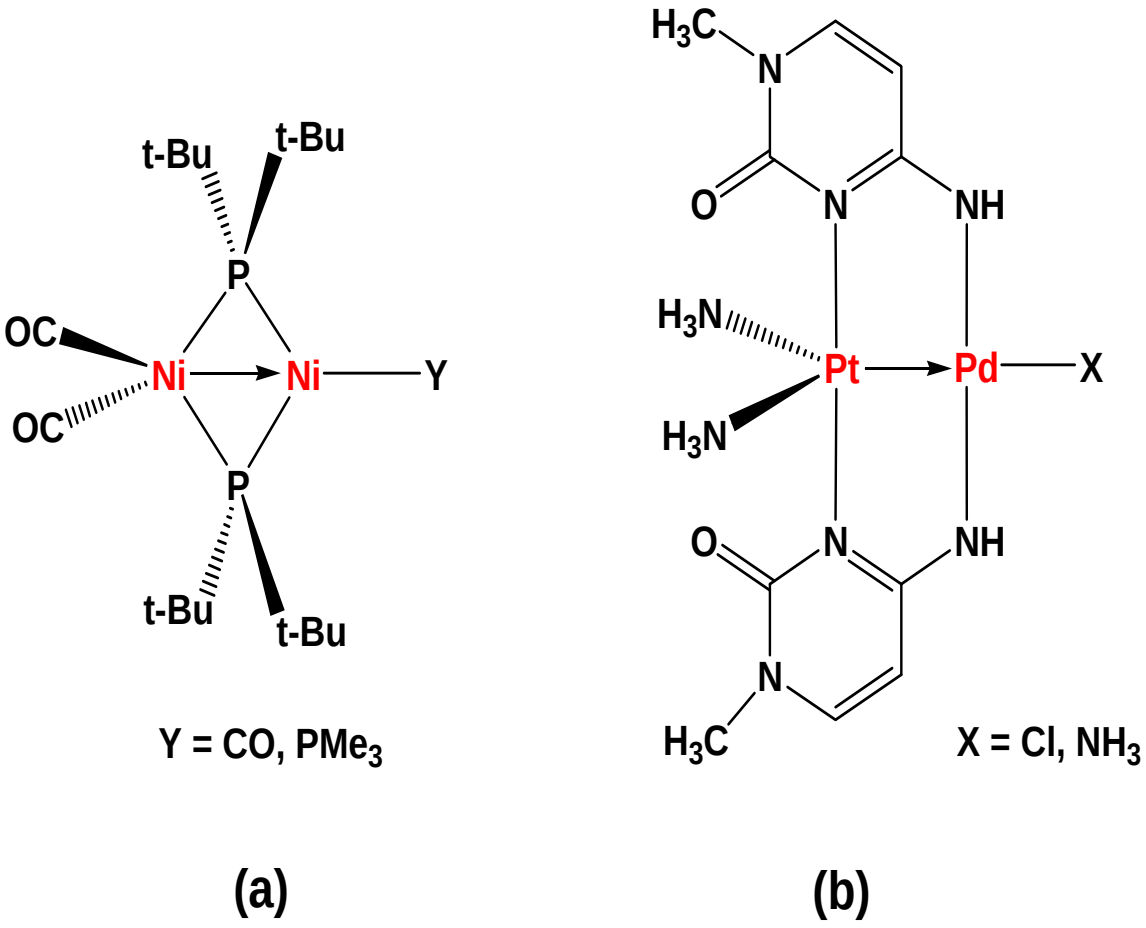

Scheme 1.3. Dative bonds between homo and heterobimetallic complexes.[8,9]

[8] R. A. Jones, A. L. Stuart, J. L. Atwood and W. E. Hunter, *Organometallics*, **1983**, *2*, 874-878.
[9] M. Krumm, B. Lippert, L. Randaccio and E. Zangrando, *J. Am. Chem. Soc.*, **1991**, *113*, 5129-5130.

1.1.2. Weak Metal-Metal bonding

a) d^8-d^8 systems

According to the molecular orbital diagram at the beginning of this chapter, d^8-d^8 present a Metal-Metal bond order of zero. However, during the last four decades several bi- or polymetallic d^8 complexes have been found to show weak Metal-Metal bonding interactions, both in solution and solid-state.[5,10] For instance, $[M(2\text{-phos})_2]Cl$ and $[M(2{=}phos)_2]Cl$ (M= Ir, Rh; 2-phos is 1,2- bis (diphenylphosphino) ethan and 2=phos is cis 1,2- bis(diphenlphosphino) ethylene) are able to form oligomeric Metal-Metal bonded chains in solution and in the solid state.[10] In 1974 Professor Hary B. Gray proposed that this weak Metal-Metal interactions are the result of a symmetry allowed interaction between filled atomic d_z^2 orbitals and empty p_z orbitals (scheme 1.3). This interaction is strong enough to form weak Metal-Metal bonds in solid state and even in solution.[10]

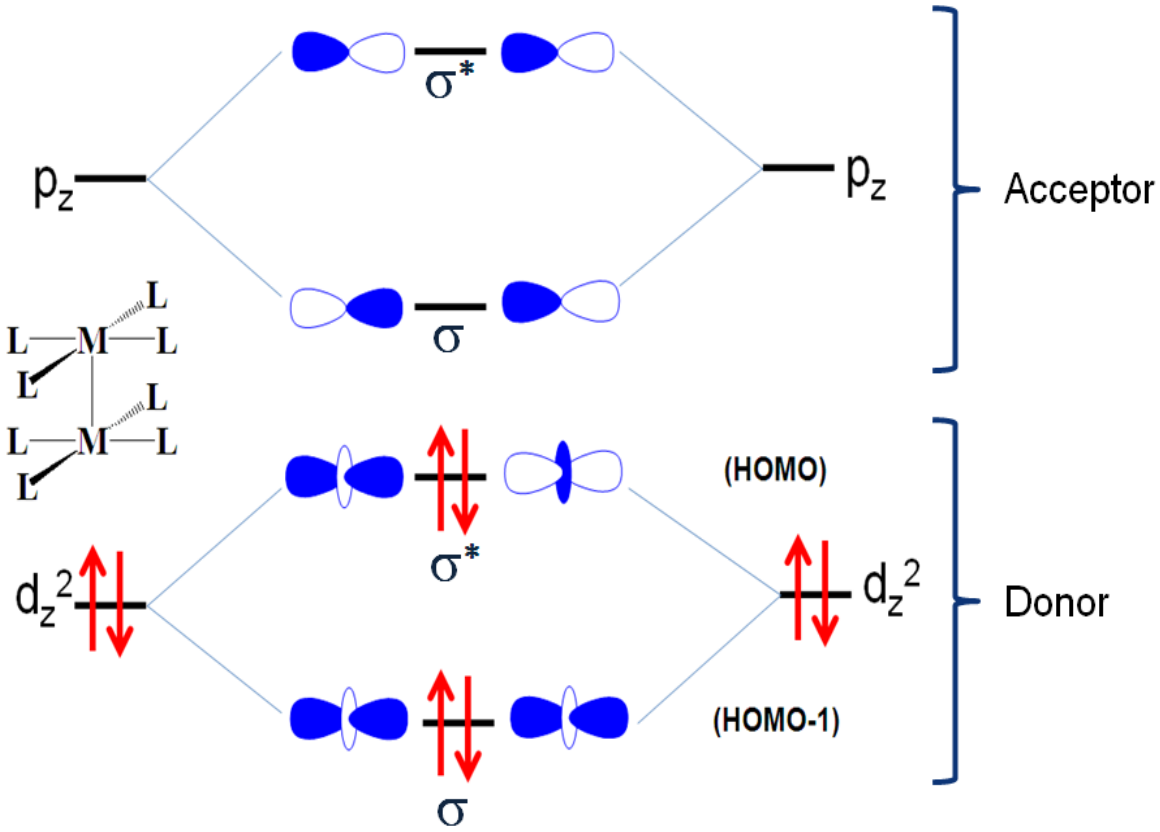

Scheme 1.3. Molecular orbital diagram for the interaction of filled atomic d_z^2 orbitals with empty p_z orbitals in square planar geometry.

[10] G. L. Geoffroy, M. S. Wrighton, G. S. Hammond and H. B. Gray, *J. Am. Chem. Soc.*, **1974**, *96*, 3105-3108.

The physical and chemical properties, especially electrical conductivity, of d^8-d^8 systems are of particular interest for their potential applications in molecular electronics.[11] Such attractive interactions are mainly observed between the elements of the second and third rows of transition metal atoms such as Rh(I)[10], Ir(I)[10], Pd(II)[12] and Pt(II)[12]. As a consequence of weak metal-metal interactions, compounds containing these metals can arrange in one directional structure by two ways, as detailed below:

I) Supramolecular assemblies by stacking square-planar complexes.

Tetracyanoplatinate, $K_2Pt(CN)_4$, commonly called KCPs (potassium cyanoplatinate), is one of the examples that shows weak Metal-Metal interaction by stacking square planar complexes. These systems are formed by chains of $[Pt(CN)_4]^{2-}$ anion complexes with intermolecular Pt-Pt distances of 3.4 Å (scheme 1.4).[13] This distance is indicative of a bonding interaction because is shorter than sum of the van der Waals radius of Pt centers (Van der Waals radius of one Pt is 175 pm).

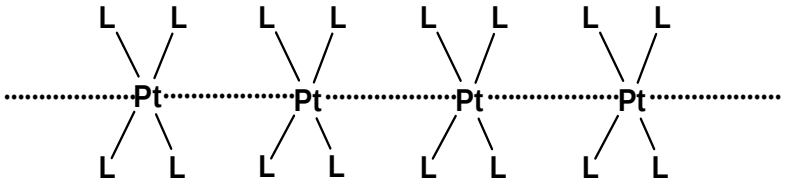

Scheme 1.4. General example of supramolecular assembly by stacking square-planar complex of Pt ($L=CN^-$).[13]

The weak interaction that directs linear ordination is described as the overlapping of full atomic $5d_z^2$ orbitals with empty p_z orbitals. Interestingly, a significant electrical conductivity for the $K_2[Pt(CN)_4]$ was found to be 5×10^{-7} $S.cm^{-1}$.[13] However, such value can be considerably increased by partial oxidation of the metal centers. Formation of electron holes randomly distributed in the mixed valence structures is the origin of

[11] a) J. S. Miller, *Extended Linear Chain Compounds,* Plenum Press, New York, **1982.** b) J. S. Miller and A. J. Epstein, *Prog. Inorg. Chem.,* **1976**, *20,* 1-151. c) G. A. Ozin and A. C. Arsenault, *Nanochemistry: A chemical approach to nanomaterials*, RSC Publishing, Cambridge, **2005**. d) J. K. Bera, and K. R. Dunbar, *Angew. Chem. Int. Ed.,* **2002**, *41,* 4453-4457.
[12] A. Kobayashi, T. Kojima, R. Ikeda and H. Kitagawa, *Inorg. Chem.,* **2006**, *45*, 322-327.
[13] M. Williams, *Adv. Inorg. Chem. Radiochem.,* **1983**, *26,* 235-268.

many interesting properties (electrical, magnetic and optical).[14] Partial oxidation of the systems based on square planar is directly associated with a shortening of the metal-metal distances. Salts arising from the partial oxidation of KCP are known as Krogmann's salts, which can be classified as anion deficient such as $K_2Pt(CN)_4Br_{0.3}.3H_2O$ (Pt-Pt 2.88 Å) or as cation deficient such as $K_{1.75}Pt(CN)_4.1.5H_2O$ (Pt-Pt 2.96 Å). These compounds behave as one-dimensional metallic conductors,[15] becoming very attractive due to their potential applications as molecular wires.[16] For instance, through partial oxidation can be obtained a distinctive KCP of formula $K_2[Pt(CN)_4X_{0.3}.nH_2O]$ (X=Cl, Br, n=3), with short Pt-Pt distances (2.78 Å). The electric conductivity is changed from 5×10^{-7}, in the reduced structure, to 1000 $S.cm^{-1}$ in the oxidized chain.[13] Partially oxidized KCP materials represent the first inorganic "molecular wires" ever designed.[14] Metal-Metal bonding in the oxidized KCPs can be described as a mixture of d^8-d^8 and d^7-d^8 interactions, being considerably stronger than purely d^8-d^8. However it is noteworthy that weak d^8-d^8 interactions are strong enough to prearrange the systems in linear structures, which later on, after oxidation become good conductors.

II). Supramolecular assemblies by stacking bimetallic complexes.

Columnar structures have also been observed for bimetallic compounds. For instance, bimetallic units of Pt(II), are formed through bridging ligands such as dithioacids[17] (scheme 1.5). As presented in scheme 1.6 the electronic structure of chains formed by dimeric units significantly differ from that observed for 1D structure formed from organization of monomeric units. As a consequence of an expanded d_{σ}^* molecular orbital formed by two d_z^2 atomic orbitals, two main features are observed in 1D metal-dimer systems: a) a decrease in electron repulsion compared with the monomer-chain type, due to the antibonding d_{σ}^* character of the $M(d_z^2)$-$M(d_z^2)$ direct overlap. b) an extension of the limit of the interactive distance between adjacent units that can go from 3.3 Å in monomeric based systems to 3.9 Å in the dimer-chain type.[12] Such effects result in a significant enhancement of metallic conduction. This is especially true for

[14] a) R. Mas-Ballest, J. Gomez-Herrero and F. Zamora, *Chem. Soc. Rev.,* **2010**, *39*, 4220-4233. b) J. Gomez-Herrero and F. Zamora, *Adv. Mater.,* **2011**, *23*, 5311-5317.
[15] S. A. Cotton, *Chemistry of Precious Metals*, Blackie Academic and Professional press, **2009**.
[16] D. Y. Wu, T. L. Zhang, *Prog. Chem.*, **2004**, *16*, 911-917.
[17] C. Bellitto, A. Flamini, O. Piovesana and P. F. Zanazzi, *Inorg. Chem.,* **1980**, *19*, 3632-3636.

Pt(II) based chains because Pt has a larger d_{z^2} orbital than Ni or Pd, resulting in a large transfer integral for overlap of d_{z^2} orbitals along the 1D chain, leading to wider electronic bands and, consequently, a stabilized metallic state.[12]

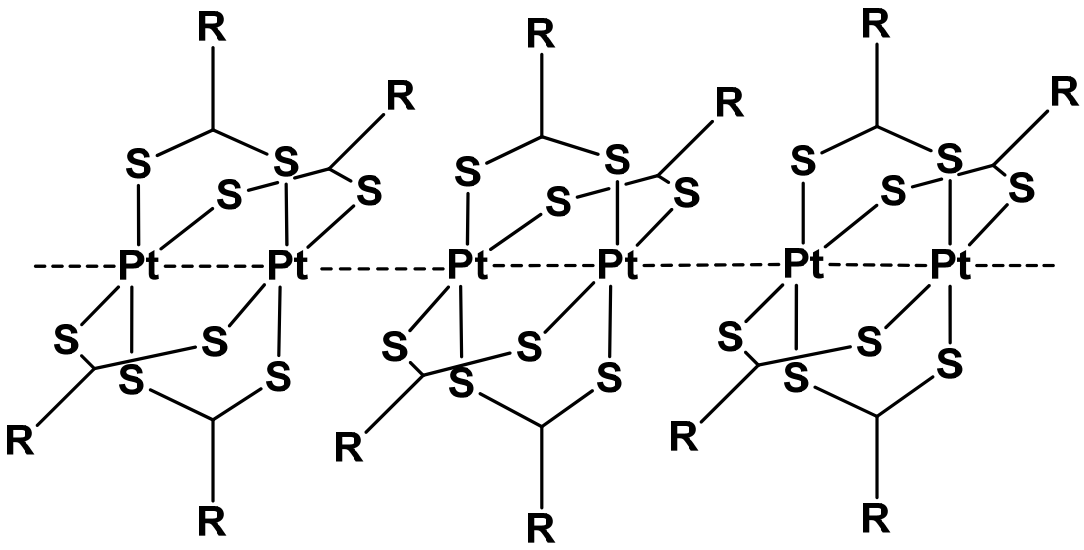

Scheme 1.5. The example of polymers with Intra- and inter molecular interaction of bimetallic units of Pt(II) and dithioacids as bridging ligand.[17]

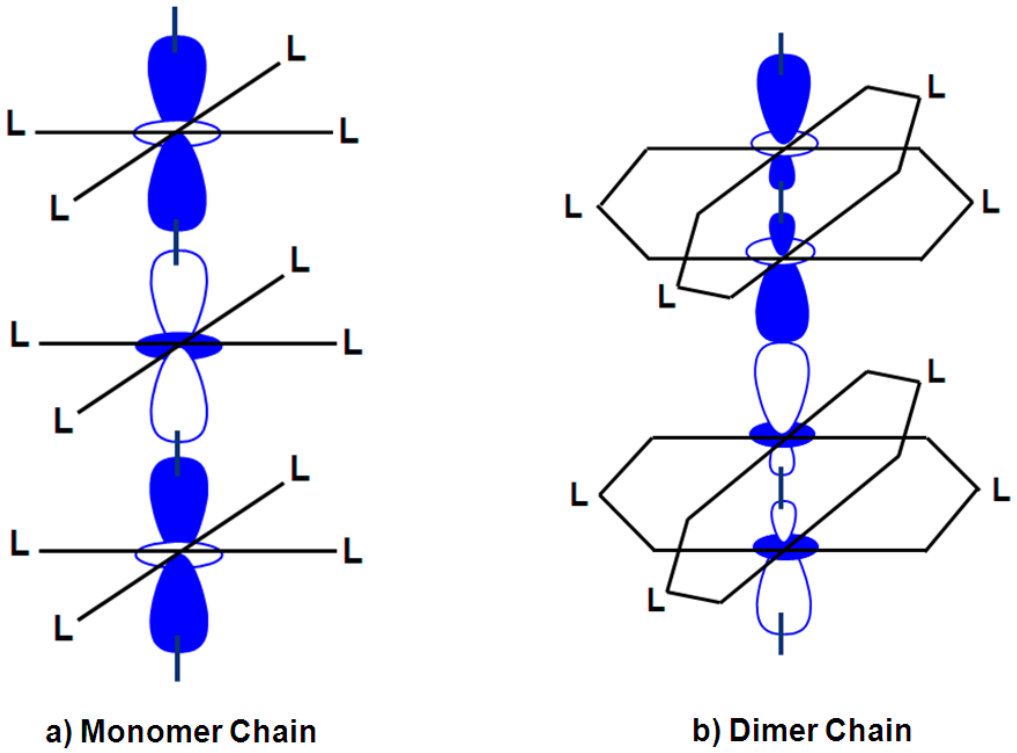

Scheme 1.6. Schematic description of 1D chain structures with (a) monomeric and (b) dimeric units. Orbitals represent the HOMO of those units.[12]

b) d^{10}-d^{10} system

Weak Metal-Metal interactions are also observed in d^{10}-d^{10} systems (full $d_{x^2-y^2}$ orbitals are involved in metal bonding).[18] In this case, like d^8-d^8 combinations, the closed-shell metal centers, instead of repulsion, show attractive interactions. Considering orbital interactions, such weak bonding can be described considering interaction between full n5d and (n+1)s/p orbitals, which are close in energy for effective orbital overlap.[18] In addition, d^{10}-d^{10} interactions are unusually strong due to relativistic effects which are specially significant for heavy metals, which are the cases where electrons' speed is a significant fraction of the light speed. As a result of relativistic effects s–orbitals decrease substantially in energy and p–orbitals also decrease, but to a lesser extent. This enhances their nuclear shielding effect, causing d– and f–orbitals to increase in energy. Thus, energy gap between 6s/6p and 5d in molecular orbitals decreases, which allows a better overlap and stronger interactions and it reaches the maximum between Au(I) centers.[18]

One of the most common example of d^{10}-d^{10} systems is the interaction between Au(I) centers known as "Aurophilicity". Schmidbaur et al. for the first time introduced the term of "Aurophilicity" to describe such special kind of interactions exhibited by Au(I) compounds.[19] It is now accepted and recognized that small mononuclear complexes of gold with intermolecular aggregation via short sub-van der Waals Au(I)···Au(I) interaction contacts of *ca.* 3.05 Å is associated with a bonding energy in the range of 5−10 kcal mol^{-1}.[19] This energy is comparable to typical hydrogen bonds. So Au(I)···Au(I) interaction by analogy to hydrogen bonding would have a similar role in the supramolecular organization of gold(I) compounds.

Although the other d^{10} ion metals in gold group also exhibit Metal-Metal interactions known as "metallophilicity" (or more specifically, "cuprophilicity" for Cu(I) and "argentophilicity" for Ag(I)),[20] aurophilic attraction is found to be as the strongest one. Even for other heavy metals similar metallophilic interactions exist, such

[18] a) P. Pyykkö and Y. Zhao, *Angew. Chem. Int. Ed. Engl.,* **1991**, *30*, 604-605. b) A. Görling, N. Rösch, D. E.Ellis and H. Schmidbaur, *Inorg. Chem.,* **1991**, *30*, 3986-3994. c) O. D. Häberlen, H. Schmidbaur and N. Rösch, *J. Am. Chem. Soc.,* **1994**, *116*, 8241-8248.

[19] a) H. Schmidbaur, *Chem. Soc. Rev.,* **1995**, *24*, 391-400. b) H. Schmidbaur, *Gold: Progress in Chemistry, Biochemistry, and Technology*, John Wiley & Sons, Chichester, **1999**.

[20] a) C. M. Che, Z. Mao, V. M. Miskowski, M. C. Tse, C. K. Chan, K. K. Cheung, D. L. Phillps and K. H. Leung, *Angew. Chem. Int. Ed.,* **2000**, *39*, 4084-4088. b) C. M. Che, M. C. Tse, M. C. W. Chan, K. K. Cheung, D. L. Phillips and K. H. Leung, *J. Am. Chem. Soc.,* **2000**, *122*, 2464-2468.

as mercury or between heavy atoms of different elements such as Hg(II)-Au(I)[21] or in d^{10}-d^8 systems like Hg(II)-Pt(II)[22], and Hg(II)-Pd(II)[23]. Remarkably none of these other interactions are as strong as aurophilicity.[24]

As a consequence of this supramolecular interaction, and taking advantage of the structural versatility of Au(I) centers, a variety of structures with interesting optical and/or luminescence properties have been reported.[25] The aurophilic interaction that hold Au(I) building blocks together via self-assembly reactions can form linear "molecular wires",[26] clusters,[27] rings,[28] catenanes[29] or polymeric structures.[30]

These complexes display very interesting photophysical properties, such as luminescence, that are induced by the presence of intermetallic interactions. Selected examples of luminescent supramolecular architectures built through Au–Au interactions, both in the solid state and/or in solution are shown in scheme 1.7. These structures are based on the supramolecular assembly of mononuclear, binuclear or trinuclear building blocks.[31] Different parameters such as aggregation state, concentration, temperature and solvent can have an effect on luminescent properties.[32]

Several studies have found a direct correlation between the emission properties of gold(I) derivatives and aurophilic interactions. As a consequence, much attention has been paid on the possibility of switching "on" and "off" the emission of Au(I) compounds by favoring or restricting Au…Au (aurophilic) contacts, for their potential as molecular sensors, probes or optical devices.[33] Additionally, aurophilicity can be used as a controlling force in crystal engineering, in self assembly electronic devices.[32]

---

[21] A. Burini, J. P. Fackler, R. Galassi, T. A. Grant, M. A. Omary, M. A. Rawashdeh-Omary, B. R. Pietroni and R. J. Staples, *J. Am. Chem. Soc.*, **2000**, *122*, 11264-11265.
[22] a) L. R. Falvello, J. Fornies, A. Martin, R. Navarro, V. Sicilia and P. Villarroya, *Inorg. Chem.*, **1997**, *36*, 6166-6171. b) R. Jószai, I. Beszeda, A. C. Bényei, A. Fischer, M. Kovács, M. Maliarik, P. Nagy, A. Shchukarev, and I. Tóth, *Inorg. Chem.,* **2005**, *44*, 9643-9651.
[23] K. Mieock, J.T. Thomas and P.G. Francois, *J. Am. Chem. Soc.*, **2008,** *130*, 6332-6333.
[24] B. Assadollahzadeh and P. Schwerdtfege, *Chemical Physics Letters*, **2008,** *462*, 222-228.
[25] a) V. W. W. Yam and E. C. C. Cheng, *Top. Curr. Chem.,* **2007**, *281*, 269-309. b) R. J. Puddephatt, *Coord. Chem. Rev.,* **2001**, *216*, 313-332. c) V. W. W. Yam and E. C. C. Cheng, *Chem. Soc. Rev.,* **2008**, *37*, 1806-1813. d) H. Schmidbaur and A. Schier, *Chem. Soc. Rev.,* **2012**, *41*, 370-412.
[26] M. J. Irwin, G. Jia, N. C. Payne and R. J. Puddephatt, *Organometallics,* **1996**, *15*, 51-57.
[27] V. W. W. Yam, E. C. C. Cheng and K. K. Cheung, *Angew. Chem. Int. Ed.,* **1999**, *38*, 197-199.
[28] M. J. Irwin, L. M. Rendina, J. J. Vittal and R. J. Puddephatt, *J. Chem. Soc. Chem. Commum.,* **1996**, 1281-1283.
[29] a) C. P. McArdle, M. J. Irwin, M. C. Jennings and R. J. Puddephatt, *Angew. Chem. Int. Ed.,* **1999**, *38*, 3376-3378. b) C. P. McArdle, J. J. Vittal and R. J. Puddephatt, *Angew. Chem. Int. Ed.,* **2000**, *39*, 3819-3822.
[30] M. C. Brandys and R. J. Puddephatt, *J. Chem. Soc. Chem. Commum.,* **2001**, 1280-1282.
[31] a) N. L. Coker, J. A. Krause Bauer and R. C. Elder, *J. Am. Chem. Soc.*, **2004**, *126*, 12-13. b) M. A. Mansour, W. B. Connick, R. J. Lachicotte, H. J. Gysling and R. Eisenberg, *J. Am. Chem. Soc.*, **1998**, *120*, 1329-1330. c) A. Hayashi, M. M. Olmstead, S. Attar and A. L. Balch, *J. Am. Chem. Soc.*, **2002**, *124*, 5791-5795.
[32] A. Laguna, *Modern Supramolecular Gold Chemistry: Gold-Metal Interactions and Applications*, Wiely-VCH press, **2008**.
[33] C. Corti and R. Holliday, *Gold: Science and Applications,* CRC press, **2010**.

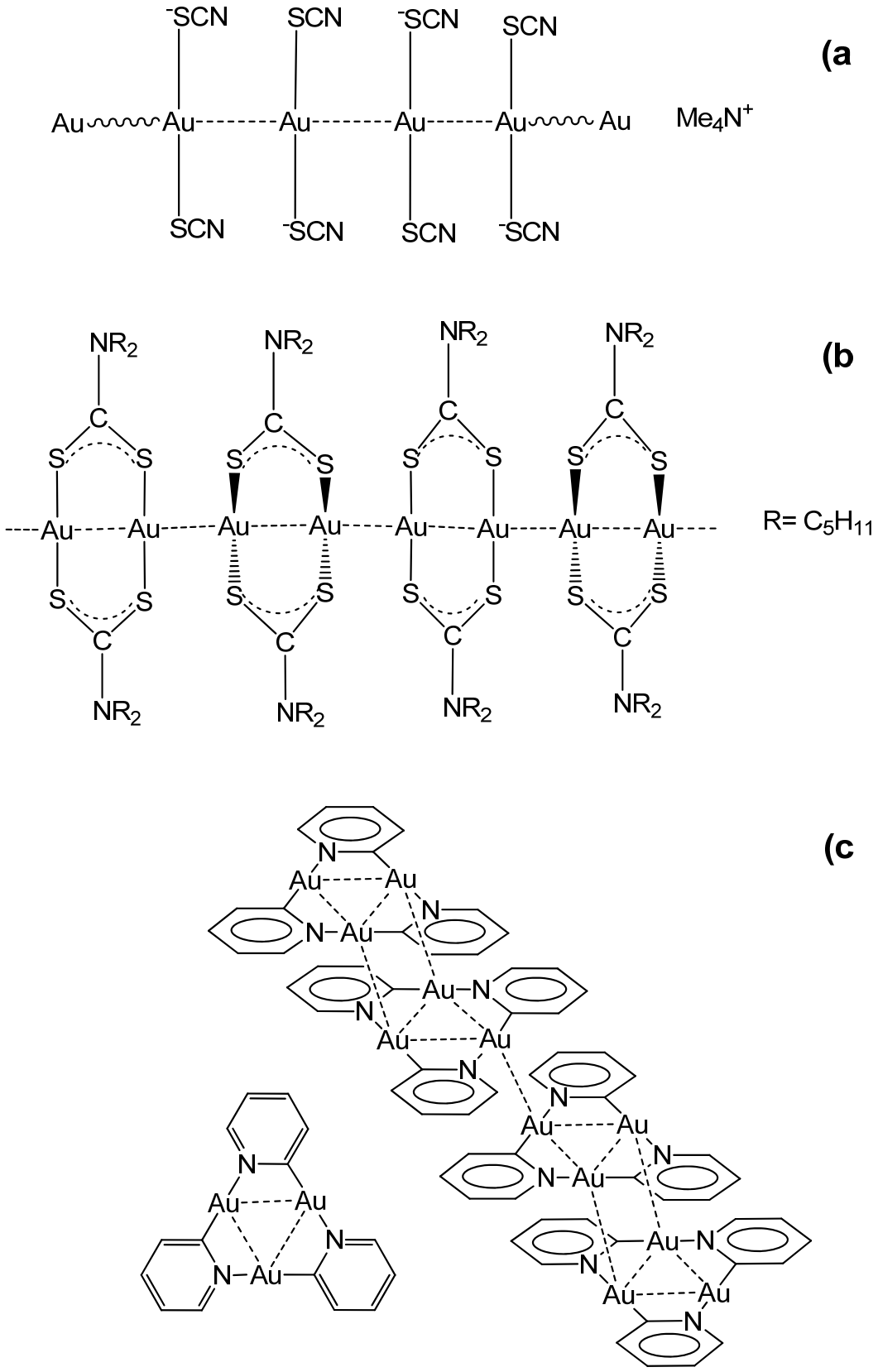

Scheme 1.7. Luminescent supramolecular architectures base on mononuclear, binuclear and trinuclear systems of gold.[31]

1.2. Metal-Ligand interactions as driving force for supramolecular assemblies

In addition to weak Metal-Metal interactions, a second strategy to assemble 1D metallo-structure is the use of bridging ligands that hold together the chains through Metal-Ligand bonding. In scheme 1.8 are presented two binding modes in which ligands can assemble metal centers in a linear geometry.

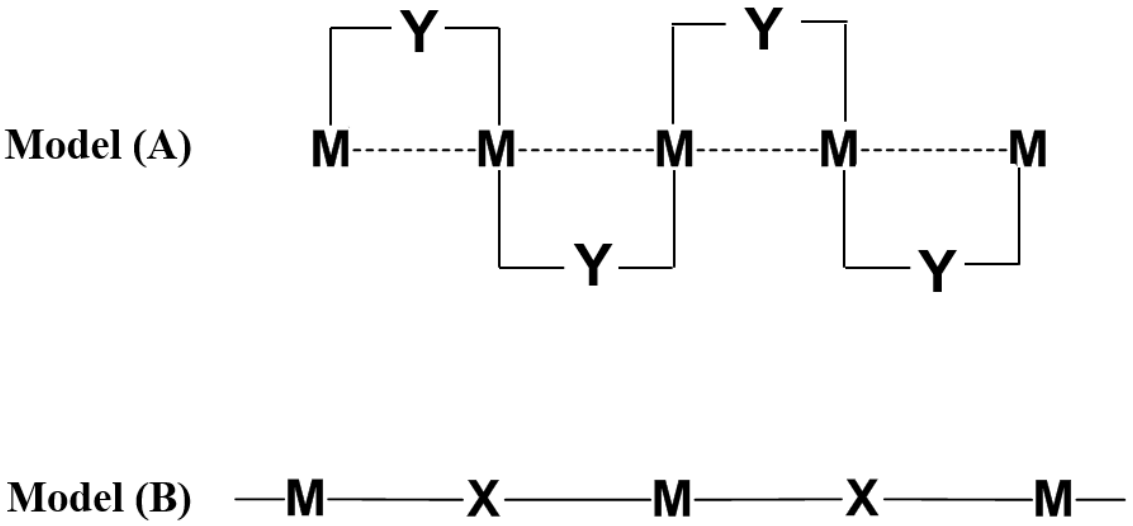

Scheme 1.8. General classification of bridging ligands. Model A: M= metals and Y= Carboxylate, Dithiocarboxylate, Xanthate ligands, etc and Model B: M= metal and X= CN, Cl, Br, I, etc.

a) Model A

In this model, linking ligands such as carboxylates, dithiocarboxylates, carbamates, dithiocarbamates, xanthates, etc use two donor atoms that interact with two metal centers holding together a chain (scheme 1.9).[34] Assembly of chains is competitive with formation of bimetallic and cyclic oligomeric structures. Such equilibriums are determined by several factors such as lability of Metal-Ligand bonding or ratio between metal sizes and distances enforced by bidentate ligands. This binding mode allows to hold the metal centers close enough (less than twice the van der Waals radius) to have weak interaction resulting from the forces from ligands to compress the Metal-Metal distances.

[34] a) V. J. Catalano, M. A. Malwitz and A. O. Etogo, *Inorg. Chem.*, **2004**, *43*, 5714-5724. b) F. Liu, W. Chen and D. Wang, *Dalton Trans.*, **2006**, 3015-3024.

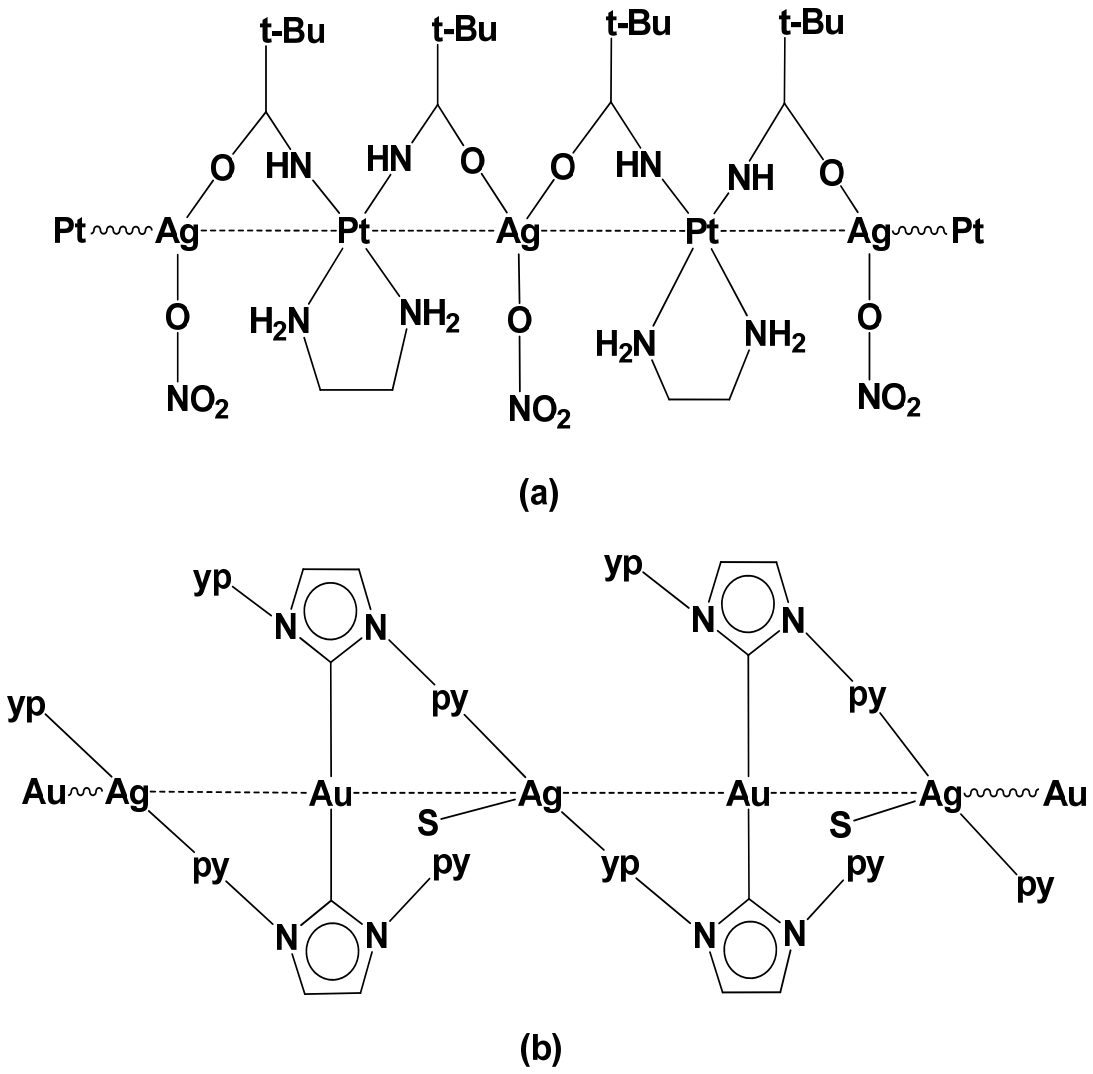

Scheme 1.9. Some examples of model A that were reported in Cambridge Structural Database (CSD).[36]

One important example of this model is $[Pd(C_2H_3O_2)_2]_n$.[35] The X-ray structure of palladium(II) acetate is trimeric, consisting of an equilateral triangle of Pd atoms each pair of which is bridged with two acetate groups in a butterfly conformation (figure 1.2 (a)).[36] However, when palladium(II) acetate is prepared in a slightly different way a pale pink powder is obtained, which have an structure consisting of infinite chains in which the coordination geometry around each Pd is square planar (figure 1.2 (b) and (c)).[37] The structure of $[Pd(C_2H_3O_2)_2]_n$ has been described as *catena*-poly [palladium(II)- di-μ-

[35] V. I. Bakhmutov, J. F. Berry, F. A. Cotton, S. Ibragimov and C. A. Murillo, *Dalton Trans.*, **2005**, 1989-1992.
[36] A. C. Skapski and M. L. Smart, *J. Chem. Soc. D.*, **1970**, 658-659.
[37] S.D. Kirik, S.F. Mulagaleev and A.I. Blokhin, *Acta. Cryst. C.*, **2004**, 449-450.

acetato-κ^4*O*:*O*′] with a linear arrangement of the palladium atoms separated by less than 3A°.[37]

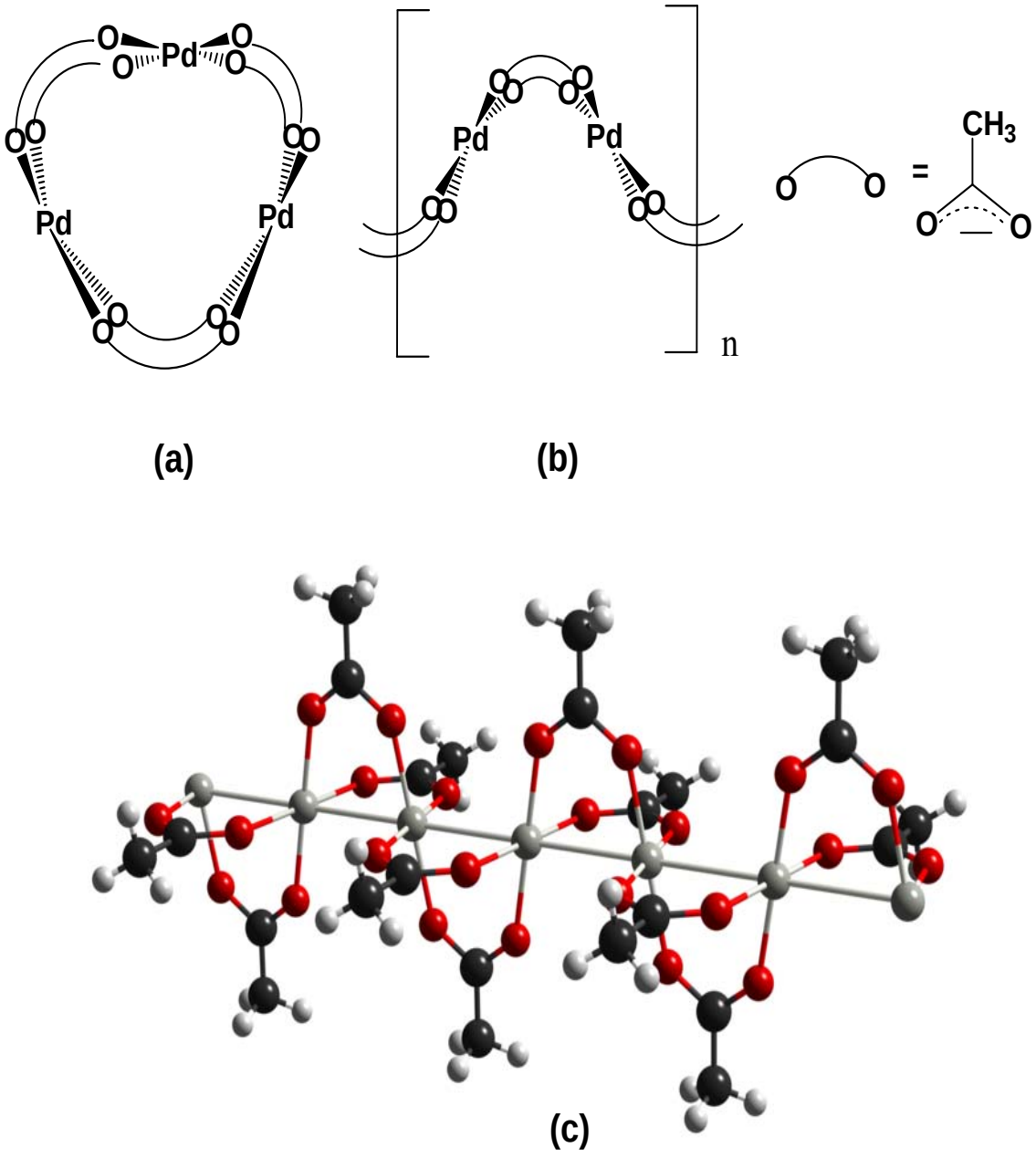

Figure 1.2. Different structures of $[Pd(C_2H_3O_2)_2]_n$. a) butterfly conformation b) linear chain c) ball and stick model of structure b (Pd=grey, O=red, C=black and H= white).[36,37]

This model also has been observed in Au(I) compounds.[38] For instance, as shown in scheme 1.10, in the polymeric one dimensional chain of [Au$_2$(n-pentyl-

[38] M-R. Azani, O. Castillo, M. L. Gallego, T. Parella, G. Aullon, O. Crespo, A. Laguna, Santiago Alvarez, R. Mas-Balleste and Felix Zamora, *Chem. Eur. J.*, **2012**, *18*, 9965-9976.

dithiocarboxylate)$_2$], the dithiocarboxylato groups act as bridging ligands between the gold centers. The distance between adjacent Au(I) centers is 2.962-3.028 A, which is shorter than twice the van der Waals radius in metallic gold (3.32 A), indicating aurophilic interactions.[38]

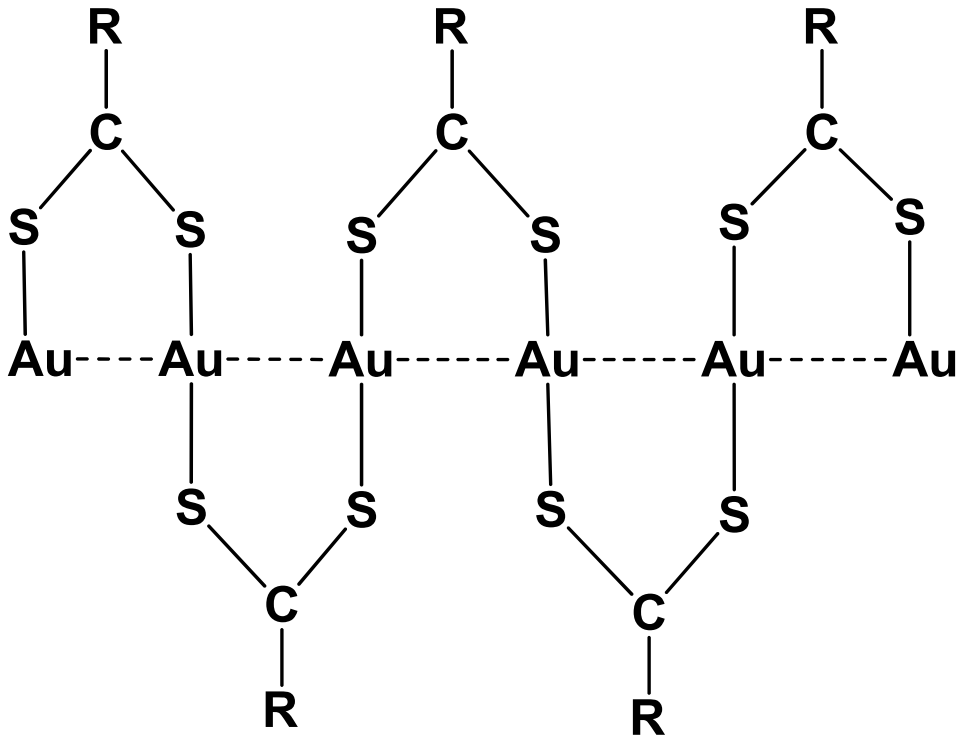

Scheme 1.10. Metal-Ligand interaction in [$Au_2(RCS_2)_2$] (R= C_5H_{11}).[38]

b) Model B

Linear supramolecular polymers following the structure shown in model B can be based on discrete units or on bimetallic fragments.

MX polymers are a typical example of linear structures based on the assembly of monometallic units. Such structures can be described as hetero- or homo-metallic polymers with metal centers with different oxidation states.[39] For instance, Wolffram red salt consists on linear chains of -Pt^{2+}-Cl^--Pt^{4+}-Cl^-- where each Pt^{4+} or Pt^{2+} centers are coordinated to four tetragonal ethyl amines.[40] Conductive properties of such polymers are in the order of 10^{-6} S.cm^{-1}.[41]

[39] M. Yamashita,T. Ishii, H. Matsuzaka, T. Manabe, T. Kawashima, H. Okamoto and H. Kitagawa, *Inorg. Chem.,* **1999**, *38*, 5124-5130.
[40] H. Tanino and K. Kobayashi, *J. Phys. Soc. Jap.,* **1983**, *52*, 1446-1456.
[41] a) H. Toftlund and P. W. Jensen, *Chem. Phys. Lett.,* **1987**, *142*, 286-290. b) G. Givaja, P. Amo-Ochoa, C. J. Gomez-Garcia and Felix Zamora, *Chem. Soc. Rev.,* **2012**, *41*, 115-147.

On the other hand, there are several possible ways to connect bimetallic building blocks to form linear structures. One possible approach for the formation of linear chains involves the inclusion of metal-halide cores as linkers. In this regard, reaction of K_2MCl_4 (M= Pd, Pt) with the cationic complex $Rh_2(acam)_4^+$ (acam= CH_3CONH_2) generated linear structures.[42] Another strategy to prepare one-dimensional compounds could be the use of metal-cyanide compounds as linkers to form heterobimetallic polymers. The ability to form both σ and π interactions of μ-CN ligands allows strong electronic coupling between the linked metal centers significantly affecting their physical properties. In addition, reversibility of MCN-M bonds makes possible structural integrity by means of self healing processes.[43]

A particular case of linear coordination polymers are the so called as MMX (scheme 1.11). Such chains can be described as one-dimensional structures constituted by bimetallic units with paddle wheel geometry linked by halide bridging ligands. This structural family is specially relevant due to their interesting physical properties.[41] For instance, those based on ruthenium, dicarboxylate $[Ru_2(RCO_2)_4I]_n$ (R = alkyl group), have shown magnetic properties.[44] However, the most exciting feature of such polymers is their electrical conductivity. For instance, polymers of formula $K_4[Pt_2(pop)_4X]_n .H_2O$ (where pop = $P_2O_5H_2^{2-}$ and X = Cl, Br, I), where the formal oxidation state of the Platinum atoms is +2.5, are considered as a new type of semiconductor.[45] Formation of these compounds involves oxidation of the precursor $[Pt_2(pop)_4]^{4-}$. Conductivity values for crystalline sample fall in the range of 10^{-4}-10^{-3} $S \cdot cm^{-1}$ at room temperature.[46]

The most studied case of MMX polymers are undoubtedly the chains formed by diplatinum units with dithioacid ligands linked by iodide anions according to the general formula $[Pt_2(RCS_2)_4I]_n$ (R = alkyl group). Here, the formal oxidation state of Pt atoms is +2.5. These polymers deserve special consideration because they show metallic

[42] Z. Yang, M. Ebihara and T. Kawamura, *Inorg. Chim. Acta.*, **2006**, *359*, 2465-2471.
[43] M. Yao,Q. Zheng, F. Gao, Y. Li and J. Zuo, *Sci. China. Chem.*, **2012**, *55*, 1022-1030.
[44] a) M. C. Barral, R. Gonzalez-Prieto, R. Jimenez-Aparicio, J. L. Priego, M. R. Torres and F. A. Urbanos, *Eur. J. Inorg. Chem.,* **2003**, 2339-2347. b) M. C. Barral, R. Gonzalez- Prieto, R. Jimenez-Aparicio, J. L. Priego, M. R. Torres and F. A. Urbanos, *Eur. J. Inorg. Chem.,* **2004**, 4491-4501. c) M. C. Barral, R. Jimenez-Aparicio, D. Perez Quintanilla, J. L. Priego, E. C. Royer, M. R. Torres and F. A. Urbanos, *Inorg. Chem.,* **2000**, *39*, 65-70.
[45] C. M. Che, F. H. Herbstein, W. M.Schaefer, R. E. Marsh and H. B. Gray, *J. Am. Chem. Soc.,* **1983**, *105*, 4604-4607.
[46] L. G. Butler, M. H. Zietlow, C. M. Che, W. P. Schaefer, S. Sridhar, P. J. Grunthaner, B. I. Swanson, R. J. H. Clark and H. B. Gray, *J. Am. Chem. Soc.,* **1988**, *110*, 1155-1162.

conductivity in crystal state at room temperature[47], which makes them very attractive towards several potential applications.[48]

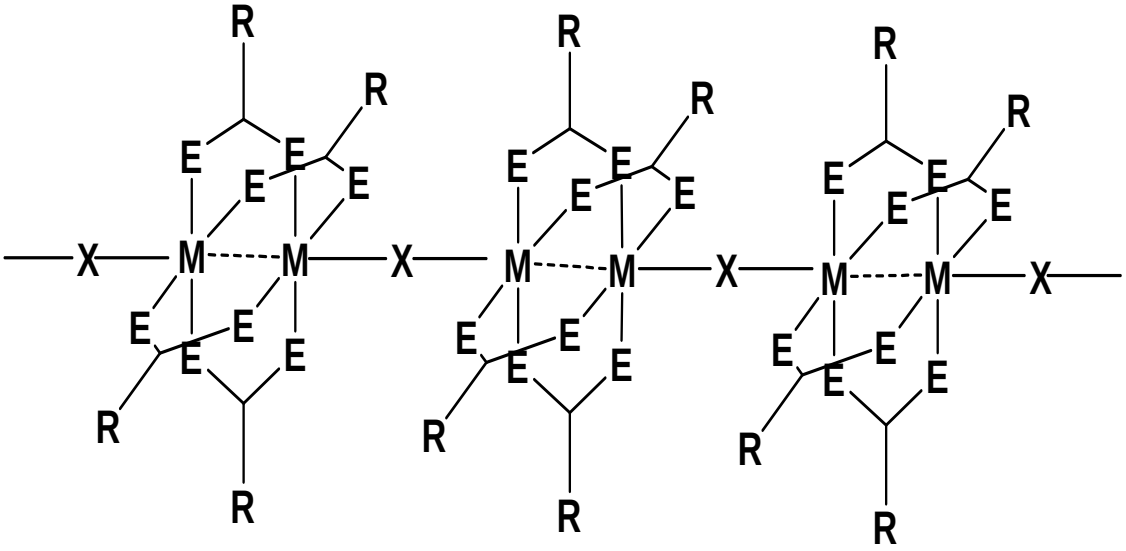

Scheme 1.11. MMX structure. (M= Pt, Ni, Pd, Ru – E=O, S – X= Br, I)

The first polymer of this class was synthesized by Bellito et al. in 1983 with the formula $[Pt_2(CH_3CS_2)_4I]_n$.[49] Individual crystals of this compound shown conductivity values of 13 $S \cdot cm^{-1}$ at room temperature.[47] However, for analogous nickel polymer lower values of electrical conductivity (5×10^{-6} $S.cm^{-1}$) were observed.[50]

The structure of $[Pt_2(RCS_2)_4I]_n$ chains can be described with different models of charge distribution, as shown below [51]:

(i) an averaged-valence state (AV): • • • $M^{+2.5}$ - $M^{+2.5}$ - X - $M^{+2.5}$ - $M^{+2.5}$ - X• • •

(ii) a charge polarization state (CP): • • • M^{+2} - M^{+3} - X - M^{+2} - M^{+3} - X • • •,

(iii) a charge density wave state (CDW): • • • M^{+2} - M^{+2} -X - M^{+3} - M^{+3} - X • • •

(iv) an alternate charge polarization state (ACP): • • • M^{+2} - M^{+3} - X - M^{+3} - M^{+2} -X • • •

Varying the temperature or exerting a compression in a uniaxial system can provoke variations in M-M and M-X distances in the crystal structure and induce phase

[47] M. Mitsumi, T. Murase, H. Kishida, T. Yoshinari, Y. Ozawa, K. Toriumi, T. Sonoyama, H. Kitagawa and T. Mitani, *J. Am. Chem. Soc.,* **2001**, *123*, 11179-11192.
[48] a) H. Kitagawa, N. Onodera, J. S. Ahn and T. Mitani, *Synthetic Metals,* **1997**, *86*, 1931-1932. b) M. Mitsumi, S. Umebayashi, Y. Ozawa, K. Toriumi, H. Kitagawa and T. Mitani, *Chemistry Letters,* **2002**, *258*-259.
[49] C. Bellitto, A. Flamini, L. Gastaldi and L. Scaramuzza, *Inorg. Chem.*, **1983**, *22*, 444-449.
[50] C. Bellito, G. Dessy and V. Fares, *Inorg. Chem.,* **1985**, *24*, 2815-2820.
[51] Y. Wakabayashi, A. Kobayashi, H. Sawa, H. Ohsumi, N. Ikeda and H. Kitagawa, *J. Am. Chem. Soc.,* **2006**, *128*, 6676-6682.

transitions.[52] Recent studies carried out with different dithiocarboxylate alkyl ligands have shown that the length of the alkyl chains determines the phase stability. As an example of the structural diversity of these materials, crystals of $[Pt_2(n\text{-pentyl}CS_2)_4I]$ show a transition from semiconductor to metallic with the increase of the temperature and a second metallic–metallic transition at 330 K inferred by electrical conductivity measurements. X-ray diffraction studies carried out at different temperatures (100, 298, and 350 K) confirm the presence of three different phases: ACP (below 210 K), an unusual AV state with three fold Pt–Pt–I unit-repetition (between 210 and 324 K) and AV (above 324 K).[53]

During last several years, the topic of MMX coordination polymers has gained renewed attention in the area of nanomaterials. In particular, our group has been interested in the isolation on surfaces of nanostructures based on MMX, with the aim of using such chains as molecular wires. Thus, in the group has been a primary goal the direct electrical measurement of isolated single chains of MMX. With this aim, several techniques to isolate nanostructures from bulk samples have been developed. One approach is based on direct sublimation of MMX crystals, and further reorganization on surfaces to generate linear nanostructures. Following this approach recently has been reported the isolation of nanoribbons of $[Pt_2(CH_3CS_2)_4I]_n$ on mica[54] and SiO_2 (as shown in figure 1.3),[55] which allowed to measure, for the first time, electrical conductivity of bundles of MMX chains at the nanoscale.

[52] H. Ito, Y. Hasegawa, H. Tanaka, S. Kuroda, M. Mitsumi and K. Toriumi, *J. Phys. Soc. Jpn.,* **2003**, *72*, 9, 2149-2152.
[53] a) S. Ikeuchi, K. Saito, Y. Nakazawa, M. Mitsumi, K. Toriumi and M. Sorai, *J. Phys. Chem. B,* **2004**, *108*, 1, 387-392. b) H. Tanaka, Y. Hasegawa, H. Ito, H. Kuroda, T. Yamashita, M. Mitsumi and K. Toriumi, *Synthetic Metals,* **2005**, *152*, 141-144.
[54] L. Welte, A. Calzolari, R. di Felice, F. Zamora and J. Gomez-Herrero, *Nat. Nanotechnol.,* **2010**, *5*, 110-115.
[55] C. Hermosa, J. V. lvarez, M-R. Azani, C. J. Gomez-Garcia, M. Fritz, J. M. Soler, J. Gomez-Herrero, C. Gomez Navarro and F. Zamora, *Nat. Commun.,* **2013**, *4*, 1709-1715.

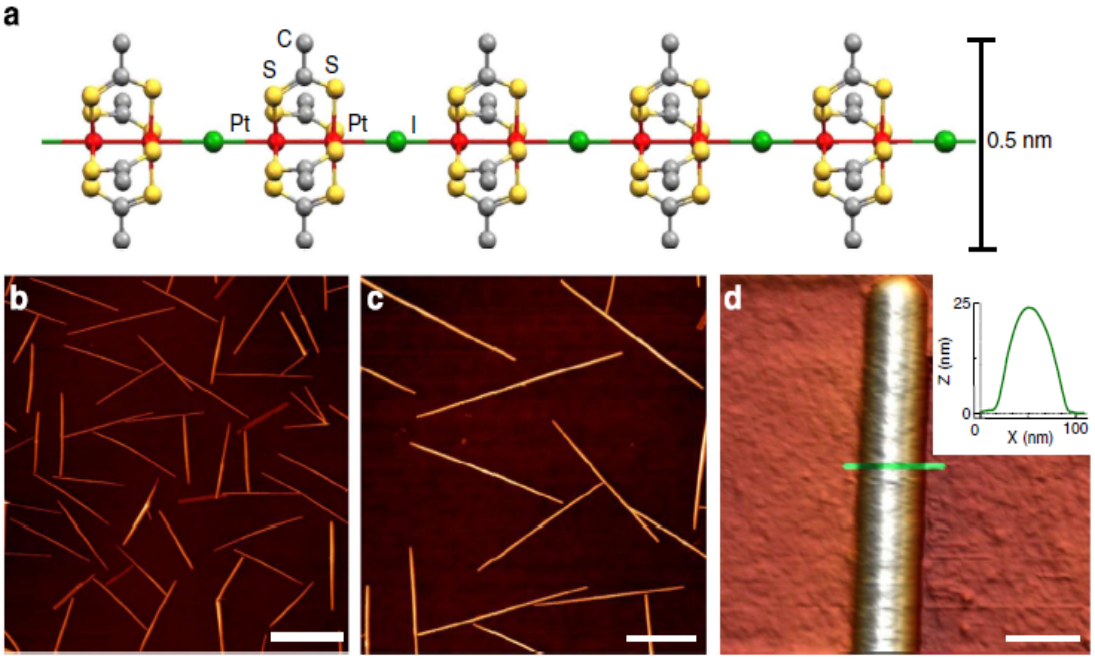

Figure 1.3. a) Structure of a $[Pt_2(CH_3CS_2)_4I]_n$ single fiber. (b,c,d) AFM images of nanoribbons on a SiO_2 substrate where the straightness and height homogeneity can be appreciated. The inset in d is a profile acquired on the green line of the corresponding image, where the cross-section of the ribbons can be determined. Typical dimensions of the nanoribbons are 10 µm × 100 nm × 20 nm. Scale bars, 8, 4 and 0.1 µm (for b, c and d, respectively).[55]

In a more recent study, MMX chains of formula $[Pt_2(n\text{-pentylCS}_2)_4I]_n$ were assembled on surfaces from solutions.[56] In that case, was observed the formation of nanocrystals and bundles, but single chains were not observed.

Heterometallic MM′X chains have also been obtained. For instance, the polymer containing Pt(II) and Ru(III) in the formula formula $[\{PtRh(PVM)_2(en)\}Cl_3 \cdot 3H_2O]_n$ (where en = ethylenediamine and PVM= $tBuCONH^-$) was isolated in 2007.[57] Also in our group recently MM′X monodimensional chains of $[Ni_{0.6}\ Pt_{1.4}(EtCS_2)_4I]$ and $[Ni_{0.1}Pd_{0.3}Pt_{1.6}(EtCS_2)_4I]$ were obtained. The electrical properties of the mixed MM′X polymer revealed a semiconducting character, while magnetic susceptibility measurements confirmed a temperature independent AV ground state.[58] However, the examples of heterometallic MM′X chains are still very scarce and there are not clear synthetic routes to build up polymers that combine physical properties of diverse metal centers.

[56] A. Guijarro, O. Castillo, L. Welte, A. Calzolari, P. J. Sanz Miguel, C. J. Gomez-Garcia, D. Olea, R. D. Felice, J. Gomez-Herrero and Felix Zamora, *Adv. Funct. Mater.*, **2010**, *20*, 1451-1457.
[57] K. Uemura, K. Yamasaki, K. Fukui and K. Matsumoto, *Eur. J. Inorg. Chem.*, **2007**, 809-815.
[58] G. Givaja, O. Castillo, E. Mateo, A. Gallego,C. J. Gomez-Garcia, A. Calzolari, R. D. Felice and Felix Zamora, *Chem. Eur. J.*, **2012**, *18*, 15476-15484.

1.3. Goals of this work.

From the fast overview of the literature shown above, it is clear that weak metal-metal interaction between Au(I) or Pt(II) centers is a powerful driving force to trigger spontaneous self-assembly processes to generate supramolecular structures of variable complexity. In a similar way, weak metal-ligand interactions in MMX chains confer to this family of coordination polymers an outstanding ability to spontaneously assemble and disassemble. Despite these facts are widely reported, not always are well understood. In particular, there are several open questions relating the factors that govern assemblies both in solid state and in solution. This thesis is aimed to contribute to shed light to some of these questions referred to the assembly of bimetallic units.

In a first approach bimetallic [AuL_2] compounds will be examined to understand the factors that affect the obtention of supramolecular polymetallic entities in solution. Obvious factors, such as steric crowding, and more subtle parameters, such as electronic structure of axial ligands will be examined. In addition, the consequences of the intrinsic ability to self-assembly of bimetallic gold compounds, on the structures found in crystal phase, will be discussed.

In a similar study, the behavior in solution of bimetallic [Pt_2L_4] species will be analyzed, in the quest of a systematic determination of the factor that could allow to control an modulate spontaneous assembly of linear structures through Pt(II)···Pt(II) weak interactions.

Taking a further step, we will apply the concepts and methods developed in the study of supramolcules based in Au(I)···Au(I) or Pt(II)···Pt(II) interactions to gain a deeper understanding of the ability shown by $[Pt_2L_4I]_n$ to assemble and disassemble. For the first time, such processes will be studied in solution and the conclusions obtained will be applied to the isolation of polymer chains on surfaces, which represents a new twist on the way to use such materials as molecular wires.

Thus, in this thesis are presented some novel insights on the molecular and electronic structures of supramolecules in solution, which are presented and related with their spectroscopic features, from both an experimental and a theoretical point of view. These results will contribute to the rational design of complex architectures based on the assembly of metal–organic building blocks.

1.4. Collaboration and scientific contributions of other researchers

A scientific study with the objectives described above requires a multidisciplinary approach. Thus, some of the work needed falls far from the expertise of the one who presents this thesis, and consequently several collaborations have been required. Without the scientific contributions of such experts this work would be impossible. In particular, Dr. Oscar Castillo from university of Pais Vasco has been the responsible of the resolution of the crystal structures by X-ray diffraction. Dr. Teodor Parella from Autonoma University of Barcelona measured DOSY-NMR spectra of gold compounds. Luminescence measurements for Au(I) compounds were made by Olga Crespo under the supervision of Professor Antonio Laguna in the University of Zaragoza. Isolation of nanometric structures from MMX polymers by soft lithography techniques has been carried out by Professor Massimiliano Cavallini, Dr. Denis Gentili, Arian Shehu and Francesca Leonardi from Institute for Nanostructured Materials of CNR of Bologna (CNR-ISMN). Dr. Eva Mateo-Marti from Astrobiology Center (CSIC-INTA) of Madrid has collaborated in the analysis by XPS of Nanostructured MMX. AFM measurements of the MMX chains on surface were obtained by Cristina Hermosa (Department of Inorganic Chemistry, UAM) under the supervision of Professor Julio Gomez-Herrero (Department of Condensed Matter Physics, UAM) .The computational and theoretical studies for gold complexes have been made by Professor Santiago Alvarez and Dr. Gabriel Aullon from University of Barcelona. For the study of assembly and disassembly of structures $[Pt_2L_4]_n$ and $[Pt_2L_4I]_n$ theoretical calculations, paying special attention to the simulation of spectroscopic features by means of TD-DFT methods, have been carried out by Dr. Alejandro Perez Paz and Leonardo A. Espinosa Leal under the supervision of Professor Angel Rubio.

Chapter 2

II. Results and discussions

2.1. Gold(I)···Gold(I) Interaction:

In this thesis, in the beginning, the comparison of six series of analogous dinuclear Au(I) compounds containing dithiocarboxylate or xanthate ligands and their ability for the supramolecular assembly are discussed (scheme 2.1).

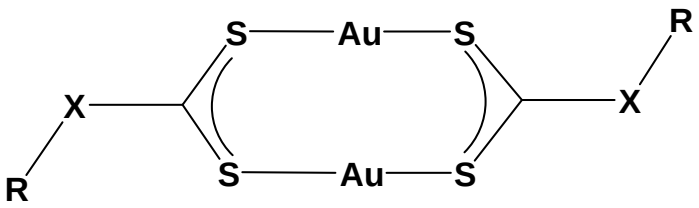

R	X = CH_2	X = O
R = $CH_3(CH_2)_2$	1	4
R = $(CH_3)_2CH_2$	2	5
R = $CH_3(CH_2)_3$	3	6

Scheme 2.1. Gold compounds studied in this thesis.

2.1.1. Synthesis of gold(I) Complexes:

Synthesis of gold(I) complexes with using dithiocarboxylate ligands has an important drawback because of achieving low yields.[59] For instance, by using the synthetic procedure described by our group, with using an Au(I) starting material, such as $K[Au(CN)_2]$ with dithiocarboxylic acid in a 1:1 ratio, high yields were not always achieved.[59] Thus, obtaining higher yield for same Au(I) complexes with this type of ligands needs to explore alternative synthetic strategies.

Here, the yields were increased up to 70% (based on gold) by reacting one equivalent of the Au(III) starting material $Na[AuCl_4]$ with three equivalents of the deprotonated dithiocarboxylic acid. The excess of two equivalents of ligand act as reducing agent to reduce Au(III) to Au(I). So, the remaining equivalent of the dithiocarboxylate coordinates to Au(I) center efficiently and rapidly. In polar media $[Au_2L_2]_n$ species precipitate immediately (scheme 2.2).

[59] M. L. Gallego, A. Guijarro, O. Castillo, T. Parella, R. Mas-Balleste and F. Zamora, *Cryst. Eng. Comm.,* **2010**, *12*, 2332-2334.

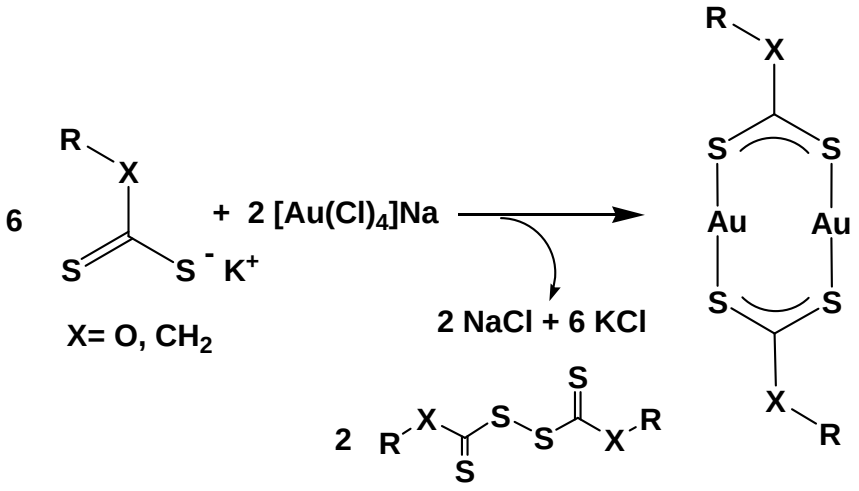

Scheme 2.2. Synthetic route followed in this thesis to obtain compounds of the formula $[Au_2L_2]$.

The same synthetic procedure was applied to synthesis of high yield Au(I) complexes with using xanthate ligands. The yields of over 70% of $[Au_2L_2]$ were obtained. X-ray quality single crystals of these compounds were obtained by slow vapor diffusion of diethyl ether on solutions of gold(I) compounds in CS_2 at 4 ºC.

2.1.2. In crystal phase

Crystal structures of homoleptic Au(I) compounds significantly depend on the types of ligands that used. For instance, Au(I) complexes with dithiocarboxylate ligands show an outstanding ability to generate oligomeric/polymeric structures by means of the μ-kS:kS' bridging mode. In these structures both intra- and inter-molecular supramolecular interactions can be found in one crystal structure. Although, in the crystalline phase of $[Au_2(\text{isobutyl-dithiocarboxylato})_2]$ two polymorphic forms have been found and reported: one formed by polymeric $[AuL]_n$ chains and other formed by discrete $[Au_2L_2]$ bimetallic units.[59]

In Au(I) compounds with xanthate ligands different crystalline structures in comparison with Au(I)-dithiocarboxylate compounds are formed. All structures known for Xanthato ligands consist on discrete dimeric entities in which the metal centres are joined by double xanthate bridges and create planar eight-member $Au_2S_4C_2$ rings. Although, because of the nature of ligand, always strong intramolecular aurophilic interaction between the gold(I) centres are found, but not always strong intermolecular aurophilic interaction are observed between dimetallic units. The significant

intramolecular interaction only have observed in [Au_2(isopropyl-xanthate)$_2$] with Au···Au at around of 3.0 Å.

In the case of Au(I)-dithiocarbamate, double bridged dimmers were observed. These compounds tend to establish short Au··Au intermolecular distances that result in strong intermolecular aurophilic interactions. In the Cambridge structural database for Au(I)-dithiocarbamate compounds, there is only one ligand that provides both double bridged dimers and single-bridge-based (oligomeric) structures. Although, using the high concentration of initial gold salt can create more favorable dimeric units than single-bridge crystal structure.[60]

In overall, according to data in Cambridge structural database (CSD) for these three types of bridging ligands, it appears that there is a higher tendency of the dithiocarboxylato ligands to provide single-bridge-based structures (rings and chains) than in the case of xanthate and dithiocarbamate ligands, where double bridged dimers have preference. Additionally, in spite of xanthate, dithiocarbamate compounds prefer to establish intermolecular aurophilic interactions between dimetallic units (scheme 2.3). The different behavior of dithiocarboxylato, xanthato, and dithiocarbamato ligands has been attributed to their electron-donor or -withdrawing nature.

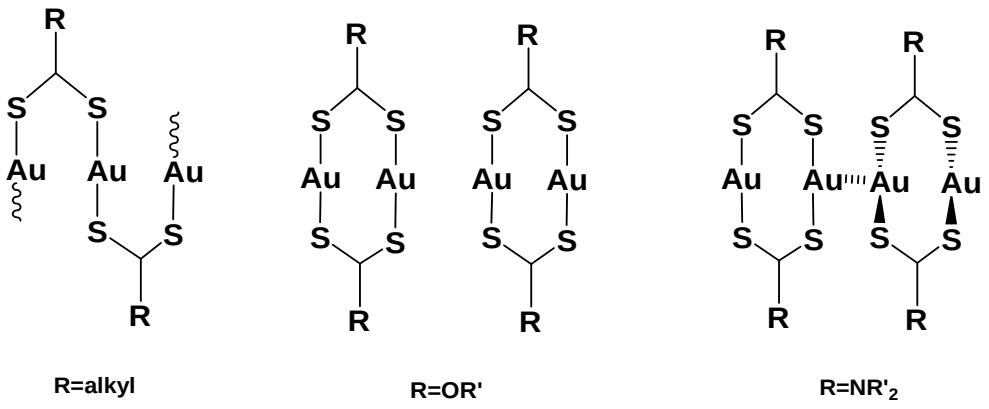

Scheme 2.3. Preferred structural motifs for homoleptic Au(I) compounds containing dithiocarboxylato, xanthato or dithiocarbamato ligands.

It is also worth mentioning that the distribution of intermolecular contacts in the CSD show maxima centered at 3.2 Å and 3.5 Å for Au···Au and Au···S contacts, respectively, whereas the S···S short contacts are spread in the range of 3.4 Å to 5.8 Å.

2.1.3. In solution

[60] B. C. Tzeng, W. H. Liu, J. H. Liao, G. H. Lee and S. M. Peng, *Cryst. Growth Des.,* **2004**, *4*, 573–577.

An interesting feature of compound **1-3** with rather different crystal structures is an identical behavior of them in solution (in CS_2). In fact, in the solution discrete analogous $[Au_2L_2]$ entities formed by cleaving the polymeric/ oligomeric $[AuL]_n$ structures found in the crystal phase. Variable temperature UV-vis data shows that by decreasing the temperature, a new feature at slightly lower energies starting to form and disappears upon heating. The temperature and concentration dependence on this new feature is indicative the spontaneous self assembly in the solution. ^1H NMR approved the presence of three different species at comparable concentrations coexist at 240 K in the solutions. To test the notion of the different nuclearities of the observed species, diffusion coefficients (D) were measured from DOSY spectra[61] of a solution at the same temperature. According to diffusion coefficient values, the species with a higher hydrodynamic radius (i.e., lower D) are more favorable at lower temperatures. The values obtained in all cases were compatible with the presence of a dimetallic, a tetrametallic, and a hexametallic species $[Au_2L_2]_n$ (n = 1, 2, 3) (scheme 2.4).

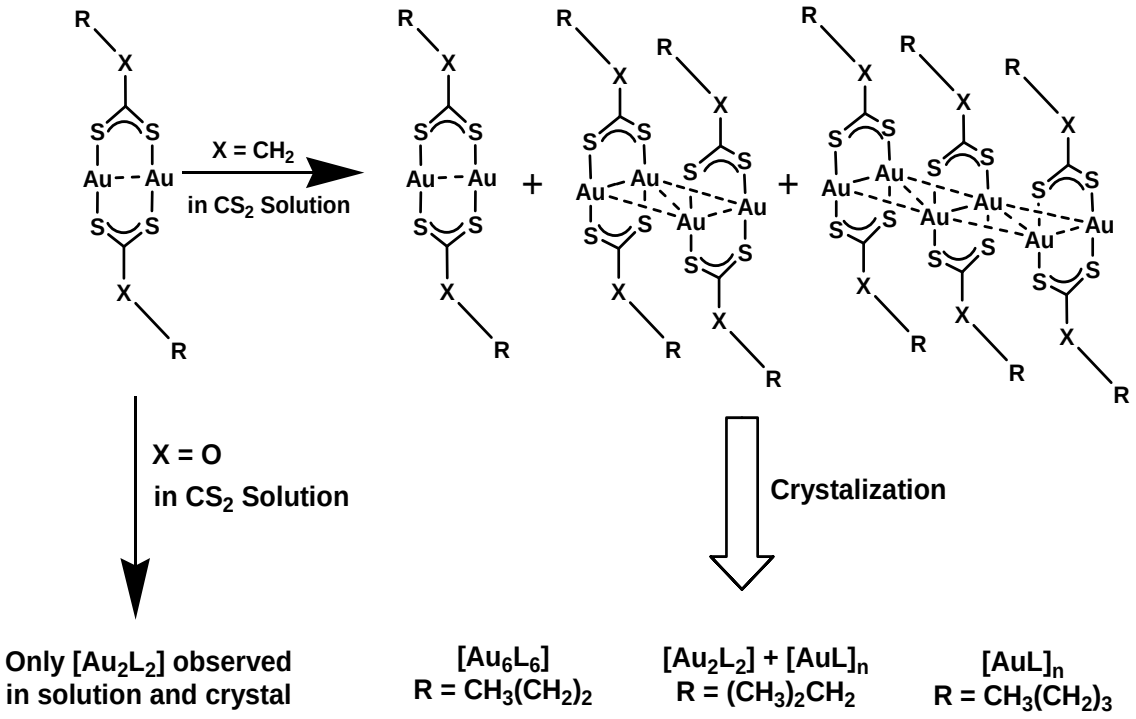

Scheme 2.4. Behavior in solution observed when $[Au_2L_2]_n$ (L = dithiocarboxilate or xanthate) are dissolved in CS_2.

The same reaction condition was performed for analogous Au(I)–xanthate compounds. Surprisingly, for Au(I) compounds with xanthate ligands upon decreasing

[61] P. S. Pregosin, P. G. A. Kumar and I. Fernandez, *Chem. Rev.,* **2005**, *105*, 2977-2998.

the temperature, no spectroscopic changes (UV-vis and NMR) were observed. Thus, although the spontaneously aggregation were observed for Au(I)-dithiocarboxylato complexes in solution, analogous complexes with xanthate ligands did not show such behavior. Thus, according to the crystal structure of compounds, it is clear that when aggregation in solution for the dithiocarboxylate compounds observed high nuclearities have been found in the their crystal phases. In the case of Au(I)-dithiocarboxylate compounds, from the corresponding discrete dimeric $[Au_2L_2]$ entities present in solution both oligomeric/polymeric structures and the discrete dimeric ones are generated. Thus, it seems the formation of the oligomeric/polymeric $[Au_2L_2]_n$ structures take place through a previous intermolecular aggregation stage of the dimers interfered by the intermolecular aurophilic contacts. The deference behavior of analogue complexes with xanthate or dithiocarboxylato ligands, is a case of sublet modulation of the supramolecular interactions. So, pay attention to this point that steric congestion is equivalent for analogous dithiocarboxylate and xanthate ligands, the tuning of aurophilic assembly should rely on electronic effects.

2.1.4. Luminescent study:

The luminescent studies were done by collaboration with the group of Professor Antonio Laguna. All of the compounds show red emissions at 77 K, but only compound **5** is emissive in the solid state at room temperature. The origin of the emissions in many thiolate gold complexes is ligand (thiolate, L) to gold (metal, M) charge-transfer (LMCT) transitions.[62] In addition, gold···gold interactions may also lead to luminescence in many polygold derivatives and metal-centered (MC) transitions.[63] When more than one metallic atom involved in the charge transfer transitions, LMMCT transitions can occurred. This case is available only when there is an interaction between metal-metal centers. In luminescence properties of Au(I) compounds, it is difficult to evaluate the influence of the aurophilia interactions in the origin of the emissions.

[62] a) J. M. Forward, D. Bohmann, J. P. Fackler and R. J. Staples, *Inorg. Chem*., **1995**, *34*, 6330-6336. b) B. C. Tzeng, C. K. Chan, K. K. Cheung, C. M. Che and S. M. Peng, *Chem. Commun.,* **1997**, 135-136. c) V. W. W. Yam, C. L. Chan, C. K. Li and K. M. C. Wong, Coord. *Chem. Rev.,* **2001**, *216*, 173-194. d) E. R. T. Tiekink and J. G. Kang, *Coord. Chem. Rev.,* **2009**, *253*, 1627-1648. e) B. C. Tzeng, H. T. Yeh, Y. C. Huang, H. Y. Chao, G. H. Lee and S. M. Peng, *Inorg. Chem.,* **2003**, *42*, 6008-6014. f) V. W. W. Yam and K. M. C. Wong, *Chem. Commun.,* **2011**, *47*, 11579-11592.

[63] a) A. Vogler and H. Kunkely, *Coord. Chem. Rev.,* **2001**, *219*, 489-507. b) A. Laguna, *Modern Supramolecular Gold Chemistry*, Wiley-VCH press, **2008**. c) V. W. W. Yam and K. K. W. Lo, *Chem. Soc. Rev.,* **1999**, *28*, 323-334.

The similar emission maxima found for all the complexes in the solid state. It can approve that intramolecular interactions play a more important role than intermolecular interaction in luminescent properties. The origin of emissions observed in complexes **1–6** are charge transfer transitions from ligand (L) to metal–metal (MM) centers (LMMCT). Only in compound **6** a broad band with two maxima was observed. It has not been possible to separate two different bands upon changing the excitation energy. So, it could be due to a dual LMMCT and MC characters.

2.1.5. Computational study:

The computational and theoretical studies were done by collaboration with the group of Professor Santiago Alvares. The computational studies approved that not only Au…Au interaction act as driving forces for assemblies in these complexes, but also Au···S and S···S interactions between dimetallic units play important role in the crystal structures.[64] Typically, when the Au···Au distance is around 3Å, there is maximum intermolecular interactions between Au(I) centers. The Au···S interactions are stabilizing at longer distances (with a minimum at around 3.5 Å) and S…S interaction are destabilizing out of this range 3.8–4.0 Å. These theoretical data have a good agreement with crystallographic data.

Comparing the computational studies with analyzing the crystal structures published for $[Au_2L_2]$ units (L=dithiocarboxylates, xanthates, or dithiocarbamates), shows that interplay of the three intermolecular interactions and of their different distance dependence can reflect in the relative orientation of the dinuclear $[Au_2L_2]$. The results show that Au···Au distances larger than 3.5 Å only compatible with coplanar orientations and Au···Au distances shorter than 3.3 Å are only compatible with a rotated structures, *i.e.* with S-Au···Au-S torsion angles larger than 30º. This effect is shown in figure 1.2 that is interdimer Au···Au distances $[Au_2L_2]$ (L=dithiocarboxylates, xanthates, or dithiocarbamates) as a function of the S-Au···Au-S torsion angle.

[64] a) D. D. Heinrich, J. C.Wang and J. P. J. Fackler, *Acta Cryst. C.,* **1990**, *46*, 1444-1446. b) M. A. Mansour, W.B. Connick, R. J. Lachicotte, H. J. Gysling and R. Eisenberg, *J. Am. Chem. Soc*., **1998**, *120*, 1329-1330. c) R. Hesse and P. Jennische, *Acta Chem. Scand.,* **1972**, *26*, 3855-3859. d) S. Y. Ho and E. R. T. Tiekink, *Z. Kristall. New Cryst. Struct*., **2002**, *217*, 589-591.

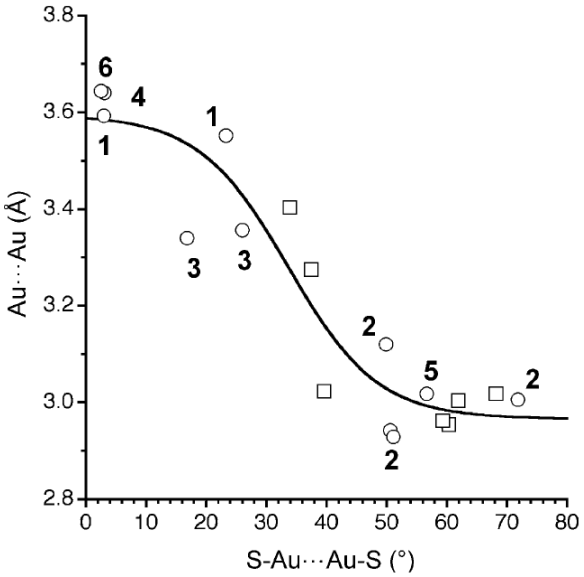

Figure 2.1. Relationship between the intermolecular Au···Au distance and the S-Au···Au-S torsion angle in compounds **1–6** (circles) and in dithiocarbamates (squares).[38]

Relative orientation of the interacting AuS_2 coordination moieties, defined by the Au-Au···Au angles (ω), is another geometrical parameter that can effect on total interaction energy between two $[Au_2L_2]$ units. The data in CSD shows that when ω angle is higher than 30º the Au···Au distances are longer than 3.88 Å. It is suggesting that the perpendicular orientation has the most stabilizing interaction energy. The calculated interaction energy of two dimetallic units with fixed intermolecular Au···Au distance of 3.0 Å via varying Au- Au···Au angles (ω) shows that the interaction energy varies little for deviations of less than 10º from a perpendicular arrangement, but become much more destabilizing at larger angles.

More stable configuration of the $[Au_2L_2]_2$ structure with each ligand (dithiocarboxylato or xanthate), theoretically was optimized and shown in figure 2.2. The structure with stacked $Au_2S_4C_2$ rings, shifted along the Au–Au direction to form Au_4 rhombuses, and also rotated relative to each other, has the most stable geometry. This stable geometry provides a perfect balance between three intermolecular interactions with Au···Au contacts at distances of around 3.0 Å and four Au···S contacts at 3.5 Å or shorter, with avoiding S···S short contacts.

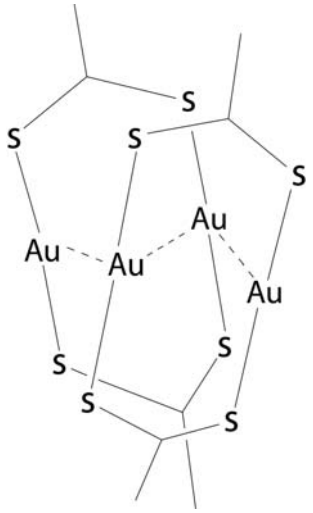

Figure 2.2. The most stable theoretical geometry of the $[Au_2L_2]_2$ structure.

2.2. Platinum(II)···Platinum(II) Interaction:

In this part, the comparison of three analogous dinuclear Pt(II) compounds containing different dithiocarboxylate ligands and their ability for the supramolecular assembly are discussed (scheme 2.5).

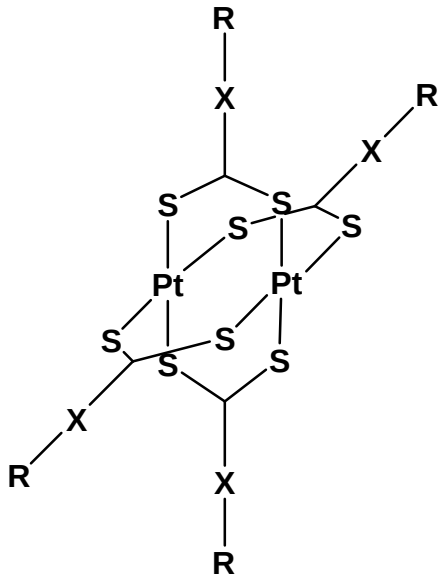

R	X = CH_2
R = $CH_3(CH_2)_2$	7
R = $(CH_3)_2CH_2$	8
R = $CH_3(CH_2)_3$	9

Scheme 2.5. Pt(II) compounds studied in this thesis.

2.2.1. In crystal phase

According to CSD, all compounds with the formula $[Pt_2L_4]$ ($L=RCS_2$) show linear arrangements in their crystal structures that dimetallic units are stacked to each other by intermolecular Pt(II)···Pt(II) distances (3.0–3.4 Å). Only in the case of $[Pt_2(CH_3CS_2)_4]$, the Pt…Pt distance is not short.[22] In fact, this linear arrangement is quasi-one-dimensional chains based on collinear dimetallic units that are directed with short intra- and interdimeric Pt-Pt distances (scheme 2.6).

This structure consists on discrete dimeric entities in which two Pt centers are joined by four μ-dithiocarboxylate kS:kS' ligand bridges and creates windmill-shape arrangement. It is worth to mention that steric hindrance of substituent dithiocarboxylate ligands can influences on the interdimeric Pt···Pt distances. It means by using bulkier substituent, the interdimer Pt···Pt distance become longer. This effect was observed in compound **7-9** that show interdimeric Pt...Pt distances 3.12, 3.26 and 3.14 Å respectively. In compound **8** with bulkier ligand the distances between Pt atoms

in dimetallic unit is longer than the rest. According to previous publication of our group, this effect is reflected on the electrical properties measured on single crystals. In fact, the conductivity measured in single crystals show a significant dependence on the intermolecular metal-to-metal distances. It has been observed that shorter Pt-Pt distances have higher conductivity.[65] In these structures, existence of long distances between Pt…S is out of range that consider even as weak interaction.

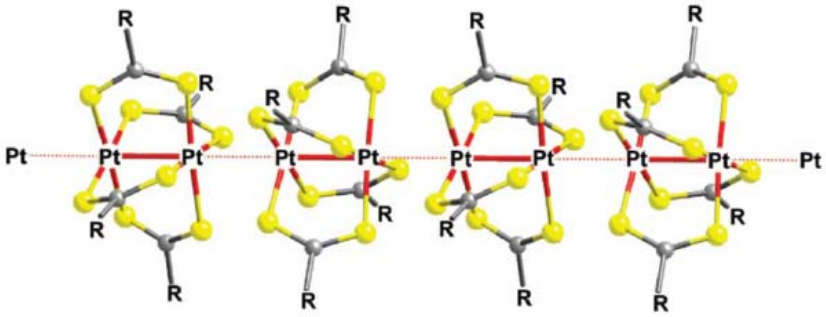

Scheme 2.6. Supramolecular 1-D arrangement observed in crystalline samples of $[Pt_2L_4]$ compounds.

2.2.2. In solution

$[Pt_2L_4]$ compounds show a thermochromic behavior in non-coordinative solvents, which depends on temperature, concentration, solvent and nature of ligand. In general, in UV-vis experiments, by decreasing the temperature, a new band appears in the red/near infrared region and disappears upon heating. This process is reversible and it also depends on concentration. These observations approved reversible aggregation processes in solution. Here, to determine the degree of aggregation, in spite of Au(I) compounds, variable-temperature (VT)-^{1}H NMR measurements did not allowed to distinguish signals from different oligomers. In fact, expected increase of the viscosity of the solvent at lower temperatures and dynamic behavior of this system that results in fast chemical exchange could be the reasons for this observation.

A detailed comparison of UV-vis features in different concentration for compound **9** (compound **9** was chose because of higher solubility) in CH_2Cl_2 revealed that not only by decreasing the concentration, relative intensity decrease, but also narrow peak with a change in the wavelength range be observed. In other hand, for concentrated solutions a wide band in the range of 500–1000 nm appears at low temperature, while a narrower

[65] A. Guijarro, O. Castillo, A. Calzolari, P. J. S. Miguel, C. J. Gomez-Garcia, R. Felice and F. Zamora, *Inorg. Chem.,* **2008**, *47*, 9736-9738.

band is observed for diluted solutions. This observation for concentrated solutions may be due to the overlap of different absorption bands of different species with a various degrees of nuclearity.

To understand about the degree of aggregation in the solution the theoretical simulation with group of Professor Angel Rubio was done. The theoretical simulation of the optical on the species of $[Pt_2(CH_3CS_2)_4]_n$ (n=1– 4) (figure 2.3) revealed that more species with higher degree of aggregation produce in the solution by decreasing the temperature. The calculated most intense absorption peaks for the different $[Pt_2L_4]_n$ species are found at approximately λ= 410, 570, 686 and 770 nm for the series n= 1–4. The theoretical simulation indicate there is a direct relation between the length of the oligomer and the energy of the optical transition associated to Pt···Pt aggregations. In fact, by increasing the oligomer chain the optical transitions shift to the lower energy. By comparing the experimental data with computed spectra, it is clear that at room temperature only monomeric $[Pt_2L_4]$ species are present in the solution, whereas at low temperature the existence of a mixture of $[Pt_2L_4]_n$ species with different nuclearities are observed. Furthermore, the calculations also were shown that the different intermolecular Pt···Pt distance can change the position of the band peak in the visible region.

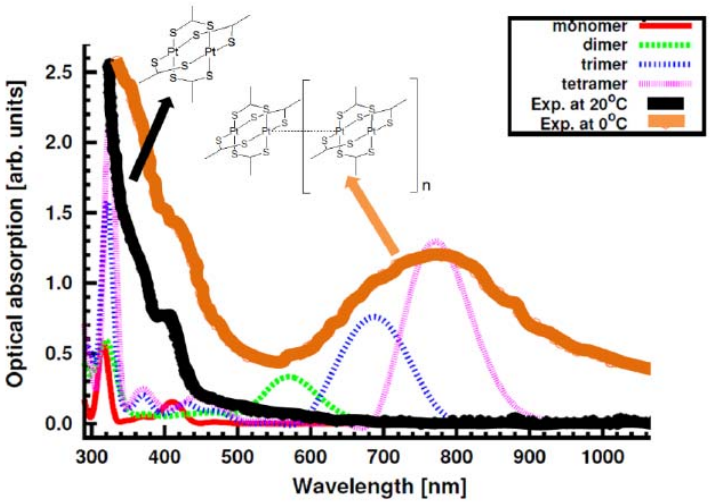

Figure 2.3. Experimental UV-vis spectra of $[Pt_2(CH_3CS_2)_4]$ at 20ºC or 0ºC in CH_2Cl_2, together with the calculated spectra for $[Pt_2(CH_3CS_2)_4]_n$ (n=1-4).

Some parameters such as the nature of ligand L or the solvent can be affected on supramolecular assembly of compounds $[Pt_2L_4]$. Under the same conditions, the steric hindrance of ligands can effect on aggregation of dimetallic units. For instance,

association of shortest chain ligand of dithiocarboxylate class ($R=CH_3CS_2^-$) is easier than other longer linear chains in the solution. In fact, in the solution free motion of linear chains provokes significant hindrance, which increases with increasing the length of the alkyl group. This hindrance is less in crystal phase, because ordered packing minimizes steric repulsive interactions. In the case of bulkier ligand contains a branched R group the approaching of the dimetal units is considerably more difficult than for compounds that contain linear R groups and more steric repulsive interaction is expected in solution than crystal phase.

The effect of the solvent in self-assembly of compounds $[Pt_2L_4]$ in solution has been explored by using different solvents such as CH_2Cl_2, $CHCl_3$, THF and CS_2. It is interesting that in the same conditions, only certain degree of self-assembly was observed in CH_2Cl_2 and (in less extent) $CHCl_3$ while CS_2 and THF hampered the association in solution. This effect can be explained by coordinative ability of THF and CS_2, which can result in weak interactions between the solvent molecules and the platinum centres. The small difference effect, between CH_2Cl_2 and $CHCl_3$ (non-coordinative solvents) on the assembly are probably related to salvation effects.

The idea of self-assembly of $[Pt_2L_4]$ at low temperature, was used by some of our group to create the $[Pt_2(CH_3CS_2)_4]$ nanofibers on an appropriate surface.[66] AFM images of solutions of $[Pt_2(CH_3CS_2)_4]$ in CH_2Cl_2 at 20ºC and at -50ºC were shown in figure 2.4. These images show amorphous material at room temperature and nanofibers at low temperature for this solution.

[66] R. Mas-Balleste, R. Gonzalez-Prieto, A. Guijarro, M. A. Fernandez-Vindel and F. Zamora, *Dalton Trans.,* **2009**, 7341-7343.

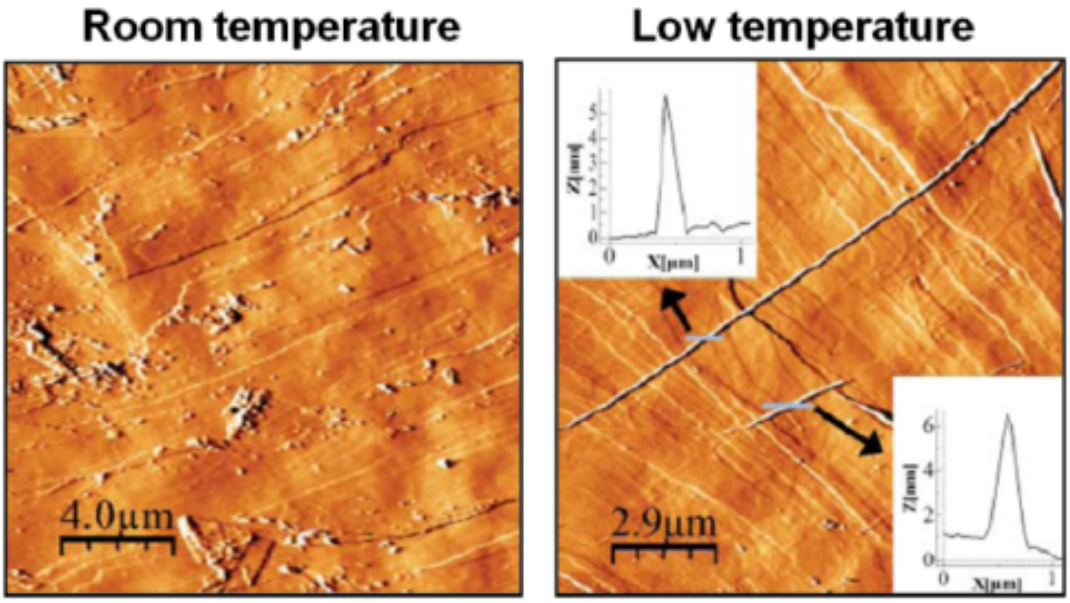

Figure 2.4. AFM images of solutions of $[Pt_2(CH_3CS_2)_4]$ in CH_2Cl_2 at 20ºC and at -50ºC. Only amorphous material on HOPG was observed at room temperature, while the nanofibers were formed at -50 ºC.[66]

2.3. MMX Chains:

In this part, the comparisons of three analogous MMX compounds containing different dithiocarboxylate ligands and their ability for the supramolecular assembly are discussed (scheme 2.7).

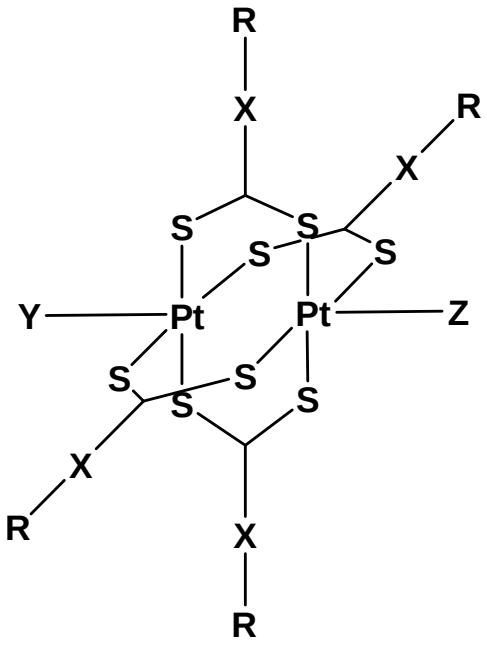

R	(X = CH2), (Y or Z= I)	(X = CH2), (Y and Z=I)
R = $CH_3(CH_2)_2$	10	13
R = $(CH_3)_2CH_2$	11	14
R = $CH_3(CH_2)_3$	12	15

Scheme 2.7. MMX and MMXX compounds studied in this thesis.

2.3.1. In crystal phase

The crystal structure of MMX compounds (M=Pt and X=I) consist of linear 1D chains generated by repetition of the Pt– Pt–I– entities. Each pair of Pt atoms is bridged by four dithiocarboylate ligands, and the pairs are interconnected by means of linear iodine bridges (scheme 2.8). The cohesive forces that hold the MMX chains together are Pt···I interdimer metal–ligand interactions. Although the chains interact weakly by means of van der Waals forces between S…S of alkyl chains, thus leading to a rather 1D anisotropic material. The crystal structures of **10** and **12** have been previously published and described as the MMX chain type like the other compounds of this

family.[67] The attempts to obtain crystals of MMX chains of **11** have been unsuccessful. In the MMX structures, the metals can have different oxidation state (as mentioned in first chapter: AV, CP, CDW and ACP) in the crystal structures according to use different conditions such as different temperatures.

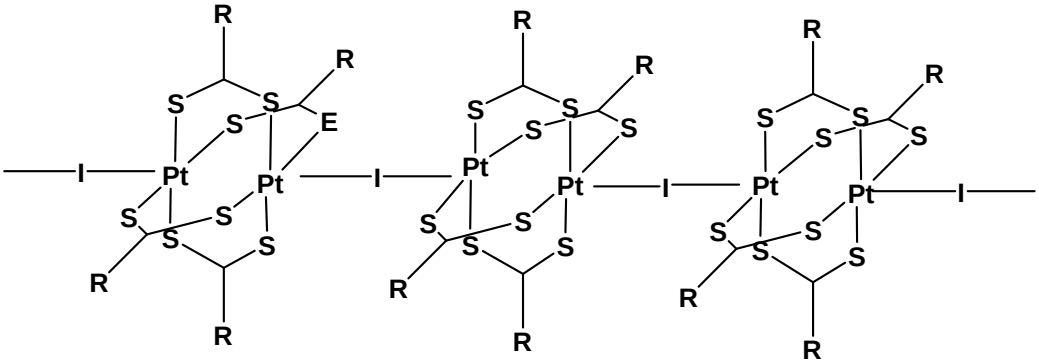

Scheme 2.8. The structure of a MMX as a pseudo-one-dimensional arrangement.

2.3.2. In solution

In spite of the polymeric nature of the structure found in the solid state, MMX compounds show a shocking ability to dissolve in a variety of organic solvents and a surprising tendency to recrystallize, thus recovering the polymeric structure. The significant ability of the $[Pt_2(RCS_2)_4I]_n$ chains to reversibly self assembly from solution is an uncommon behavior for other metal-organic polymers and raises the questions of which species are present in solution, and which factors have an effect on their subsequent reassembly.[68] In order to address these important factors, the spectroscopic features of compounds **10-12** dissolved in different solvent such as CH_2Cl_2, $CHCl_3$, THF and CS_2 were analyzed and compared with those of the $[Pt_2(RCS_2)_4]$ and $[Pt_2(RCS_2)_4I_2]$ precursors.

The spectroscopic data revealed the dissociation of $[Pt_2(RCS_2)_4I]_n$ into an equimolar mixture of $[Pt_2(RCS_2)_4]$ and $[Pt_2(RCS_2)_4I_2]$ in the solution. In fact, ^{1}H NMR spectrum of $[Pt_2(RCS_2)_4I]_n$ in different solvents was shown an overlapping of the spectra of species $[Pt_2(RCS_2)_4]$ and $[Pt_2(RCS_2)_4I_2]$. Additionally, the UV-vis spectrum of a 1 mM solution of $[Pt_2(RCS_2)_4I]_n$ for compound **10-12** can be understood as the

[67] a) A. Guijarro, O. Castillo, L. Welte, A. Calzolari, P. J. S. Miguel, C. J. Gomez-Garcia, D. Olea, R. di Felice, J. Gomez-Herrero and F. Zamora, *Adv. Funct. Mater.,* **2010**, *20*, 1451-1457. b) M. Mitsumi, K. Kitamura, A. Morinaga, Y. Ozawa, M. Kobayashi, K. Toriumi, Y. Iso, H. Kitagawa and T. Mitani, *Angew. Chem. Int. Ed.,* **2002**, *41*, 2767-2771.

[68] D. Gentili, G. Givaja, R. Mas-Balleste, M. R. Azani, A. Shehu, F. Leonardi, E. Mateo-Marti, P. Greco, F. Zamora and M. Cavallini, *Chem. Sci.,* **2012**, *3*, 2047-2051.

result of overlapping the UV-vis spectra separately measured from 0.5 mM CH_2Cl_2 solutions of precursors $[Pt_2(RCS_2)_4]$ and $[Pt_2(RCS_2)_4I_2]$.

According to spectroscopic data, it is clear that by dissolving MMX compounds of **10-12,** two different diamagnetic dimetallic compounds containing two Pt(II) centres (in the case of $[Pt_2(RCS_2)_4]$) or two Pt(III) centres (for $[Pt_2(RCS_2)_4I_2]$) are formed (scheme 2.9). This observation also was confirmed by EPR spectra that no paramagnetic signal was observed for solutions.

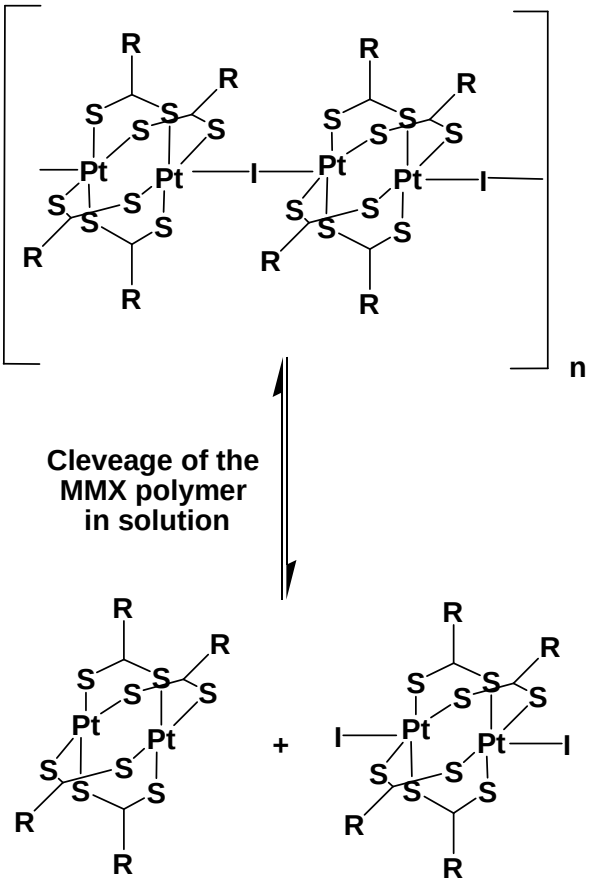

Scheme 2.9. Representation of the dissociation processes in solution of crystals of **10-12**.

In previous part, the (re)assembly ability of the $[Pt_2(RCS_2)_4]$ precursor to associate via reversible weak $d^8 \bullet\bullet\bullet d^8$ interactions in solution, were mentioned. In fact, UV-vis spectrums of compound **7-9** at low temperature indicated the assemblies of dimetallic species (MM…MM) with present new bands at 600-700 nm. So, similar behavior was observed for solutions of $[Pt_2(RCS_2)_4I]_n$. Additionally, a new band at 820 nm appeared in the spectrum of $[Pt_2(RCS_2)_4I]_n$ in CH_2Cl_2 at low temperature. According to this point that this new feature was not observed for the solutions of pure precursors $[Pt_2(RCS_2)_4]$

or $[Pt_2(RCS_2)_4I_2]$ at low temperature, this new band should be related to the assembly of $[Pt_2(RCS_2)_4]$ and $[Pt_2(RCS_2)_4I_2]$ (MM…XMMX) to generate $[Pt_2(RCS_2)_4I]_n$ chains (scheme 2.10).

The ratio between these assemblies MM…MM and MM…XMMX in compound **10** was affected by the overall concentration of MMX, being the MM…MM assembly less favored at lower concentrations. These results can be useful to understand the process of MMX polymer formation from solution.

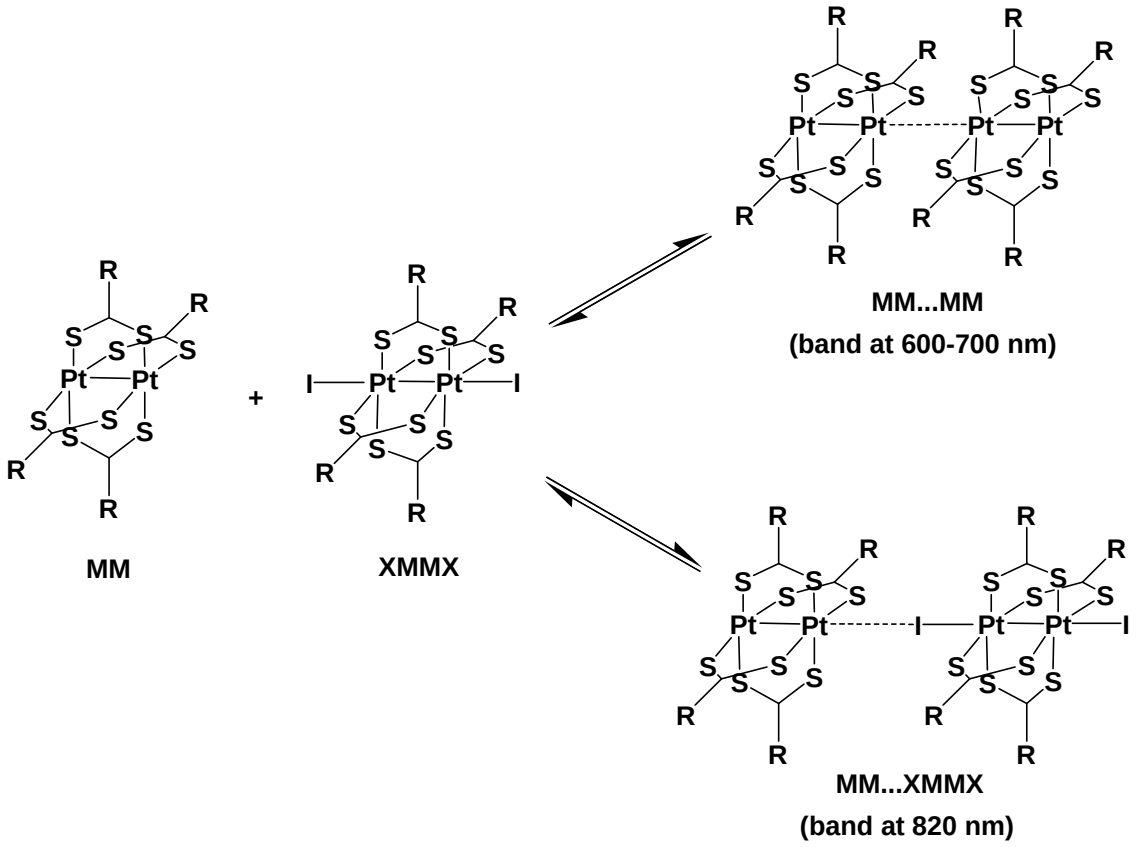

Scheme 2.10. Representation of reassembly processes in solution for solutions of $[Pt_2(RCS_2)_4I]_n$.

2.3.2.1. Effect of ligand on (re)assembly in solution

Effect of ligand can be primarily discussed regarding the results obtained by UV-vis at low temperature in CH_2Cl_2 for compound **10-12** (figure 2.5). Temperature dependence of the molar absorptivity of signals at around 700 nm and 820 nm that appears at low temperatures in 1 mM solutions of **10-12** was shown in figure 2.6. Behavior of compounds **10-12** can rationalize in terms of effective bulkiness in solution of dithiocarboxylate ligand. When ligand contains a ramified R group (compound **11**)

the approaching of bimetallic units especially in 700 nm region (MM…MM) that is related to MM aggregations is definitively more difficult than compounds **10** and **12** which contain linear R groups. While, the bridging iodide anion in MM···XMMX separates the MM units in such a way that steric repulsion is much less critical than in MM···MM supramolecules. Between **10** and **12** supramolecular assemblies are favored for **10**, because has shorter chain.

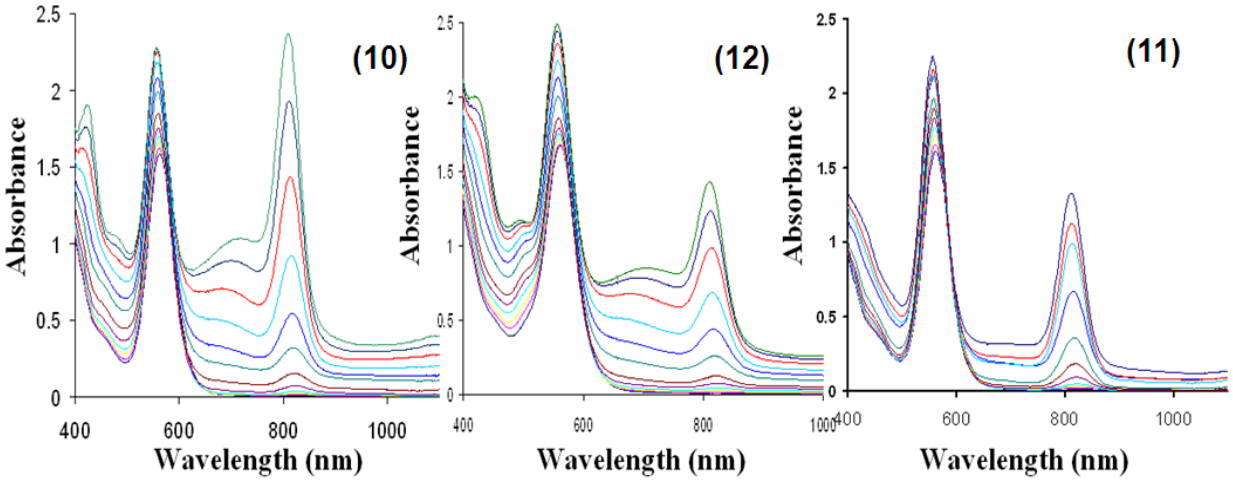

Figure 2.5. UV-vis spectrum of a 1 mM solution of **10**, **12** in CH_2Cl_2 (from 20 ºC to -90) and **11** (from 20 ºC to -80).

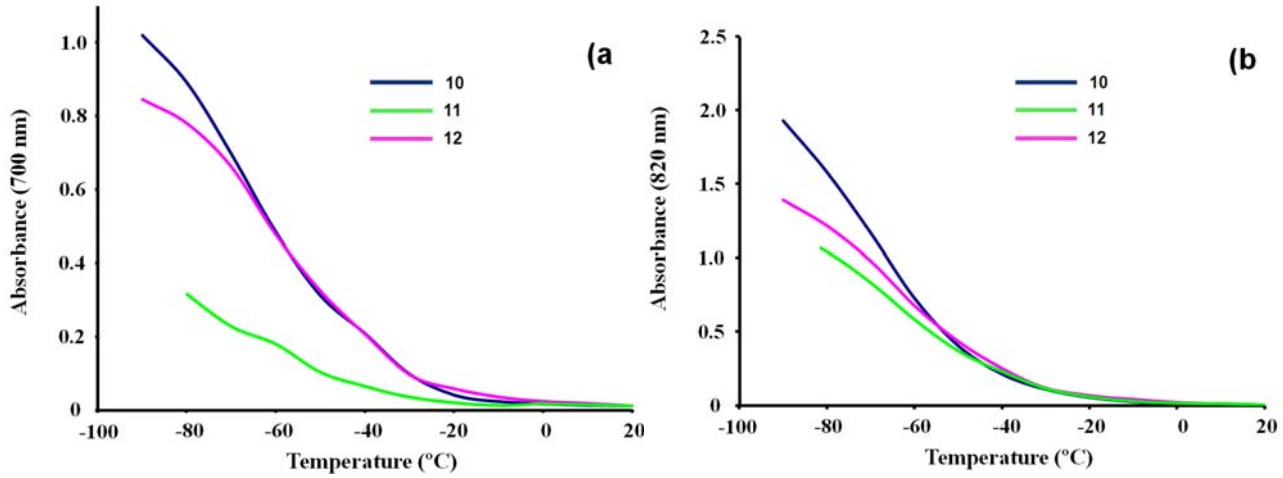

Figure 2.6. The temperature dependence of the molar absorptivity of signals at 700 nm (a) and 820 nm (b) that appears at low temperatures in 1 mM solutions of **10-12** in CH_2Cl_2.

2.3.2.2. Effect of solvent on (re)assembly in solution

The effect of solvent in self-assembly of compounds **10-12** in solution has been examined comparing the behaviour of solutions using as a solvent CH_2Cl_2, $CHCl_3$, THF and CS_2. However, to compare the inherent ability of compound **10-12** to associate in solution in different solvents, unique conditions (the same concentration) have to be used. They showed comparable trends. Thus, at the same conditions, while certain degree of self-assembly in CH_2Cl_2 and $CHCl_3$ was observed, CS_2 and THF hampered the association in solution. This effect can be easily justified considering the known coordinative ability of such solvents, which can result in weak metal-ligand interactions between the solvent molecules and the Pt(II) centres, which make more difficult self-assembly of MM...MM in the 700 nm region through Pt···Pt interactions (as observed in previous part) and assembly of MM...XMMX around 820 nm. Notwithstanding this, in THF as a less coordinating solvent in comparison with CS_2, when the temperature is low enough; new features in the lower energies region appear, indicating certain degree of self-assembly.

Pay attention to previous part (aggregation of MM…MM units), the difference between coordinative and non-coordinative solvents was expected. In the case of non-coordinative solvents a surprising difference was observed between CH_2Cl_2 and $CHCl_3$. In fact in the case of CH_2Cl_2 the assembly is favored toward MM···MM interactions, in spite of the CHCl3 that direct the assemblies more to MM···XMMX aggregation. In a previous part, the association of MM pure precursors was shown less favorable in $CHCl_3$ than CH_2Cl_2. This effect was observed again in this study for the MM···MM association, but not for the MM···XMMX assembly. The reasons may be due to more efficient way of $CHCl_3$ to solvate and block the MM units, which shifts the equilibrium toward the XMMX···MM assembly.

2.3.2.3. Effect of ligth on reassembly in solution

In UV-vis experiments of THF, an unexpected observation took place. Continuous irradiation of MMX solutions enhanced their ability to generate supramolecular assemblies in solution. This reversible photo induced assembly process is probably due to the photo-dissociation of the THF···MM interaction (figure 2.7). Accordingly, the pure MM precursor shows some degree of photo induced association, but to a much

lower extent. This proposed photo-dissociation mechanism would lead to a slowly release of "free" MM species, which in the presence of an excess of XMMX would preferentially form the complex MM···XMMX.

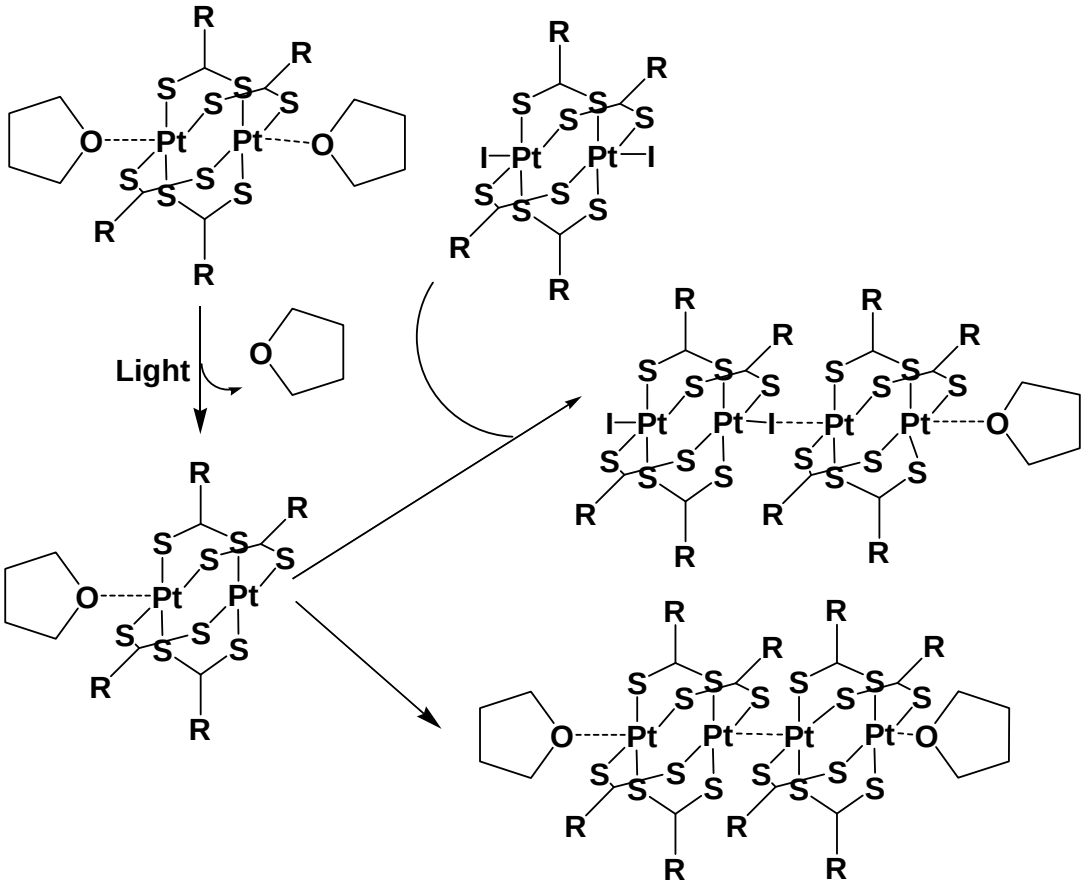

Figure 2.7. Representation of the photo-dissociation of compound **10-12** in THF.

2.3.3. Form solution to surface:

The possibility of producing MMX nanostructures on surface in collaboration with the group of Professor Julio Gomez-Herrero was explored. They investigated the effect of temperature on the nanostructures of $[Pt_2(CH_3CS_2)_4I]_n$, which formed based on sublimation of crystalline samples, after deposition of the solution of MMX polymer. The deposition of solution on mica at 0 ºC created single/few MMX chains with 0.5-2.5 nm in height and several microns in length. By more decreasing the temperature, the formation of long chains was restricted. This observation may be due to the present of oligomeric species that already formed at lower temperature in the solution. In fact, it can limit the diffusion of the building blocks at the solution/surface interface and so can restrict the formation of long chains at lower temperatures. In overall, these results, for

the first time, shows the isolation of single chain of $[Pt_2(CH_3CS_2)_4I]_n$ on mica, which is an insulator substrate suitable for further electrical characterization.

2.3.3.1. Formation of patterned conductive nanostructures by Nanolithography

The producing of MMX nanostructures on surface by Nanolithography method in collaboration with the group of Professor Massimiliano Cavallini was investigated. According to the excellent reversibility in the depolymerization/repolymerization process of MMX, the micromolding in capillaries (MIMIC)[69] and lithographically controlled wetting (LCW)[70] for compound **10** were used to fabricate ordered patterns of parallel sub-micrometric wires (μ-wires) (figure 2.8).

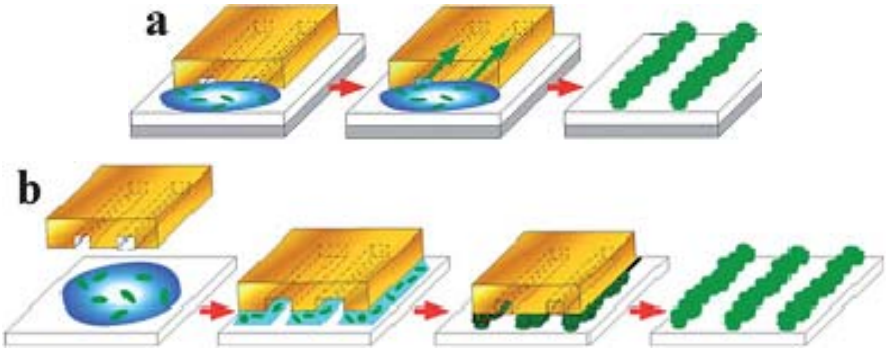

Figure 2.8. A schematic representation of (a) micromolding in capillaries (MIMIC) and (b) lithographically controlled wetting (LCW).

Optical micrograph of μ-wires and parallel μ-wires (width 900 nm, height 124 nm, periodicity 1.5 μm) on pre-fabricated gold electrodes that were printed by MIMIC was shown in Figure 2.9. Also Morphological characterizations were shown in Figures 2.10 and 2.11.

[69] E. Kim, Y. N. Xia and G. M. Whitesides, *Nature*., **1995**, *376*, 581-584.

[70] M. Cavallini and F. Biscarini, *Nano Lett.,* **2003**, *3*, 1269-1271.

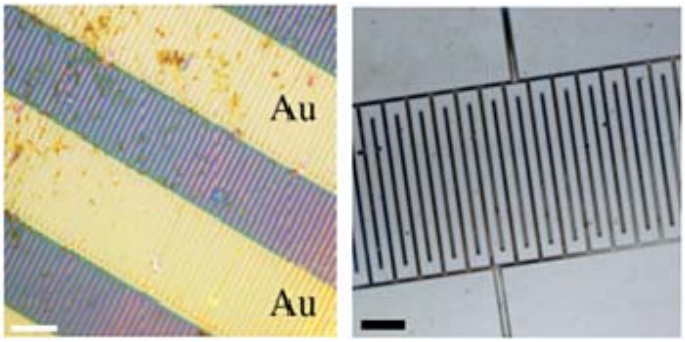

Figure 2.9. Microfabrication by unconventional wet lithography. An optical image (scale bar = 10 μm) of parallel μ-wires printed onto Au surface (right). An optical micrograph (scale bar = 100 μm) of interdigitated comb-like electrodes of $[Pt_2(n\text{BuCS}_2)_4I]_n$ printed on silicon oxide by LCW (left).

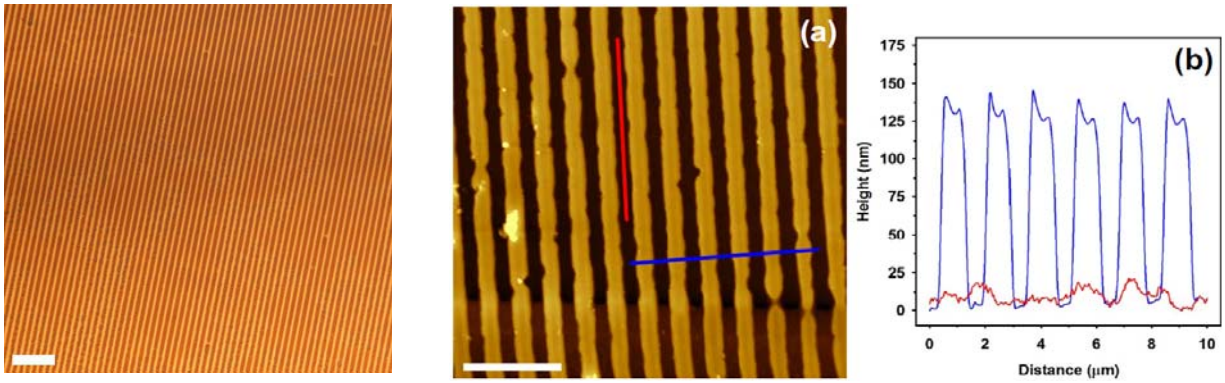

Figure 2.10. a) AFM morphology (scale bar = 5 μm), and b) AFM profiles of $[Pt_2(n\text{BuCS}_2)_4I]_n$ wires patterned on gold electrodes (LCW, parallel lines, 2 mg/mL in CH_2Cl_2).

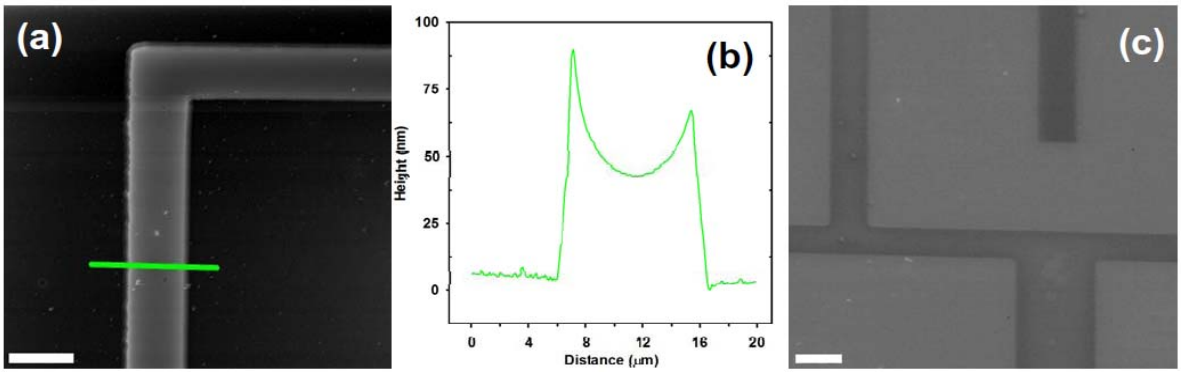

Figure 2.11. a) AFM image (scale bar = 10 μm), b) AFM profile, and c) SEM (scale bar = 10 μm) of $[Pt_2(n\text{BuCS}_2)_4I]_n$ pattern on silicon oxide (LCW, interdigitated comb-like, 2 mg/mL in CH_2Cl_2).

The electrical characterization by obtaining the I–V curve was revealed a near Ohmic behaviour within the range of +50 to -50 V (figure 2.12).

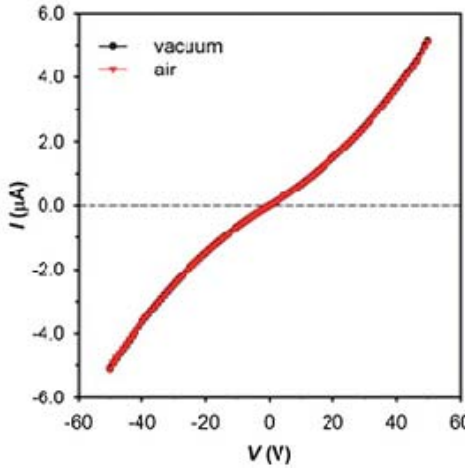

Figure 2.12. Current vs. voltage characteristics of the wires were formed by unconventional wet lithography in the air and vacuum.

It is interesting and important that the electrical behaviour of the wires, were not changed by passing time (for 6 months) in air at room temperature and in high humidity. In fact, by using different environmental conditions, no sign of hysteresis or any other electrical deterioration were observed. This is a very important issue for electronic applications. The high current density of ca. 5 A cm^{-2} at 50 V was estimated for these wires by assuming that the current spreads across the entire section of the wires. These data for sub-micrometric wires is comparable to and, in some cases, even better than corresponding metallic wires.[71]

2.3.4. Theoretical and computational studies

The computational and theoretical studies were done by collaboration with the group of Professor Angel Rubio. They computed binding energies of the association processes of MMX structures by using DFT calculations. They considered $[Pt_2(CH_3CS_2)_4I]_n$ as the simplest representative compound of the family $[Pt_2(RCS_2)_4I]_n$ chains to minimize the computational costs. Different supramolecules were considered for this study: dimer (XMMX-MM), trimers (XMMX-MM-XMMX and MM-XMMX-MM) and tetramer complex (XMMX-MM-XMMX-MM). The calculated data was shown that the required energy to dissociate one dimetallic unit from dimer, trimer or tetramer in asymmetric cleavage is less than symmetric dissociation in all cases. This

[71] a) D. A. Serban, P. Greco, S. Melinte, A. Vlad, C. A. Dutu, S. Zacchini, M. C. Iapalucci, F. Biscarini and M. Cavallini, *Small*., **2009**, *5*, 1117-1122. b) P. Greco, M. Cavallini, P. Stoliar, S. D. Quiroga, S. Dutta, S. Zachini, M. C. Lapalucci, V. Morandi, S. Milita, P. G. Merli and F. Biscarini, *J. Am. Chem. Soc.,* **2008**, *130*, 1177-1182.

energy is of the order of a hydrogen bond. In fact this finding proved the absence of EPR signals in our experimental data that was observed for MMX solutions.

In the association process, they approved that the driving force for the Pt-Pt···I-Pt-Pt-I interaction arises from the interaction between the occupied $5p_z$ atomic orbitals (donor) of the iodine atom with the empty $6p_z$ orbitals (acceptor) of the platinum atom in MM. Such a donor–acceptor interaction is classified in the range of supramolecular interactions because is much weaker than the regular metal–ligand bonding. In overall, the computational data claim to consider MMX compounds as molecular aggregates rather than coordination polymers. Such an interpretation is fully consistent with the observed experimental behavior.

To validate experimental UV-vis spectroscopic data, they calculated the spectra of $[Pt_2(RCS_2)_4I]_n$ oligomers by using time-dependent density functional theory (TDDFT). Optical spectra from TDDFT calculations were shown in figure 2.13. It is clear that spectra calculated for the dimer and tetramer are significantly different from the experimental observations. So, the TDDFT calculations suggest the formation of trimers in solution.

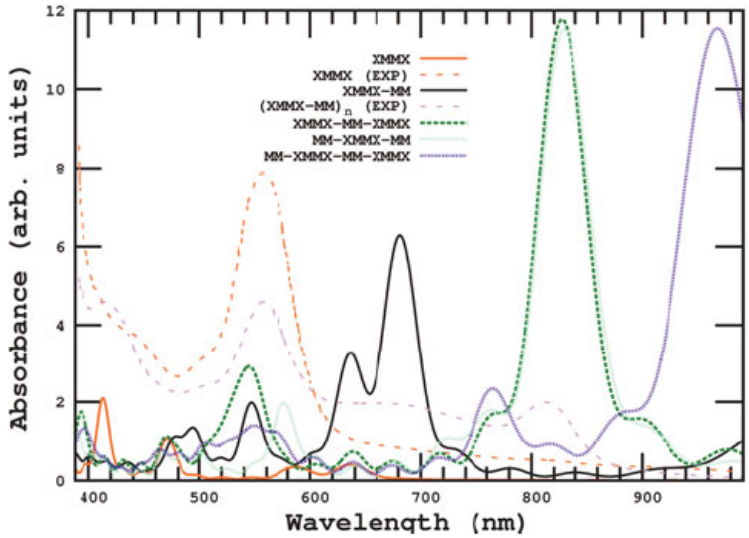

Figure 2.13. Calculated real-time TDDFT spectra for XMMX and its different oligomers with MM in gas phase at the PBE level using the OCTOPUS code. The computed spectra are normalized by the number of monomers. Only the polarization along the molecular chain was considered. For comparison the experimental spectra measured in CH_2Cl_2 solution at -60 ºC for compound **10** (EXP, in legend) and its related XMMX monomer (red dashes) are also shown.

Chapter 3

III. Articles

Article 1

Title: The Structural Diversity Triggered by Intermolecular Interactions between $Au^{I}S_2$ Groups: Aurophilia and Beyond

Autors: Mohammad-Reza Azani, Oscar Castillo, M. Luz Gallego, Teodor Parella, Gabriel Aullón, Olga Crespo, Antonio Laguna, Santiago Alvarez*, Rubén Mas-Ballesté* and Félix Zamora*

Journal: Chemistry - A European Journal

Year: 2012

Volume / Pages: 18 (32) / 9965-9976.

CHEMISTRY
A EUROPEAN JOURNAL

FULL PAPER

DOI: 10.1002/chem.201200999

The Structural Diversity Triggered by Intermolecular Interactions between Au^IS_2 Groups: Aurophilia and Beyond

Mohammad-Reza Azani,[a] Oscar Castillo,[b] M. Luz Gallego,[a] Teodor Parella,[c] Gabriel Aullón,[d] Olga Crespo,[e] Antonio Laguna,[e] Santiago Alvarez,*[d] Rubén Mas-Ballesté,*[a] and Félix Zamora*[a]

Abstract: The present study is aimed at elucidating the factors that direct the assembly of a specific family of Au^I species. The assembly of Au^I centers and dithiocarboxylato or xanthato ligands results in a surprising structural diversity observed by single-crystal X-ray diffraction. However, in solution, just evidences for discrete bimetallic $[Au_2L_2]$ species have been observed. Interestingly, when dithiocarboxylato ligands have been used, a reversible supramolecular assembly has been observed forming the supramolecules of formulae $[Au_2L_2]_2$ and $[Au_2L_2]_3$. Initial studies on luminescent properties have been carried out at variable temperature. All the compounds show red emissions in the solid state at very similar energies, suggesting that the intramolecular interactions play a more relevant role in the luminescent properties than the intermolecular ones. The computational studies indicate that not only Au···Au interactions, but also Au···S and S···S ones play a role in the structure and energetic of the supramolecular species, as well as for the choice between supramolecular association or intramolecular oligomerization.

Keywords: aurophlicity · density functional calculations · luminescence · polymers · supramolecular chemistry

Introduction

The systematic use of weak interactions to assemble complex structures is the ultimate challenge in supramolecular chemistry.[1] Usually, dipolar/electrostatic interactions, such as hydrogen bonding, are the main tool to build suprastructures. Despite the wide variety of highly interesting structures obtained through this strategy, it seems difficult that such assemblies could confer special electrical or optical properties. However, there is another kind of weak interactions that, in principle, could have a significant impact on the properties of the self-assembled suprastructures. Specifically, recent reports suggest that weak metal–metal interactions can be used to build up complex structures.[2] Such attractive interactions are mainly observed between Pt^{II}, Ag^I, or Au^I centers. In particular, the most common of such interactions is the enhanced tendency of Au^I centers to establish weak $Au^I\cdots Au^I$ bonding, known as aurophilia.[3] This phenomenon is a consequence of a combination of dispersion forces and the mixing of filled 5d-based molecular orbitals and empty molecular orbitals of appropriate symmetry derived from the 6s and 6p orbitals.[4] As a consequence of this supramolecular interaction, and taking advantage of the structural versatility of Au^I centers, a variety of structures with interesting optical and/or electrical properties have been reported.[5,6]

Thus, getting deeper insights on the concept that could allow for a control of the chemical and physical characteristics of polymetallic gold(I) compounds is still an important challenge in inorganic chemistry. Some outstanding technological implications of such developments could be the self-assembly of complex molecular systems in the search for electronic devices of nanometric dimensions. The study of the influence of the nature of ligands on the nuclearity and

[a] M.-R. Azani, Dr. M. L. Gallego, Dr. R. Mas-Ballesté, Dr. F. Zamora
Departamento de Química Inorgánica
Universidad Autónoma de Madrid
28049 Madrid (Spain)
E-mail: felix.zamora@uam.es
Homepage: http://www.nanomater.es

[b] Dr. O. Castillo
Departamento de Química Inorgánica
Facultad de Ciencia y Tecnología
Universidad del País Vasco, Apartado 644
48080 Bilbao (Spain)

[c] Dr. T. Parella
Servei de Ressonància Magnética Nuclear
Universitat Autónoma de Barcelona
08193 Bellaterra (Spain)

[d] Dr. G. Aullón, Prof. Dr. S. Alvarez
Departament de Química Inorgànica and
Institut de Química Teòrica i Computacional
Universitat de Barcelona, Martí i Franquès 1-11
08028 Barcelona (Spain)
E-mail: santiago.alvarez@qi.ub.es

[e] Dr. O. Crespo, Prof. Dr. A. Laguna
Departamento de Química Inorgánica
Instituto de Síntesis Química y Catálisis Homogénea (ISQCH).
Universidad de Zaragoza-CSIC
Pedro Cerbuna 12, 50009, Zaragoza, (Spain)

Supporting information for this article is available on the WWW under http://dx.doi.org/10.1002/chem.201200999.

CHEMISTRY
A EUROPEAN JOURNAL

ChemPubSoc
Europe

electronic structure of gold(I) compounds is a valuable contribution towards this goal.

Considering the enhanced affinity of gold(I) centers toward sulfur atoms, ligands containing the $-CS_2^-$ donor groups (dithiocarbamates, xanthates, and dithiocarboxylates) offer excellent perspectives to obtain a variety of new gold-containing complexes with unprecedented structural, chemical, and physical features.

In this work, we address the comparison of the electronic structure and ability for the supramolecular assembly of a series of analogous dinuclear Au^I compounds containing dithiocarboxylate or xanthate ligands (Scheme 1). Gold chemistry with this kind of ligands is scarcely represented. Just three structures of homoleptic compounds containing dithiocarboxylato ligands and Au^I are included in the Cambridge structural database (CSD): 1) the tetranuclear gold(I) dithioacetate compound $[Au(MeCS_2)]_4$, which has a rhombic Au_4 array,[7] 2) the hexametallic compound of the formula $[Au_6(o\text{-}CH_3C_6H_4CS_2)_6]$, in which the six gold atoms of the Au_6 cluster are coplanar forming an equilateral triangle with three Au atoms in the vertices and three metal atoms at the center of the edges,[8] and 3) in our recent effort to explore this chemistry, we found that by using the ligand $^-S_2CCH_2CH(CH_3)_2$ (L) two different entities can be formed in the crystalline phase: the dimetallic complex $[Au_2L_2]$ and the coordination polymer $[AuL]_n$.[9]

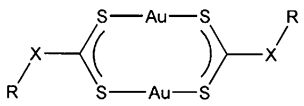

	X = CH_2	X = O
R = $CH_3(CH_2)_2$	1	4
R = $(CH_3)_2CH_2$	2	5
R = $CH_3(CH_2)_3$	3	6

Scheme 1. Compounds studied in this work.

Similarly, gold xanthate complexes are very scarce, however, they have shown interesting structures and optical properties. In particular, the following complexes containing xanthate ligands have been reported: $[(PPh_3)_2AuS_2COEt]$,[10] $[(CEP)_2AuS_2COR]$ (CEP = tris(cyanoethyl)phosphine; R = Me, Et, Bu),[10] $[(CH_3)_2AuS_2CO\text{-}2,6\text{-}C_6H_3(CH_3)_2]$,[11] and the heterobridged ylide complex $[Au_2(\mu\text{-}(CH_2)PPh_2)(\mu\text{-}S_2COR)]$ (R = Me, Et, *i*Pr).[12] The only homoleptic xanthate Au^I compound structurally characterized was reported a few years ago by Fackler et al.[13] and consists of a dimetallic structure of the formula $[Au_2(n\text{Bu-xanthate})_2]$.

The limited examples presented above suggest that these types of ligands would provide a versatile framework, in which a diversity of coordination geometry and nuclearity can be achieved. Therefore, the first goal of this work is to explore the different structural possibilities that $^-S_2C\text{-}X\text{-}R$ (X = CH_2, O; R = $(CH_2)_nCH_3$ (n = 2, 3), $CH(CH_3)_2$) could offer as ligand to coordinate Au^I centers. Taking a step further, we analyzed the electronic structure of gold compounds with such ligands and its consequences on the ability of such compounds to perform molecular recognition through Au···Au aurophilic interactions.

Overall, the results presented in this work provide some valuable insights on how aurophilia, and other weak interactions, can direct the assembly of supramolecules or even coordination polymers. This is a new step towards the design of complex architectures based on the 1D structure by assembly of metal–organic building blocks.

Results and Discussion

Synthesis: A schematic representation of the compounds prepared is provided in Scheme 1. In this work we overcome an important drawback that was found by using the synthetic procedure described in our previous efforts on isolation of Au^I–dithiocarboxylato compounds.[9] In our previous report, by using an Au^I starting material, such as $K[Au(CN)_2]$, to react with dithiocarboxylic acid in a 1:1 ratio, high yields were not always achieved with the range of ligands used in this work. Thus, we felt the need to explore alternative synthetic strategies to obtain the corresponding Au^I–dithiocarboxylato complexes. We increased the yields up to 70% (based on gold) by reacting three equivalents of the deprotonated dithiocarboxylic acid with one equivalent of the Au^{III} starting material $Na[AuCl_4]$. The excess of two equivalents of ligand was consumed as reducing agent to obtain Au^I centers and, according to the reaction shown in Scheme 2, supposedly the disulfide product (which has never been isolated). Once the Au^{III} is reduced the remaining equivalent of the dithiocarboxylate coordinates the Au^I center rapidly and efficiently. In polar media such as the reaction mixture (for more details see the Experimental Section) the $[Au_2L_2]_n$ species precipitate immediately, pushing forward the reaction towards a nearly complete conversion. Interestingly, recrystallization of compounds **1**–**3** in CS_2 obtained by this procedure resulted in identical structures than that obtained by our previously reported "low yield" method based on the reaction of $K[Au(CN)_2]$ and dithiocarboxylic acid under neutral conditions in ethanol.

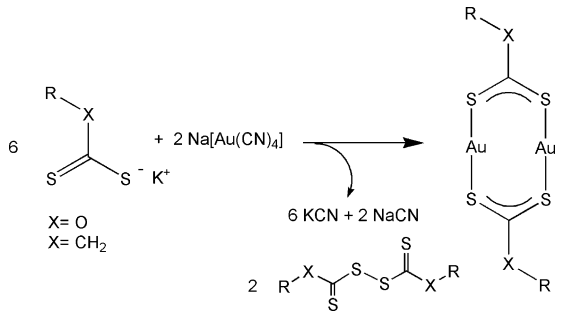

Scheme 2. Synthetic route followed in this work to obtain compounds of the formula $[Au_2L_2]$.

The same synthetic procedure was applied to the obtention of Au^I–xanthate compounds with excellent results. In this case, addition of a base was not required because the

xanthate ligands were used in their commercial form as potassium salts. Potassium xanthate salts are soluble in H_2O and yields of over 70% of $[Au_2L_2]$ were obtained by reacting such solutions containing three equivalents of the deprotonated ligand and one equivalent of $Na[AuCl_4]$ as a starting material.

Solid-state characterization: Compounds [Au_2(*n*Bu-dithiocarboxylato)$_2$] (**1**) and [Au_2(*n*-pentyl-dithiocarboxylato)$_2$] (**3**), were crystallized following the same procedure but different structures were found (see the Experimental Section for some additional details). The crystal structure of compound **1** is comprised of arrowtip-shaped hexanuclear clusters in which bridging dithiocarboxylato ligands hold together the six gold(I) centers in an alternating way (Figure 1 a). Considering only classical covalent bonds (i.e., disregarding Au···Au interactions), this molecule can be described as a remarkable 24-member $Au_6S_{12}C_6$ ring. There are two crystallographically independent arrow-shaped hexameric rings; both of them are planar but tilted 24.2° relative to each other. The dithiocarboxylate ligands, that present their usual μ-κS:κS′ bridging mode, are nearly perpendicular to the Au_6 mean plane. On the other hand, although the dicarboxylato-bridged Au–Au distances show little dispersion (2.965–3.033 Å), the Au-Au-Au angles present values ranging from 67 to 145°. The great dispersion of the Au-Au-Au angles could be due to the presence of significant intramolecular Au···Au (3.297–3.380 Å). Such interactions cannot be understood as the direct consequence of the dithiocarboxylato coordination requirements (Table S1 in the Supporting Information). Additionally, there is structural evidence of intermolecular S···S (3.269–3.598 Å) and Au···S (3.428-3.579 Å) contacts that might play some role in the fine-tuning of the packing of neighboring molecules in the crystal. Interestingly, the intermolecular distances between the gold centers are long (3.546–3.879 Å), ruling out intermolecular aurophilic interactions.

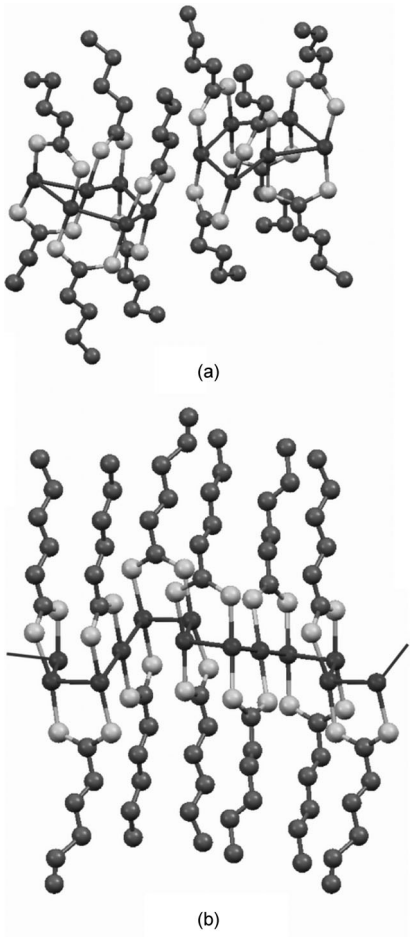

Figure 1. Coordination entities found in compounds **1** (a) and **3** (b).

The presence of an additional methylene group in the dithiocarboxylato ligand has a dramatic effect on the structure found by single-crystal X-ray diffraction. Thus, the structure of [Au_2(*n*-pentyl-dithiocarboxylate)$_2$] (**3**) consists on a polymeric 1D chain. The dithiocarboxylato groups act as bridging ligands between the gold centers in the 1D chain (Figure 1 b). The short distances between adjacent centers (Au···Au distances of 2.962–3.028 Å) within the polymeric chain are indicative of aurophilicity. The sinuous non-linear pattern of the gold centers within the chain, that present Au···Au···Au angles that range from 68 to 180°, could be attributed to weaker additional intrachain Au···Au (3.344–3.356 Å) and Au···S (3.48–3.52 Å) interactions between fourth neighbors with the pattern as shown in structure **7** (Scheme 3). At the same time, kinking of the chain avoids S···S contacts shorter than 3.6 Å except between nearest neighbors. Also the S-Au-Au-S dihedral angle within the chelate ring of the dithiocaboxylato ligands, ranging from 0 to 19°, can be explained by the tilting of the S-Au-S units in order to favor short Au···S contacts between fourth neighbors. Neighboring chains are also connected by a host of Au···S and S···S interactions, leading to a 2D assembly of the polymeric chain in which the aliphatic chains of the dithiocarboxylato ligand spread outwards of the supramolecular sheets giving rise to a lamellar structure assembled along the crystallographic *c* direction by means of the van der Waals interactions established between the aliphatic residues.

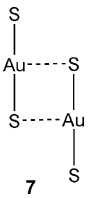

7

Scheme 3. Representation of the long range interactions found for compound **3** (named as **7**).

The structural data concerning compound **2**, [Au_2(isobutyldithiocarboxylato)$_2$], have been previously reported by us,[9] indicating the existence in the crystalline phase of two polymorphic forms formed by discrete $[Au_2L_2]$ bimetallic units and polymeric $[AuL]_n$ chains, respectively.

The structures of [Au_2(*n*-propyl-xanthate)$_2$] (**4**) and [Au_2(isopropyl-xanthate)$_2$] (**5**), are composed by discrete dimeric entities in which the metal centers are joined by double μ-κS:κS′ xanthate bridges leading to essentially planar eight-member $Au_2S_4C_2$ rings (Figure 2). This structural feature is in contrast with the higher aggregation found

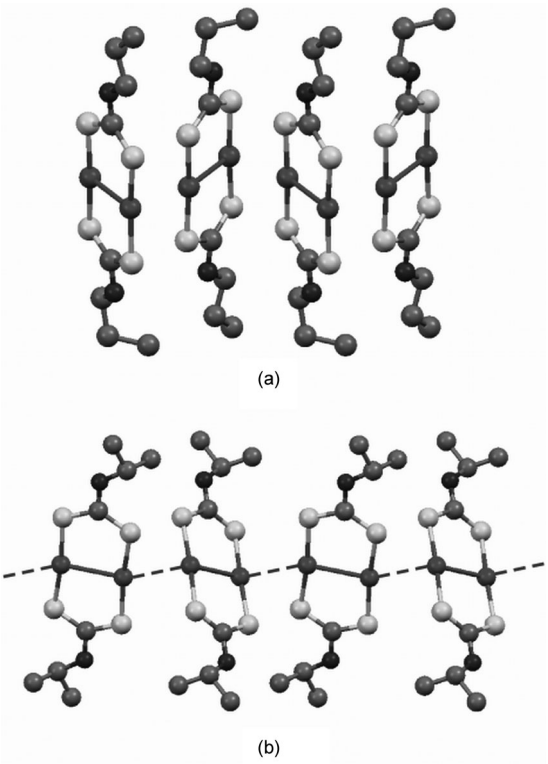

Figure 2. View of the structures of compounds **4** (a) and **5** (b). Dashed lines indicate intermolecular Au···Au contacts.

for compounds **1** and **2**. The average values for the Au–S bond lengths do not show significant deviations between the two structures (2.30 and 2.28 Å for compounds **4** and **5**, respectively). Also, the S-Au-S angle is very similar for the two compounds (173.1 and 172.0° for compounds **3** and **5**, respectively). The short intramolecular Au···Au distances in the two complexes (2.841 and 2.807 Å for compounds **4** and **5**, respectively) are indicative of a strong intramolecular aurophilic interaction between the gold(I) centers (Table S2 in the Supporting Information). These values are significantly shorter that those found in compounds **1** and **2**, in which a single μ-κS:κS′ dithiocarboxylato bridge is shared by each pair of neighboring metal centers.

The intermolecular interactions are the most significant difference between the crystal structures of compounds **4** and **5**. In compound **4**, the shortest intermolecular Au···Au distance (3.636 Å) suggests that the supramolecular assembly of the dimeric entities takes place essentially through Au···S (3.584 Å) contacts with four neighbors, achieved by a shift of neighboring molecules perpendicular to the Au–Au unit, in the way shown in structure **7**. This is not the case for compound **5**, for which relatively close intermolecular contacts between adjacent gold atoms (3.018 Å) give rise to an assembly of the $[Au_2(\text{isopropyl-xanthate})_2]$ units in a kinked chain that shows also S···S (3.575 Å) contacts. Interchain interactions in compound **5** occur also through Au···S contacts at 3.587 Å between dimers shifted as shown in structure **7**. The structural characterization of $[Au_2(n\text{-butyl-xanthate})_2]$ (**6**), that is also comprised of discrete dimeric entities, has been reported previously by Fackler et al.[13] In that structure, dimers are also shifted as to match Au···S distances of about 3.62 Å.

The overall crystal structure of the reported compounds consists always of a central sheet, in which the gold and sulfur atoms are located, surrounded by the aliphatic chains of the ligands spreading outwards and giving rise to a lamellar structure assembled by means of van der Waals interactions among the aliphatic residues.

In order to get deeper insight into the factors that direct the structure of the gold dithiocarboxylato complexes and gold complexes with analogues ligands, a search in the CSD was performed (Figure 3). It appears that there is a higher tendency of the dithiocarboxylato ligands to provide single-

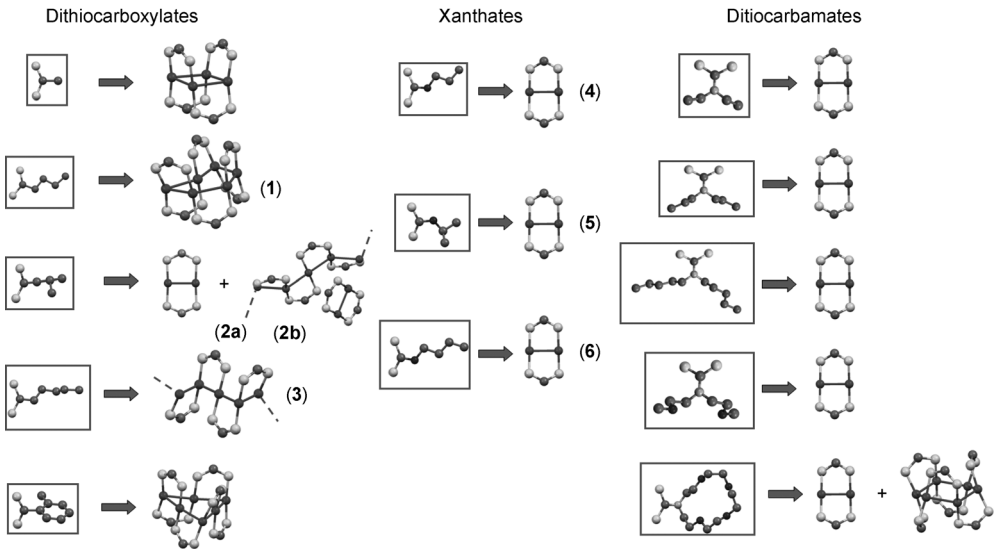

Figure 3. Schematic representation of the crystal structures found in the CSD for gold complexes containing dithiocarboxylato ligands and analogous ligands.

bridge-based structures (rings and chains) than in the case of xanthate and dithiocarbamate ligands, where double-bridged dimers are preponderant. As shown in Figure 3, there are two examples in which the same ligand provides the two types of structures. In the case of the dithiocarbamate, the authors state that only a severe increase of the concentration of gold in the reaction media, depending on the selection of the solvent, allows to overcome the appearance of the more favorable dimeric-based crystal structure.[14] The different behavior of dithiocarboxylato, xanthato, and dithiocarbamato ligands has been attributed to their electron-donor or -withdrawing nature. Interestingly, taking into account that both oligomeric/polymeric structures and the discrete dimeric ones are generated from the same discrete dimeric $[Au_2L_2]$ entities present in solution, it is reasonable to assume that the formation of the oligomeric/polymeric $[Au_2L_2]_n$ structures take place through a previous intermolecular aggregation stage of the dimers mediated by the intermolecular aurophilic contacts. Thus, when aggregation in solution is observed (for the dithiocarboxylato compounds) high nuclearities have been found in the crystal phase.

For the subsequent discussion it is also worth mentioning that the distribution of intermolecular contacts between Au–S units in the CSD present maxima centered at 3.2 and 3.5 Å for Au···Au and Au···S contacts, respectively, whereas the S···S short contacts are spread between 3.4 and 5.8 Å with no clear maximum.

Studies of the behavior in solution: Although rather different crystal structures have been found for compounds **1–3**, an identical behavior in solution (in CS_2) is observed for these three compounds. This fact suggests that the polymeric/oligomeric $[Au_2L_2]_n$ structures found in the crystal phase are cleaved to form discrete analogous $[Au_2L_2]$ entities. Accordingly, as already reported for compound **1**,[9] UV/Vis data from solutions of compounds **2** and **3** present strong evidences of spontaneous self-assembly that depends on the temperature and the concentration of the gold compound. In Figure 4 such effect is shown for complexes **1–3**. Initially, at room temperature the $[Au_2L_2]$ species have an intense absorption at high energies in the UV region ($\lambda_{max}=374$, 373, and 377 nm for compounds **1**, **2**, and **3**, respectively). Lowering the temperature triggers the formation of a new feature at slightly lower energies ($\lambda_{max}=385$, 390, and 392 nm for compounds **1**, **2**, and **3**, respectively). Consistently with an aggregation process, the ratio between the intensities of both features depends on the concentration, that is, the absorption at lower energies being enhanced at higher concentrations. Interestingly, the aggregation process is reversed upon heating. Such reversibility suggests that weak supramolecular interactions are the driving force of the observed self-assembly in solution, which do not imply major rearrangements in the structure, such as those observed in the crystal structures. In order to verify whether a ligand effect can be found in such process, the same study has been performed for analogous Au^I–xanthate compounds (**4–6**). Surprisingly, under the same reaction conditions, for compounds with xanthate ligands the appearance of a new spectroscopic feature is not observed upon decreasing the temperature (see the Supporting Information). Thus, although dithiocarboxylate-containing compounds spontaneously aggregate in solution, analogous complexes with xanthate ligands do not show such a behavior.

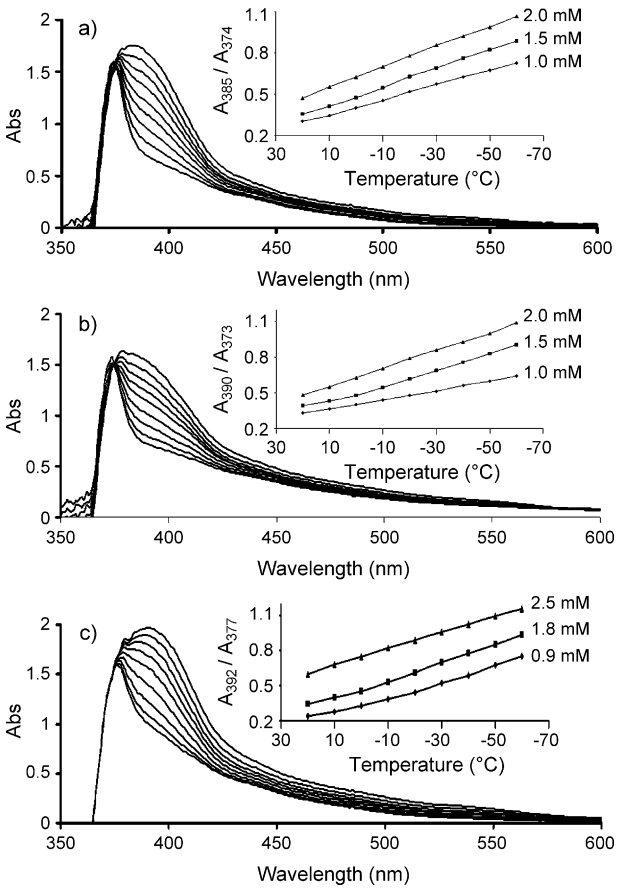

Figure 4. Variable-temperature UV/Vis measurements, by using a cell with an optical path of 0.2 cm, for solutions in CS_2 of a) compound **1** (2.0 mM from 20 to −60 °C), b) compound **2** (2.0 mM from 20 to −60 °C), and c) compound **3** (2.5 mM from 20 to −60 °C). Spectra were taken from 10 to 10°. The insets show the concentration- and the temperature-dependence of the UV/Vis features of each compound.

The appearance of different species in the solutions of $[Au_2L_2]$ (L = dithiocarboxylato) by lowering the temperature is also observed by ^{1}H NMR spectroscopy. Interestingly, although significant differences on the nuclearity of compounds **1–3** have been observed in the crystal structures, similar degrees of aggregation in solution have been observed by means of NMR measurements, for the three compounds. The more diagnostic feature to monitor such phenomena is the signal corresponding to the CH_2 group directly attached to the dithiocarboxylato moiety, which appears in the region from $\delta=2.7$–3.0 ppm in the spectra of **1–3** in a 3:1 $CS_2/CDCl_3$ mixture. At lower temperatures, signals at lower field become prominent. In fact, at 240 K, for complexes **1–3**, three different species co-exist in solution at

comparable concentrations. The assessment of the degree of association in solution was obtained by measuring diffusion coefficients (D) from DOSY spectra of a solution at 240 K. Similar sets of values of D were obtained for compounds **1**–**3** (Table 1). According to the measured diffusion coefficient values, the species with a higher hydrodynamic radius (i.e., lower D) become more favorable at lower temperatures. Assuming that all three species have similar spherical shapes, the ratio between the measured hydrodynamic radii is consistent with the presence of a dimetallic, a tetrametallic, and a hexametallic species $[Au_2(L)_2]_n$ ($n=1$, 2, 3) (see the Supporting Information).

Table 1. Diffusion coefficient values measured for compounds **1**–**3** at 240 K in a 3:1 $CS_2/CDCl_3$ mixture.

	$D1$[a]	$D2$[a]	$D3$[a]	$D2/D1$ (0.74)[b]	$D3/D2$ (0.86)[c]
1	7.76	5.89	5.01	0.76	0.85
2	6.50	4.83	4.19	0.74	0.87
3	6.76	5.01	4.47	0.74	0.89

[a] Values expressed in $10^{-10}\,m^2s^{-1}$. [b] Values in parenthesis correspond to the expected ratio $D2$/D1 for species $[Au_2(L)_2]$ and $[Au_2(L)_2]_2$. [c] Values in parenthesis correspond to the expected ratio $D3/D2$ for species $[Au_2(L)_2]_2$ and $[Au_2(L)_2]_3$.

The fact that the UV/Vis spectra of solutions of compounds **4**–**6** do not change at low temperature is also consistent with the NMR measurements, which do not show any effect by decreasing the temperature. However, the question of whether the nature of the compound in solution is a dimetallic one or if there are some stable species of higher nuclearity, required the measurement of diffusion coefficients from DOSY spectra. The D values obtained from these experiments for the unique species observed in each case are very close to those found for the bimetallic dithiocarboxylato-containing analogues (in the three cases the value of D is measured as approximately $7.7\times10^{-10}\,m^2s^{-1}$). Thus, it is experimentally established that compounds **4**–**6** do not aggregate in solution under the conditions that triggers the assembly of their dithiocarboxylate analogues **1**–**3**.

This is a case of subtle modulation of the supramolecular interactions between compounds containing Au^I centers. Considering that steric congestion is equivalent for analogous dithiocarboxylato and xanthato ligands, the tuning of aurophilic assembly should rely on electronic effects. In order to shed some light on the structures that can result from such assemblies and their electronic description, theoretical calculations at the MP2 level have been performed.

Luminescent studies: Only compound **5** is emissive in the solid state at room temperature, whereas all of the compounds show red emissions at 77 K (Table 2, Figure 5). Lifetime measurements and the Stokes shift point out to a phosphorescent nature of the luminescence. Such transitions are forbidden transitions enabled by the spin–orbit coupling, which is most prominent in heavy atoms.

Table 2. Luminescence maxima (λ_{em}) and excitation maxima (λ_{ex}) and lifetime (τ) found in the solid state for complexes **1**–**6**.

	77 K		298 K	
	λ_{em} [nm] (τ [μs])	λ_{ex} [nm]	λ_{em} [nm] (τ [μs])	λ_{ex} [nm]
1	687 (30)	br (376–591)		
2	776 (24)	456, 599		
3	673 (26)	371, 490		
4	680 (133)	406		
5	686 (150)	367, 410		
6	608 (27), 694 (42)	366, 491	575 (9)	371

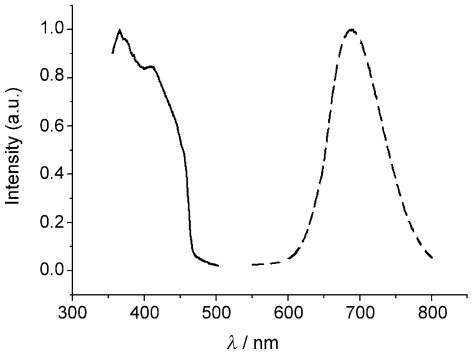

Figure 5. Solid-state emission (-----) and excitation (——) spectra of complex **5** (77 K).

Luminescent thiolate gold complexes are well known and ligand (thiolate, L) to gold (metal, M) charge-transfer (LMCT) transitions have been claimed as the origin of the emissions in many cases.[15] In addition gold···gold interactions are known to be responsible for the emissions observed in many polygold derivatives and metal-centered (MC) transitions may also lead to luminescence.[6a,16] These gold···gold interactions may play a relevant role and then more than one metallic atom can be involved in the charge-transfer transitions, which are symbolized as LMMCT transitions. The influence of the gold···gold distance on the emission wavelength of thiolate gold complexes has been analyzed[16a] and it has been described that a reduction of the metallic distance leads to a red shift of the emission maxima. Nevertheless it is not possible to deduce the presence or not of aurophilic interactions from the emission energy value.

We propose that the emissions observed in complexes **1**–**6** are originated by ligand (L) to metal–metal (MM) charge-transfer transitions. It is difficult to evaluate the influence of the metallic interactions in the origin of the emissions. In this sense it is interesting to notice that compound **6** displays a broad band with two maxima (Figure 6). It has not been possible to separate two different bands upon changing the excitation energy and a complicated origin may be suspected. Then a dual LMMCT and MC character could also be possible.

Considering that different inter- and intramolecular Au···Au interactions are observed in the compounds studied herein, the different possible contribution of both types of metal···metal interactions to the luminescence can be taken

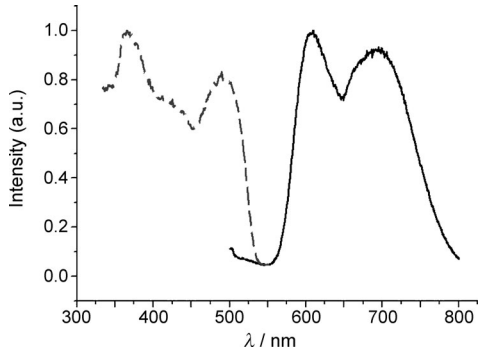

Figure 6. Solid-state excitation (-----) and emission (——) spectra of complex **6** (77 K).

into account. If the intermolecular aurophilic interactions would govern the luminescence, the different scenarios would lead to different energy maxima. The similar emission maxima found for all the complexes in the solid state lead to the proposal that the intramolecular interactions play a more important role in the luminescent properties and the intermolecular ones are not so relevant. Overall, we propose that the emissions in compounds **1**–**6** are due mainly to ligand-to-gold–gold charge-transfer transitions involving the gold centers, although the participation of MC transitions may not be excluded.

Relationship between solid state and species in solution: A surprising feature of compounds **1**–**3** is their spontaneous interconversion between the structures found in solution and those found in the crystal phase. In fact, when a crystal is dissolved in CS_2 the behavior found is the above presented, but recrystallization from such solutions results in the formation of crystals with the structures already presented, as proved by X-ray diffraction.

This kind of rearrangement requires some degree of lability of the dithiocarboxylato ligand. However, the calculated energetic cost for the cleavage of one Au–S bond in $[Au_2L_2]$ is higher than 40 kcal mol^{-1} for the ethyldithiocarboxylato and methylxanthato ligands, too high to expect this process to occur spontaneously at room temperature. Then, how can it occur? To answer this question it is relevant to quote that compounds **1**–**3** are only soluble in CS_2. Considering that CS_2 can act as a ligand, coordination of the solvent to the Au^I centers could assist the reorganization process that results in the oligomeric/polymeric forms observed in the crystal structures. To test this notion, calculations have been performed on the stabilization that results from coordination of a CS_2 molecule to a gold center in a $[Au_2L_2]$ molecule where a ligand acts as a monodentate ligand toward each gold atom. A computational study shows that coordination of a CS_2 solvent molecule is endergonic by about 8 kcal mol^{-1} for both the ethyldithiocarboxylato and the methylxanthato dinuclear complexes. Such a solvent coordination might assist the partial dissociation of one bidentate ligand, which in its absence costs more than 40 kcal mol^{-1}. The reasons why the two different ligands employed behave differently regarding the formation of oligomers is still unclear. However, it is found the trend that the compounds that show supramolecular aggregation in solution are the ones that crystallize in oligomeric/polymeric structures. Thus, it seems reasonable to assume that the approaching of discrete bimetallic compounds through supramolecular interactions, is a first step required to from oligomeric/polymeric arrangements. In any case, a much more detailed mechanistic study would be needed to study the possible dimer–oligomer reaction.

Computational study: In order to rationalize the variety of structural patterns found for the supramolecular arrangement of the di- and oligonuclear compounds prepared, we have carried out computational studies at the MP2 level of theory, capable of reasonably evaluating the relevant intermolecular interactions. We performed calculations on $[Au_2L_2]_2$ (L = S_2C-X, X = Et, NMe_2, and OMe) structures with the three relative orientations illustrated in Scheme 4. The values of interaction energies found between the $[Au_2L_2]$ units are shown in Table 3. The interaction energy

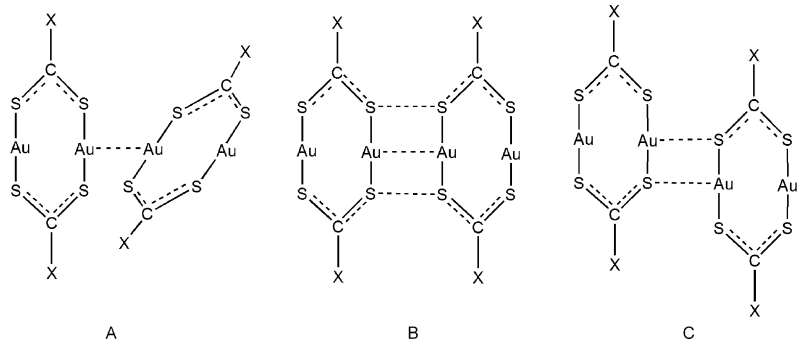

Scheme 4. Representation of the calculated structures.

Table 3. Basis Set Superposition Error (BSSE)-corrected interaction energies between dinuclear $[Au_2L_2]$ complexes with interacting topologies A–C (see Scheme 4) at fixed intermolecular distances, where L being a dithiocarboxylate (X = CH_2Me), dithiocarbamate (X = NMe_2), or xhanthate (X = OMe).

X	D[a]	E(A) [kcal mol^{-1}]	E(B) [kcal mol^{-1}]	E(C) [kcal mol^{-1}]
CH_2Me	3.0	−9.74	+10.69	−0.91
	3.5	−7.51	−4.62	−4.82
	4.0	−4.74	−4.94	−3.90
NMe_2	3.0	−7.32	+5.14	+2.50
	3.5	−5.52	−4.47	−3.88
	4.0	−3.18	−3.70	−3.35
OMe	3.0	−8.84	+5.54	+0.46
	3.5	−6.94	−6.02	−4.69
	4.0	+4.39	−5.48	−3.19

[a] Values expressed in angstroms (Å).

between two $[Au_2L_2]$ units in structure A can be attributed to an Au···Au attraction. For structure C, the calculated interaction energy corresponds to two Au···S interactions. Finally, the difference between interaction energies found between two $[Au_2L_2]$ compounds in structures B and A corresponds to twice the S···S interaction. These results allowed us to estimate the distance dependence of the pairwise Au···Au, Au···S, and S···S interactions as shown in Figure 7.

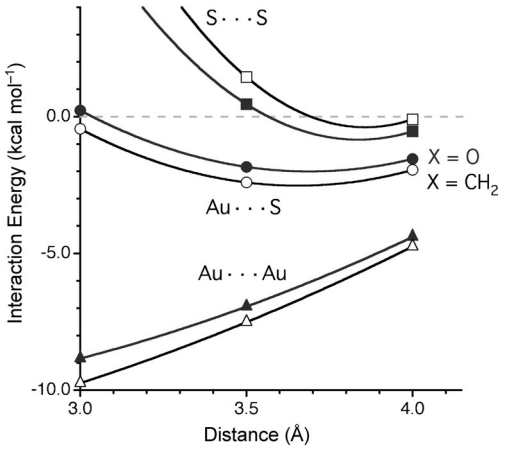

Figure 7. BSSE-corrected pairwise interaction energies for the supramolecular interactions between Au_2L_2 dimers A–C (Scheme 4), evaluated from the results given in Table 3.

Figure 7 shows that the most stabilizing intermolecular interaction is that between two gold atoms, with a minimum at a rather short Au···Au distance (3.0 Å or less). The Au···S interactions are also stabilizing at somewhat longer distances (with a minimum at around 3.5 Å), whereas S···S interactions are destabilizing at short distances and only slightly stabilizing at 3.8–4.0 Å. For that reason, in the parallel arrangement B the attractive Au···Au interaction is not enough to make the supramolecular assembly favorable at 3.0 Å. At longer distances, at which the Au···Au attraction could overweight the S···S repulsions in B, topology C can compete by means of its two attractive Au···S interactions. At distances longer than 3.5 Å, the slipped geometry C becomes even more stable than the assembly through bare aurophilic interactions as in A.

The interplay of the three intermolecular interactions and of their different distance dependence is nicely reflected in the relative orientation of the dinuclear $[Au_2L_2]$ units found in the crystal structures of the dithiocarboxylates **1**–**3**, the xanthates **4**–**6**, and the dithiocarbamates (retrieved from the CSD). A representation of the interdimer Au···Au distances as a function of the S-Au···Au-S torsion angle (Figure 8) shows that Au···Au distances shorter than 3.30 Å are only compatible with a rotated structure, that is, with S-Au···Au-S torsion angles larger than 30° (as in compounds **2** and **5**). Nearly

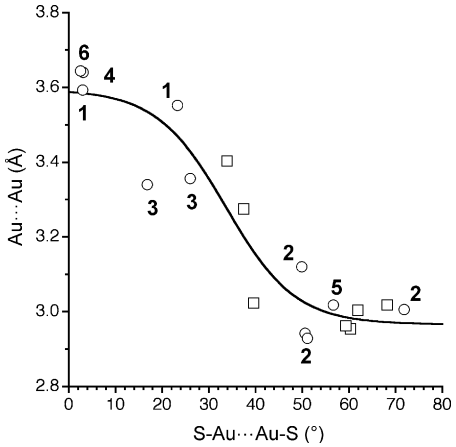

Figure 8. Relationship between the intermolecular Au···Au distance and the S-Au···Au-S torsion angle in compounds **1**–**6** (circles) and in dithiocarbamates (squares).[17]

coplanar intermolecular interactions as found in complexes **1**, **4**, and **6**, in contrast, appear at distances larger than 3.5 Å.

Next, we have optimized the structures of dimers of the dinuclear complexes, $[Au_2L_2]$ with dithiocarboxylato and xanthato ligands, as well as tetranuclear complexes with alternating bridges as found in reference [7], akin to the hexanuclear complex **1**, and the results are summarized in Table 4. Three energy minima were found for the dimer of the dithiocarboxylato complex (**8a**–**c**) and two for that of the xanthate complex (**9a** and **b**), and one minimum each for the corresponding tetramers (**8t** and **9t**, respectively).

The most stable dimers with each ligand, **8a** and **9a** (Figure 9), present structures with stacked $Au_2S_4C_2$ rings, shifted along the Au–Au direction to form Au_4 rhombuses, and also rotated relative to each other (as calibrated by an

Table 4. Energies and structural parameters for dimers of the dinuclear complexes of dithiocarboxylate (**8a**–**c**) and dithioxanthate (**9a** and **b**), as well as for the corresponding tetramers **8t** and **9t** (Figure 9). Only contacts shorter than 3.60 Å are given. E_{int} is the BSSE-corrected interaction energy between two monomers; τ is the twist angle measured by the Au-Au···Au-Au torsion; E_{rel} is the calculated energy relative to that of the most stable $[Au_2L_2]$ dimer.

	Dithiocarboxylate				Xanthate		
	8a	**8b**	**8c**	**8t**	**9a**	**9b**	**9t**
E_{int} [kcal mol^{-1}]	−12.45	−10.64	−11.3		−10.96	−9.96	
E_{rel} [kcal mol^{-1}]	0.00			−0.76	0.00		+0.80
τ [°]	23	61	97	21	23	20	18
Au···Au [Å]	2.91	3.19	2.94	2.86[a]	2.98	3.05	2.87[a]
	3.02	3.19			3.14	3.05	
	3.07				3.14		
Au···S [Å]	3.34	3.18	3.10	>3.60	3.38	>3.90	>3.80
	3.38	3.19	3.10		3.39		
	3.46	3.19	3.45		3.43		
	3.53	3.19	3.47		3.43		
S···S [Å]	3.52	3.48	3.43	>3.60[b]	3.55	3.54	>3.60[b]
	3.57	3.48	3.45		3.56	3.54	
		3.58	3.45			3.54	
		3.58	3.50			3.54	

[a] Intramolecular. [b] Interligand.

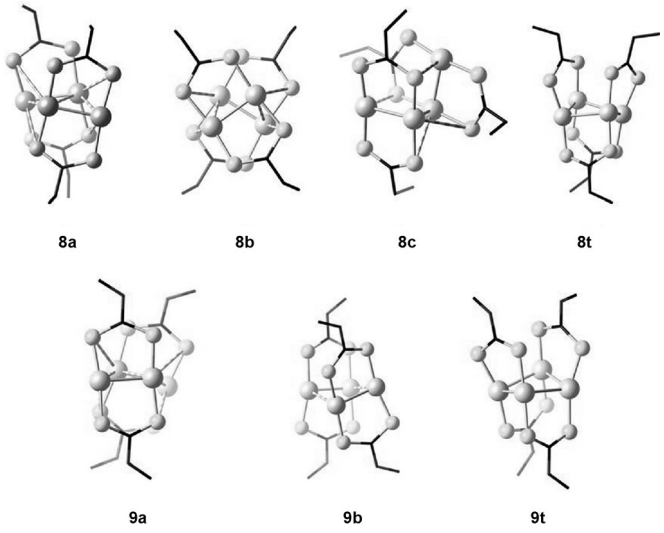

Figure 9. Optimized structures for dimers of the dinuclear Au complexes with ethyldithiocarboxylate (**8a–c**) and methyldithioxanthate (**9a** and **b**) ligands, and for the corresponding tetramers **8t** and **9t**. Striped cylinders represent intermolecular contacts at distances of 3.5 Å or shorter. Hydrogen atoms not shown for simplicity.

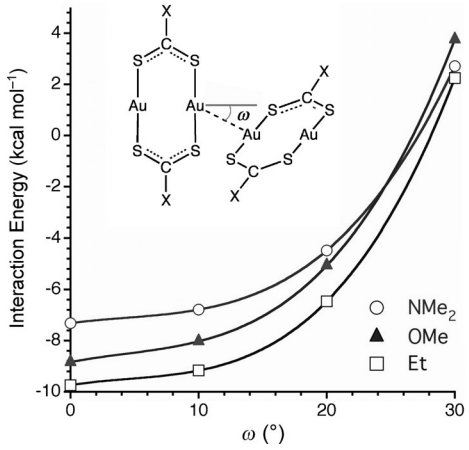

Figure 10. Angular dependence of the interaction energy between dinuclear Au complexes with dithiocarboxylato, dithiocarbamato, and xanthato ligands, calculated at the MP2 level and corrected for the BSSE (○ = NMe_2, ▲ = OMe, and □ = Et).

Au-Au···Au-Au torsion angles τ of 23°). The resulting arrangement facilitates the existence of three intermolecular Au···Au contacts at distances of around 3.0 Å and four Au···S contacts at 3.5 Å or shorter, whereas avoiding S···S short contacts (only two contacts at less than 3.6 Å appear in each case), in excellent agreement with the conclusions drawn from the analysis of the models A–C (Scheme 4) and with the distribution of the experimental intermolecular distances and torsion angles discussed above. The other energy minima found for the dimers are relatively close in energy, and differ in the relative arrangement of the two monomers, achieved through different degrees of shift and rotation. The different arrangements observed combine different number of Au···Au intermolecular contacts at varying distances with the number and distance of the Au···S contacts (see **8a** and **8c**), thus resulting in nearly isoenergetic structures. Still another factor that may influence the total interaction energy is the relative orientation of the interacting AuS_2 coordination moieties, because an analysis of all short contacts between those units in the CSD shows that the Au···Au distances are all longer than 3.88 Å when a gold atom deviates from the normal to the other AuS_2 group by more than 30°, suggesting that the interaction energy is most stabilizing at the perpendicular orientation. Therefore, two Au···Au interactions in **9b** at practically straight angles could be nearly as stabilizing as three interactions in **9a** that deviate 15° from the perpendicular direction. Such an angular dependence of the strength of the aurophilic interaction is confirmed by the results of BSSE-corrected interaction energy calculations between two dinuclear molecules at a fixed intermolecular Au···Au distance of 3.0 Å and varying Au-Au···Au angles (ω). Our results for similar dithiocarboxylato, dithiocarbamato, and xanthato ligands (Figure 10) show that the interaction energy varies little for deviations of less than 10° from a perpendicular arrangement, but become much less stabilizing at larger angles, which is in excellent agreement with the experimental angular distribution of the intermolecular contacts between AuS_2 groups.

The optimized structure for the tetramers with alternating bridges is very similar for the dithiocarboxylato and the xanthato ligands. The main difference with the dimers of the dinuclear molecules is that all the Au–Au contacts are now intramolecular and therefore shorter, due to the small bite of the bidentate ligands, whereas all Au···S and S···S distances are substantially longer. The two effects nearly compensate each other and the energy difference between the molecular and supramolecular species is rather small. However, there is an opposing trend in the dithiocarboxylate and xanthate cases: although for the former ligand the tetramer is slightly more stable than the dimer of dinuclear complexes, for the latter the opposite situation appears. Such a difference can probably be attributed to the slightly more stabilizing nature of the Au···Au interactions in the dithiocarboxylato compounds (Figure 7), and is consistent with our finding that they form oligonuclear systems such as complex **1** and the one reported by Piovesana et al.[7] However, we cannot rule out that the formation of intermolecular-associated dimers or oligomers could be the result of kinetic rather than thermodynamic control.

Conclusion

From the results presented in this work it can be inferred that aurophilic assemblies are highly dependent on subtle changes on the ligands that hold together the gold centers in bimetallic molecules of the general formula $[Au_2L_2]$. In this work we used a series of analogous dithiocarboxylate and xanthate ligands to study their behavior in solution and their structural characteristics in the crystalline phase. With

respect to their behavior in solution, we observed that compounds with dithiocarboxylato ligands can reversibly aggregate in solution through supramolecular interactions, whereas xanthate compounds do not show this phenomenon. The steric hindrance of the selected ligands is the same between analogous dithiocarboxylato and xanthato ligands. Thus, the diversity of the behavior observed in this work should be understood as a delicate balance of diverse subtle weak interactions that concur at the same time, not only Au···Au, Au···S, or S···S, but probably also solvation forces or interactions between the CH_2R or OR groups.[18]

Luminescence studies carried out at variable temperature showed that all the compounds present emission at similar wavelengths in the solid state suggesting that the intramolecular interactions play a more relevant role in the luminescent properties than the intermolecular ones. Ligand-to-metal–metal charge-transfer (LMMCT) transitions are postulated as the origin of the emissions.

The computational studies presented here indicate that not only Au···Au interactions, but also Au···S and S···S ones have a say in the structure and energetic of the supramolecular species, as well as for the choice between supramolecular association or intramolecular oligomerization. Such effects result in the rich structural diversity observed in the crystal phase. Xanthate-containing compounds appear as discrete bimetallic molecules, eventually connected through Au···Au interactions forming a chain (compound **4**), or through weaker Au···S interactions forming layers (compounds **5** and **6**). The dithiocarboxylato analogues may appear, in addition, as oligonuclear molecules. Overall, this work presents new tools for designing complex structures of different nuclearity that contain sulfur-bonded Au^I centers with short contacts, which can have potential interest for the engineering of molecular conductive devices.

Experimental Section

Materials and methods: All reagents were purchased from Aldrich and used as received. $CS_2 \geq 99.9\%$ was purchased from Sigma Aldrich and used without further purification. Diethyl ether was purchased from Carlo Erba and used without further purification.

The synthesis of dithicarboxylic acids was carried out following a procedure previously reported.[19] Spectroscopic characterization of the obtained compounds was performed by means of elemental analysis, UV/Vis and ^{1}H NMR spectroscopy, and single-crystal X-ray diffraction.

^{1}H NMR spectra were recorded on a Bruker AMX-300 spectrometer. C, H, S elemental analyses were performed on a PerkinElmer 240-B microanalyzer.

DOSY NMR experiments were carried out on a 600 MHz AVANCE Bruker spectrometer equipped with a 5 mm triple-resonance inverse broadband probe head and a *z*-gradient coil. Experiments were recorded at several temperatures for samples of 5–10 mg of compounds **1**–**6** dissolved in a 1:3 $CDCl_3/CS_2$ solvent mixture. The measurement of *D* were performed at 240 K by using the double-stimulated echo (DSTE) pulse sequence, by using a diffusion time of 150 ms, and a LED delay of 5 ms. For each experiment, sine-shaped PFGs, with a duration of 2 ms followed by a recovery delay of 100 μs were incremented from 2–95 % of the maximum strength in 16 equally spaced steps. Signal intensities of a given resonance were adjusted to: $A_g = A_o \exp(-\gamma^2 g^2 \delta^2 (4\Delta - \delta) D)$; where A_g and A_o are the signal intensities in the presence and absence of PFG, respectively, γ is the gyromagnetic ratio ($rad\,s\,g^{-1}$), *g* is the strength of the diffusion gradients ($gauss\,cm^{-1}$), *D* is the diffusion coefficient of the observed spins ($cm^2\,s^{-1}$), δ is the length of the diffusion gradient (s), and Δ is the diffusion time (s). Data were processed by using the software package included into the TOPSPIN software. In all samples, the residual solvent signal of $CHCl_3$ showed a *D* value of $17.4 \times 10^{-10}\ m^2 s^{-1}$.

Electronic absorption spectra were recorded on an Agilent 8452 diode array spectrophotometer over a 190–1100 nm range in 0.1, 0.2, and 1 cm quartz cuvettes thermostatted by a Unisoku cryostat.

Steady-state photoluminescence spectra were recorded with a Jobin–Yvon Horiba Fluorolog FL-3–11 spectrometer by using band pathways of 3 nm for both excitation and emission. Phosphorescence lifetimes were recorded with a Fluoromaxphosphorimeter accessory containing a UV xenon flash tube. Coefficients of determination (R^2) to first order exponential functions are 0.99.

Computational details: Calculations were carried out by using the Gaussian 09 package.[20] A perturbation method with introduction of correlation energy through the second order Möller–Plesset approach was used (MP2).[21] Relativistic effective core potentials from the Stuttgart–Dresden group were used to represent the innermost electrons of the gold atoms and its basis set of valence double-ζ quality associated known as SDD,[22] by adding an *f*-polarization function.[23] The basis set for the main group elements (S, C, O, and H) was of triple-ζ quality,[24] and included a *d*-polarization function in the sulfur atoms.[23] Energies in carbon disulfide solution ($\varepsilon = 2.61$) were taken into account by PCM cal-

Table 5. Crystallographic data and structure refinement details of compounds **1** and **3**–**5**.

	1	**3**	**4**	**5**
formula	$C_{30}H_{54}Au_6S_{12}$	$C_6H_{11}AuS_2$	$C_8H_{14}Au_2O_2S_4$	$C_8H_{14}Au_2O_2S_4$
M_r	1981.25	344.24	664.36	664.36
crystal system	monoclinic	triclinic	orthorhombic	monoclinic
space group	*P*2/*c*	$P\bar{1}$	$P2_12_12_1$	*C*2/*c*
a [Å]	18.9785(12)	8.7491(3)	6.7406(4)	28.848(3)
b [Å]	14.0398(5)	12.7363(6)	7.4325(4)	4.4854(4)
c [Å]	18.1941(7)	20.8084(9)	28.251(2)	10.9343(11)
α [°]	–	95.366(4)	–	–
β [°]	112.399(6)	91.064(3)	–	105.498(5)
γ [°]	–	108.389(4)	–	–
V [Å^3]	4482.1(4)	2187.82(16)	1415.36(15)	1363.4(2)
Z	4	10	4	4
ρ_{calcd} [$g\,cm^{-3}$]	2.936	2.613	3.118	3.237
μ [mm^{-1}]	20.148	17.204	21.279	22.090
T [K]	100(2)	150(2)	293(2)	100(2)
reflns collected	18109	19358	6522	7702
unique data/parameters	17914/337	8790/396	3011/148	1511/69
reflns with $I \geq 2\sigma(I)$	4059	5097	2589	1294
R_{int}	0.0891	0.0664	0.1001	0.0793
GOF[a]	0.741	1.023	1.007	1.056
final *R* indices				
$[I>2\sigma(I)]$ $R1$[b]/w$R2$[c]	0.0446/0.0857	0.0522/0.1072	0.0556/0.1433	0.0640/0.1766
all data $R1$[b]/w$R2$[c]	0.1216/0.0956	0.0923/0.1112	0.0630/0.1486	0.0720/0.1888

[a] $S = [\Sigma w(F_0^2 - F_c^2)^2/(N_{obs} - N_{param})]^{1/2}$. [b] $R1 = \Sigma ||F_0| - |F_c||/\Sigma |F_0|$. [c] $wR2 = [\Sigma w(F_0^2 - F_c^2)^2/\Sigma w F_0^2]^{1/2}$; $w = 1/[\sigma^2(F_0^2) + (aP)^2]$ where $P = (\max(F_0^2, 0) + 2Fc^2)/3$ with $a = 0.0291$ (**1**), 0.0394 (**3**), 0.0971 (**4**), and 0.1455 (**5**).

culations,[25] keeping the geometry optimized for gas-phase (single-point) calculations.

X-ray data collection and crystal structure determination: The single-crystal X-ray diffraction data collections were done for compounds **1** and **3**–**5** on an Oxford Diffraction Xcalibur diffractometer with graphite-monochromated $Mo_{K\alpha}$ radiation ($\lambda = 0.71073$ Å). The data reduction was done with the CrysAlisPro and X-RED programs.[26] All the structures were solved by direct methods by using the SIR92 program[27] and refined by full-matrix least-squares on F^2 including all reflections (SHELXL97).[28] All calculations were performed using the WINGX crystallographic software package.[29] Due to the usual disorder present in compounds containing long alkyl chains, the alkyl chains of the dithiocarboxylate and xanthate ligands was refined by imposing soft restraints on the C−C distances and C-C-C angles. Crystal parameters and details of the final refinements of compounds **1** and **3**–**5** are summarized in Table 5. CCDC 871929 (**1**), 871930 (**3**), 871931 (**4**), 871932 (**5**), and 871933 (**6**), contain the supplementary crystallographic data for this paper. These data can be obtained free of charge from The Cambridge Crystallographic Data Centre via www.ccdc.cam.ac.uk/data_request/cif..

Synthesis and characterization

*Synthesis of gold(I)–dithiocarboxylato compounds (**1**–**3**)*: $Na[AuCl_4]\cdot 2H_2O$ (238.8 mg, 0.6 mmol) was dissolved in water (2 mL). A solution of the corresponding dithiocarboxylic acid (1.8 mmol) and KOH (100.8 mg, 1.8 mmol) in water (4 mL) was added to this orange solution. The mixture was stirred for 5 min. Then the red solid was filtered, washed with diethyl ether, dried under vacuum, and recrystallized from a 1:1 CS_2/diethyl ether mixture (132 mg, 76% for **1**; 151 mg, 82% for **2**; 163 mg, 71% for **3**). X-ray quality single crystals of these compounds were obtained by slow vapor diffusion of diethyl ether on a solution of gold(I) isopentyl dithiocarboxylate in CS_2 at 4 °C.

Analysis for compound **1**: ^{1}H NMR (300 MHz, 298 K, $CDCl_3/CS_2$ 3:1, $SiMe_4$): $\delta = 0.99$ (t, $J = 7.2$ Hz), 1.38–1.45 (m), 1.80–1.91 (m), 2.96 ppm (t, $J = 7.6$ Hz); IR (KBr): $\tilde{\nu} = 901$ (s), 991 (s), 1132 (s), 1207 (w), 1458 (w), 1624 (m), 2853 (m), 2951 (s), 3413 cm^{-1} (s); elemental analysis calcd (%) for $C_{10}H_{18}Au_2S_4$: C 18.2, H 2.7, S, 19.4; found: C 17.8, H 2.7, S 19.4.

Analysis for compound **2**: ^{1}H NMR (300 MHz, 298 K, $CDCl_3/CS_2$ 3:1, $SiMe_4$): $\delta = 1.07$ (d, $J = 6.3$ Hz), 2.21–2.38 (m), 2.82 ppm (d, $J = 7.2$ Hz); IR (KBr): $\tilde{\nu} = 849$ (m), 991 (s), 1147 (s), 1240 (w), 1456 (w), 1624 (m), 2858 (w), 2947 (m), 3410 cm^{-1} (s); elemental analysis calcd (%) for $C_{10}H_{18}Au_2S_4$: C 18.2, H 2.7, S 19.4; found: C 17.4, H 2.7, S 19.2.

Analysis for compound **3**: ^{1}H NMR (300 MHz, 298 K, $CDCl_3/CS_2$ 3:1, $SiMe_4$): $\delta = 0.97$ (t, $J = 7.0$ Hz), 1.36–1.43 (m), 1.34–1.48 (m), 1.82–1.94 (m), 2.95 ppm (t, $J = 7.5$ Hz); IR (KBr): $\tilde{\nu} = 934$ (s), 1010 (s), 1134 (s), 1201 (w), 1465 (m), 1622 (w), 2847 (m), 2922 (s), 3404 cm^{-1} (s); elemental analysis calcd (%) for $C_{12}H_{22}Au_2S_4$: C 20.9, H 3.2, S 18.6; found: C 20.7, H 3.2, S 18.6.

*Synthesis of gold(I)–xanthate compounds (**4**–**6**)*: $Na[AuCl_4]\cdot 2H_2O$ (167.1 mg, 0.42 mmol) was dissolved in water (2 mL). A solution of the corresponding potassium xanthate salt (1.26 mmol) in water (4 mL) was added to this orange solution. The mixture was stirred for 5 min. Then the red solid was filtered, washed with diethyl ether, dried under vacuum, and recrystallized from CS_2/diethyl ether (115 mg, 75% for **4**; 102 mg, 72% for **5**; 134 mg, 79% for **6**). X-ray quality single crystals of these compounds were obtained by slow vapor diffusion of diethyl ether on a solution of the corresponding gold(I) xanthate in carbon disulfide at 4 °C.

Analysis for compound **4**: ^{1}H NMR (300 MHz, 298 K, $CDCl_3/CS_2$ 3:1, $SiMe_4$): $\delta = 1.11$ (t, $J = 7.5$ Hz), 1.97–2.05 (m), 4.52 ppm (t, $J = 6.5$ Hz); IR (KBr): $\tilde{\nu} = 1057$ (s), 1104 (m), 1140 (m), 1200 (s), 1377 (w), 1456 (m), 1632 (m), 2869 (w), 2965 (m), 3398 cm^{-1} (s); elemental analysis calcd (%) for $C_8H_{14}O_2Au_2S_4$: C 14.4, H 2.1, S 19.3; found: C 14.0, H 2.2, S 19.0.

Analysis for compound **5**: ^{1}H NMR (300 MHz, 298 K, $CDCl_3/CS_2$ 3:1, $SiMe_4$): $\delta = 1.55$ (d, $J = 6.5$ Hz), 5.45–5.53 ppm (m); IR (KBr): $\tilde{\nu} = 1037$ (s), 1087 (s), 1137 (m), 1213 (s), 1379 (m), 1456 (m), 1608 (w), 2911 (w), 2973 (m), 3430 cm^{-1} (s); elemental analysis calcd (%) for $C_8H_{14}O_2Au_2S_4$: C 14.4, H 2.1, S 19.3; found: C 14.3, H 2.2, S 19.2.

Analysis for compound **6**: ^{1}H NMR (300 MHz, 298 K, $CDCl_3/CS_2$ 3:1; $SiMe_4$): $\delta = 1.06$(t, $J = 7.2$ Hz), 1.5 8–1.65 (m), 1.94–2.01 (m), 4.56 ppm (t, $J = 6.5$ Hz); IR (KBr): $\tilde{\nu} = 1051$ (s), 1124 (w), 1143 (m), 1195 (s), 1381 (w), 1455 (m), 1621 (w), 2863 (m), 2950 (m), 3427 cm^{-1} (s); elemental analysis calcd (%) for $C_{10}H_{18}O_2Au_2S_4$: C 17.3, H 2.1, S 18.5; found: C 17.0, H 2.6, S 18.2.

Acknowledgements

This work was supported by the MICINN (projects MAT2010-20843-C02-01, PLE2009-0065, ACI2009-0969, CTQ2011-23862-C02 and CTQ2010-20500-C02-01), Comunidad de Madrid (S-0505/MAT/0303), Gobierno Vasco (IT477-10), and Generalitat de Catalunya (2009-SGR-1459). R. M.-B. thanks the Spanish M.E.C. for funding through the 'Ramón y Cajal' program.

[1] J. M. Lehn, *Proc. Natl. Acad. Sci. USA* **2002**, *99*, 4763–4768.
[2] a) J. K. Bera, K. R. Dunbar, *Angew. Chem.* **2002**, *114*, 4633–4637; *Angew. Chem. Int. Ed.* **2002**, *41*, 4453–4457; b) F. A. Cotton, R. A. Walton, *Multiple Bonds Between Metal Atoms*, Oxford, **1993**, p. .
[3] a) H. Schmidbaur, A. Schier, *Chem. Soc. Rev.* **2008**, *37*, 1931–1951; b) P. Pyykkö, *Chem. Soc. Rev.* **2008**, *37*, 1967–1997.
[4] a) A. Vogler, H. Kunkely, *Chem. Phys. Lett.* **1988**, *150*, 135–137; b) P. Pyykkö, Y. F. Zhao, *Angew. Chem.* **1991**, *103*, 622–623; *Angew. Chem. Int. Ed. Engl.* **1991**, *30*, 604–605; c) Y. Jiang, S. Alvarez, R. Hoffmann, *Inorg. Chem.* **1985**, *24*, 749–757; d) P. K. Mehrotra, R. Hoffmann, *Inorg. Chem.* **1978**, *17*, 2187–2189; e) A. Dedieu, R. Hoffmann, *J. Am. Chem. Soc.* **1978**, *100*, 2074–2079; f) K. M. Merz, R. Hoffmann, *Inorg. Chem.* **1988**, *27*, 2120–2127; g) M. A. Carvajal, S. Alvarez, J. J. Novoa, *Chem. Eur. J.* **2004**, *10*, 2117–2132; h) E. O'Grady, N. Kaltsoyannis, *Phys. Chem. Chem. Phys.* **2004**, *6*, 680–687.
[5] a) V. W.-W. Yam, E. C.-C. Cheng, *Top. Curr. Chem.* **2007**, *281*, 269–309; b) R. J. Puddephatt, *Coord. Chem. Rev.* **2001**, *216*, 313–332; c) J. C. Vickery, M. M. Olmstead, E. Y. Fung, A. L. Balch, *Angew. Chem.* **1997**, *109*, 1227–1229; *Angew. Chem. Int. Ed. Engl.* **1997**, *36*, 1179–1181.
[6] a) V. W.-W. Yam, E. C.-C. Cheng, *Chem. Soc. Rev.* **2008**, *37*, 1806–1813; b) H. Schmidbaur, A. Schier, *Chem. Soc. Rev.* **2012**, *41*, 370–412.
[7] a) B. Chiari, O. Piovesana, T. Tarantelli, P. F. Zanazzi, *Inorg. Chem.* **1985**, *24*, 366–371; b) O. Piovesana, P. F. Zanazzi, *Angew. Chem.* **1980**, *92*, 579–580; *Angew. Chem. Int. Ed. Engl.* **1980**, *19*, 561–562.
[8] J. A. Schuerman, F. R. Fronczek, J. Selbin, *J. Am. Chem. Soc.* **1986**, *108*, 336–337.
[9] M. L. Gallego, A. Guijarro, O. Castillo, T. Parella, R. Mas-Balleste, F. Zamora, *CrystEngComm* **2010**, *12*, 2332–2334.
[10] Z. Assefa, R. J. Staples, J. P. Fackler, *Inorg. Chem.* **1994**, *33*, 2790–2798.
[11] C. Paparizos, J. P. Fackler, *Inorg. Chem.* **1980**, *19*, 2886–2889.
[12] M. Bardaji, P. G. Jones, A. Laguna, M. Laguna, *Organometallics* **1995**, *14*, 1310–1315.
[13] A. A. Mohamed, I. Kani, A. O. Ramirez, J. P. Fackler, *Inorg. Chem.* **2004**, *43*, 3833–3839.
[14] B. C. Tzeng, W. H. Liu, J. H. Liao, G. H. Lee, S. M. Peng, *Cryst. Growth Des.* **2004**, *4*, 573–577.
[15] a) J. M. Forward, D. Bohmann, J. P. Fackler, R. J. Staples, *Inorg. Chem.* **1995**, *34*, 6330–6336; b) B. C. Tzeng, C. K. Chan, K. K. Cheung, C. M. Che, S. M. Peng, *Chem. Commun.* **1997**, 135–136; c) V. W. W. Yam, C. L. Chan, C. K. Li, K. M. C. Wong, *Coord. Chem. Rev.* **2001**, *216*, 173–194; d) E. R. T. Tiekink, J. G. Kang, *Coord. Chem. Rev.* **2009**, *253*, 1627–1648; e) B. C. Tzeng, H. T. Yeh, Y. C. Huang, H. Y. Chao, G. H. Lee, S. M. Peng, *Inorg. Chem.* **2003**, *42*, 6008–6014; f) V. W. W. Yam, K. M. C. Wong, *Chem. Commun.* **2011**, *47*, 11579–11592.

[16] a) J. M. Forward, J. P. Fackler, Jr., Z. Assefa in *Optoelectronic Properties of Inorganic Compounds* (Eds.: M. Roundhill, J. P. Fackler, Jr.), Plenum, New York, **1999**, Chapter 6; b) A. Vogler, H. Kunkely, *Coord. Chem. Rev.* **2001**, *219*, 489–507; c) J. M. López-de-Luzuriaga in *Modern Supramolecular Gold Chemistry* (Ed.: A. Laguna), Wiley-VCH, **2008**, p. 347; d) V. W. W. Yam, K. K. W. Lo, *Chem. Soc. Rev.* **1999**, *28*, 323–334; e) V. W. W. Yam, C.-H. Tao in *Gold: Science and Applications* (Eds.: C. Corti, R. Holliday), CRC Press, **2010**, Chapter 5, pp. 69–87; f) C.-M. Che, S.-W. Lai in *Gold Chemistry: Applications and Future Directions in the Life Sciences* (Ed.: F. Mohr), Wiley-VCH, **2009**, Chapter 5, pp. 249–281; g) J. B. Foley, A. E. Bruce, M. R. M. Bruce, *J. Am. Chem. Soc.* **1995**, *117*, 9596–9597; h) P. Schwerdtfeger, A. E. Bruce, M. R. M. Bruce, *J. Am. Chem. Soc.* **1998**, *120*, 6587–6597.

[17] a) D. D. Heinrich, J.-C. Wang, J. P. J. Fackler, *Acta Crystallogr. Sect. C.* **1990**, *46*, 1444–1446; b) M. A. Mansour, W. B. Connick, R. J. Lachicotte, H. J. Gysling, R. Eisenberg, *J. Am. Chem. Soc.* **1998**, *120*, 1329–1330; c) R. Hesse, P. Jennische, *Acta Chem. Scand.* **1972**, *26*, 3855–3859; d) S. Y. Ho, E. R. T. Tiekink, *Z. Kristallogr. New Cryst. Struct.* **2002**, *217*, 589–591.

[18] J. Echeverría, G. Aullon, D. Danovich, S. Shaik, S. Alvarez, *Nat. Chem.* **2011**, *3*, 323–330.

[19] J. M. Beiner, C. G. Andrieu, A. Thuillie, *C. R. Seances Acad. Sci. Ser. B* **1972**, *274*, 407–410.

[20] Gaussian 09, Revision A.01, M. J. Frisch, G. W. Trucks, H. B. Schlegel, G. E. Scuseria, M. A. Robb, J. R. Cheeseman, G. Scalmani, V. Barone, B. Mennucci, G. A. Petersson, H. Nakatsuji, M. Caricato, X. Li, H. P. Hratchian, A. F. Izmaylov, J. Bloino, G. Zheng, J. L. Sonnenberg, M. Hada, M. Ehara, K. Toyota, R. Fukuda, J. Hasegawa, M. Ishida, T. Nakajima, Y. Honda, O. Kitao, H. Nakai, T. Vreven, J. A. Montgomery, Jr., J. E. Peralta, F. Ogliaro, M. Bearpark, J. J. Heyd, E. Brothers, K. N. Kudin, V. N. Staroverov, R. Kobayashi, J. Normand, K. Raghavachari, A. Rendell, J. C. Burant, S. S. Iyengar, J. Tomasi, M. Cossi, N. Rega, J. M. Millam, M. Klene, J. E. Knox, J. B. Cross, V. Bakken, C. Adamo, J. Jaramillo, R. Gomperts, R. E. Stratmann, O. Yazyev, A. J. Austin, R. Cammi, C. Pomelli, J. W. Ochterski, R. L. Martin, K. Morokuma, V. G. Zakrzewski, G. A. Voth, P. Salvador, J. J. Dannenberg, S. Dapprich, A. D. Daniels, Ö. Farkas, J. B. Foresman, J. V. Ortiz, J. Cioslowski, D. J. Fox, Gaussian, Inc., Wallingford CT, **2009**.

[21] C. Møller, M. S. Plesset, *Phys. Rev.* **1934**, *46*, 618–622.

[22] D. Andrae, U. Haussermann, M. Dolg, H. Stoll, H. Preuss, *Theor. Chim. Acta* **1990**, *77*, 123–141.

[23] A. Schäfer, C. Huber, R. Ahlrichs, *J. Chem. Phys.* **1994**, *100*, 5829–5835.

[24] A. Schäfer, H. Horn, R. Ahlrichs, *J. Chem. Phys.* **1992**, *97*, 2571–2577.

[25] a) J. Tomasi, M. Persico, *Chem. Rev.* **1994**, *94*, 2027–2094; b) C. Amovilli, V. Barone, R. Cammi, E. Cances, M. Cossi, B. Mennucci, C. S. Pomelli, J. Tomasi, *Adv. Quantum Chem.* **1999**, *32*, 227–261.

[26] CrysAlisPro, version 1.171.35.15, Agilent Technologies, Yarnton, UK., **2011**.

[27] A. Altomare, M. Cascarano, C. Giacovazzo, A. Guagliardi, *J. Appl. Crystallogr.* **1993**, *26*, 343.

[28] SHELXL-97, Program for Crystal Structure Refinement, G. M. Sheldrick Universität Göttingen, Göttingen (Germany), **1997**.

[29] L. J. Farrugia, *J. Appl. Crystallogr.* **1999**, *32*, 837.

Received: March 23, 2012
Published online: July 10, 2012

CHEMISTRY
A EUROPEAN JOURNAL

Supporting Information

The Structural Diversity Triggered by Intermolecular Interactions between $Au^{I}S_2$ Groups: Aurophilia and Beyond

Mohammad-Reza Azani,[a] Oscar Castillo,[b] M Luz Gallego,[a] Teodor Parella,[c] Gabriel Aullón,[d] Olga Crespo,[e] Antonio Laguna,[e] Santiago Alvarez,*[d] Rubén Mas-Ballesté,*[a] and Félix Zamora*[a]

chem_201200999_sm_miscellaneous_information.pdf

CONTENTS

Crystallographic data

Table S1. Selected bond lengths (Å) for compounds **1** and **3**. [a]

Compound **1**		Compound **3**	
Au1–S11	2.316(4)	Au1–S1	2.313(4)
Au2–S12	2.276(5)	Au2–S2	2.309(5)
Au2-S21	2.283(5)	Au2–S3	2.306(5)
Au3-S22	2.296(5)	Au3-S4	2.305(4)
Au3-S32^{i}	2.291(4)	Au3-S5	2.297(4)
Au4-S31	2.296(5)	Au4-S6	2.298(4)
Au5-S41	2.314(5)	Au4-S7	2.298(4)
Au6-S42	2.281(6)	Au5-S8	2.287(5)
Au6-S51	2.287(5)	Au5-S9	2.289(4)
Au7-S52	2.295(5)	Au6-S10	2.304(4)
Au7-S62^{ii}	2.308(5)	Au1-Au2	2.9615(6)
Au8-S61	2.310(6)	Au2-Au3	2.9874(9)
Au1-Au2	2.9685(8)	Au3-Au4	2.9927(8)
Au2-Au3	2.9836(9)	Au4-Au5	3.0285(9)
Au3-Au4	2.9757(8)	Au5-Au6	2.9833(6)
Au5-Au6	2.9653(7)		
Au6-Au7	3.0334(9)		
Au7-Au8	2.9910(7)		

[a] Symmetry codes: (i) 1-x, y, -z+1/2; (b) 1-x, y, -z-1/2.

Table S2. Selected bond lengths (Å) for compounds **4** and **6**. [a]

Compound **4**		Compound **6**	
Au1–S1	2.300(5)	Au1–S1	2.291(7)
Au1–S3	2.310(5)	Au1–S2	2.274(7)
Au2-S2	2.296(5)	Au2–S3	2.289(7)
Au2-S4	2.299(5)	Au2-S4	2.312(7)
Au1-Au2	2.8414(10)	Au1-Au2	2.8494(15)

[a] Symmetry codes: (i) 1-x, y, -z+1/2; (b) 1-x, y, -z-1/2.

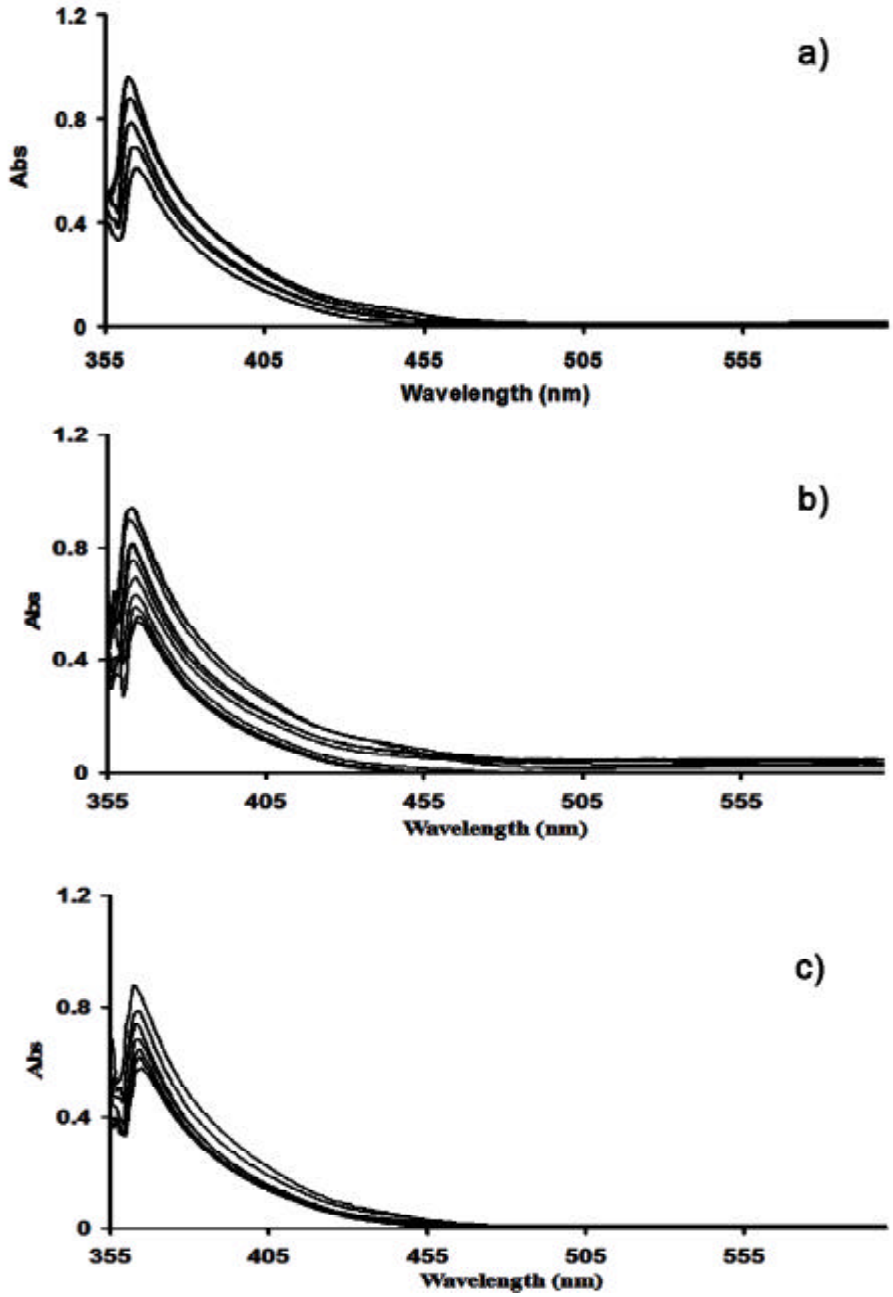

Figure S1. Variable-temperature UV-vis spectra, using a cell with an optical path of 0.2 cm, for 2.5 mM solutions in CS_2 of a) compound **4** (20 to -60ºC); b) compound **5** (20 to -60ºC); c) compound **6** (20 to -40ºC) .

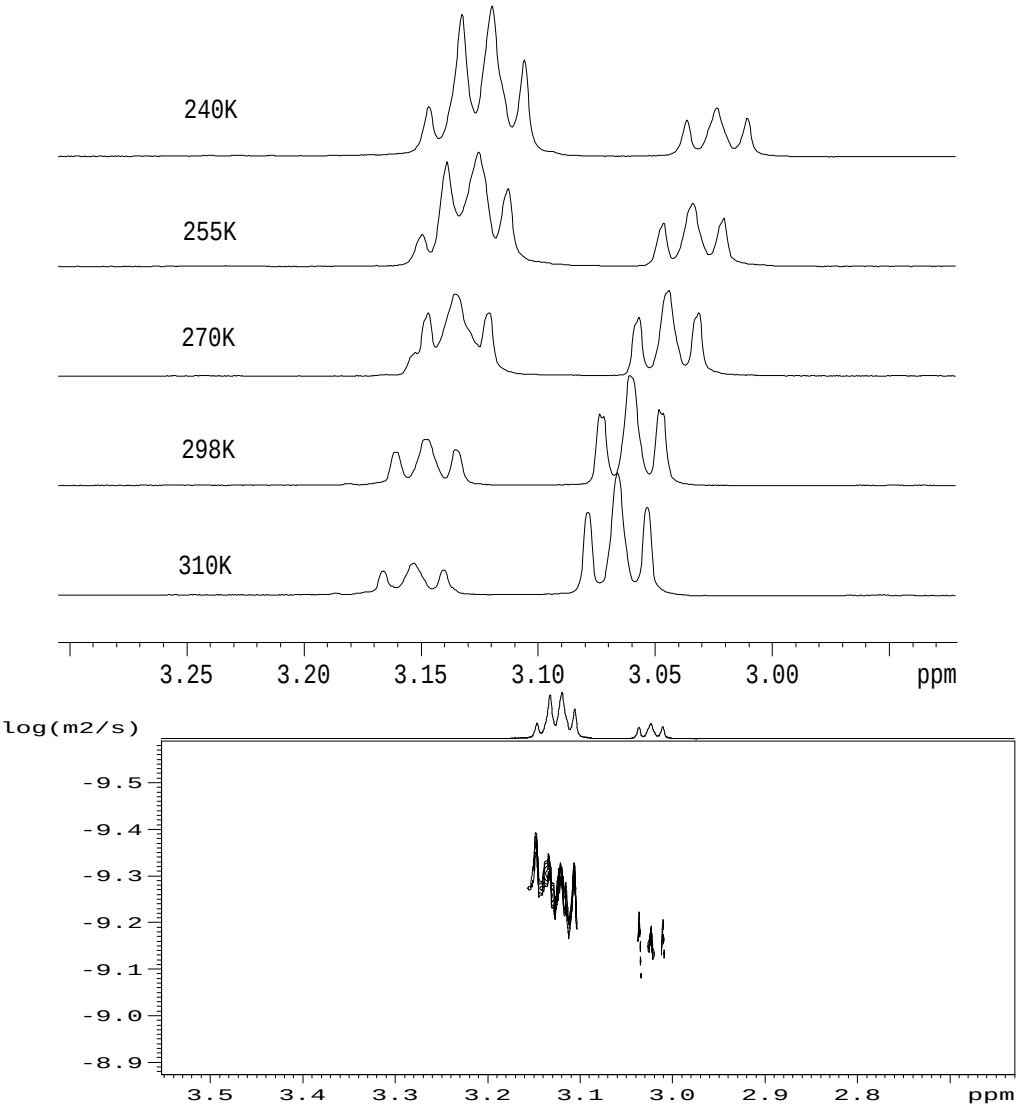

Figure S2. Variable-temperature ^{1}H and DOSY NMR spectrum at 240K of a solution of **1** in a mixture of $CS_2/CDCl_3$.

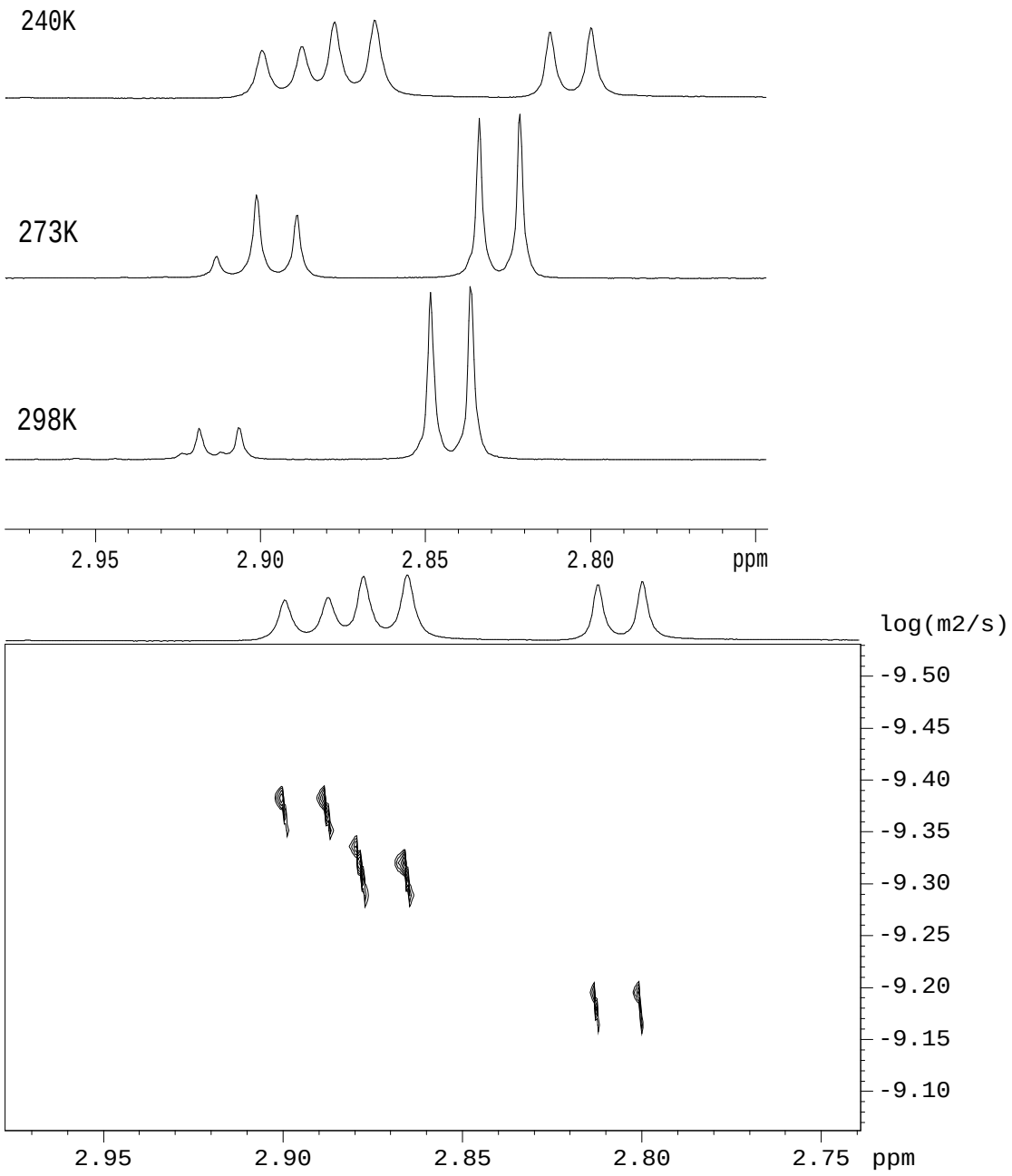

Figure S3. Variable-temperature ^{1}H and DOSY NMR spectrum at 240 K of a solution of **2** in a mixture of $CS_2/CDCl_3$.

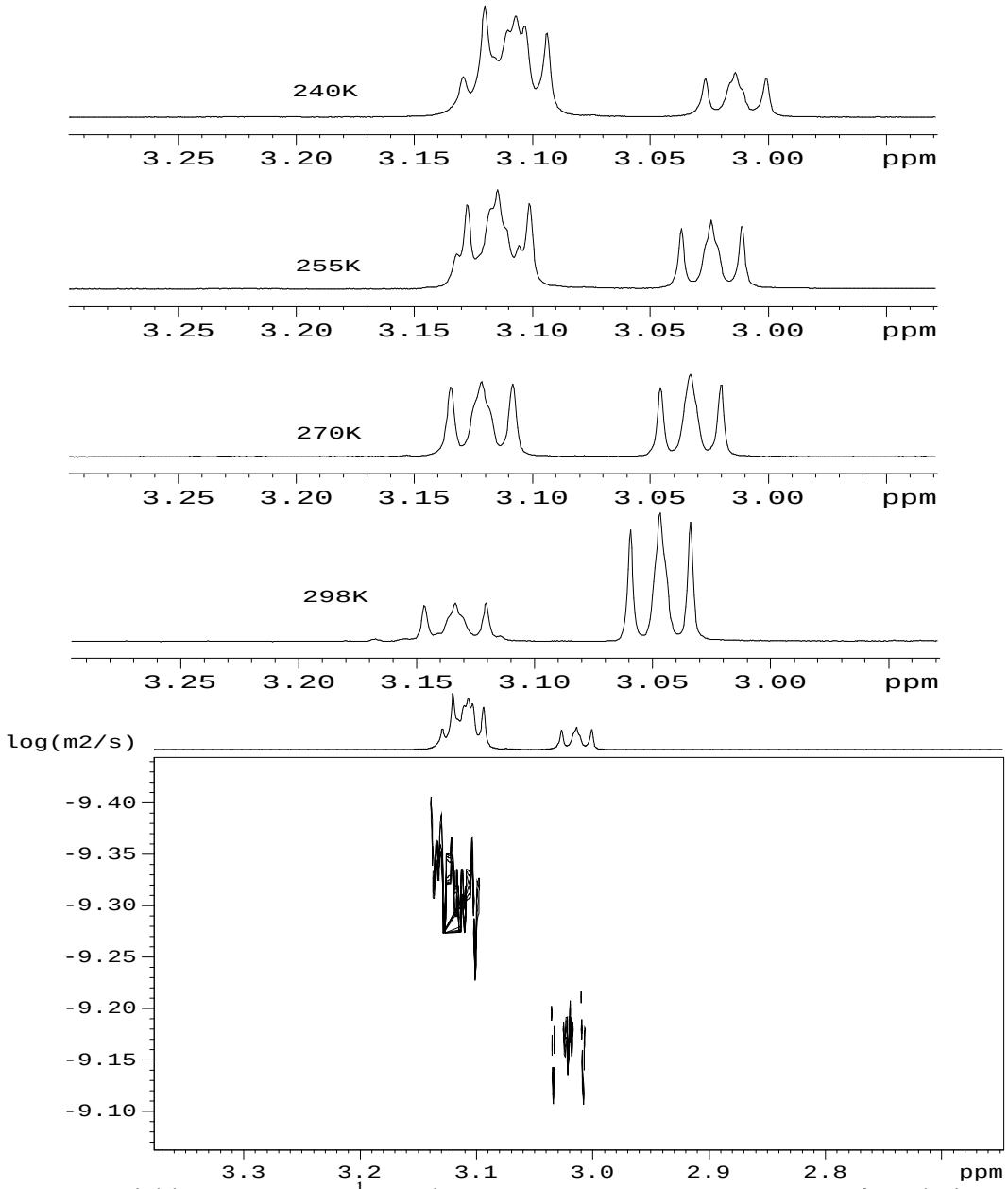

Figure S4. Variable-temperature ^{1}H and DOSY NMR spectrum at 240 K of a solution of **3** in a mixture of $CS_2/CDCl_3$.

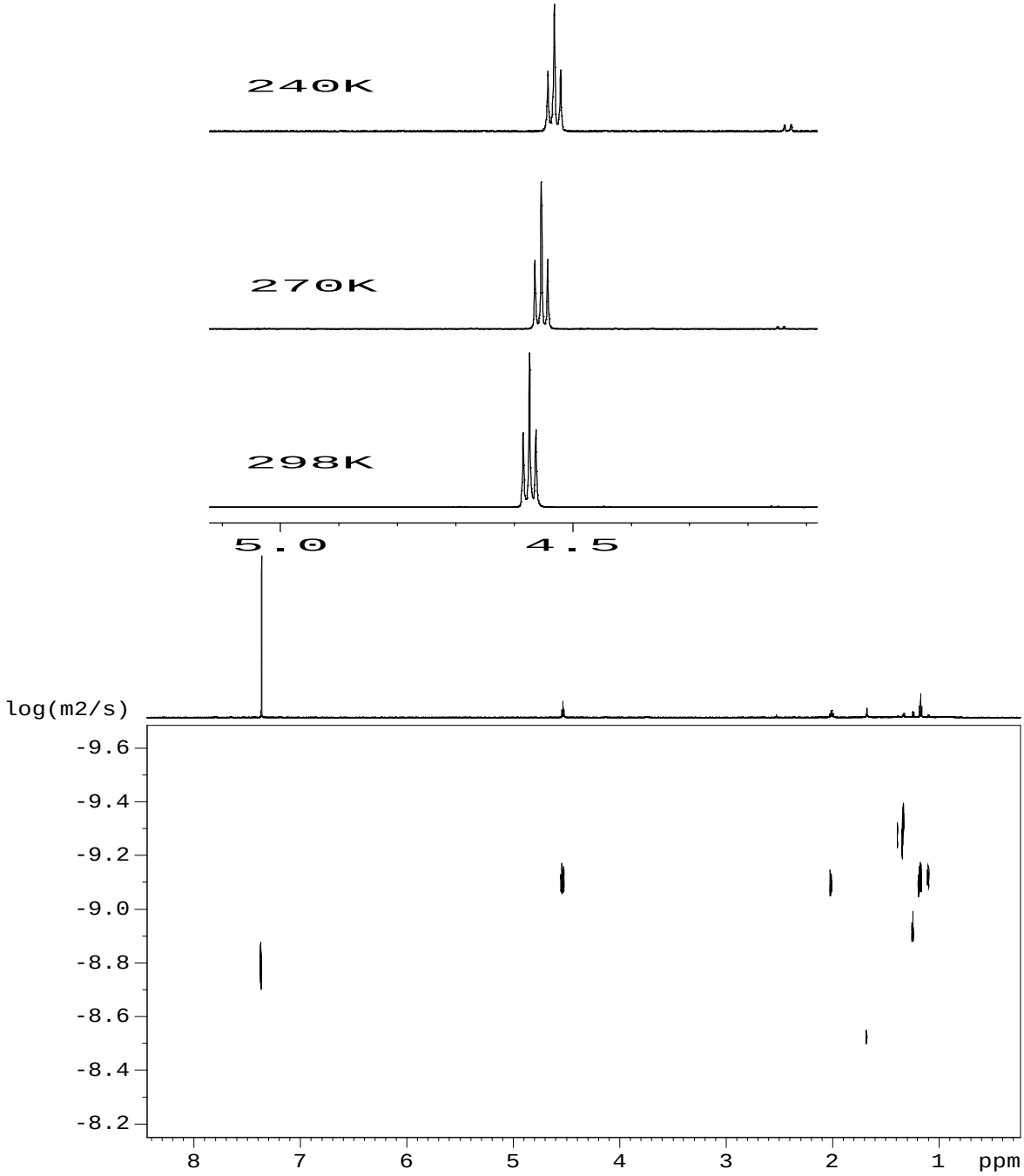

Figure S5. Variable-temperature ^{1}H and DOSY NMR spectrum at 240K of a solution of **4** in a mixture of $CS_2/CDCl_3$.

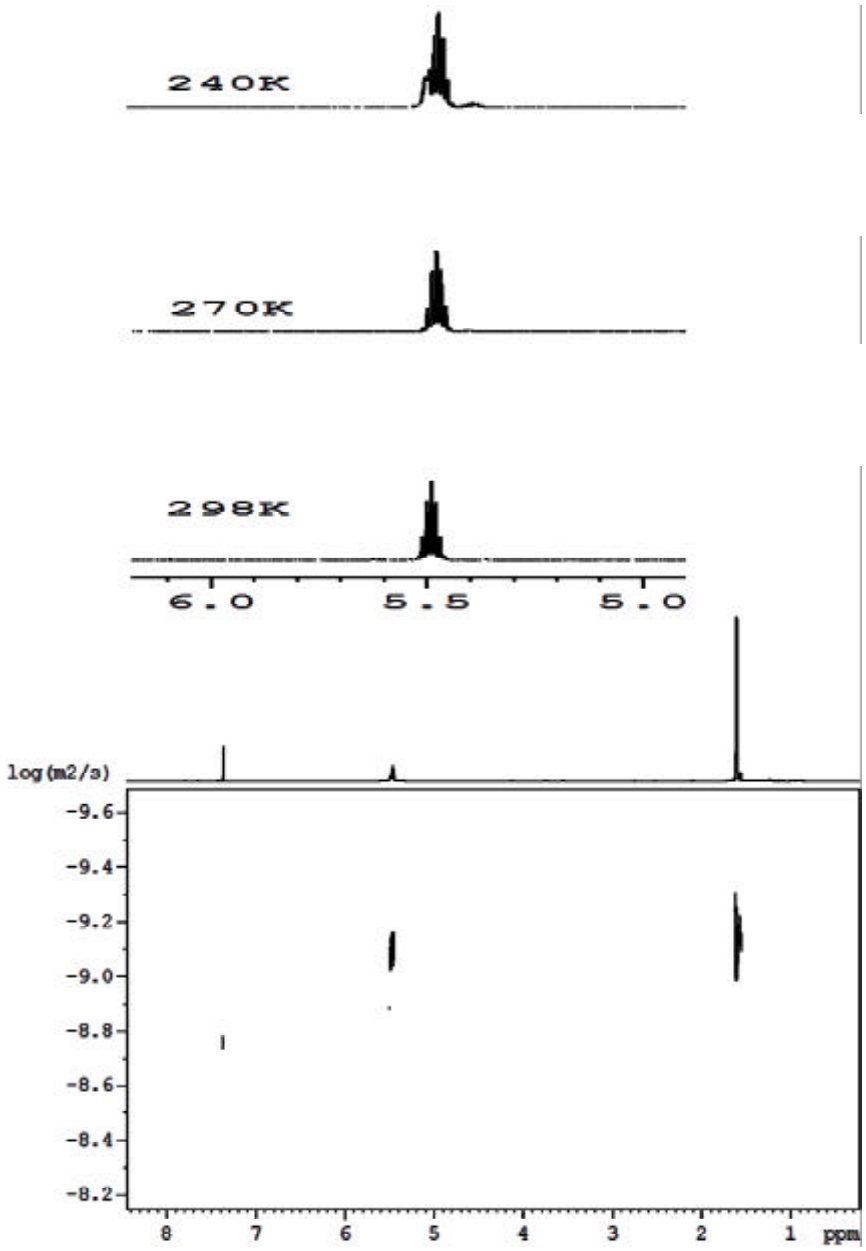

Figure S6. Variable-temperature ^{1}H and DOSY NMR spectrum at 240 K of a solution of **5** in a mixture of $CS_2/CDCl_3$.

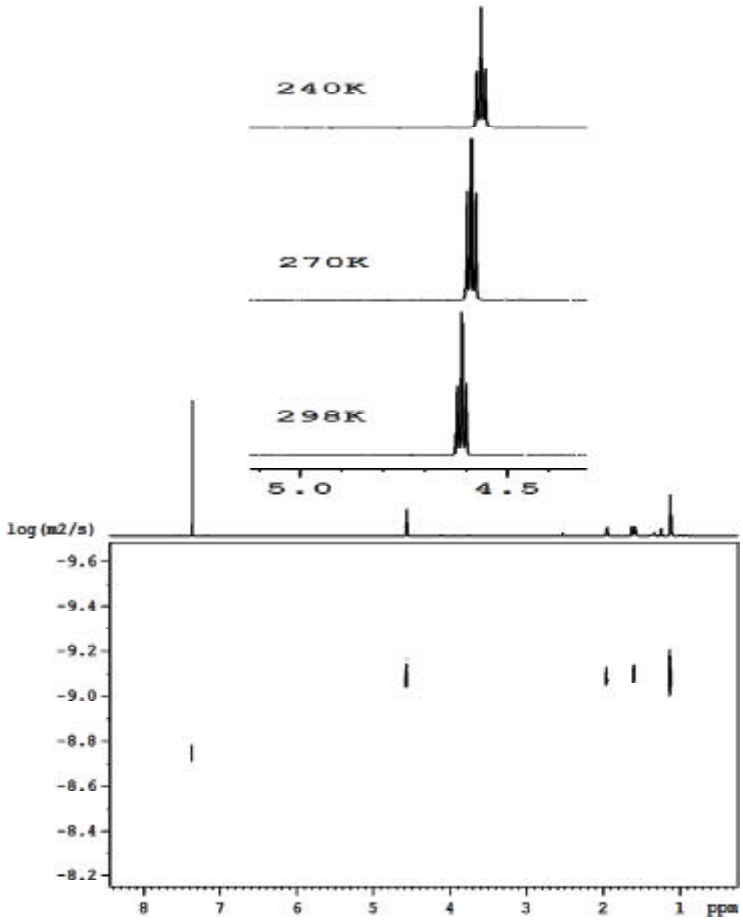

Figure S7. Variable-temperature ^{1}H and DOSY NMR spectrum at 240K of a solution of **6** in a mixture of $CS_2/CDCl_3$.

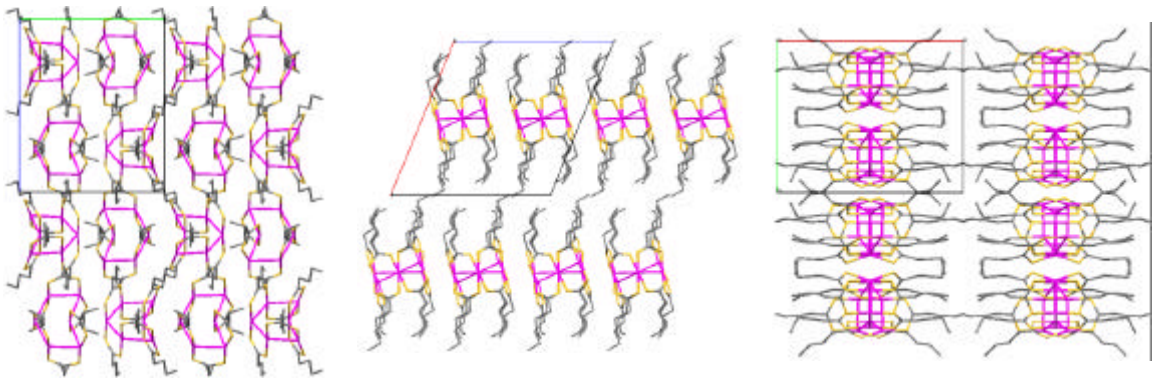

(a) (b) (c)

Figure S8. Projections of the crystal packing of compound 1 along the crystallographic axis a (a), b (b) and c (c). The disorder of the aliphatic chains has been omitted for clarity.

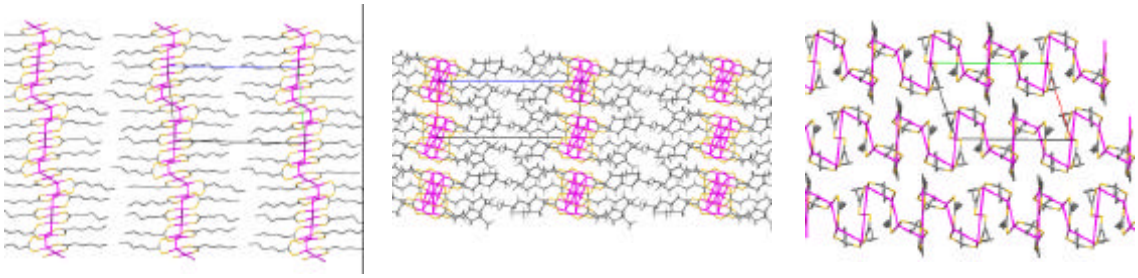

(a) **(b)** **(c)**

Figure S9. Projections of the crystal packing of compound **3** along the crystallographic axis a (a), b (b) and c (c).

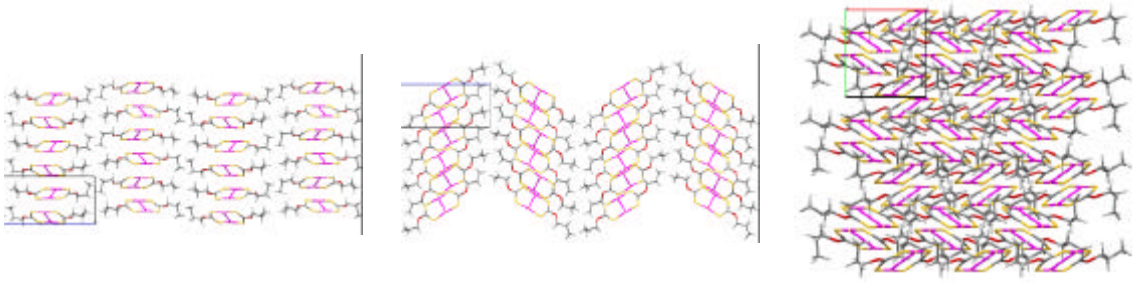

(a) (b) (c)

Figure S10. Projections of the crystal packing of compound **4** along the crystallographic axis a (a), b (b) and c (c).

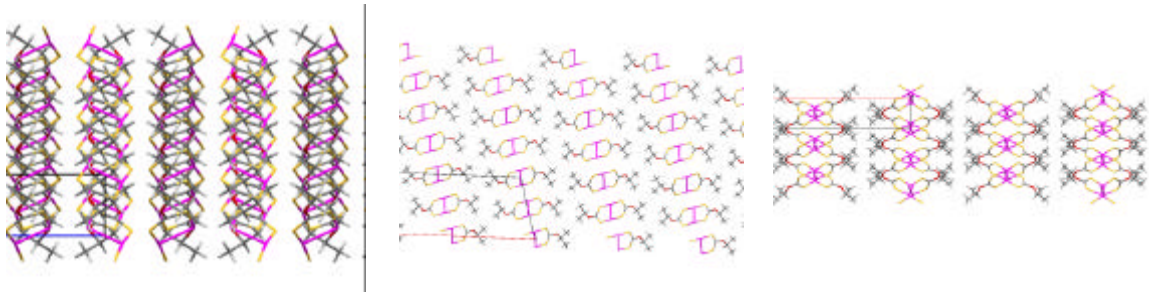

(a) (b) (c)

Figure S11. Projections of the crystal packing of compound **5** along the crystallographic axis a (a), b (b) and c (c).

Article 2

Title: Supramolecular Assembly of Diplatinum Species through Weak PtII···PtII Intermolecular Interactions: A Combined Experimental and Computational Study

Autors: Alejandro Pérez Paz, Leonardo A. Espinosa Leal, Mohammad-Reza Azani, Alejandro Guijarro, Pablo J. Sanz Miguel, Gonzalo Givaja, Oscar Castillo, Rubén Mas-Ballesté*, Félix Zamora* and Angel Rubio*

Journal: Chemistry - A European Journal

Year: 2012

Volume / Pages: 18 (43) / 13787-13799.

CHEMISTRY
A EUROPEAN JOURNAL

FULL PAPER

DOI: 10.1002/chem.201201962

Supramolecular Assembly of Diplatinum Species through Weak $Pt^{II}\cdots Pt^{II}$ Intermolecular Interactions: A Combined Experimental and Computational Study

Alejandro Pérez Paz,[a] Leonardo A. Espinosa Leal,[a] Mohammad-Reza Azani,[b] Alejandro Guijarro,[b] Pablo J. Sanz Miguel,[b] Gonzalo Givaja,[b] Oscar Castillo,[c] Rubén Mas-Ballesté,*[b] Félix Zamora,*[b] and Angel Rubio*[a]

Abstract: The present study elucidates the factors that govern the spontaneous self-assembly of a family of dimetal $[Pt_2L_4]$ (L = dithiocarboxylato ligand) complexes. Experimental data show that variables such as temperature, concentration, solvent and the nature of the ligand L have a critical effect on the reversible self-assembly of supramolecular $[Pt_2L_4]_n$ entities. In solution, new UV/Vis spectroscopic features emerge at low temperatures and/or high concentrations, which are attributed to the formation of oligomeric $[Pt_2L_4]_n$ species. The description of intermolecular Pt···Pt interactions, the main driving force for the association, was addressed from a computational perspective. The contributions from intermolecular Pt···S and S···S interactions to these supramolecular assemblies were found to be repulsive. Experimental UV/Vis data have been interpreted by means of computational spectroscopy.

Keywords: computational chemistry · density functional calculations · metal–metal interactions · platinum · supramolecular chemistry

Introduction

A main goal in supramolecular chemistry is the understanding of weak intermolecular interactions that can result in self-assembly processes.[1] Although hydrogen bonding has been widely studied, other interactions such as weak metal–metal interactions remain less explored.[2] Among these, the tendency of gold compounds to aggregate through Au−Au bonds is the most familiar phenomenon, known as aurophilicity.[3] However, this is not the only metal–metal supramolecular interaction, and weak $d^{10}\cdots d^{10}$ bonding has also been observed for Ag^I and Cu^I centres.[4] Similarly, $d^8\cdots d^8$ interactions have been reported for some Pt^{II} compounds. This weak metal–metal interaction can result in columnar stacks formed by one-dimensional chains of aligned coordination complexes (Scheme 1).[5]

The linear structures formed by the stacking of square-planar monomer complexes have shown interesting properties. For example, tetracyanoplatinates, $K_2Pt(CN)_4X_{0.3}\cdot n H_2O$ (X = Cl, Br, $n = 3$), commonly called KCPs, were one of the first examples showing electrical conductivity.[6] These systems are formed by the stacking of square-planar $[Pt(CN)_4]^{n-}$anion complexes.[7] The structures are formed by

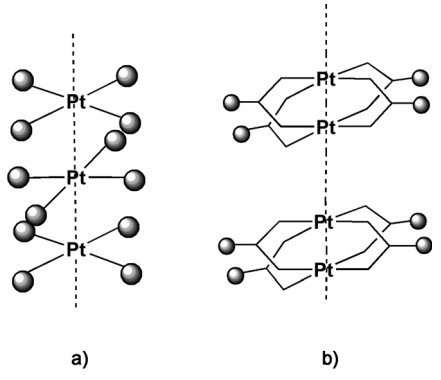

Scheme 1. Schematic illustration of the columnar structures originating from the stacking of a) square planar mononuclear platinum complexes and b) dinuclear complexes.

[a] Dr. A. Pérez Paz, L. A. Espinosa Leal, Prof. A. Rubio
Nano-Bio Spectroscopy Group and
ETSF Scientific Development Centre
Departamento de Física de Materiales
Universidad del País Vasco
Centro de Física de Materiales
CSIC-UPV/EHU-MPC and DIPC
Av. Tolosa 72, 20018 Donostia, San Sebastián (Spain)
E-mail: angel.rubio@ehu.es

[b] M.-R. Azani, Dr. A. Guijarro, Dr. P. J. Sanz Miguel, G. Givaja, Dr. R. Mas-Ballesté, Dr. F. Zamora
Departamento de Química Inorgánica
Universidad Autónoma de Madrid, 28049 Madrid (Spain)
E-mail: ruben.mas@uam.es
felix.zamora@uam.es

[c] Dr. O. Castillo
Departamento de Química Inorgánica
Facultad de Ciencia y Tecnología
Universidad del País Vasco, UPV/EHU
Apartado 644, 48080 Bilbao (Spain)

Supporting information for this article is available on the WWW under http://dx.doi.org/10.1002/chem.201201962.

CHEMISTRY
A EUROPEAN JOURNAL
ChemPubSoc Europe

the overlapping of $5d_{z^2}$ orbitals, which are strongly affected by the Pt–Pt intermolecular distances. The anisotropic conductive properties of the KCPs are connected to their metal–metal distances. The electrical conductivity for the $K_2[Pt(CN)_4]$ (5×10^{-7} S cm^{-1}) is substantially increased upon partial oxidation of the KCPs. This is related to a shortening of the Pt–Pt distances, which become close to what is found in the platinum metal (2.78 Å). KCP-based materials represent the first inorganic "molecular wires" ever designed.[8]

In a similar approach, analogous columnar systems have been formed with dimetallic precursors.[9] These discrete dinuclear complexes with intermolecular metal–metal interactions have fascinating magnetic and electrical properties.[2b] Some of them have been shown to be suitable as precursors for weakly bound one-dimensional metal chains.[10] Recently, it has been shown that linear arrangements in crystalline samples of such compounds can result on different conductivity properties, which are highly dependent on the Pt···Pt distances determined by the nature of the dithiocarboxylato ligands. In a previous report, it has been demonstrated that the compound $[Pt_2(S_2C(CH_2)_5CH_3)_4]$ undergoes reversible aggregation processes in solution as observed by a characteristic thermochromic behaviour.[11] More recently, we have reported that such aggregations also occur in compound $[Pt_2(S_2CCH_3)_4]$ and that can trigger the formation of nanofibers on surfaces.[10a]

A deeper understanding of the chemical principles that direct such assemblies is of great interest due to the potential impact on the bottom-up assembly of conductive 1D nanostructures of these principles. This work aims to provide answers by means of a combination of experimental and theoretical insights to hitherto unexplored points concerning supramolecular assembly. Specifically, the factors (nature of ligands, solvents and other physical parameters) that have an influence on such self-associations are explored. The results observed in solution will be discussed and related with the structures found in the monocrystals. In addition, novel insights on the molecular and electronic structures of supramolecules in solution are presented and related with their spectroscopic features.

Results and Discussion

Crystal structure of compounds 1 and 2: All the reported crystal structures for compounds of the formula $[Pt_2L_4]$ show linear arrangements that are directed by intermolecular $Pt^{II}\cdots Pt^{II}$ interactions.[12] There is only one exception to this tendency for a polymorph reported of $[Pt_2(S_2CCH_3)_4]$, which does not show short Pt···Pt distances.[13] In contrast, in this structure Pt···S distances of 3.51 Å can be found. These values were previously interpreted as evidence that Pt···S interactions directed the packing of $[Pt_2(S_2CCH_3)_4]$ units. However, such long distance is in the limit of what can be considered as weak interaction and probably is just the result of packing effects in the condensed phase. Below, the possibility of Pt···S interactions are discussed from a theoretical perspective. On the other hand, in the rest of the reported structures, the metal···metal distances fall in the range between 3.08 and 3.39 Å, below the sum of their van der Waals radii (3.5 Å). As shown in Table S2 in the Supporting Information, such distances depend on the nature of the organic fragment attached to the dithiocarboxylate group. Bulkier ligands, such as C_6H_{11}–CS_2^- or $(CH_3)_2CH$–CH_2–CS_2^-, result in longer intermolecular Pt···Pt distances.

In this work, the crystal structure of two new $[Pt_2L_4]$ complexes has been determined. In particular two $[Pt_2L_4]$ (L = C_4H_9–CS_2^-) complexes have been studied: one with the linear alkyl chain ($CH_3(CH_2)_3$–CS_2^-) and the other with a branched alkyl group ($(CH_3)_2CHCH_2$–CS_2^-). The intermolecular Pt···Pt distances observed in these two new structures are very different depending on the steric hindrance imposed by the ligand. Thus, for the complex with the linear alkyl chain a Pt···Pt distance of 3.12 Å is found, whereas for the branched isomer this distance increases up to 3.26 Å. The possible relation of this effect with the behaviour in solution is discussed below.

The crystal structures of compounds **1** and **2** consist of quasi-one-dimensional chains based on collinear alignment of $[Pt_2(S_2CR)_4]$ dinuclear entities with short intra- and interdimeric Pt–Pt distances (Figure 1). The dinuclear entities

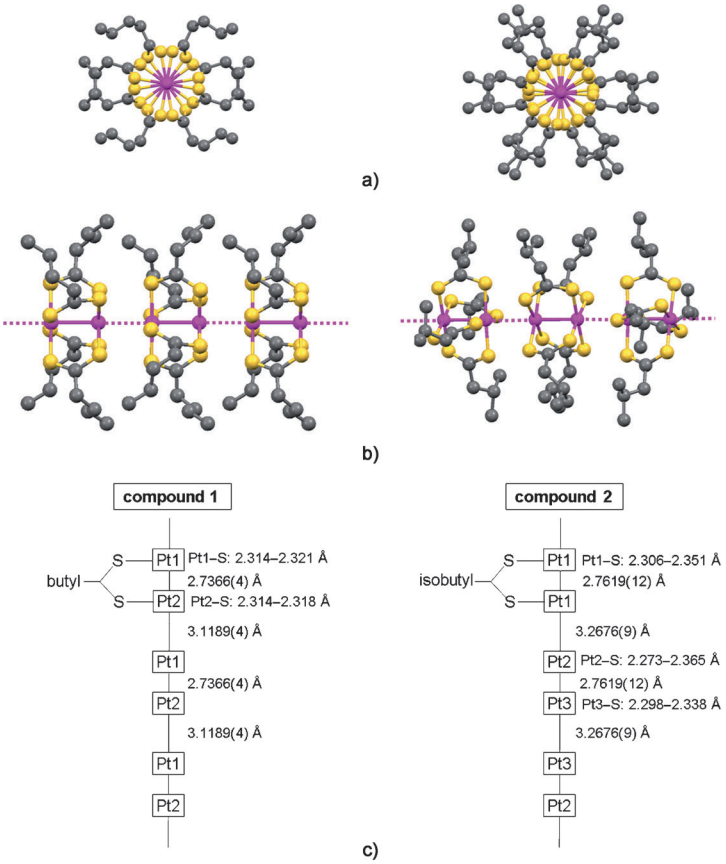

Figure 1. a) Front view, b) side view and c) structural parameters of the quasi-one-dimensional chains present in compounds **1** and **2**. The hydrogen atoms have been omitted for clarity (magenta = Pt, grey = C, yellow = S).

show a windmill-shaped arrangement in which four μ-dithiocarboxylato-κS:κS' ligands bridge two Pt^{II} centres with a metal···metal distance in the range 2.737–2.768 Å. The metal coordination environment consists of four sulphur atoms defining the equatorial plane from which the platinum atoms deviate 0.051–0.064 Å inwards from the dimer. Above and below this plane, there are placed the other platinum atom of the dimer and a platinum atom from the next dinuclear unit. The two PtS_4 squares of the dinuclear entity are rotated by 21.72–26.04° from the eclipsed arrangement. The complexes are stacked collinearly along the intradinuclear Pt–Pt axis by means of short interdimer Pt–Pt distances: 3.119–3.337 Å. Adjacent PtS_4 squares belonging to different dimers are also rotated by 44.08–44.44° for compound **1** and 32.61–38.68° for compound **2**. The analysis of the crystal structure of these compounds together with the previously published examples of diplatinum dithiocarboxylate chains suggests that the steric hindrance of the substituents of the dithiocarboxylato ligands influences the interdimeric Pt···Pt distances: the bulkier is the substituent, the longer is the interdimer Pt···Pt distance 3.119 (**1**) versus 3.268 Å (**2**).

Supramolecular assembly of compound 3 in CH_2Cl_2: In addition to the complexes with the novel structures reported herein, we included in this study the complex $[Pt_2(S_2C(CH_2)_4CH_3)_4]$ (**3**). A crystal structure of this compound has been previously reported in a recent work.[10b] In the present study, compound **3** offers the advantage of its high solubility, which allowed the study of self-aggregation in solution in a wide range of concentrations avoiding precipitation processes.

Figure 2 shows the thermochromic behaviour observed in 2–0.2 mM solutions of **3** in CH_2Cl_2. By decreasing the temperature, a new broad band appears in the red/near-infrared region as observed previously for complexes $[Pt_2(S_2C(CH_2)_5CH_3)_4]$ and $[Pt_2(S_2CCH_3)_4]$.[11] This is a very wide band that disappears upon heating and re-appears when the solution is cooled down again. The dependence upon the concentration of such absorbance indicates that it is due to reversible aggregation processes in solution. Similar observations for complex $[Pt_2(S_2C(CH_2)_5CH_3)_4]$ were previously proposed as a result of an equilibrium between the species $[Pt_2L_4]$ and $[Pt_2L_4]_2$.[11] However, our detailed studies of this phenomenon indicate that a more complex scenario should be considered. In fact, the gradual redshift of the appearing band while decreasing the temperature suggests, according to our theoretical results, that the average size of the supramolecular entities present in solution increases at lower temperatures.

A first attempt to characterise the species $[Pt_2L_4]_n$ ($n=1$, 2, …) present in solution was carried out by means of variable-temperature (VT)-^{1}H NMR measurements. Unfortunately, lowering the temperature did not allow us to distinguish signals from different oligomers. The only variation observed in the ^{1}H NMR spectra while decreasing the temperature, is the widening of signals, which is especially dramatic for the signal corresponding to the protons closer to the platinum centres (Figure S1 in the Supporting Information). Such an effect could be explained by the dynamic behaviour of this system that results in fast chemical exchange, together with the expected increase of the viscosity of the solvent at lower temperatures. Accordingly, theoretical calculations performed with the species $[Pt_2(S_2CCH_3)_4]$ and $[Pt_2(S_2CCH_3)_4]_2$ (see below) suggest that protons remote from the Pt centres by four bonds are insensitive to association processes.

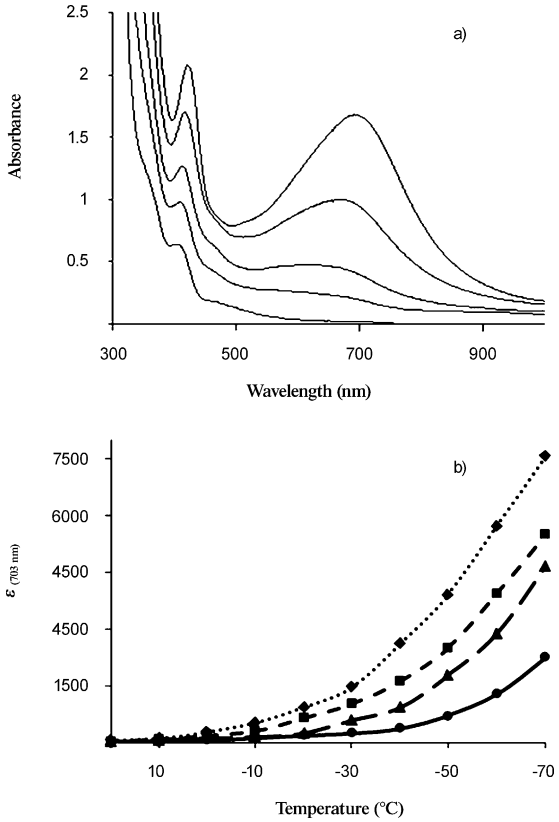

Figure 2. a) UV/Vis measurements for a 2 mM solution of **3** in CH_2Cl_2 at temperatures from 20 to −60°C (difference between spectra is 20°C). b) Concentration–temperature (20 to −60°C) dependence of the relative absorbance observed at $\lambda=703$ nm (◆=2, ■=1, ▲=0.5, and ●=0.2 mM).

A detailed comparison of UV/Vis features observed in 2 and 0.2 mM solutions of **3** in CH_2Cl_2, allows us to note that, by decreasing the concentration, not only a decrease of the relative intensity is observed, but also a change in the wavelength range where this absorbance can be observed (Figure 3). Although for concentrated solutions a wide band in the range of 500–1000 nm appears at low temperature, a narrower band is observed for diluted solutions. This difference is attributed to the overlap of different absorption bands due to different species with a diverse degree of nuclearity generated at low temperature for concentrated solutions. However, for diluted conditions, a narrower distribution of nuclearities should be present in solution. This interpretation is further supported by the theoretical simulation of the optical features of the species $[Pt_2(S_2CCH_3)_4]_n$ ($n=1$–4) (see below).

CHEMISTRY
A EUROPEAN JOURNAL

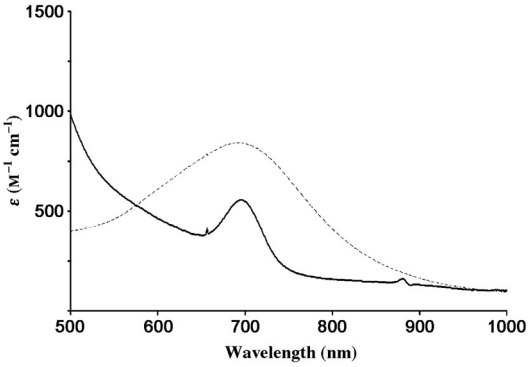

Figure 3. Comparison of the relative absorbance in the range 500–1000 nm observed for a 0.2 mM solution of **3** in CH_2Cl_2 at −70 °C (bold line) and that observed for a 2 mM solution (dashed line).

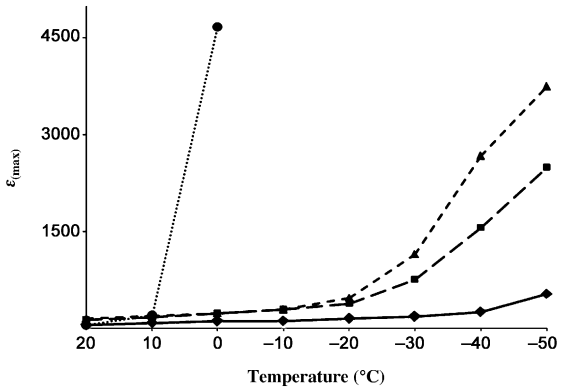

Figure 4. Measured temperature dependence of the absorbance in the near-infrared region of compounds **1**–**3** (0.5 mM, ▲=**1**, ◆=**2**, ■=**3**) and $[Pt_2(S_2CCH_3)_4]$ (0.2 mM; ●) in CH_2Cl_2. For each compound, the respective maximum is taken into account.

Supramolecular assembly of compounds 1, 2 and 3—effect of the ligand: The ability of compound **3** to self-assemble in solution has been compared with that of compounds **1** and **2**. This comparison offers a new tool to evaluate the factors that have an effect on the aggregation of compounds of the general formula $[Pt_2L_4]$. A first difficulty that appears in this comparative study is the different solubility that each compound can offer in a common solvent such as CH_2Cl_2. Thus, in all cases, it is not possible to force the conditions (temperature and concentration) to maximise aggregation. In the present study the compound most reluctant to precipitate is compound **3**, for which it is possible to reach a major degree of aggregation at low temperature and high concentration. However, under the same conditions, when no precipitation is observed for any of the compounds studied, compound **3** is not the one that shows a major tendency to aggregate.

The effect of the ligand can be primarily discussed regarding the results obtained in CH_2Cl_2. Figure 4 represents the temperature dependence of the molar absorptivity of the signal at around 700 nm that appears at low temperatures in a 0.5 mM solutions of compounds **1**–**3**. For comparison, the data obtained for a 0.2 mM solution of $[Pt_2(S_2CCH_3)_4]$ in CH_2Cl_2 previously reported are also included.[10a] Interestingly, there is an evident effect of the ligand that can be related to the steric hindrance that each dithiocarboxylato ligand present in solution. Thus, for R−CS_2 when R = CH_3 association in solution is observed at temperatures not far from room temperature (≈0 °C). It is worth noting that compound $[Pt_2(S_2CCH_3)_4]$ has a poor solubility. As a consequence, only diluted solutions (≈0.2 mM) of this compound could be analysed. However, even at such low concentration association in solution is easier than with any other diplatinum complex. In contrast, for bulkier ligands much lower temperatures are needed to trigger self-assembly. The behaviour of compounds **1**–**3** can be rationalised in terms of the effective bulkiness of the dithiocarboxylato ligand in solution. When the ligand contains a branched R group (compound **2**) the approaching of the dimetal units is definitively more difficult than for compounds **1** and **3**, which contain linear R groups. Between compounds **1** and **3**, supramolecular assembly is favoured for compound **1**, because the R group is a shorter chain. It is also interesting to compare these tendencies with the trend that the intermolecular Pt···Pt distances in the single crystals follows (Table S2 in the Supporting Information). For compounds $[Pt_2(S_2CCH_3)_4]$, **1** and **3**, this distance is practically indistinguishable, which is in contrast with the different tendency to aggregate in solution. This apparent contradiction is easily rationalised by taking into account that the steric hindrance of the ligands has not the same effect in solution than in the crystalline samples. Ordered packing minimises steric repulsive interactions especially where linear alkyl chains are present in the structure. However, free motion of such chains in solution provokes significant hindrance, which increases with the length of the alkyl group. This concept is less applicable to branched chains (as in compound **2**), which present a high steric hindrance in solution that cannot be as well overcome in the ordered packing of the crystalline samples.

Supramolecular assembly of compounds 1–3 in $CHCl_3$, THF and CS_2—effect of solvent: The effect of the solvent in self-assembly of compounds **1**–**3** in solution has been examined by comparing the behaviour of the solutions by using CH_2Cl_2, $CHCl_3$, THF and CS_2 as solvent. Compounds **1**–**3** show comparable trends. For clarity, the discussion is centred on the results found for complex **3** (for results obtained by using complexes **1** and **2**, see Figures S2 and S3 in the Supporting Information). Figure 5 shows the UV/Vis spectra of 1 mM solutions of compound **3** in the different solvents at −50 °C, which is the limit temperature that prevents precipitation in all investigated solvents. It is worth to note that the solubility in CS_2 and THF is greater than in $CHCl_3$, allowing measurements at temperatures as low as −100 °C, where some supramolecular association is observed (Figures S4–S6 in the Supporting Information). However, to compare the inherent ability of compound **3** to associate in solution in different solvents, unique conditions (such as shown in Figure 5) have to be used. Thus, under the same conditions,

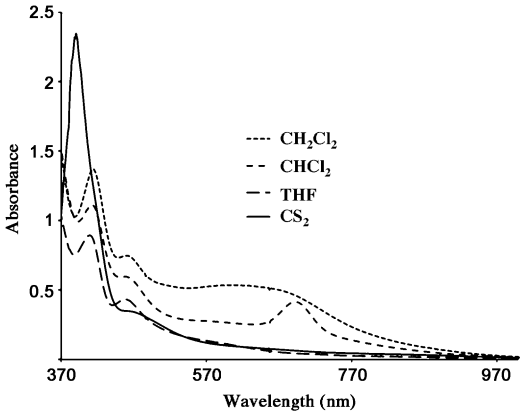

Figure 5. UV/Vis measurements for 1 mM solutions of **3** in CH_2Cl_2, $CHCl_3$, CS_2 and THF at −50 °C.

whereas a certain degree of self-assembly in CH_2Cl_2 and (in less extent) in $CHCl_3$ is observed, CS_2 and THF hamper the association in solution. This effect could, in principle, be justified considering the known coordinative ability of such solvents, which can result in weak metal–ligand interactions between the solvent molecules and the platinum centres. In addition, solvation effects could also account for the observed trend. In any case, when the temperature is low enough, new features in the visible region appear, indicating a certain degree of self-assembly. In THF and CS_2 the new maximum absorbance appear at higher energies, which, in accordance with theoretical calculations (see below), is indicative for lower degrees of aggregation (Figures S4–S6 in the Supporting Information).

To test the conjecture that the solvent competes for coordinating $[Pt_2L_4]$, we have performed geometry optimisations of one solvent molecule (THF and CS_2 were considered) with one $[Pt_2L_4]$ monomer frozen at its experimental structure (see the Supporting Information for the relaxed structures). The calculations were performed by using the PBE exchange correlation functional.[14] For THF, we observed a clear attractive interaction between its oxygen atom and the Pt centre of the monomer (distance Pt···O = 3.15 Å). For CS_2, we found that only a linear configuration; that is, Pt-Pt···S-C-S, leads to a stable van der Waals complex (Pt···S = 3.52 Å), whereas the perpendicular configuration is repulsive.

Despite the lower solubility in $CHCl_3$, it is possible to note a greater tendency of **3** to aggregate in this solvent than in CS_2 and THF. However, CH_2Cl_2 is still the solvent that maximises the self-assembly. The near-infrared feature observed at low temperature for 1 mM solutions of compound **3** in $CHCl_3$ is symmetric and narrower than that observed in CH_2Cl_2 under the same conditions. Thus, $CHCl_3$ solutions at low temperature seem to generate a more limited number of species than that in CH_2Cl_2. Interestingly, 1 mM solutions in $CHCl_3$ at −50 °C present a UV/Vis spectrum that is almost identical to the one observed for 0.2 mM solutions in CH_2Cl_2 at −60 °C. Thus, the data obtained suggest that, in comparison with what is observed in CH_2Cl_2, in $CHCl_3$ compounds of the formula $[Pt_2L_4]$ present a lower tendency to reversibly aggregate. As explained above, in this case the difference in polarity between both solvents, and thus their different ability to solvate the dimetal precursor $[Pt_2L_4]$, is probably the fact that determines the supramolecular aggregation to form oligomers of formula $[Pt_2L_4]_n$.

Theoretical modelling: In this section, we present an elaborate study of the ground- and excited-state properties of the Pt···Pt linear chain structures by using a combination of basis sets and (time-dependent)/density functional theory (TD)/DFT methodologies.[15] We analyse the performance of different numerical approaches in the description of the electronic and optical properties of various $[Pt_2L_4]_n$ clusters and offer a detailed explanation of the experimental results. To minimise calculation times, all calculations have been carried out with the representative compound $[Pt_2L_4]$ with $L = S_2CCH_3$.

The crystallographic data show that $[Pt_2L_4]$ forms stable chains in the solid phase. In solution, the formation of $[Pt_2L_4]_n$ aggregates is also observed. The stability of these supramolecular entities is due to persistent weak intermolecular metal···metal interactions, which are in general difficult to describe by standard DFT methods. In addition, the presence of heavy transition-metal atoms and the large size of the system render the modelling of such structures a challenge with current theoretical approaches. According to theoretical calculations, relativistic and electronic correlation effects are thought to be important in the stability of such aggregates.

To describe accurately the energetics of $[Pt_2L_4]$ dimerisation, our efforts demonstrate that it is necessary to use a complete basis set and to go beyond the widely used DFT methods. Thus, more sophisticated approaches are required to predict Pt···Pt bond lengths comparable with the available crystallographic experimental data. Theoretical insights on the molecular and electronic structures of $[Pt_2L_4]_n$ supramolecules, as well as further analysis of the electronic transitions responsible for UV/Vis spectra are accounted below.

Properties in the electronic ground state—structure and energetics: As discussed previously, the intermolecular association process occurs through weak $d^8 \cdots d^8$ interactions between Pt atoms. The $[Pt_2L_4]_2$ structure was optimised by using different exchange-correlation DFT functionals and basis sets. The binding energies (see the Supporting Information) have been obtained from optimisations starting from a structure rearranged to facilitate the Pt···Pt contacts. Calculations were corrected for the basis set superposition error (BSSE).[16] As shown in the Supporting Information, we found that DFT performs poorly at describing accurately the energetics of this kind of interactions and yields binding energies, which are greatly scattered. For example, the widely used exchange-correlation functionals BLYP and B3LYP[17] predict a repulsive interaction between the monomers, a situation that even the long-range corrected func-

tional CAM-B3LYP[18] is not able to correct. By using the experimental structure and the PBE[14] functional in the complete basis set limit, we obtained a reasonable binding energy of -1.44 kcal mol^{-1}. After extensive testing, we concluded that for the purpose of the present work, which is the characterisation of the spectral properties of weakly bound metal complexes, the PBE functional family (which includes its hybrid version PBE0[19]) is the best, providing a good compromise between accuracy and computing time.

Kawamura and co-workers[11] reported the only experimental estimate available for the dimerisation energy of $[Pt_2(S_2C(CH_2)_5CH_3)_4]$. According to that study, the dimerisation is moderately exothermic ($\Delta H = -13$ kcal mol^{-1}), but entropically disfavoured ($\Delta S = -0.041$ kcal mol^{-1}). The change in the Gibbs free energy at $-20\,^{\circ}C$ is approximately -2.63 kcal mol^{-1}. To put these numbers in context, they should be compared with the thermal energy at the same temperature (0.50 kcal mol^{-1}). This comparison shows the weakness of the Pt···Pt interaction, which is favoured at sufficiently low temperatures to overcome the entropic cost of self-association.

We explored the possibility that Pt···S could lead to the formation of $[Pt_2L_4]_n$ supramolecular structures. In principle, one would expect some kind of attraction between Pt and S atoms of adjacent monomers. However, in our calculations, we always found that intermolecular Pt···S interaction is a repulsive one in $[Pt_2(S_2C(CH_2)_5CH_3)_4]$ and never leads to a stable structure on its own. The lack of Pt···S donor–acceptor interactions is probably due to the fact the platinum-based empty orbitals are at energies very distant from that of sulphur-based full atomic orbitals.

Geometry optimisations at distinct Pt···Pt distances were performed by taking an eclipsed disposition of the sulphur atoms between monomers as starting structure. We observed that as the monomers are brought together, a relative rotation occurs between them so as to break the eclipsed conformation of adjacent sulphur groups. This is indicative that intermolecular S···S interactions become also repulsive at the Pt···Pt equilibrium distance in $[Pt_2L_4]_2$. The preferred structure adopts a staggered conformation and the dihedral angle agrees well with crystallographic data (the experimental dihedral angle S-Pt···Pt-S is 44^0). Thus, we emphasise that attractive Pt···Pt interactions are mainly responsible for the self-association of $[Pt_2L_4]$ species.

We also found a strong variation of the intramolecular Pt···Pt equilibrium distances, which are greatly scattered from 3.0 Å at the LDA level to 3.8 Å with the GGA functional (the sum of the van der Waals radii for Pt is 3.50 Å). For reasons that are still unclear, here we found that LDA (unlike GGA/hybrid functionals) seems to yield reasonable Pt···Pt intermolecular distances as already reported for aurophilic interactions[20] and for Pd^{II} and Pt^{II} pyrophosphato complexes.[21] In addition, we note that the equilibrium Pt···Pt distance becomes smaller when the geometrical optimisation is performed in the presence of dichloromethane as solvent with the PCM model. Given the difficulty of reproducing the experimental geometry (in particular, the Pt···Pt interaction) with DFT, we decided to use the crystallographic structure in most of our subsequent calculations.

A differential analysis of the charge redistribution due to dimerisation of $[Pt_2L_4]$ is shown in Figure 6. The charges were computed at the PBE0 level with the LANL2TZ basis set for platinum and 6-311+G** on the rest of atoms for the crystallographic $[Pt_2L_4]_2$ structure and its dissociated form. Upon binding, the natural population analysis[22] shows that the Pt atoms in the intermolecular region donate almost 0.05 electrons, which flow mostly to the nearby sulphur atoms, whereas the distant sulphur and methyl groups remain virtually unaffected by the dimerisation. Interestingly, this analysis highlights the leading role of the bridging ligands of the $[Pt_2L_4]_2$ dimetal structure in the assembly of $[Pt_2L_4]_n$ through Pt···Pt interactions. Specifically, NPA shows the ability of the sulphur atoms to accommodate a part of the charge donated by the platinum atoms resulting in a synergic effect in the stable linear structures. A similar behaviour is found for the Mulliken charge differential analysis (see the Supporting Information) but a more pronounced charge transfer between the atoms is observed.

The presence of dichloromethane as the solvent does not significantly change the charge differential analysis described above. The only difference is that the solvent indu-

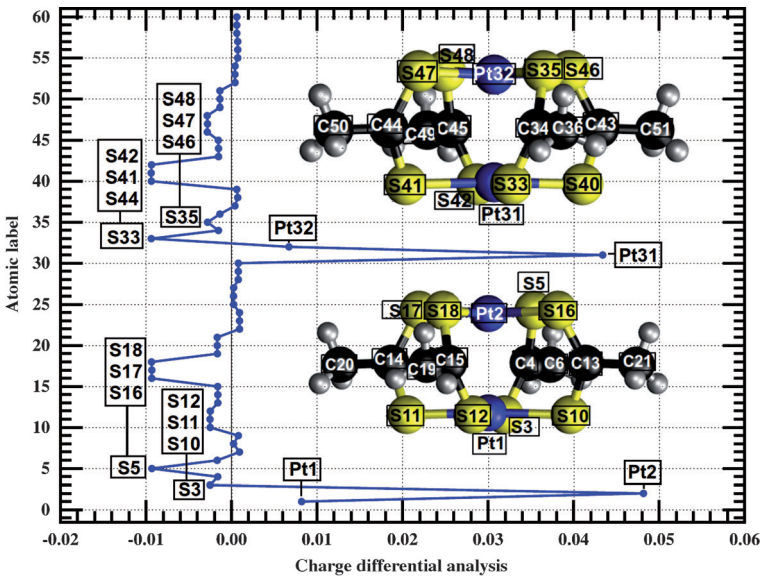

Figure 6. Calculated differential charges ($q_{exp} - q_{separated}$) by using NPA (natural population analysis) between the separated and the experimental $[Pt_2L_4]_2$ structure at the PBE0 level with the LANL2TZ basis set on all platinum atoms and 6-311+G** on the rest. Values were calculated by using the Gaussian 09 package.[23]

ces a somewhat larger charge separation in the polarisable atoms such as sulphur and also the carbon atoms directly attached to them.

It is worth mentioning that, from Figure 6, there is no appreciable change in the distribution of the charge in the methyl groups of $[Pt_2L_4]$ or $[Pt_2L_4]_2$ (and presumably of the larger linear chains). Thus, ^{1}H NMR spectroscopy is expected to be insensitive to follow the aggregation process, as we confirmed experimentally. Moreover, a theoretical determination of the ^{1}H chemical shift values shows no significant variation between the $[Pt_2L_4]$ and $[Pt_2L_4]_2$ proton signals (see the Supporting Information). Undoubtedly, the ^{195}Pt NMR technique would be better suited to monitor the self-association process between $[Pt_2L_4]$ monomers than ^{1}H NMR spectroscopy. However, our attempts to discern signals in experimental ^{195}Pt NMR data in this system were unsuccessful, probably due to a fast chemical exchange behaviour.

As a first approach to understand the electronic description of the Pt···Pt bonding between monomer species, Figure 7 shows the energy variation of selected Kohn–Sham molecular orbitals with the Pt···Pt distance in a $[Pt_2L_4]_2$ system. The energies and orbitals are computed at the PBE level on a real space grid by using the OCTOPUS code.[24] The first thing to notice is that the energy and the shape of the displayed unoccupied orbitals are practically independent of the Pt···Pt distance. Also, the HOMO−3 is unaffected because it is a MO localised exclusively in one monomer. The HOMO and HOMO−1 levels remain degenerate from 14 up to 6 Å. Further decrease of the intermonomeric distance induces an energy splitting of these MOs. Figure 7b shows that the HOMO becomes a σ antibonding combination of mainly $5d_{z^2}$ (65%) character with a significant contribution of the $6p_z$ (4%) and 6s (10%) orbitals of Pt and its energy increases upon dimer formation. Conversely, the HOMO−1 is of σ bonding nature and becomes stabilised upon dimerisation.

Pure d^8···d^8 interactions, that is, the combination of adjacent occupied Pt $5d_{z^2}$ orbitals alone is not sufficient to explain a neat stabilisation of these supramolecular aggregates because the theoretical bond order is zero. Of course, similar association is predicted to be much stronger for d^7···d^7 interactions, where the σ bonding combination of the d_{z^2} orbitals is occupied (HOMO) and the σ antibonding combination is unoccupied (LUMO). Thus, Pt^{II}···Pt^{II} attraction should be explained according to more subtle interactions.

The current understanding of the driving force of such weak metal–metal interaction involves a symmetry-allowed mixing between atomic orbitals of adjacent Pt atoms along the Pt–Pt vector (z direction), namely, the occupied (donor) $5d_{z^2}$ and the empty (acceptor) $6p_z$ and 6s orbitals.[25] This overlap (we confirmed the participation of the $6p_z$ and 6s atomic orbitals to the HOMO and HOMO−1 combinations for $[Pt_2L_4]_2$, see above) strengths the Pt–Pt interaction within each monomer and, at the same time, results in a lobe expansion of the frontier MOs that protrudes away the monomers favouring their subsequent intermolecular Pt···Pt

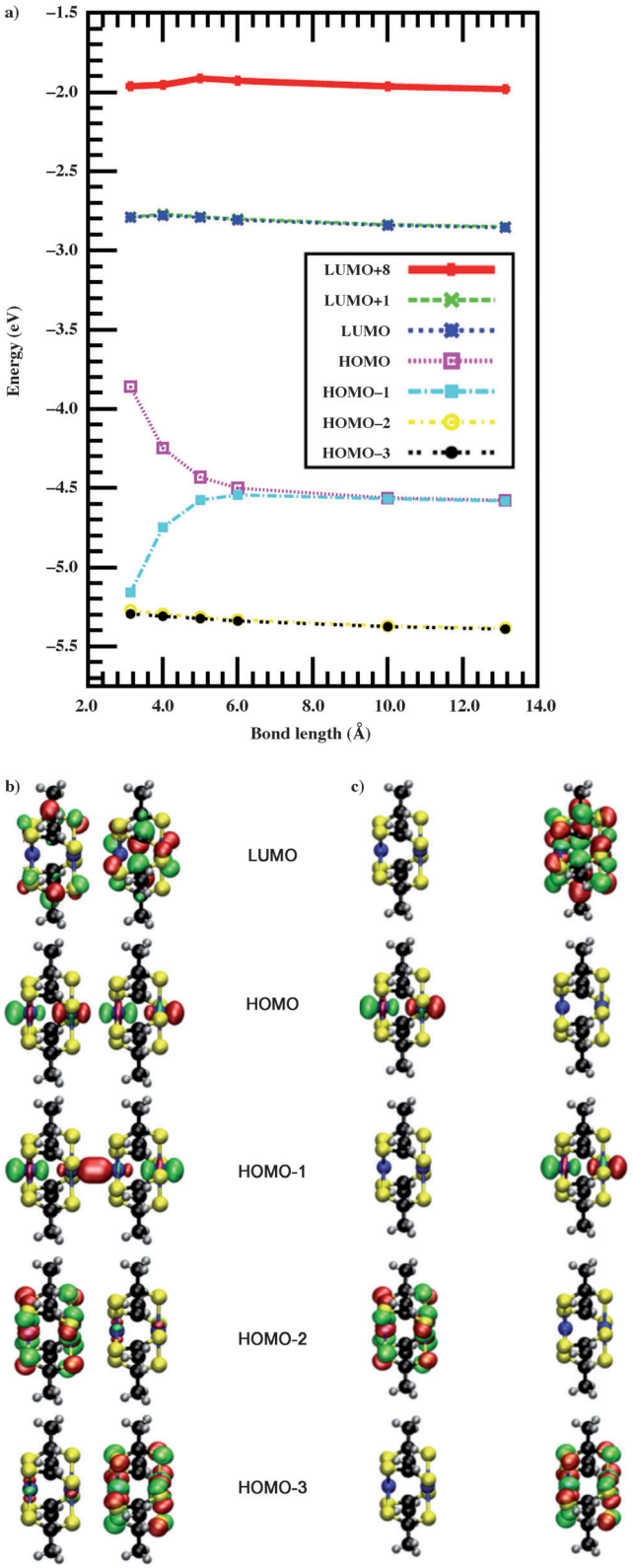

Figure 7. a) Energy variation of selected Kohn–Sham orbitals with the distance between two monomeric $[Pt_2L_4]$ species. Isosurface representation (enclosing 80% of the charge) of these orbitals at the experimental geometry (b) and at a Pt···Pt distance of 10 Å (c). Values were calculated by using the OCTOPUS code[24] and the PBE[14] exchange-correlation functional.

CHEMISTRY
A EUROPEAN JOURNAL

self-association.[11] This explanation supports the experimental evidence that short intramolecular Pt–Pt distances are also accompanied by short intermolecular Pt···Pt distances.[11] Based on these qualitative ideas of the molecular orbital theory, Alvarez and co-workers have investigated the correlation between the pyramidalisation angle α (i.e., Pt···Pt–L) and the Pt···Pt distance in various dimetal compounds including dithiocarboxylato complexes of Pt^{II}.[26]

To compare our calculations on $[Pt_2L_4]_n$ ($n=1$–4) clusters with the results expected for an infinitely long chain ($n\rightarrow\infty$), we undertook the study of the electronic properties of the 1D periodic system at the LDA level. Figure 8 (left) displays the calculated electronic band structure along the chain direction (x axis). The plot features a nearly constant LUMO level and a highly dispersive HOMO band, which becomes degenerate with the HOMO−1 state at the edge of the first Brillouin zone (BZ). A direct band gap of 0.505 eV was calculated at the Γ point, which is very close to the PBE value of 0.44 eV previously reported.[10b] Thus, the periodic system is predicted to be a semiconductor at this level of theory, in accordance to the aforementioned study. Our computed band gap (0.505 eV) agrees well with the extrapolated value (0.388 eV) from different HOMO–LUMO energies of the OCTOPUS calculations for $[Pt_2L_4]_n$ ($n=1$–4) polymers of increasing length n (fit band gap(n) = 0.388+1.405/n eV). The difference in energy between the HOMO at the Γ point and the edge of the BZ is 1.30 eV, which is also in good agreement with the PBE value of 1.26 eV, previously reported.[10b] In addition, we estimated the effective hole mass from a parabolic fit of the top valence band at the Γ point. Our result (0.12, in units of the free electron mass) is, however, in contrast to the reported PBE value (0.50).[10b] Figure 8 (middle) also displays the projected density of the states (PDOS) of the periodic system and shows the important contribution of the platinum 6p and 5d atomic orbitals to the bands involved in the visible optical transitions in the periodic system.

Finally, Figure 8 (right) depicts the HOMO at selected wave vectors of the BZ of the isolated periodic chain. At the Γ point (Figure 8, right, top), the HOMO has σ character and features a fully antibonding combination of the platinum $5d_{z^2}$ orbitals (with a slight involvement of the 3p orbitals of the sulphur atoms) between adjacent monomers (the chain direction is now the x axis). Similar findings were found in our discrete cluster calculations (Figure 7). At the edge of the BZ (Figure 8, right, bottom), however, the HOMO features an alternating pattern of bonding–antibonding σ combination of the same orbitals, which becomes degenerated with the HOMO−1 due to the presence of two monomers within the computational cell. Due to its partial bonding character, the HOMO at the edge of the BZ is more stable than the (purely antibonding) HOMO at the Γ point (Figure 8, left).

Excited-state properties—analysis of optical spectra: Because the HOMO in all $[Pt_2L_4]$ compounds is of σ* character and involves mostly Pt atoms, a complete basis set on these atoms is essential to reproduce an accurate spectrum. The basis set effect on the optical spectrum is examined in the Supporting Information. The OCTOPUS code allows us to achieve the complete basis set limit on all atoms faster than ordinary quantum chemistry codes (such as Gaussian),

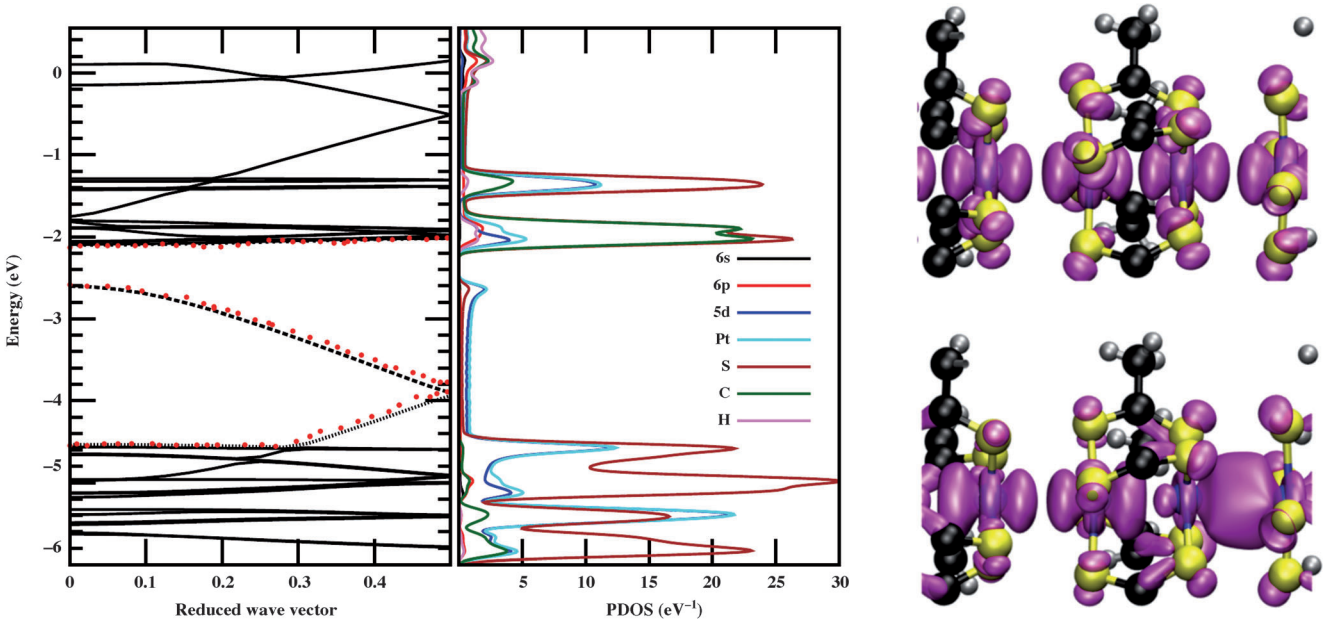

Figure 8. Electronic properties of an isolated periodic chain of $[Pt_2L_4]_2$ computed at the LDA level. Left) Electronic band structure: dashed lines show the frontier molecular orbitals. The reduced wave vector is in units of $2\pi/L$ with $L=11.801$ Å. The PBE band structures from reference [10b] are displayed by the red dots and agree very well with our LDA results. Middle) Projected density of states (PDOS). Right) Electronic density (enclosing a 90% of the charge) of the highest occupied molecular orbital (HOMO) at selected points in the first Brillouin zone (BZ): at the Γ point (right, top) and at the edge of the BZ (right, bottom).

which are typically based on atom-centred basis sets. Specifically, in the case of Pt, we found that the available atom-centred basis sets (e.g., LANL2DZ and LANL2TZ) are not flexible enough. The complete basis set limit for latter methods becomes prohibitively expensive due to the size of the systems in this work. Due to the aforementioned limitations, a real-space method was chosen to study the optical absorption of $[Pt_2L_4]$ systems.

As for the choice of exchange-correlation functional, previous works have shown that PBE provides a relatively good description of the optical properties of organic complexes (with some known deficiencies that are not relevant here). Moreover, in view of the reasonable predicted energetics already discussed and the correct reproduction of the experimental spectra, we decided to carry out the optics calculations with the PBE functional.

In our experimental study, we interpret the broad band at 760 nm in the UV/Vis spectra of concentrated solutions of $[Pt_2L_4]$ at low temperature as an indication of the formation of oligomeric $[Pt_2L_4]_n$ species. In order to further elucidate this assignment, we theoretically investigated the spectroscopic properties of isolated $[Pt_2L_4]_n$ ($n=1$–4) species.

Figure 9a shows the UV/Vis spectra from real-time TDDFT calculations at the PBE level for $[Pt_2L_4]_n$ ($n=1$-4) computed by using the OCTOPUS code. Geometries used for these calculations were obtained from the crystalline structure without further modification. The system is assumed to be isolated in all spatial directions. The optical absorption for the three directions of polarisation for $[Pt_2L_4]_n$ ($n=1$–4) in vacuum (Figure 9b) shows that most of the visible transitions are polarised along the axis passing through the platinum atoms.

The calculated most intense absorption peaks for the different $[Pt_2L_4]_n$ species are found at approximately $\lambda=410$, 570, 686 and 770 nm for the series $n=1$–4. These peaks correspond to neutral excitations from the HOMO (mostly a σ* combination of the Pt $5d_{z^2}$ orbitals) to unoccupied orbitals of σ character involving the sulphur ligands. An isosurface representation of the most relevant orbitals in the optical transitions is given in Figure 10. In the monomer, $[Pt_2L_4]$, the involved orbitals are from the HOMO to the LUMO+6 (63%) level. For the dimer, $[Pt_2L_4]_2$, the transition involves the HOMO to the LUMO+8 (83%). In $[Pt_2L_4]_3$, the contribution is more mixed but still the behaviour is the same (σ* to σ). Here, the excitation from the HOMO to the LUMO+12 (34%) is the most important transition. Finally, for $[Pt_2L_4]_4$ the main contribution is from the HOMO to the LUMO+16 (67%). It is worth mentioning that LDA (Perdew–Zunger parameterisation[27]) yields similar spectra as PBE in the low energy range (see the Supporting Information).

Our calculations show that the position of the band peak in the visible region is very sensitive to the intermolecular Pt···Pt distance (see the Supporting Information). This phenomenon partially contributes to the broadening of this band when $[Pt_2L_4]$ is found in solution. From Figure 7a, we can rationalise this behaviour for $[Pt_2L_4]_2$ due to the closing

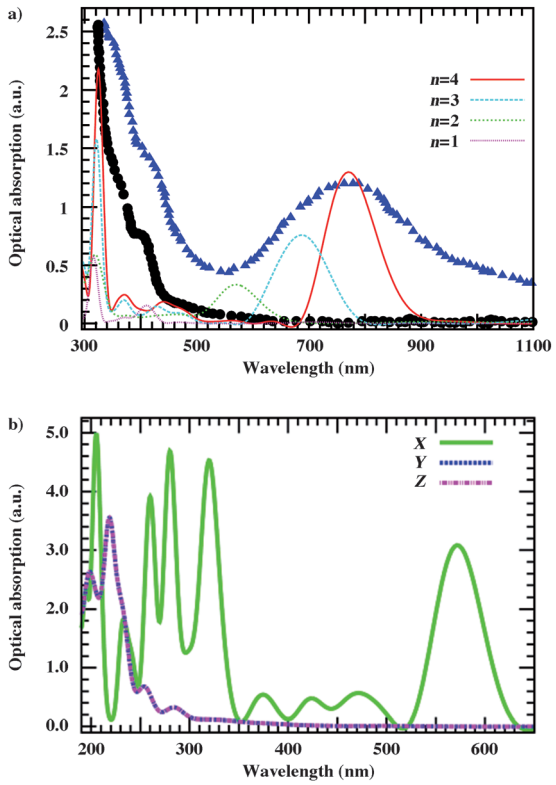

Figure 9. a) Calculated real-time TDDFT spectra for different isolated $[Pt_2L_4]_n$ ($n=1$–4) species at the PBE level by using the OCTOPUS code.[24] The spectra are normalised by the number of $[Pt_2L_4]$ monomers. The experimental spectra of $[Pt_2L_4]$ in solution at 20 (black dots) and 0 °C (blue triangles) are also shown. b) Spectra for the isolated dimer along all polarisation directions. Note that the experimental broad band centred at $\lambda=760$ nm (blue triangles) is due to the formation of $[Pt_2L_4]_n$ ($n>1$) polymers due to intermolecular Pt···Pt interaction and that it is polarised along this direction.

of the gap between the HOMO and the LUMO+8 levels upon decreasing the Pt···Pt distance. Interestingly, for the $[Pt_2L_4]_2$ dimer, the energy variation of the HOMO is responsible for this redshift, whereas the LUMO+8 is unaffected by the Pt···Pt distance.

Comparison of the broad band observed in the experimental spectrum (blue triangles in Figure 9a) with our computed spectra clearly suggests that at room temperature only monomeric $[Pt_2L_4]$ species are present, whereas at low temperature a mixture of $[Pt_2L_4]_n$ species with different nuclearities coexists. The observed thermochromic effect of the experimental absorption spectra of $[Pt_2L_4]$ in solution is an indication that a reversible equilibrium exists between the monomer and a mixture of various complexes of different nuclearity.[1]

[1] Assuming that in solution only the monomer (M) and the dimer (D) coexist, the exact expression (assuming additivity in the law of Lambert–Beer) for the average molar extinction coefficient is $\varepsilon(\lambda)=\frac{\varepsilon_D}{2}+(\varepsilon_D-2\varepsilon_M)\frac{1-\sqrt{1+8K[M_0]}}{8K[M_0]}$, where $\varepsilon(\lambda)=\frac{A(\lambda)}{d[M_0]}$, $A(\lambda)$ is the measured absorbance, d is the optical path length, $K=\frac{[D]}{[M]^2}$ is the equilibrium constant of the dimerisation and $[M_0]$ is the initial concentration of the monomer.

CHEMISTRY
A EUROPEAN JOURNAL

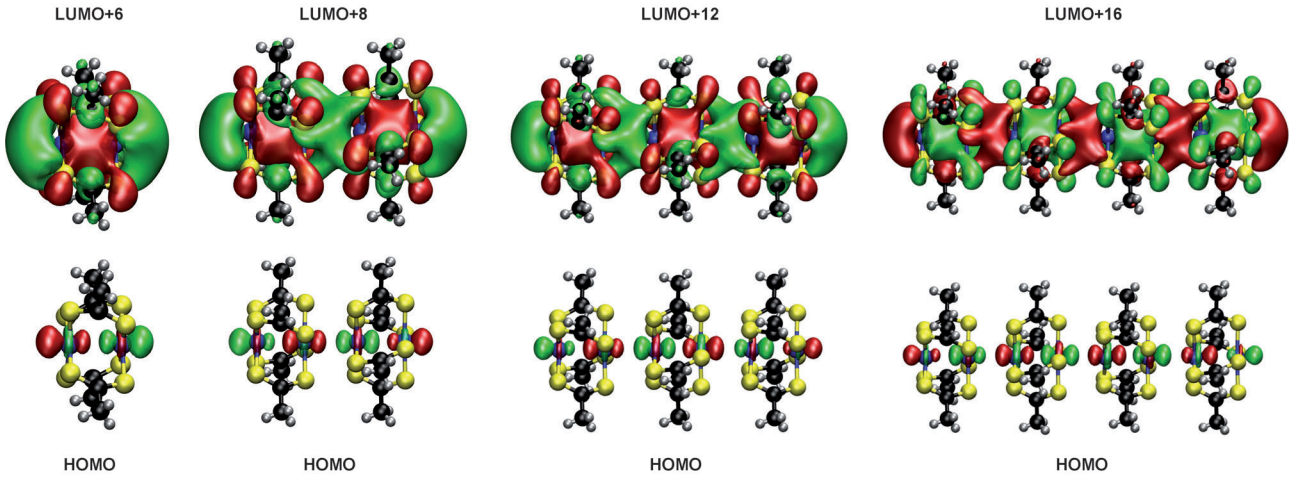

Figure 10. Main Kohn–Sham orbitals involved in the most intense low energy transition for $[Pt_2L_4]_n$ (with $n=1$–4 increasing from left to right) at the PBE level. The isosurface contours correspond to 20% of the maximum value.

We also consider the effect of the explicit solvent (dichloromethane) on the optical spectrum of $[Pt_2L_4]_2$ and we found that the visible part of the signal remains unchanged with respect to vacuum. Only in the high-energy region we observed the dichloromethane signal as expected for this transparent solvent (see the Supporting Information).

Our results of the theoretical spectra of $[Pt_2L_4]_n$ ($n=1$–4) clearly indicate that increasing the length of the oligomer results in a decrease of the energy of the optical transition associated to Pt···Pt aggregations. To take this trend to its limit, we analysed the optical properties of an isolated periodic chain of the dimer $[Pt_2L_4]_2$. The optical properties of the infinite chain were computed with the YAMBO code[28] by using the LDA wavefunctions produced previously by the PWscf program.[29] As shown in the Supporting Information and Figure 8, for the periodic calculation we used LDA because it yields nearly the same spectra as the PBE functional. The absorption spectrum within the random-phase approximation (RPA) level is shown in Figure 11. A total of 300 bands, 17 irreducible wave vectors in the 1D first BZ, and a plane wave cut-off of 16.25 Ry were sufficient to obtain a reasonably converged spectrum. As a convergence test, the RPA spectra were also calculated with quantum espresso (QE in legend) by using a very high kinetic energy cut-off (60 Ry) to show that the main features are still well captured by the lower cut-off (16.25 Ry) of the YAMBO calculations.

As expected for 1D systems (and also found for the $[Pt_2L_4]_n$ ($n=2$–4) clusters) the response in the chain direction (x) is much stronger that in the perpendicular (y, z) directions. The RPA spectra for light polarised in the x direction features a prominent central band with two strong peaks at $\lambda=400$ and 500 nm. Inclusion of local field effects (LF, in the legend of Figure 11) improves the RPA spectrum significantly by shifting those peaks to higher energies as well as by reducing its intensity. Thus, the anisotropy of the system is already evident at the RPA level even though we

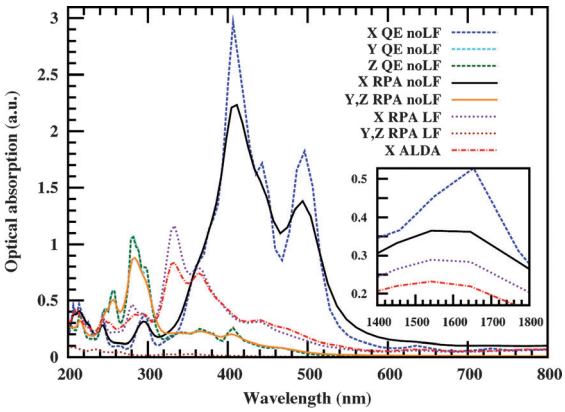

Figure 11. Calculated optical absorption spectra of an isolated periodic chain of $[Pt_2L_4]$ at the LDA level. In the legend, RPA stands for the random-phase approximation; (no)LF means that local field effects are (not) included in the response function; ALDA refers to a TDDFT calculation within the adiabatic LDA approximation; QE means that the spectrum was calculated with the quantum espresso code;[29] all other spectra are calculated with the YAMBO package.[28]

were neglecting many body effects, which would require expensive GW/Bethe–Salpeter calculations.[30] LF effects were converged with 300 reciprocal lattice vectors for the dimension of the response matrix. Interestingly, we found no peak in the low-energy region of the visible spectrum (500–800 nm). However, we observed the appearance of a broad band in the near-infrared region at 1600 nm, which is consistent with a dramatic redshift due to an infinite chain of the 600 nm band found for $[Pt_2L_4]_2$. Finally, a linear response TDDFT calculation within the adiabatic LDA (ALDA, in the legend of Figure 11) approximation hardly changes the LF-RPA results.

Conclusion

In this work, we demonstrate that the tendency of $[Pt_2L_4]$ to form persistent supramolecular entities can be extended to a family of compounds containing dithiocarboxylato ligands. This aggregation, which occurs through Pt···Pt interactions, can be modulated by several variables. First, high concentration and low temperatures favour the formation of $[Pt_2L_4]_n$. Species with different nuclearity are observed, although decreasing the initial monomer concentration results in a narrower distribution of polymeric species. Second, the supramolecular assembly of $[Pt_2L_4]$ in solution can also be tuned by the nature of the ligand L. In principle, bulkier ligands inhibit the formation of oligomeric species. For example, this trend is observed in the crystal structures comparing the intermolecular Pt···Pt distances of linear versus branched ligands. Interestingly, although the length of the linear chains does not affect the intermolecular interactions in the crystal phase, it has an important impact in solution. Lastly, the solvent can also affect the supramolecular aggregation of the diplatinum complexes. Solvents containing donor atoms (such as the oxygen atom in THF or the sulphur atoms in CS_2) disfavour the aggregation by coordination to the Pt metal centre. Thus, the orbitals in the platinum centres are readily available to interact (although weakly) with the coordinating solvent molecules. However, the effect of the solvent can be more subtle as illustrated by the different results observed in CH_2Cl_2 and $CHCl_3$, where the polarity probably plays a leading role.

Theoretical simulations confirm that $[Pt_2L_4]$ species binds through weak intermolecular Pt···Pt interactions. Intermolecular Pt···S and S···S interactions between monomers have been found to be repulsive at all levels of calculations. The description of the weak Pt···Pt interaction has been particularly challenging due to issues with basis set incompleteness and limitations of current implementation of density functional theory. The description of Pt···Pt binding requires consideration of orbitals beyond the frontier ones because the HOMO is in fact of σ* character, whereas the HOMO−1 is of σ character. This weak metal–metal attraction is mediated by the interaction between the platinum $5d_{z^2}$ and $6p_z$ atomic orbitals (the chain direction is along the z axis). In addition, the soft sulphur atoms in the dithiocarboxylato ligands assist the supramolecular assembly by accommodating the electronic charge donated by the Pt atoms involved in the Pt···Pt interaction.

From our extensive comparative study by using different methodologies, we found that a complete basis set limit is essential in order to properly describe the optical properties of these compounds. Theoretical calculations of the optical spectra allowed us to elucidate the nature of the low-energy transitions that appear at low temperature. Our calculations clearly show that the appearance of such a band is due to oligomeric species that keep their cohesion through Pt···Pt interactions. Further increasing the nuclearity of $[Pt_2L_4]_n$ decreases the energy of these optical transitions, the extreme case is the periodic isolated chain (a model of the crystal phase), which shows an absorbance, which is shifted to the infrared region. The broad band in the visible region is attributed to transitions from the HOMO, which is a σ* combination of the $5d_{z^2}$ and the $6p_z$ orbital of the Pt atoms, to unoccupied molecular orbitals delocalised on the sulphur ligands.

Overall, our results lead to important advances in the understanding of how diplatinum species can assembly into 1D conductive supramolecular polymers, offering valuable hints in the search for a bottom-up assembly of molecular electronic devices.

Experimental Section

Materials and methods: All reagents were purchased from Sigma Aldrich and used as received. The solvent CS_2 (purity $\geq$99.9%) was also purchased from Sigma Aldrich and used without further purification. The synthesis of the dithicarboxylic acids was carried out following a procedure previously reported.[31] Structural characterisation of the compounds was performed by means of elemental analysis, UV/Vis and ^{1}H NMR spectroscopy as well as single-crystal X-ray diffraction analysis. ^{1}H NMR spectra were recorded on a Bruker AMX-300 spectrometer. C, H, S elemental analyses were performed on a Perkin–Elmer 240-B microanalyser. Electronic absorption spectra were recorded on an Agilent 8452 diode array spectrophotometer over a 190–1100 nm range in 0.1, 0.2 and 1 cm quartz cuvettes thermostatted by a Unisoku cryostat.

Synthesis of $[Pt_2(S_2C(CH_2)_3CH_3)_4]$ (1) and $[Pt_2(S_2CCH_2CH(CH_3)_2)_4]$ (2): The compounds were prepared following the procedure previously reported by Mitsumi et al.[32] The brown solid obtained upon keeping the solution 24 h at 4 °C was filtered off, washed with cold -hexane and dried under vacuum. Crystals of suitable size for X-ray diffraction analysis were obtained upon slow cooling of a solution of the complex dissolved in hot dichloromethane.

Compound **1**: 73% yield; ^{1}H NMR (500 MHz, $CDCl_3$): δ = 2.78 (t, J = 7.5 Hz, 3H), 1.79–1.69 (m, 2H), 1.39–1.30 (m, 2H), 0.85 ppm (t, J = 7.5 Hz, 2H); IR (KBr): $\tilde{\nu}$ = 2951 (vs), 2928 (vs), 1146 (s), 1009 cm^{-1} (vs); elemental analysis calcd (%) for $C_{20}H_{36}S_8Pt_2$ (923.1955): C 26.0, H 3.9, S 27.8; found: C 25.8, H 3.8, S 27.7.

Compound **2**: 71% yield; ^{1}H NMR (500 MHz, $CDCl_3$) :δ = 2.63 (d, J = 7.5 Hz, 6H), 2.23–2.14 (m, 1H), 0.90 ppm (d, J = 7.5 Hz, 2H); IR (KBr): $\tilde{\nu}$ = 3432 (m), 2952 (s), 1155(s), 1003 cm^{-1} (vs); elemental analysis calcd (%) for $C_{20}H_{36}S_8Pt_2$ (923.1955): C 26.0, H 3.9, S 27.8; found: C 25.9, H 3.8, S 27.6.

Crystallographic measurements: Crystal data were collected by using $Mo_{K\alpha}$ radiation on a Bruker SMART 6K CCD diffractometer (for compound **1**) or on a Xcalibur diffractometer (for compound **2**). The structures were solved by direct methods by using the SIR92 program[33] and refined by full-matrix least-squares on F^2 including all reflections (SHELXL97).[44] All calculations were performed by using the WINGX crystallographic software package.[45] All non-hydrogen atoms were refined anisotropically.

Crystal data for compound **1**: $C_{20}H_{36}Pt_2S_8$; M_r = 923.15; T = 296(2) K; orthorhombic; space group: *Pccn*; a = 26.494(3), b = 9.1068(7), c = 11.7111(10) Å; V = 2825.7(4) Å^3; Z = 4; ρ_{calcd} = 2.170 g cm^{-3}; $\mu(Mo_{K\alpha})$ = 10.491 mm^{-1}; θ_{max} = 30.54°; 37835 reflections collected, 4318 unique reflections (R_{int} = 0.0713); final $R1$ = 0.0319 and $wR2$ = 0.0811 [$I > 2\sigma(I)$]; $R1$ = 0.0402 and $wR2$ = 0.0893 (all data); $\rho_{max/min}$ 4.374/−6.057 Å^{-3}.

Crystal data for compound **2**: $C_{20}H_{36}Pt_2S_8$; M_r = 923.15; T = 100(2) K; orthorhombic; space group: *Ccc2*: a = 18.1699(15), b = 23.304(3) c = 20.019(3) Å; V = 8476.7(18) Å^3; Z = 12; ρ_{calcd} = 2.170 g cm^{-3}; $\mu(Mo_{K\alpha})$ = 10.491 mm^{-1}; θ_{max} = 26.19°; 15567 reflections collected, 7392 unique reflections (R_{int} = 0.0611); final $R1$ = 0.0580 and $wR2$ = 0.1411 [$I > 2\sigma(I)$];

$R1 = 0.1402$ and $wR2 = 0.1990$ (all data); Flack parameter = 0.05(10); $\rho_{max/min}$ 2.810/−1.845 Å^{-3}.

CCDC 876196 (**1**) and 876197 (**2**) contain the supplementary crystallographic data for this paper. These data can be obtained free of charge from The Cambridge Crystallographic Data Centre via www.ccdc.cam.ac.uk/data_request/cif.

Computational details: The electronic properties of the $[Pt_2L_4]$ compounds both in the ground and in the excited state were investigated by using different computational methods, most of them based on the density functional theory[33] and its time-dependent extension (TDDFT).[34]

In the first part, we analysed the stability of the small clusters in their ground states by using Gaussian 09[23] with different exchange-correlation functionals. We describe the Pt atoms with the standard double- and triple-zeta quality basis sets (LANL2DZ and LANL2TZ)[36] with the effective core potential (ECP)[36a,37] approach and the 6-311+G**[38] basis on the other atoms. In some cases, we used the PCM (polarisable continuum model)[39] to study the effect of the solvent in the conformation.

A study of the change of the frontier orbitals during the dimerisation processes in the gas phase was performed by using the OCTOPUS code.[24] With this approach, all quantities are defined on the real space by using a numerical mesh. A simulation box made with centred spheres with radii of 6.0 Å and a grid spacing of 0.18 Å. We used the PBE[14] exchange-correlation functional. Norm-conserving Troullier–Martins pseudopotentials[40] were used for the non-valence electrons. The geometries were taken from our crystallographic data without further modification.

To calculate the periodic $[Pt_2L_4]_2$ chain structure in vacuum, we used the PWscf code of the quantum espresso suite.[29] The $[Pt_2L_4]_2$ dimer of the experimental X-ray structure was placed with its chain axis oriented along the x direction in a 3D periodic orthorhombic box of the volume $11.801 \times 29.105 \times 29.105$ Å^3. Thus, the simulated system consists of a periodic chain of dimers in the x direction, whereas isolated in the perpendicular y,z plane. A total of 17 irreducible wave vectors was used to sample the first 1D Brillouin zone (BZ) along the chain axis (x). whereas only the Γ point was sampled in the perpendicular directions (y,z). The exchange and correlation term was approximated by using the Perdew–Zunger[27] parametrisation of the local-density-approximation (LDA). A norm-conserving Troullier–Martins-type pseudopotential was generated for the Pt atoms, which included scalar relativistic and non-linear core corrections to describe the interaction of the core with the ten valence electrons (5d, 6s) per Pt atom. The rest of the species (C, S and H) was described with other norm-conserving pseudopotentials so that only s and p valence orbitals were explicitly considered for these elements. The Kohn–Sham valence orbitals were expanded in a plane wave basis set up to a kinetic energy cut-off of 60 Ry. The Marzari–Vanderbilt[41] smearing with a width of 0.01 Ry was used. In total, the cell contains 224 electrons and 60 atoms with a Pt···Pt distance between the $[Pt_2L_4]$ monomers of 3.137 Å.

The optical properties of the linear $[Pt_2L_4]_n$ clusters were calculated by using the real-time TDDFT as implemented in the OCTOPUS code.[15] This methodology is highly efficient in the estimation of the excited states of molecular systems because unoccupied states are not necessary and it scales linearly with the size of the systems. The starting point is the ground state wavefunction from the different $[Pt_2L_4]$ linear crystalline structures, which are perturbed by a weak electric field in the three polarisation directions (x, y and z). The optical spectrum is proportional to the Fourier transform of the time evolution of the electric dipole moment. In all cases, the total propagation time was 30 $\hbar\,eV^{-1}$ units with a time step of 0.01 $\hbar\,eV^{-1}$ units and the exchange-correlation functional was PBE.

The study of the explicit solvent was done with the same parameters described above by using relaxed configurations with seven and twelve dichloromethane molecules solvating the $[Pt_2L_4]_2$ species (see Figure S6 in the Supporting information). The configurations were generated by using the CP2K program.[42] During all geometry optimisations, the solvent was allowed to relax whereas the $[Pt_2L_4]_2$ dimer was fixed at the experimental X-ray structure. An initially optimised configuration at the semiempirical PM6 level was placed in a cubic box of the side length 35 Å for a subsequent solvent relaxation with DFT. The exchange and correlation term was approximated by using the Perdew–Burke–Ernzerhof (PBE) functional.[14] The Gaussian-plane wave (GPW) hybrid basis set in the quickstep module of the CP2K program was used. The electronic density was expanded by using an auxiliary plane wave basis set up to a kinetic energy cut-off of 400 Ry for the calculation of the Hartree potential. The interaction of the valence electrons with the atomic cores was described by using the norm-conserving, dual space, Goedecker–Teter–Hutter (GTH) pseudopotentials for all atoms.[43] In particular, for the Pt atoms, we used the GHT-PBE-q18 pseudopotential, which describes all core electrons up to the 4f level, leaving explicitly eight electrons in the semicore (5s, 5p) and ten electrons in the valence (5d, 6s). The valence Kohn–Sham orbitals were expanded in terms of contracted Gaussian-type orbitals (GTO) of double-ζ valence-polarised (DZVP) quality for all atoms and specifically optimised for its use with the GTH pseudopotentials (DZVP-MOLOPT-GTH). A threshold of 10^{-8} a.u. for the energy change was adopted in the SCF wavefunction minimisation based on the direct inversion in the iterative subspace (DIIS) algorithm. The BFGS optimisation algorithm was stopped when the maximum gradient on any atom was less than 0.0001 a.u.

Acknowledgements

We acknowledge financial support from the European Research Council Advanced Grant DYNamo (ERC-2010-AdG, Proposal No. 267374), the Spanish Grants (FIS2011-65702-C02-01, PIB2010US-00652 and MAT2010-20843-C02-01), the ACI-Promociona (ACI2009-1036 and ACI2009-0969), the Grupos Consolidados del Gobierno Vasco (IT-319-07 and IT-477-10), the Comunidad de Madrid (S-0505/MAT/0303) and the Consolider nano THERM (Grant No. CSD2010-00044), the computational time was granted by the Barcelona Supercomputing Centre, "Red Española de Supercomputación" throughout the project QCM-2011-3-0029 and the technical and human support provided by IZO-SGI, SGIker (UPV/EHU, MICINN, GV/EJ, ERDF and ESF). L.A.E.L. acknowledges the financial support from the Spanish Research Council (CSIC) through its "Junta para la Ampliación de Estudios fellowship (JAE-Predoc-2008)" and the efficient computer cluster in San Sebastian maintained by J. Alberdi Rodriguez.

[1] J. M. Lehn, *Proc. Natl. Acad. Sci. USA* **2002**, *99*, 4763–4768.
[2] a) J. K. Bera, K. R. Dunbar, *Angew. Chem.* **2002**, *114*, 4633–4637; *Angew. Chem. Int. Ed.* **2002**, *41*, 4453–4457; b) F. A. Cotton, R. A. Walton, *Multiple Bonds Between Metal Atoms*, 2nd ed., Clarendon, Oxford, **1993**.
[3] a) H. Schmidbaur, A. Schier, *Chem. Soc. Rev.* **2008**, *37*, 1931–1951; b) P. Pyykkö, *Chem. Soc. Rev.* **2008**, *37*, 1967–1997.
[4] F. A. Cotton, X. J. Feng, M. Matusz, R. Poli, *J. Am. Chem. Soc.* **1988**, *110*, 7077–7083.
[5] a) J. S. Miller, *Extended Linear Chain Compounds*, Plenum Press, New York, **1982**; b) J. S. Miller, A. J. Epstein, *Prog. Inorg. Chem.* **1976**, *20*, 1.
[6] S. Roth, *One-dimensional Metals*, VCH, Weinheim, **1995**.
[7] M. Williams, *Adv. Inorg. Chem. Radiochem.* **1983**, *26*, 235–268.
[8] a) R. Mas-Ballesté, J. Gómez-Herrero, F. Zamora, *Chem. Soc. Rev.* **2010**, *39*, 4220–4233; b) J. Gómez-Herrero, F. Zamora, *Adv. Mater.* **2011**, *23*, 5311–5317.
[9] F. A. Cotton, C. Lin, C. A. Murillo, *Acc. Chem. Res.* **2001**, *34*, 759–771.
[10] a) R. Mas-Ballesté, R. Gónzalez-Prieto, A. Guijarro, M. A. Fernandez-Vindel, F. Zamora, *Dalton Trans.* **2009**, 7341–7343; b) A. Guijarro, O. Castillo, A. Calzolari, P. J. S. Miguel, C. J. Gomez-Garcia, R. di Felice, F. Zamora, *Inorg. Chem.* **2008**, *47*, 9736–9738; c) A. Kobayashi, T. Kojima, R. Ikeda, H. Kitagawa, *Inorg. Chem.* **2006**, *45*, 322–327.
[11] T. Kawamura, T. Ogawa, T. Yamabe, H. Masuda, T. Taga, *Inorg. Chem.* **1987**, *26*, 3547–3550.

[12] Cambridge Crystallographic Data Base, Conquest version 1.14, **2012**.
[13] C. Bellitto, A. Flamini, O. Piovesana, P. F. Zanazzi, *Inorg. Chem.* **1980**, *19*, 3632–3636.
[14] a) J. P. Perdew, K. Burke, M. Ernzerhof, *Phys. Rev. Lett.* **1996**, *77*, 3865–3868; b) J. P. Perdew, K. Burke, M. Ernzerhof, *Phys. Rev. Lett.* **1997**, *78*, 1396–1396.
[15] a) Special issue: *Chem. Phys.* **2011**, *391*, 1–176; b) M. A. L. Marques, N. Maitra, F. Nogueira, E. K. U. Gross, A. Rubio, *Lecture Notes in Physics, Fundamentals of the Time-Dependent Density Functional Theory*, Springer, Heidelberg, **2012**; c) Special issue: *Phys. Chem. Chem. Phys.* **2009**, *11*, 4421–4688.
[16] a) S. F. Boys, F. Bernardi, *Mol. Phys.* **2002**, *100*, 65–73; b) S. Simon, M. Duran, J. J. Dannenberg, *J. Chem. Phys.* **1996**, *105*, 11024–11031.
[17] a) K. Raghavachari, *Theor. Chem. Acc.* **2000**, *103*, 361–363; b) P. J. Stephens, F. J. Devlin, C. F. Chabalowski, M. J. Frisch, *J. Phys. Chem.* **1994**, *98*, 11623–11627.
[18] T. Yanai, D. P. Tew, N. C. Handy, *Chem. Phys. Lett.* **2004**, *393*, 51–57.
[19] C. Adamo, V. Barone, *J. Chem. Phys.* **1999**, *110*, 6158–6170.
[20] S. G. Wang, W. H. E. Schwarz, *J. Am. Chem. Soc.* **2004**, *126*, 1266–1276.
[21] N. Marino, C. H. Fazen, J. D. Blakemore, C. D. Incarvito, N. Hazari, R. P. Doyle, *Inorg. Chem.* **2011**, *50*, 2507–2520.
[22] a) A. E. Reed, R. B. Weinstock, F. Weinhold, *J. Chem. Phys.* **1985**, *83*, 735–746; b) A. E. Reed, F. Weinhold, *J. Chem. Phys.* **1985**, *83*, 1736–1740.
[23] Gaussian 09, Revision A.02, M. J. Frisch, G. W. Trucks, H. B. Schlegel, G. E. Scuseria, M. A. Robb, J. R. Cheeseman, G. Scalmani, V. Barone, B. Mennucci, G. A. Petersson, H. Nakatsuji, M. Caricato, X. Li, H. P. Hratchian, A. F. Izmaylov, J. Bloino, G. Zheng, J. L. Sonnenberg, M. Hada, M. Ehara, K. Toyota, R. Fukuda, J. Hasegawa, M. Ishida, T. Nakajima, Y. Honda, O. Kitao, H. Nakai, T. Vreven, J. A. Montgomery, Jr., J. E. Peralta, F. Ogliaro, M. Bearpark, J. J. Heyd, E. Brothers, K. N. Kudin, V. N. Staroverov, R. Kobayashi, J. Normand, K. Raghavachari, A. Rendell, J. C. Burant, S. S. Iyengar, J. Tomasi, M. Cossi, N. Rega, J. M. Millam, M. Klene, J. E. Knox, J. B. Cross, V. Bakken, C. Adamo, J. Jaramillo, R. Gomperts, R. E. Stratmann, O. Yazyev, A. J. Austin, R. Cammi, C. Pomelli, J. W. Ochterski, R. L. Martin, K. Morokuma, V. G. Zakrzewski, G. A. Voth, P. Salvador, J. J. Dannenberg, S. Dapprich, A. D. Daniels, O. Farkas, J. B. Foresman, J. V. Ortiz, J. Cioslowski, D. J. Fox, Gaussian Inc., Wallingford CT, **2009**.
[24] A. Castro, H. Appel, M. Oliveira, C. A. Rozzi, X. Andrade, F. Lorenzen, M. A. L. Marques, E. K. U. Gross, A. Rubio, *Phys. Status Solidi B* **2006**, *243*, 2465–2488.
[25] K. R. Mann, J. G. Gordon, H. B. Gray, *J. Am. Chem. Soc.* **1975**, *97*, 3553–3555.
[26] G. Aullón, P. Alemany, S. Alvarez, *Inorg. Chem.* **1996**, *35*, 5061–5067.
[27] J. P. Perdew, A. Zunger, *Phys. Rev. B* **1981**, *23*, 5048–5079.
[28] A. Marini, C. Hogan, M. Gruning, D. Varsano, *Comput. Phys. Commun.* **2009**, *180*, 1392–1403.
[29] P. Giannozzi, S. Baroni, N. Bonini, M. Calandra, R. Car, C. Cavazzoni, D. Ceresoli, G. L. Chiarotti, M. Cococcioni, I. Dabo, A. Dal Corso, S. de Gironcoli, S. Fabris, G. Fratesi, R. Gebauer, U. Gerstmann, C. Gougoussis, A. Kokalj, M. Lazzeri, L. Martin-Samos, N. Marzari, F. Mauri, R. Mazzarello, S. Paolini, A. Pasquarello, L. Paulatto, C. Sbraccia, S. Scandolo, G. Sclauzero, A. P. Seitsonen, A. Smogunov, P. Umari, R. M. Wentzcovitch, *J. Phys. Condens. Matter* **2009**, *21*, 395502.
[30] a) L. Hedin, *Phys. Rev.* **1965**, *139*, A796–A823; b) E. E. Salpeter, H. A. Bethe, *Phys. Rev.* **1951**, *84*, 1232–1242.
[31] J. M. Beiner, C. G. Andrieu, A. Thuillie, *C. R. Seances Acad. Sci. Ser. B* **1972**, *274*, 407–410.
[32] M. Mitsumi, T. Murase, H. Kishida, T. Yoshinari, Y. Ozawa, K. Toriumi, T. Sonoyama, H. Kitagawa, T. Mitani, *J. Am. Chem. Soc.* **2001**, *123*, 11179–11192.
[33] A. Altomare, M. Cascarano, C. Giacovazzo, A. J. Guagliardi, *Appl. Crystallogr.* **1993**, *26*, 343–350.
[34] W. Kohn, *Rev.Mod. Phys.* **1999**, *71*, 1253–1266.
[35] E. Runge, E. K. U. Gross, *Phys. Rev. Lett.* **1984**, *52*, 997–1000.
[36] a) P. J. Hay, W. R. Wadt, *J. Chem. Phys.* **1985**, *82*, 299–310; b) L. E. Roy, P. J. Hay, R. L. Martin, *J. Chem. Theory Comput.* **2008**, *4*, 1029–1031.
[37] a) P. J. Hay, W. R. Wadt, *J. Chem. Phys.* **1985**, *82*, 270–283; b) W. R. Wadt, P. J. Hay, *J. Chem. Phys.* **1985**, *82*, 284–298.
[38] R. Krishnan, J. S. Binkley, R. Seeger, J. A. Pople, *J. Chem. Phys.* **1980**, *72*, 650–654.
[39] R. Cammi, J. Tomasi, *J. Comput. Chem.* **1995**, *16*, 1449–1458.
[40] N. Troullier, J. L. Martins, *Phys. Rev. B* **1991**, *43*, 1993–2006.
[41] N. Marzari, D. Vanderbilt, A. De Vita, M. C. Payne, *Phys. Rev. Lett.* **1999**, *82*, 3296–3299.
[42] The CP2K project homepage can be found under http://cp2k.berlios.de/.
[43] S. Goedecker, M. Teter, J. Hutter, *Phys. Rev. B* **1996**, *54*, 1703–1710.
[44] G. M. Sheldrick, *Acta Crystallogr. Sect. A* **2008**, *64*, 112–122.
[45] L. J. Farruigia, *J. Appl. Crystallogr.* **2012**, *32*, 837–838.

Received: June 4, 2012
Published online: September 14, 2012

Please note: Minor changes have been made to this manuscript since its publication in *Chemistry—A European Journal* Early View. The Editor.

CHEMISTRY
A EUROPEAN JOURNAL

Supporting Information

Supramolecular Assembly of Diplatinum Species through Weak $Pt^{II}\cdots Pt^{II}$ Intermolecular Interactions: A Combined Experimental and Computational Study

Alejandro Pérez Paz,[a] Leonardo A. Espinosa Leal,[a] Mohammad-Reza Azani,[b] Alejandro Guijarro,[b] Pablo J. Sanz Miguel,[b] Gonzalo Givaja,[b] Oscar Castillo,[c] Rubén Mas-Ballesté,*[b] Félix Zamora,*[b] and Angel Rubio*[a]

chem_201201962_sm_miscellaneous_information.pdf

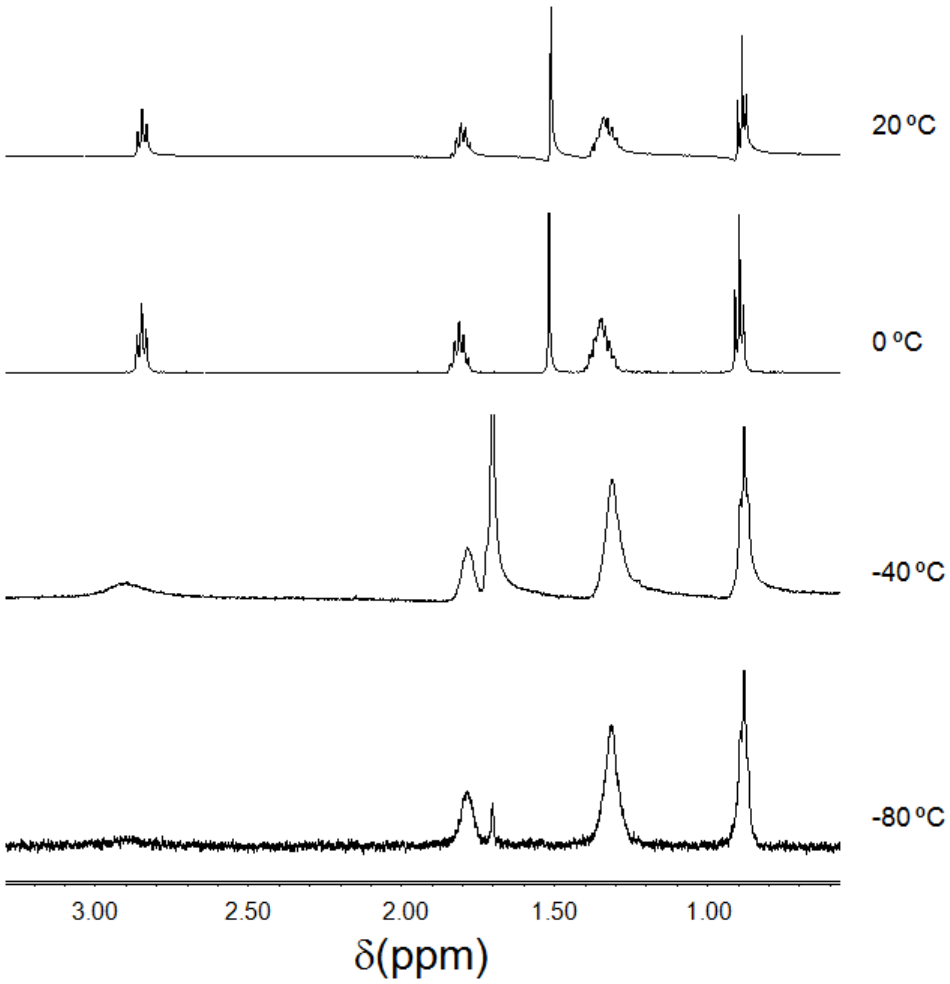

Figure S1. VT-^{1}H NMR spectra for 2 mM solutions of **3** in CD_2Cl_2.

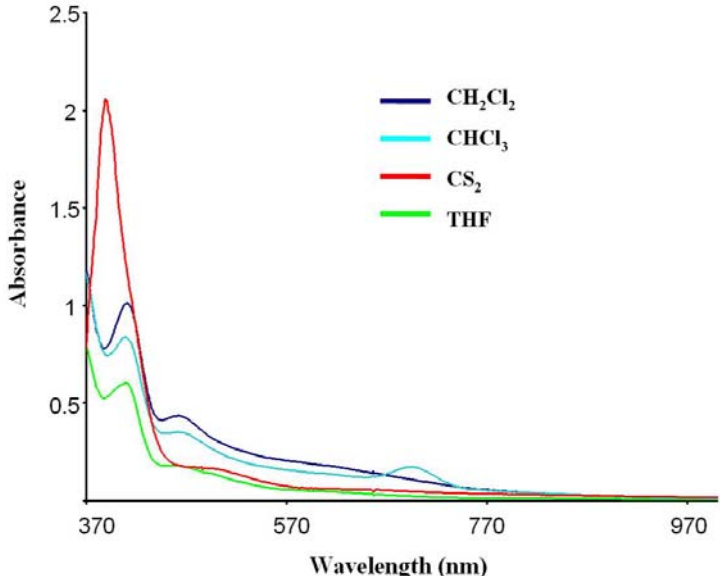

Figure S2. UV-vis spectra for 1 mM solutions of **1** in CH_2Cl_2, $CHCl_3$, CS_2 and THF at -30 ºC.

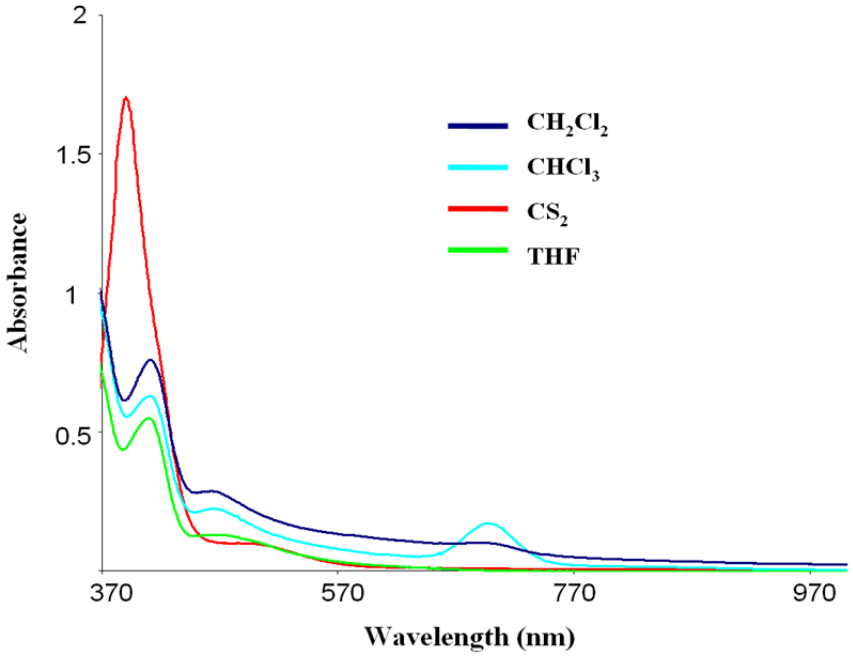

Figure S3. UV-vis spectra for 1 mM solutions of **2** in CH_2Cl_2, $CHCl_3$, CS_2 and THF at -20 ºC.

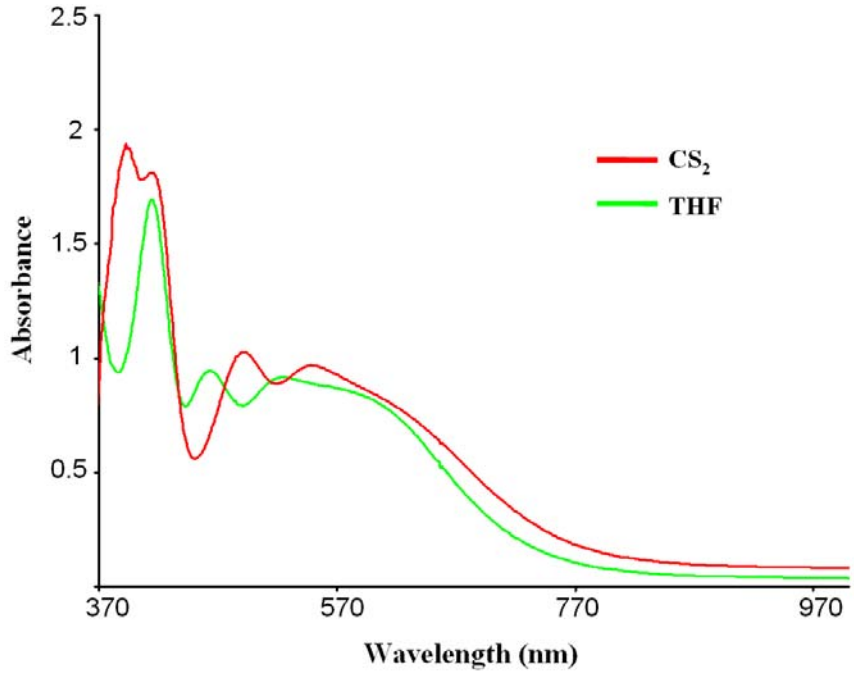

Figure S4. UV-vis spectra for 1 mM solutions of **1** in CS_2 or THF at -100 ºC.

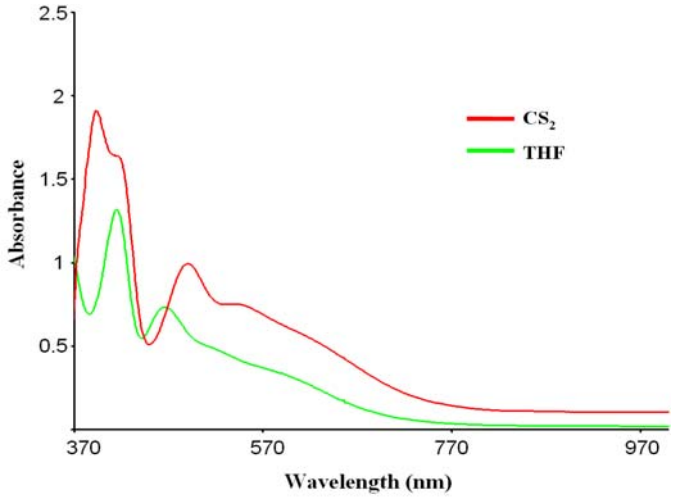

Figure S5. UV-vis measurements for 1 mM solutions of **2** in CS_2 (at -100 ºC) or THF (at -80 ºC).

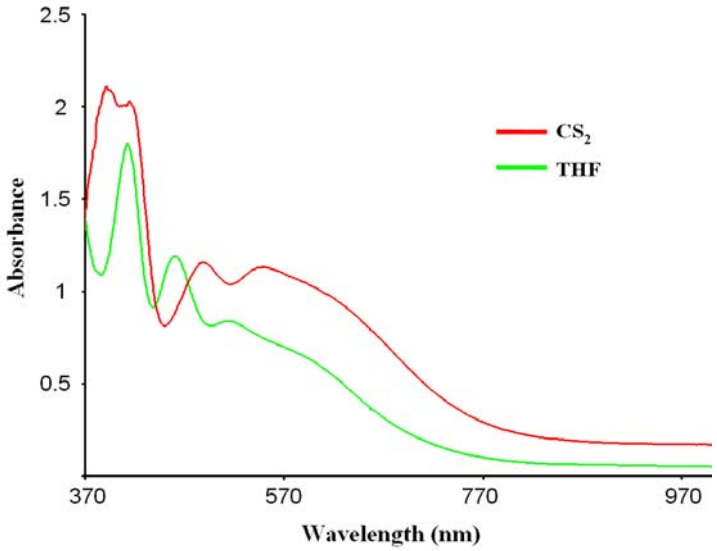

Figure S6. UV-vis spectra for 1 mM solutions of **3** in CS_2 or THF at -100ºC.

(a)

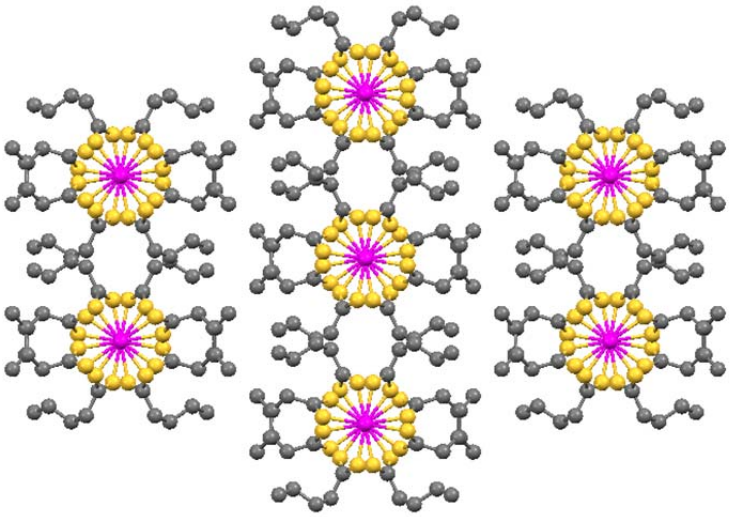

(b)

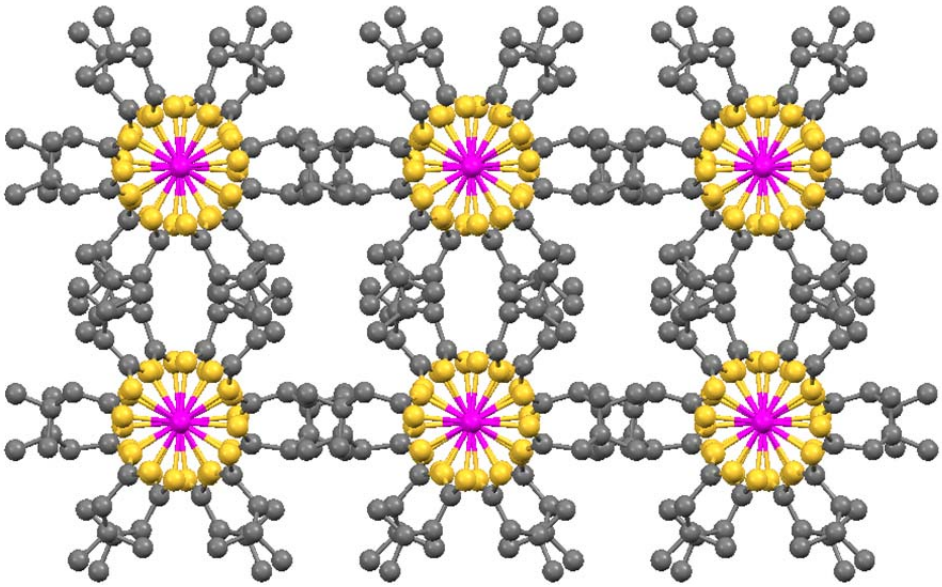

Figure S7. Crystal packing of compounds **1** (a) and **2** (b) viewed along the chain propagation axis.

Table S1. Crystallographic and structure refinement details of compounds **1** and **2**.

	1	**2**
Empirical formula	$C_{20}H_{36}Pt_2S_8$	$C_{20}H_{36}Pt_2S_8$
Formula weight	923.15	923.15
Crystal system	Orthorhombic	Orthorhombic
Space group	*Pccn*	*Ccc2*
T (K)	296(2)	100(2)
a (Å)	26.494(3)	18.1699(15)
b (Å)	9.1068(7)	23.304(3)
c (Å)	11.7111(10)	20.019(3)
V (Å3)	2825.7(4)	8476.7(18)
Z	4	12
ρ_{calc} (g cm^{-3})	2.170	2.170
μ (MoKα, mm^{-1})	10.491	10.491
Unique data/parameters	4318 / 137	7392 / 239
Reflections with I≥2σ(I)	3175	2881
R_{int}	0.0713	0.0611
GOF	1.084	0.968
Final R indices		
[I>2σ(I)] R1[a] / wR2[b]	0.0319 / 0.0402	0.0580 / 0.1411
All data R1[a] / wR2[b]	0.0811 / 0.0893	0.1402 / 0.1990

[a] $R1 = \sum||F_0|-|F_c|| / \sum|F_0|$; [b] $wR2 = [\sum w(F_0^2 - F_c^2)^2 / \sum wF_0^2]^{1/2}$; $w = 1/[\sigma^2(F_0^2) + (aP)^2 + b]$ where $P = (\max(F_0^2,0) + 2Fc^2)/3$ with a = 0.0386 (**1**) and 0.0668 (**2**); b = 8.2013 (**1**) and 0.0000 (**2**).

Table S2. Selected bond lengths (Å) of compounds **1** and **2**.[a]

Compound **1**		Compound **2**			
Pt1–S11	2.3142(12)	Pt1–S11	2.327(15)	Pt3–S32	2.299(15)
Pt1–S12	2.3213(12)	Pt1–S12b	2.353(14)	Pt3–S42	2.315(14)
Pt2–S21	2.3182(12)	Pt1–S21	2.305(15)	Pt3–S52	2.319(12)
Pt2–S22	2.3136(12)	Pt1–S22b	2.314(14)	Pt3–S62	2.338(15)
Pt1–Pt2	2.7366(4)	Pt2–S31	2.364(17)	Pt1–Pt1b	2.7619(12)
Pt1···Pt2a	3.1189(4)	Pt2–S41	2.298(9)	Pt2–Pt3	2.7680(9)
		Pt2–S51	2.324(13)	Pt1···Pt2	3.2676(9)
		Pt2–S61	2.273(16)	Pt3···Pt3c	3.3367(12)

[a] Symmetry codes: (a) x, –y+1/2, z+1/2; (b) –x+3/2, –y+1/2, z; (c) –x+1/2, –y+1/2, z.

Mulliken Calculations: Charge Differential Analysis

In Figure S8, we present a calculation of the charge differential analysis using the Mulliken methodology for the dimer $[Pt_2L_4]_2$ (with $L=S_2C(CH_2)_5CH_3$, hereafter) crystalline structure and two separated monomers $[Pt_2L_4]$ at 30 Å. We compared the Mulliken approach with the NPA (Natural Population Analysis) method, which was used in the theoretical section of the manuscript. Here, we can see that both analyses give essentially the same trends as for Pt and S atoms are concerned.

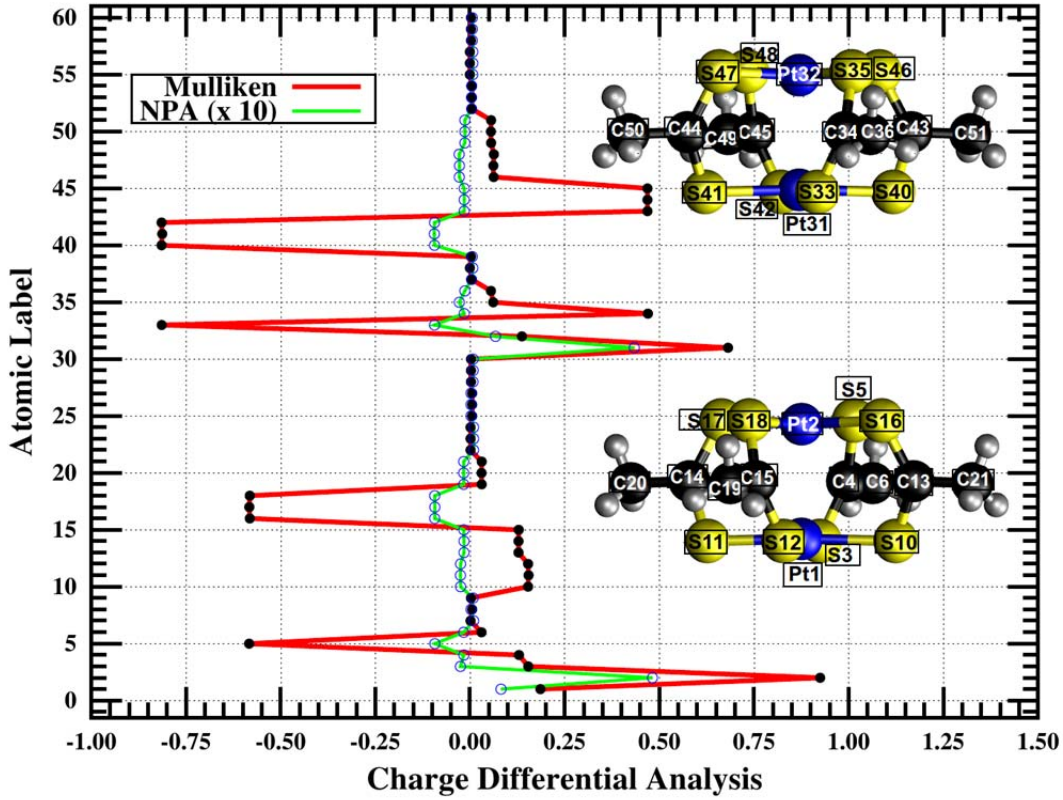

Figure S8. Calculated differential analysis using Mulliken method (in red) and NPA (Natural Population Analysis, in green) charges between the separated and the experimental $[Pt_2L_4]_2$ at the PBE0 level with LANL2TZ basis-set on the platinum atoms.

^{1}H NMR calculations for monomer and dimer

Table S3 shows the computed chemical shifts for the $[Pt_2L_4]$ and $[Pt_2L_4]_2$ structures, both in vacuum and in solvent. The latter was approximated using the PCM model. The computed proton chemical shifts are very similar between the monomer and dimer. Thus, our calculations predict that is difficult to distinguish the aggregation state of different $[Pt_2L_4]_n$ species in solution using the ^{1}H NMR technique.

Table S3. Isotropic part of the Gauge Independent Atomic orbital (GIAO) nuclear magnetic shielding tensors for protons (in ppm). All values are calculated at the same level of theory. Chemical Shifts (in ppm) are given in parentheses. Geometries were optimized at the PBE0 level using the basis sets LANL2DZ on Pt atoms and 6-311+G** for the rest.

Media/Compound	$[Pt_2L_4]$	$[Pt_2L_4]_2$	TMS
Vacuum	29.010150 (2.844950)	28.973029 (2.882071)	31.8551 (0.0)
CD_2Cl_2	28.893350 (2.90765)	28.867046 (2.933954)	31.8010 (0.0)

Optical absorption with TDDFT: influence of DFT exchange-correlation functional

Optical absorption spectra within Time Dependent Density Functional Theory (TDDFT) are commonly calculated using atom-centered basis sets. Here, we show that with the available basis-sets for the platinum, we have a problem with the calculation of the excited states for different $[Pt_2L_4]_2$ structures. In Figure S9, we show the optical absorption using both LANL2DZ and LANL2TZ basis sets and with different exchange-correlation functionals and input geometries. All computed spectra were calculated taken the first 50 single-excited states in the Casida formulation. We have that the description of the absorption in the low energy region is confusing even using the same initial geometrical structure. No clear trend is observed.

Figure S9 shows spectra computed from various geometries and different exchange correlation functionals. First, we consider the $[Pt_2L_4]_2$ crystalline geometry with CAM-B3LYP and PBE0 exchange-correlation level for the optics (lines red and dotted-green). Second, we consider the geometry obtained from the calculations using M06L functional (that gives a Pt···Pt bond distance of 3.365 Å) and CAM-B3LYP and PBE0 exchange-correlation level for the excited states (lines dashed-blue and pointed-magenta). The third level of calculation includes a model dimer (where we replaced the methyl groups in $[Pt_2L_4]_2$ by hydrogens) geometry optimized using M06L functional (lines pointed-aquamarine and dashed-yellow). The optical behavior is similar to the second group of calculations. It means that in general the influence of the methyl group attached to the final

carbons does not change significantly the optical spectrum. In the inserted box in Figure S9, we show the result for the optimized geometry at LANL2TZ using M06L functional (with a bond distance of 3.285 Å) and the same for the optics.

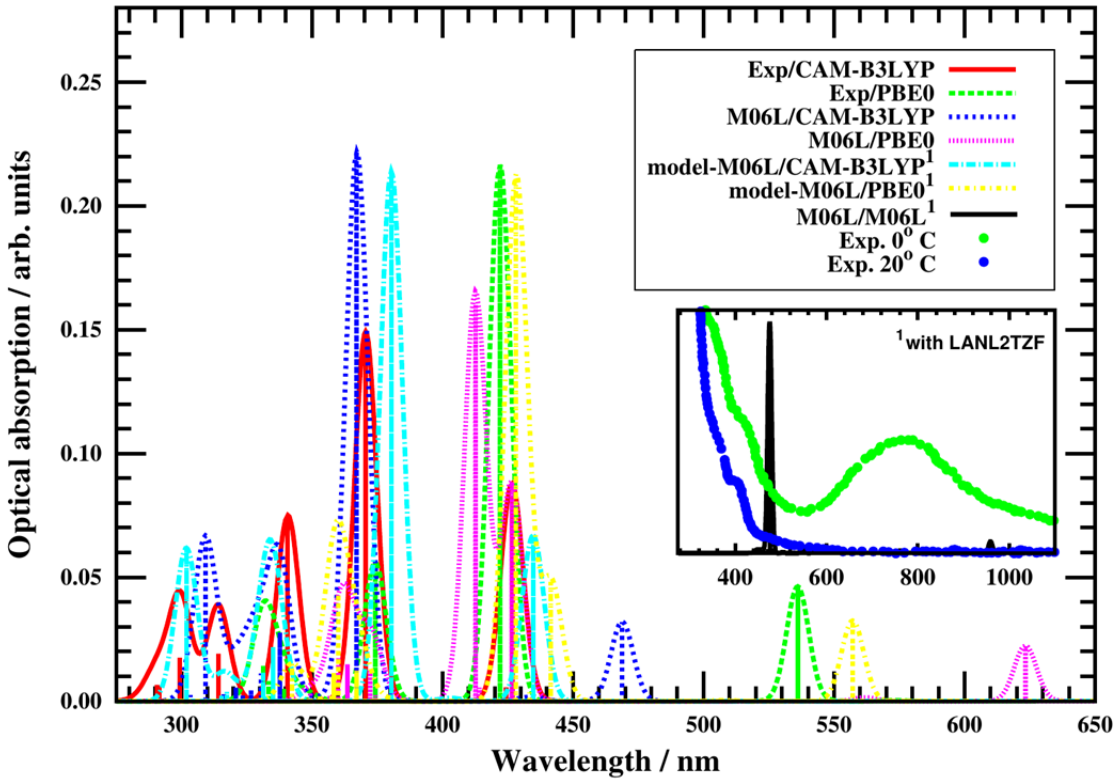

Figure S9. Optical absorption with TDDFT for different $[Pt_2L_4]_2$ structures with different exchange-correlation functional and basis-sets for Pt and input geometries. All results were obtained by using GAUSSIAN 09.

Optical absorption with real-time TDDFT at the LDA level

In the Figure S10, we present the optical absorption $[Pt_2L_4]_n$ (n=1-4) using real-time real-space methodology with the same geometrical parameters that we used for the calculation with GGA/PBE in the central part of the paper. The peaks at 416, 582, 719, and 778 nm correspond to $[Pt_2L_4]$, $[Pt_2L_4]_2$, $[Pt_2L_4]_3$ and $[Pt_2L_4]_4$ species, respectively, and they were calculated using the geometry from the crystallographic available data. The level of calculation was LDA with Perdew-Zunger exchange-correlation functional and the resulting spectra are very similar to the PBE ones reported in Fig. 9 of the main paper.

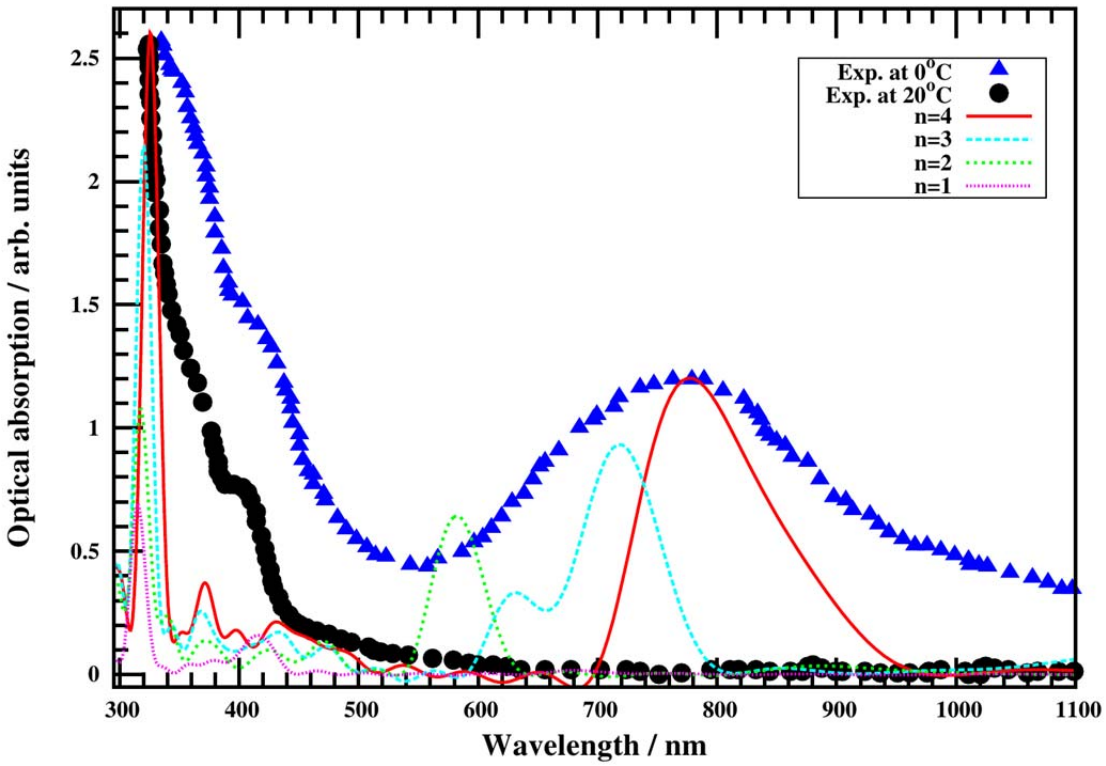

Figure S10. Computed optical absorption spectra with real-time real-space TDDFT at LDA/Perdew-Zunger level for $[Pt_2L_4]_n$ (n= 1-4) taken from crystalline structures. All values calculated with the OCTOPUS code.

Optical absorption with TDDFT: Influence of the explicit solvent

Figure S11 shows the effect on the optical absorption spectrum along the main principal axis of explicit solvent. We considered seven and twelve molecules of dichloromethane. We compare these results with the spectrum at the same level with our results in vacuum. We found that the electronic effect of CH_2Cl_2 on the visible region of $[Pt_2L_4]_n$ spectrum is negligible. We did not consider, however, the geometrical caging effect that the DCM may have on the structure of $[Pt_2L_4]$ polymers. This phenomenon could change the Pt···Pt distance resulting in a spread of the low energy band. Calculations were performed at PBE level using the OCTOPUS code. For the solvated systems, we needed to used a finite electronic temperature (with a Fermi-Dirac smearing function and a smearing of 0.08 eV) to converge the ground state.

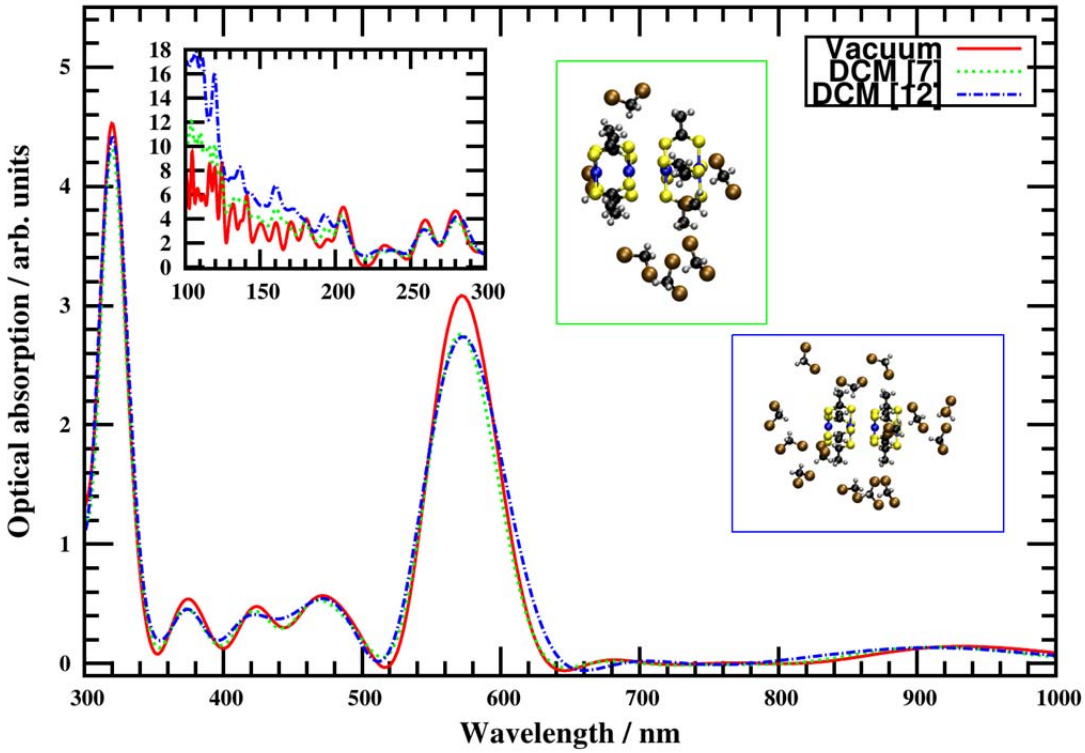

Figure S11. Solvent effect on the real-time TDDFT spectra of the dimer along the main axis of polarization. Seven (7) and twelve (12) dichloromethane molecules have been explicitly considered. The influence of the solvent on the spectra only appears at high energies and is shown in the inset. All values calculated with the OCTOPUS code.

Computed Ground State Properties: structure and energetics

Table S4. Computed binding energies (positive values indicate attractive interaction) and equilibrium distances for the dimer $[Pt_2L_4]_2$ using different exchange correlation functionals and basis sets. The LANL2DZ/LANL2TZ basis sets were used for Pt atoms and 6-311+G** on the rest. Basis set superposition error (BSSE) was corrected. [1] Values computed with the GAUSSIAN 09 package.[2] The binding energies were calculated from the difference in total energy between the relaxed $[Pt_2L_4]_2$ system and two non-interacting $[Pt_2L_4]$. The binding energy in the complete basis set limit was estimated to be 1.44 kcal/mol at the PBE level using the OCTOPUS code. [3, 4]

Functional	*Binding energy (Kcal/mol)*	*Distance (Å)*
LDA	15.78	3.016[1]
PBE	1.25	3.599[1]
CAM-B3LYP	-0.454	3.935[1]
PBE0	0.63	3.682[1,3]
	0.53	3.682[1]
	0.0	3.684[2]
	5.1	3.541[1,3] (PCM)
M06L	9.50	3.36465[1]
	9.355	3.285[2]
B97D	20.4	3.4900[1]
	20.7	3.4923[2]

[1] with LANL2DZ, [2] with LANL2TZ, [3] Without BSSE.

Regarding the binding energy of the Pt···Pt complex obtained from the above mentioned structural optimizations, we have that using highly parameterized functional such us M06-L by Truhlar and co-workers we found values around 9 kcal/mol. Using BP97-D,[5] the XC functional proposed by Grimme to include dispersion corrections, we found a binding energy around 20 kcal/mol.

The PBE family[1] (PBE, PBE0) produces the typical overbinding in the structure, as already known for other supramolecular systems.[6, 7] Similar behavior has been reported in other compounds with characteristic $d^8\cdots d^8$ (metal-metal) interactions.[1] We found that the basis set used to describe the platinum atom (if this include double or triple-ζ functions) has a

slight influence in the bond length for the same functional. However, this variation can be appreciable if highly parametrized functionals such as M06-L[8] is used. Furthermore, correcting the mentioned calculations using Basis Set Superposition Error scheme (BSSE)[3,4] does not change in more than 0.1 Å the bond length (Table 1).

Interaction of THF and CS_2 with one $[Pt_2L_4]$ monomer

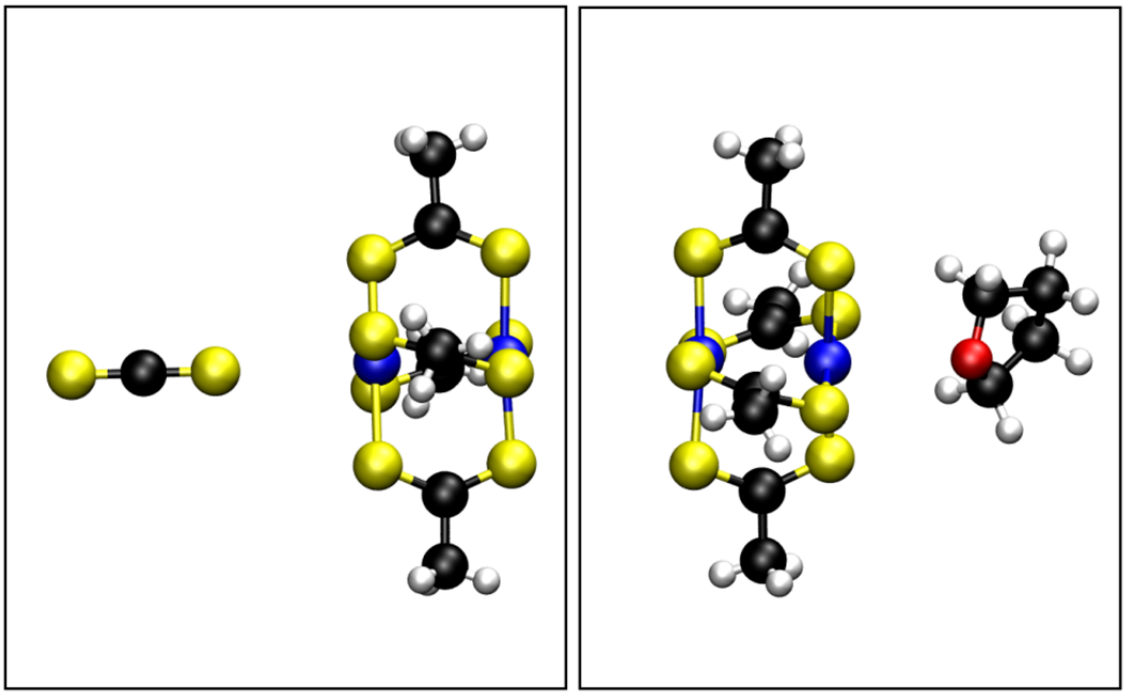

Figure S12. Relaxed solvent (Left: CS_2, Right: THF) configurations with one $[Pt_2L_4]$ monomer frozen at its experimental geometry. These relaxed structures were obtained using the CP2K code with the same parameters as described in the main paper.

References

1. C. Adamo and V. Barone, *J Chem Phys*, 1999, **110**, 6158-6170.
2. http://cp2k.berlios.de/.
3. S. F. Boys and F. Bernardi, *Mol Phys*, 2002, **100**, 65-73.
4. S. Simon, M. Duran and J. J. Dannenberg, *J Chem Phys*, 1996, **105**, 11024-11031.
5. S. Grimme, *J Comput Chem*, 2006, **27**, 1787-1799.
6. K. Raghavachari, *Theor Chem Acc*, 2000, **103**, 361-363.
7. P. J. Stephens, F. J. Devlin, C. F. Chabalowski and M. J. Frisch, *J Phys Chem-Us*, 1994, **98**, 11623-11627.
8. A. K. Wilson, T. vanMourik and T. H. Dunning, *Theochem-J Mol Struc*, 1996, **388**, 339-349.

Article 3

Title: The Isolation of Single MMX Chains from Solution: Unravelling the Assembly–Disassembly Process

Autors: Mohammad-Reza Azani, Alejandro Pérez Paz, Cristina Hermosa, Gonzalo Givaja, Julio Gómez-Herrero, Rubén Mas-Ballesté*, Félix Zamora* and Angel Rubio*

Journal: Chemistry - A European Journal

Year: 2013

Volume / Pages: 19 (46) / 15518-15529.

CHEMISTRY
A EUROPEAN JOURNAL

ChemPubSoc
Europe

DOI: 10.1002/chem.201301450

The Isolation of Single MMX Chains from Solution: Unravelling the Assembly–Disassembly Process**

Mohammad-Reza Azani,[a] Alejandro Pérez Paz,[b] Cristina Hermosa,[a] Gonzalo Givaja,[a] Julio Gómez-Herrero,[c, d] Rubén Mas-Ballesté,*[a] Felix Zamora,*[a, d] and Angel Rubio*[b]

Abstract: Herein, we provide a systematic theoretical and experimental study of the structural and optical properties of MMX (M = metal, X = halide) chains. The influence of solvent, temperature, and concentration has been analyzed to find suitable parameters for initial building-block associations in solution. By using density functional calculations, we have computed the dissociation energy of different MMX oligomers (up to the tetramer) in the gas phase. On the basis of these findings, we discuss the most likely disassembly scenario and propose a new interpretation of these compounds. We also calculated the charge redistribution that occurs upon MM + XMMX binding in vacuum. Time-dependent density functional theory (TDDFT) is used to calculate the UV/visible spectra of different MMX chains up to the tetramer in the gas phase. The implications of these theoretical findings in the analysis of our experiments are discussed in the text. The overall body of data presented suggests a new way of looking at such linear structures. By taking into account these new data, we have been able to isolate single/few MMX chains on mica.

Keywords: computational spectroscopy · density functional calculations · MMX chains · molecular wires · supramolecular assembly · surfaces

Introduction

Processability is the required condition of a material to be organized in a way suitable to form structures with specific functions. Organization of functional materials on the scale of a few nanometers, or even as molecules, is required for nanotechnological applications. This is a relevant problem, for example, in nanoelectronics in which the use of organic conductors is still restricted by their processability.

The self-organization of molecules based on noncovalent interactions have been extensively studied in solution,[1] in the solid state,[2] and on surfaces,[3] thus leading to a large variety of supramolecules with different architectures.[4] Some of these supramolecules have been constructed by using coordinative bonds.[5] In fact, the use of coordinate bonds allows the formation of an infinite association of two simple building blocks, such as metal entities and organic or inorganic ligands, with a large variety of architectures of different dimensionalities,[6] named as coordination polymers (CPs).

The kinetic lability of metal–ligand bonds[7] supports the reproducible construction of functional, highly ordered structures for a wide range of potential technological applications, including catalysis, gas storage, and separation,[8] and physical properties, such as electrical conductivity and magnetism.[9] Current interest in the development of highly conductive CPs is also motivated by their potential technological impact.[10] However, CPs are typically limited by their processability, which is mainly due to their null or low solubility.

In this context, remarkable exceptions are the so-called MMX (M = metal, X = halide) chains.[11] A MMX chain is formed by an arrangement of halide ions bridging dimetallic subunits in which metal ions (M) are connected by four ligands (e.g., pirophosphates or dithiocarboxylates). The MMX chains based on platinum, dithiocarboxylate ligands, and iodine (i.e., M = Pt and X = I) have shown metallic con-

[a] M.-R. Azani,[+] C. Hermosa, Dr. G. Givaja, Dr. R. Mas-Ballesté, Dr. F. Zamora
Departamento de Química Inorgánica
Universidad Autónoma de Madrid, 28049 Madrid (Spain)
E-mail: ruben.mas@uam.es
felix.zamora@uam.es

[b] Dr. A. P. Paz,[+] Prof. A. Rubio
Nano-Bio Spectroscopy group and
ETSF Scientific Development Centre
Departamento de Física de Materiales, Universidad del País Vasco
Centro de Física de Materiales CSIC-UPV/EHU-MPC and DIPC
Av. Tolosa 72, 20018 Donostia–San Sebastián (Spain)
E-mail: angel.rubio@ehu.es

[c] Prof. Dr. J. Gómez-Herrero
Departamento de Física de la Materia Condensada
Facultad de Ciencias
Universidad Autónoma de Madrid, 28049 Madrid (Spain)

[d] Prof. Dr. J. Gómez-Herrero, Dr. F. Zamora
Condensed Matter Physics Center (IFIMAC)
Universidad Autónoma de Madrid
28049 Madrid (Spain)

[+] These authors contributed equally to this work.

[**] M = metal, X = halide.

Supporting information for this article is available on the WWW under http://dx.doi.org/10.1002/chem.201301450.

CHEMISTRY
A EUROPEAN JOURNAL

ductivity at room temperature.[12] MMX chains are therefore promising candidates for nanoelectronic applications in which molecular wires that can transport electrical charges across long distances are required.[10,13] Furthermore, the relatively low work function (ca. 3.7 eV)[14] and the fact that thin films of MMX are almost transparent for thicknesses lower than 50 nm make this class of structure extremely appealing for molecular electronics and optoelectronics. Recently, some of us demonstrated experimentally the outstanding electrical properties of deposited MMX nanoribbons[14] and nanocrystals[15] ($[Pt_2(RCS_2)_4I]_n$; R = methyl or *n*-penthyl) on mica. The conductive nanoribbons were formed on mica by direct sublimation from crystals of $[Pt_2(methyl\text{-}CS_2)_4I]_n$ in high vacuum.[14,16]

Once the conductivity of nanostructures of MMX chains based on platinum–dithiocarboxylatos has been demonstrated, the next main challenge was the fabrication of a functional device based on these polymers. To address this goal and to exploit the depolymerization/repolymerization ability of MMX,[7] we performed the self-assembly in a spatially confined environment by using unconventional wet lithography,[17] thus obtaining sub-micrometric structures.

To gain further control over the deposition from a solution of $[Pt_2(RCS_2)_4I]_n$ chains, and with the aim of approaching the single-molecule level, the present work focuses on the understanding of the parameters that affect the assembly/disassembly process. We started by selecting $[Pt_2(RCS_2)_4I]_n$ chains with different alkyl groups at the dithiocarboxylato ligands to analyze the potential influence of steric factors. The spectroscopic experimental data obtained from solutions at different concentrations, temperatures, and solvents have been rationalized with theoretical calculations. These results have been fundamental for the rational design of nanostructures on surfaces to allow, for the first time, the isolation of single chains of $[Pt_2(RCS_2)_4I]_n$ on mica.

Results and Discussion

Dissociation in solution at room temperature: We first address the behavior in solution of the linear MMX chains of formula $[Pt_2(RCS_2)_4I]_n$ (R = $(CH_2)_4CH_3$ (**1**), $(CH_2)_3CH_3$ (**2**)). The crystal structures of **1** and **2** have been previously reported (see refs [15] and [18], respectively) and are described as the dithiocarboxylato MMX-chain type. At room temperature and in the crystalline phase, bimetallic units $[Pt_2(RCS_2)_4]^+$ are symmetrically bridged by iodide ligands. The cohesive force that hold together the MMX chains are Pt···I interdimer metal–ligand interactions. Although the chains interact weakly by means of van der Waals forces, thus leading to a rather 1D anisotropic material. Despite the polymeric nature of the structure found in the solid state, MMX compounds show a shocking ability to dissolve in a variety of organic solvents and a surprising tendency to recrystallize, thus recovering the polymeric structure. To obtain a deeper understanding on the reasons of such behavior, we analyzed the chemical nature of the species in solution that result from dissolving **1** and **2** in CH_2Cl_2, $CHCl_3$, THF, or CS_2.

At a first glance, two possibilities can be considered: 1) individual chains could be dispersed in some solvents to maintain their polymeric or oligomeric structure or 2) the chains are dissembled into their basic molecular subunits. If such is the case, two possible disassembly modes could be considered: 1) a symmetric cleavage mode, which generates a solution of paramagnetic $[Pt_2(RCS_2)_4I]^{\cdot}$ molecular species, or 2) an asymmetric cleavage mode, which generates an equimolar mixture of diamagnetic $[Pt_2(RCS_2)_4I_2]$ and $[Pt_2(RCS_2)_4]$ complexes (Scheme 1). In our attempt to search for evidence of the symmetric cleavage of MMX chains, we tried to measure EPR spectra of such solutions, but no paramagnetic signal was observed in any case. On the other hand, the fact that compounds $[Pt_2(RCS_2)_4I_2]$ and $[Pt_2(RCS_2)_4]$ are well known, easily isolable and characterizable, allowed us to compare the spectroscopic features found in the solutions of such compounds with those found in solutions of MMX chains. In this sense, ^{1}H NMR spectroscopic analysis clearly indicates that dissolving an MMX crystal always results in the formation of an equimolar mixture of $[Pt_2(RCS_2)_4I_2]$ and $[Pt_2(RCS_2)_4]$ complexes (Scheme 1). Independent of the dithioacetato ligand and regardless the nature of the solvent (polarity, coordinative ability, etc.), the same cleavage pattern is always observed. As a representative example, Figure 1 shows ^{1}H NMR spectroscopic data obtained for a solution of **2** in $CDCl_3$ relative to the features observed for precursors $[Pt_2(RCS_2)_4I_2]$ and $[Pt_2(RCS_2)_4]$ (R = $(CH_2)_3CH_3$; for additional data of **1** and **2** in a variety of solvents, see Figures S1 and S2 in the Supporting Information). Thus, from a thermodynamic point of view, an inherent preference for this pathway is observed, which will be further confirmed below by our First Principles calculations.

To determine whether the cleavage of MMX polymers into their molecular-building blocks is quantitative, we compared the UV/Vis spectroscopic features of 1 mM solutions of MMX with the spectra observed for solutions of the cor-

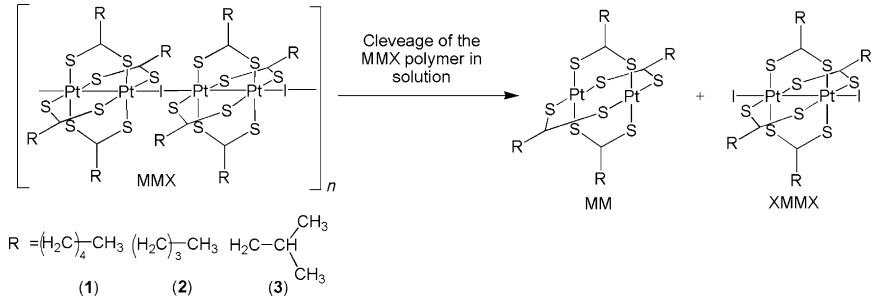

Scheme 1. Schematic illustration of the MMX-chain cleavage in solution.

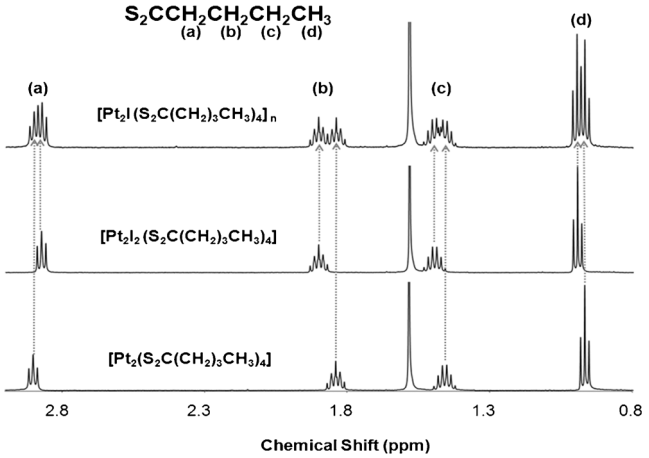

Figure 1. ^{1}H NMR spectrum obtained for a solution of **2** in $CDCl_3$ compared with the features observed for the precursors $[Pt_2(RCS_2)_4I_2]$ and $[Pt_2(RCS_2)_4]$ ($R=(CH_2)_3CH_3$).

responding $[Pt_2(RCS_2)_4I_2]$ (0.5 mM) and $[Pt_2(RCS_2)_4]$ (0.5 mM) measured independently. In all cases, the spectra of 1 mM solutions of MMX chains can be described as the addition of UV/Vis spectra obtained from 0.5 mM solutions of $[Pt_2(RCS_2)_4I_2]$ and $[Pt_2(RCS_2)_4]$. As a representative example, Figure 2 shows UV/Vis spectroscopic data obtained for a solution of **1** in CH_2Cl_2 (for **2**, see Figure S3 in the Supporting Information). Accordingly the disassembly of the MMX chains is quantitative in all cases.

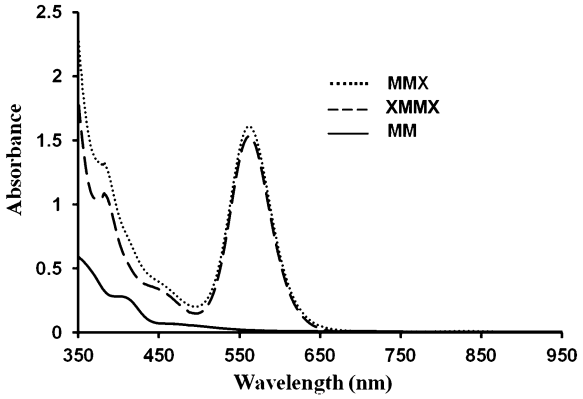

Figure 2. Comparison of the UV/Vis spectra obtained from 0.5 mM solutions of $[Pt_2(RCS_2)_4I_2]$ and $[Pt_2(RCS_2)_4]$ ($R=(CH_2)_4CH_3$) and data obtained for a 1 mM solution of **1**. All the spectra were measured at room temperature in CH_2Cl_2 with a 2 mm cell.

Reassembly of MMX chains 1–3 in CH_2Cl_2: In a recent report, we analyzed in detail the tendency of $[Pt_2(RCS_2)_4]$ fragments to self-assemble spontaneously in solution by decreasing the temperature. Following a similar approach, we studied the changes on the UV/Vis spectra of solutions of MMX at low temperature. For this study, we have added a third case with the ligand RCS_2^- ($R=CH_2CH(CH_3)_2$). Attempts to obtain crystals of MMX chains with this dithioacetato ligand have been unsuccessful. However, the $[Pt_2(RCS_2)_4I_2]$ and $[Pt_2(RCS_2)_4]$ compounds ($R=CH_2CH(CH_3)_2$) are easily isolable by using reported procedures.[12] Thus, regarding the fact that the dissolution of MMX chains are shown to be the result of dissociation into the corresponding $[Pt_2(RCS_2)_4I_2]$ and $[Pt_2(RCS_2)_4]$ building blocks, we also studied the behavior in solution of equimolar mixtures of $[Pt_2(RCS_2)_4I_2]$ and $[Pt_2(RCS_2)_4]$ ($R=CH_2CH(CH_3)_2$). Theses mixtures are considered in the following sections as solutions of the MMX polymer labeled as **3** in Scheme 1. Indeed, upon decreasing the temperature new spectroscopic features appear in the UV/Vis spectra from solutions of **1**–**3**. The specific absorption of the new bands also depends on the concentration.

Thus, the appearance of such new features is favored at higher concentrations. As a representative example, Figure 3 shows the low-temperature UV/Vis spectrum of **1** in CH_2Cl_2 relative to the spectra of the parent MM and XMMX units.

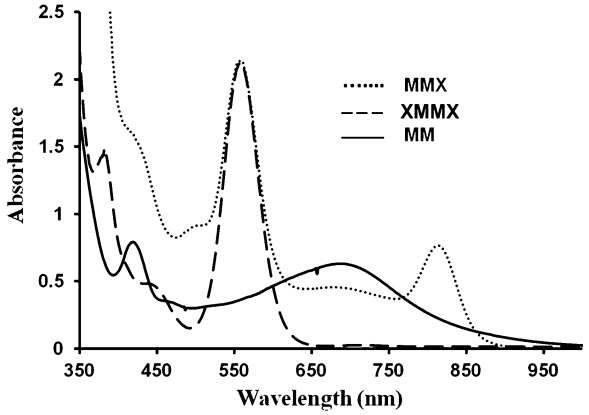

Figure 3. Comparison of the UV/Vis spectra obtained from 0.5 mM solutions of $[Pt_2(RCS_2)_4I_2]$ and $[Pt_2(RCS_2)_4]$ ($R=(CH_2)_4CH_3$) and data obtained for a 1 mM solution of **1**. All the spectra were measured at −70 °C in CH_2Cl_2 with a 2 mm cell.

The band at $\lambda=700$ nm is identical to the band recently reported for the MM···MM associations observed for pure $[Pt_2(RCS_2)_4]$. Because solutions of MMX in fact contain mixtures of MM and XMMX units, it is not surprising to observe some degree of MM···MM association under the similar conditions (concentration, temperature, solvent, etc.) that we observed previously for pure MM compounds. A second absorption appears at $\lambda=850$ nm. To discard the possibility that XMMX fragments follow somehow self-assembly processes, we measured the UV/Vis spectra of solutions of pure XMMX compounds at low temperature. No changes at low temperature were observed in such measurements. Thus, the formation of a band at $\lambda=850$ nm requires the simultaneous presence in solution of both MM and XMMX complexes. Consequently, an absorption at $\lambda=850$ nm is assigned to an association of $[Pt_2(RCS_2)_4]$ and $[Pt_2(RCS_2)_4I_2]$ similar to that observed in the MMX-chain structures (Scheme 2). An assignment of such a transition is further confirmed by First Principles optical calculations.

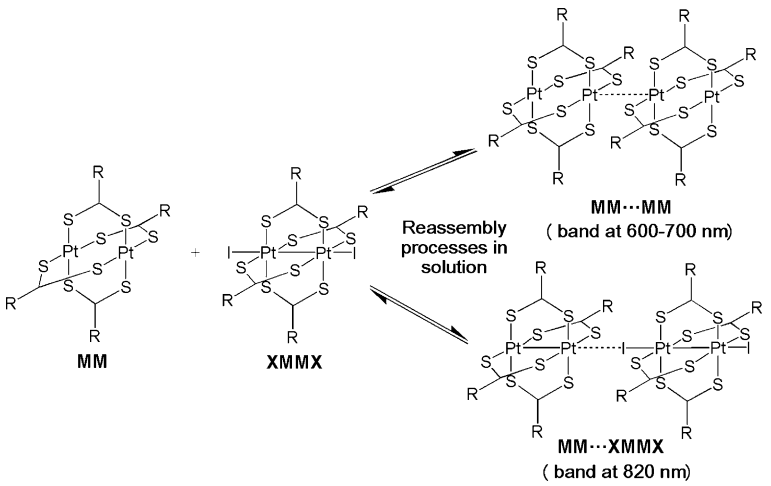

Scheme 2. Representation of the behavior observed for solutions of $[Pt_2(RCS_2)_4I]_n$.

In regard to the effect of the dithioacetato ligand, it is worth mentioning that the ratio between the MM···XMMX and MM···MM supramolecular assemblies is affected by the steric hindrance induced by each ligand. In fact, for the bulkier dithioacetato ligand in **3**, no MM···MM association is observed, and thus only the MM··XMMX assembly mode is detected by UV/Vis spectroscopic analysis. This effect is related to the different constraints imposed in the MM···MM and MM···XMMX assemblies. The bridging iodide anion in MM···XMMX separates the MM units in such a way that steric repulsion is much less critical than in MM···MM supramolecules (Figure 4).

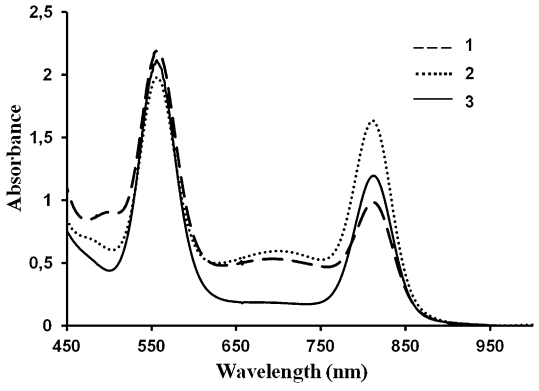

Figure 4. Comparison of the measured UV/Vis spectra obtained from 1 mM solutions of **1**–**3** measured at −80 °C in CH_2Cl_2 with a 2 mm cell.

Iodine titration: from MM to XMMX species: The observations presented above suggest that solutions of MMX in fact contain an equimolar mixture of MM and XMMX and that such a mixture results in MM···MM and MM···XMMX supramolecular assemblies at low temperature. To determine the behavior of the MM and XMMX mixtures with different molar ratios, we performed the titration of the MM compound $[Pt_2(RCS_2)_4]$ ($R=(CH_2)_4CH_3$) with variable amounts of I_2. The selection of this compound is based on its higher solubility to allow UV/Vis spectroscopic measurements at −60 °C without precipitation. Figure 5 presents the intensity of absorptions at low temperature (−60 °C) at $\lambda=550$ (due to the XMMX product), 700 (due to the MM···MM supramolecules), and 850 nm (due to the XMMX···MM supramolecular assemblies). Interestingly, up to 0.5 equivalents of I_2, a simultaneous increase of the absorbances at $\lambda=550$ and 850 nm is observed together with the decrease of the absorbance at $\lambda=$ 700 nm. This observation indicates that the $[Pt_2(RCS_2)_4]$ compound is being consumed and $[Pt_2(RCS_2)_4I_2]$ is formed to allow not only MM···MM but also MM···XMMX interactions. The behavior at 0.5 equivalents of I_2 is the same as that observed for MMX polymer **1**. From 0.5 to 1 equivalents of I_2, an increase of the absorbance at $\lambda=550$ nm is observed together with the decrease of absorbances at $\lambda=700$ and 850 nm. Curiously, the decrease of absorptions at $\lambda=700$ and 850 nm is not synchronic. Thus, the equilibrium is shifted because the MM···MM interaction is less favorable, but the MM···XMMX interaction is still possible while some MM is still present in solution at higher concentrations of $[Pt_2(RCS_2)_4I_2]$.

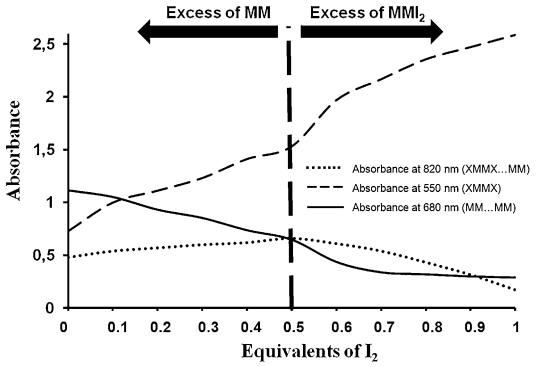

Figure 5. Intensity of absorptions at low temperature (−60 °C) at $\lambda=550$, 680 and 850 nm from a 1 mM solution of $[Pt_2(RCS_2)_4]$ ($R=(CH_2)_4CH_3$) in CH_2Cl_2 at −60 °C after the addition of variable amounts of I_2.

Effect of the solvent in the reassembly in solution: The effect of the solvent in self-assembly process of **1**–**3** in solution has been examined by comparing the behavior of the solutions with CH_2Cl_2, $CHCl_3$, THF, and CS_2 as the solvents. Compounds **1**–**3** show comparable trends. For clarity, the discussion centers on the results for complex **1** (the results

obtained with complexes **2** and **3**; see Figure S4 in the Supporting Information).

Figure 6 shows the UV/Vis spectra of 1 mM solutions of **1** in the different solvents at −60 °C, which is the limit temperature that prevents precipitation in all the investigated solvents. It is worth noting that the solubility in CH_2Cl_2, CS_2, and THF is higher than in $CHCl_3$, thus allowing measurements at temperatures as low as −90 °C at which a major degree of supramolecular association is observed only in CH_2Cl_2 (see Figure S5 in the Supporting Information). However, unique conditions are required to compare the inherent ability of **1** to associate in different solvents. Thus, under the same conditions, whereas a certain degree of self-assembly in CH_2Cl_2 and $CHCl_3$ is observed, CS_2 and THF hamper the association in solution. This effect could, in principle, be justified by considering the known coordinative ability of such solvents, which could result in weak metal–solvent or solvation interactions between the solvent molecules and the MM species, as previously reported for pure MM precursors. Therefore, blocking of the MM part hampers both the MM···MM and MM···XMMX assemblies.

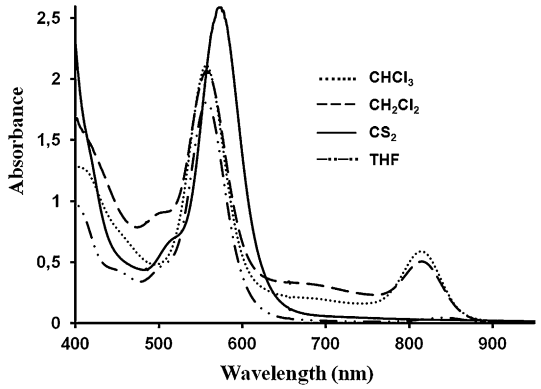

Figure 6. UV/Vis spectra measured for 1 mM solutions of **1** (2 mm cell at −60 °C) in $CHCl_3$, CH_2Cl_2, THF, and CS_2.

In addition to the expected difference between coordinative and noncoordinative solvents, a surprising difference is observed between CH_2Cl_2 and $CHCl_3$. Thus, although bands that correspond to the MM···XMMX and MM···MM interactions are present in CH_2Cl_2, the assembly is favored toward MM···XMMX interactions in $CHCl_3$ in spite of the MM···MM aggregation, which is observed in a minor proportion. In a previous study, we reported that the association of MM pure precursors was less favorable in $CHCl_3$ than in CH_2Cl_2.[19] This effect is again observed in this study for the MM···MM association, but not for the MM···XMMX assembly. The reasons for this selectivity can be understood as a more efficient way of $CHCl_3$ to solvate and block the MM units, which shifts the equilibrium toward the XMMX···MM assembly.

Photoinduced reassembly of MMX structures in THF: In the course of the UV/Vis experiments, an unexpected observation took place. Continuous irradiation of MMX solutions enhanced their ability to generate supramolecular assemblies in solution. Several light/dark cycles were essayed for **1** in THF (Figure 7). In the light phases, we left the shutter of the UV/Vis instrument open, and then irradiation over the range $\lambda = 200$–1100 nm was produced from the lamps of the instrument to the solution in the cuvette at −90 °C.

During this period (3600 s), we measured consecutive spectra, which show an increase of the band intensity at $\lambda =$ 850 nm. After the self-assembly reached its maximum, the lamp in the instrument was switched off during a dark period of 60 minutes and the sample was left in the instrument at −90 °C. After this period, no supramolecular interactions were detected in solution, but the MM···XMMX structures were reassembled by irradiating the sample again. Interestingly, the ratio of MM···MM/MM···XMMX shifted toward MM···XMMX in this system, as can be appreciated in the spectra shown in Figure 8.

This reversible photoinduced assembly process is probably due to the photo-dissociation of the THF···MM interaction. Accordingly, the pure MM precursor shows some degree of photoinduced association, but to a much lower extent. This proposed photo-dissociation mechanism would lead to a slowly release of "free" MM species, which in the presence of an excess of XMMX would preferentially form the complex MM···XMMX.

From solution to surface: temperature dependent assembly of MMX nanostructures: By taking into account the results observed concerning the temperature dependence and the effect of the solvents in the MMX solutions, we decided to explore the possibility of producing MMX nanostructures on surfaces. This object is a primary goal towards a direct

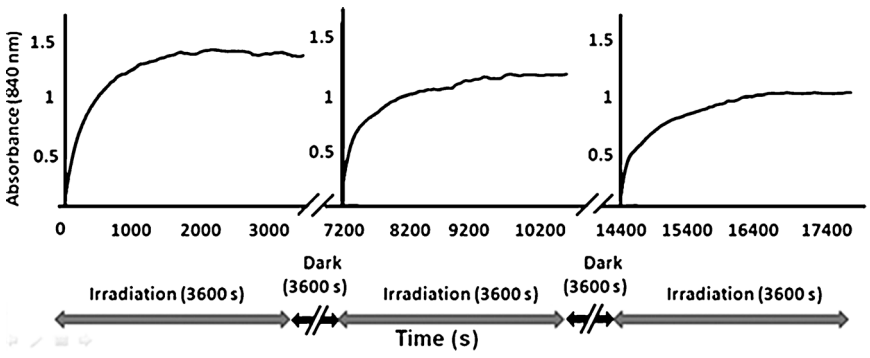

Figure 7. Variations in the absorbance at $\lambda = 840$ nm observed in a 1 mM solution of **1** in THF (2 mm cell at −90 °C) during irradiation/dark cycles. The solution was exposed to UV/Vis radiation with continuous frequencies over the range $\lambda = 200$–1100 nm.

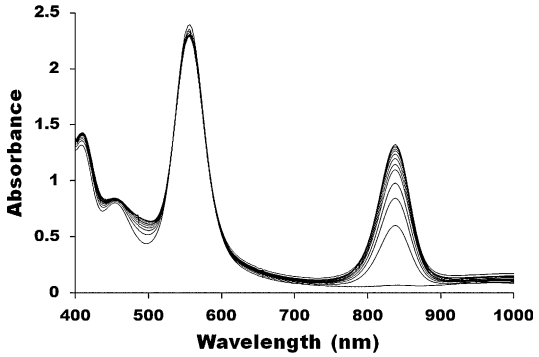

Figure 8. Time evolution of UV/Vis spectra measured during the irradiation process of a 1 mM solution of **1** in THF (2 mm cell at −90 °C). The solution was exposed to UV/Vis radiation with continuous frequencies over the range $\lambda = 200$–1100 nm. Each spectrum was recorded every 200 seconds (time increases from bottom to top).

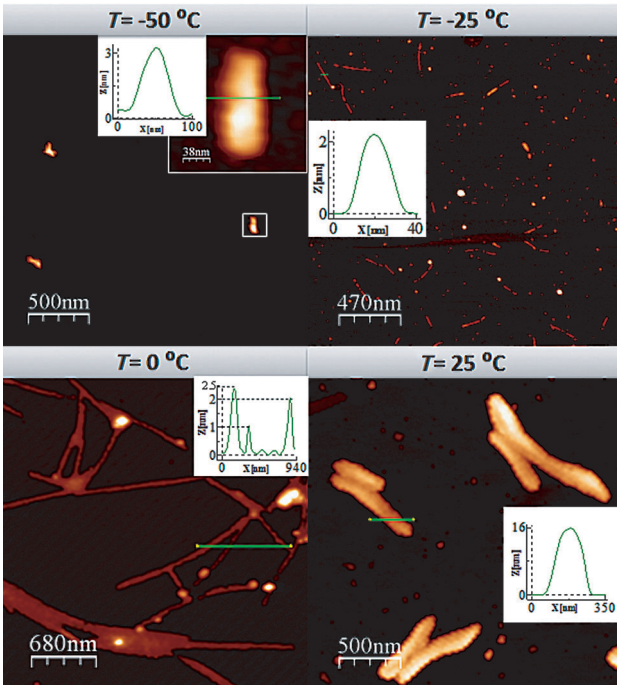

Figure 9. AFM topographic images of solutions of $[Pt_2(CH_3CS_2)_4I]_n$ in CH_2Cl_2 deposited on mica at different temperatures.

electrical measurement of isolated single chains of MMX to prove their potential as molecular wires. In this context, we have recently reported on the isolation of nanoribbons of $[Pt_2(CH_3CS_2)_4I]_n$ on mica and SiO_2, which allowed us to measure, for the first time, electrical conductivity of bundles of MMX chains on the nanoscale.[14,20] The procedure to obtain such structures was based on sublimation from crystalline samples,[16] which is somehow a surprising method for a polymeric material. However, considering the easy assembly/disassembly processes observed for MMX in solution,[21] it is now easy to rationalize how the molecular building blocks of MMX chains, namely, MM and XMMX, could be generated with thermal energy, evaporate, and fly to land on the surface and then diffuse and reassemble again to form MMX chains. In a more recent study, we tried to assemble MMX chains on surfaces from solutions.[15] In that case, the formation of nanocrystals and bundles was observed but we were unable to characterize single molecules on surfaces.

Now, by taking as a starting point the detailed study of the factors that have an effect on the assembly of MMX chains in solution by supramolecular aggregation of their MM and XMMX precursors, we revisited, from a new perspective, the problem of the assembly MMX chains on surfaces by assembly of their building blocks in solution. We investigated the effect of temperature on the nanostructures found on surfaces after deposition of solutions of a MMX polymer. A previous report followed a similar approach for the study of assembly on the surfaces of $[Pt_2(CH_3CS_2)_4]$.[19] Now, we complete our understanding of this system by analyzing the assembly on surfaces of $[Pt_2(CH_3CS_2)_4I]_n$.

Figure 9 shows the AFM topographic images obtained upon deposition of 0.1 mg mL^{-1} solutions of $[Pt_2(CH_3CS_2)_4I]_n$ in CH_2Cl_2 on mica at −50, −25, 0, and 25 °C. Although at room temperature, nanocrystals with heights of 15–25 nm are observed; single/few chains that are several microns length with heights of approximately 0.5–2.5 nm are found at 0 °C (note that a single $[Pt_2(CH_3CS_2)_4I]_n$ chain shows a diameter of approximately 0.5 nm based on X-ray diffraction measurements).[12] Decreasing the temperature to −25 °C results in the formation of shorter chains (0.5 μm) of similar heights. Furthermore, small rodlike structures (200 × 50 × 3 nm) are found at −50 °C. In principle, these findings could seem counterintuitive because bigger crystals are generally formed under slow-evaporation conditions, such as low temperature. However, our observations have to be understood by considering two factors: 1) the degree of association of the species present in solution and 2) the diffusion at the interface between solution and surface. Thus, individual molecular building blocks are in solution at 25 °C, which self-organize to form 3D crystals/nanocrystals only under saturated concentrations, reached by evaporation of the solvent. In contrast, at low-temperature oligomeric species are already preformed, which directs the final assembly toward 1D nanostructures. However, the limited diffusion of the building blocks at the solution/surface interface restricts the formation of long chains at −25 °C, and especially at −50 °C.

Overall, these results show, for the first time, the isolation of single, or near to, single chains of $[Pt_2(CH_3CS_2)_4I]_n$ on mica, which is an insulator substrate suitable for further electrical characterization.

DFT description of the XMMX···MM interaction: To gain a fundamental understanding of the association processes observed for MMX structures, we computed binding energies by using DFT calculations. To minimize computational costs, we considered $[Pt_2(RCS_2)_4I]_n$ (R = CH_3) as the simplest representative compound of the family $[Pt_2(RCS_2)_4I]_n$ chains (R = alkyl groups). For brevity, in the following, we will use the common nomenclature given in previous reports that names $[Pt_2(RCS_2)_4I_2]$ as XMMX and $[Pt_2(RCS_2)_4]$ as

MM, where in our study M refers to platinum atoms and X represents the iodine atom. The supramolecules considered herein for computation were the dimer (XMMX-MM), trimers (XMMX-MM-XMMX and MM-XMMX-MM), and lastly, the tetramer complex (XMMX-MM-XMMX-MM).

The first question to be addressed with our DFT calculations concerns the preferred mode of dissociation of $(XMMX\text{-}MM)_n$ oligomer chains in the gas phase. For the dimer MM-XMMX, we can distinguish two modes of dissociation (Scheme 3, top): the symmetric cleavage, which generates two paramagnetic species MMX, and the asymmetric breakage, which leads to the diamagnetic species XMMX and MM. For the trimers and tetramer, we consider one end of the chain and proceed similarly as in the dimer. The specific nature of the dissociation products depends on the nuclearity (shown in Scheme 3). In the calculations, whenever radicals were encountered (symmetric cleavage) we employed spin-unrestricted DFT with a fixed doublet spin state to deal with the odd number of electrons in the dissociated fragments. Thus, in this study, we do not deal with the complicated spin-state nature of the MMX compounds.

The calculated dissociation energies and pathways are described in Scheme 3. The dissociation-energy values were computed by using the real-space DFT code OCTOPUS.[22] All the investigated dissociation processes were barrierless. The calculated data show that for all the isolated oligomers, the symmetric cleavage (which leads to the production of MMX radicals) is largely suppressed with respect to asymmetric dissociation. Thus, DFT calculations predict that the asymmetric mode of cleavage is the preferred route for dissociation and that the energy cost of this mode is of the order of a hydrogen bond. This finding is consistent with the absence of EPR signals in our experimental data observed for MMX solutions. Because enthalpic factors promote the polymerization process in the gas phase up to the largest oligomer studied herein (tetramer), these data seem to suggest that the termination process could be due to the obvious entropic cost of assembly. The consistency of the dissociation energies shown in Scheme 3 was further confirmed by using a completely different methodology ab initio; that is, we double checked our binding energies with an atom-centered basis set as implemented in the Gaussian 09 package.[23] The resulting values differ within 1 kcal mol^{-1} or less (see the Supporting Information). Similar calculations using an implicit solvent (polarisable continuum model (PCM)) have extended our conclusions to same oligomers in solution (see the Supporting Information). Unlike our recent work on $[MM]_n$ oligomers,[24] we note here that the DFT methods seem to describe satisfactorily the energetics of inter-

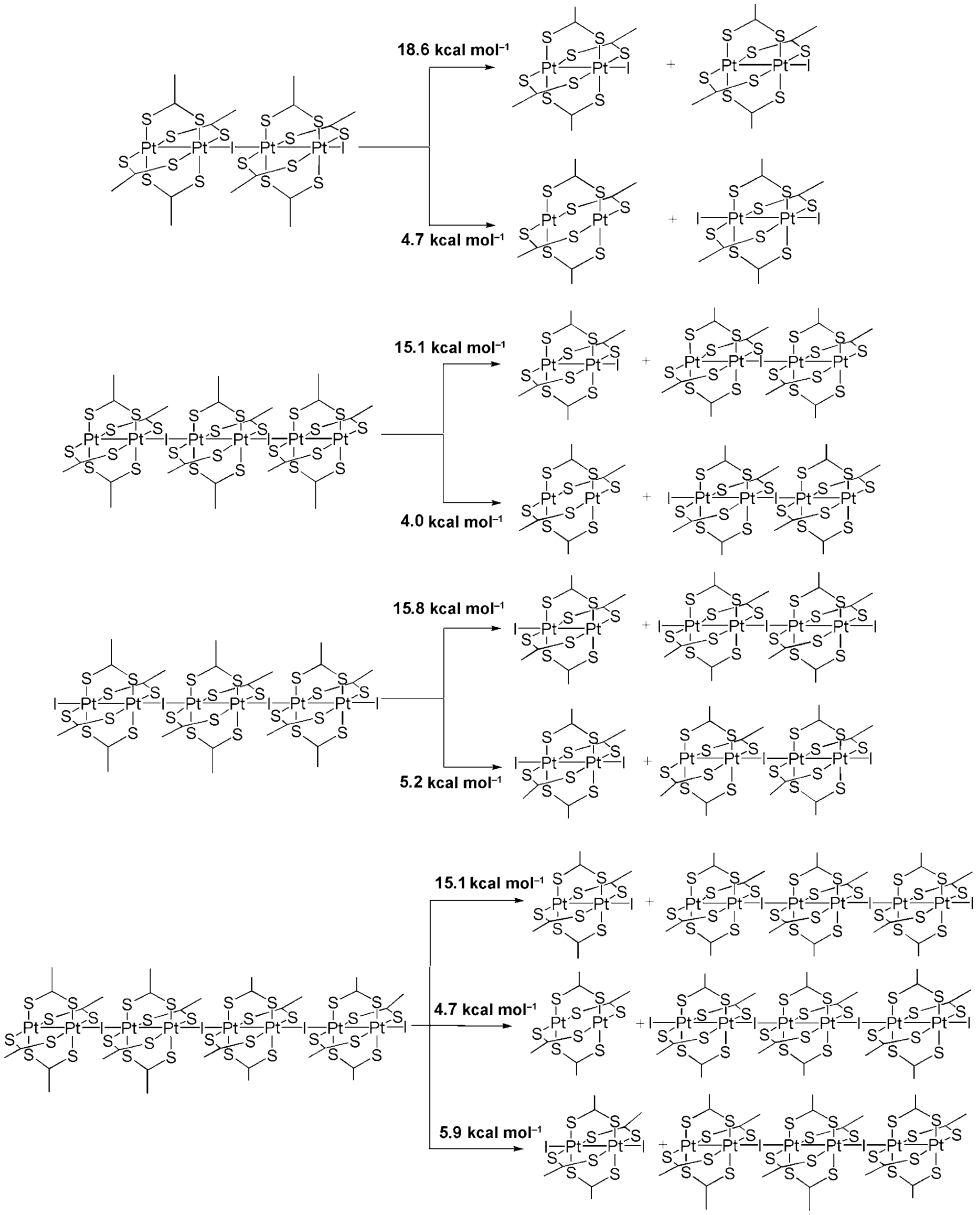

Scheme 3. Dissociation pathways of MMX oligomers from the dimer (top) up to the tetramer (bottom). Dissociation energies were calculated in the complete basis-set limit and PBE level on the gas-phase molecules.

molecular XMMX···MM associations.

The charge redistribution upon dimer formation is shown in Figure 10 following the natural population analysis (NPA) and Mulliken definitions. The differential-charge analysis is a meaningful way to characterize the charge redistribution, thus providing valuable insight into the nature of the associative process. Our results show that there is a good agreement between the NPA and Mulliken definitions for most of the atoms, except for a discrepancy in magnitude (but not in sign) for the iodine atom in the central region (labeled as 8; Figure 10). A negative (positive) value of $Q_{eq}-Q_{sep}$ means that a given atom at the equilibrium geometry is electron richer (poorer) than when the complex is dissociated. The results obtained predict that all the methyl groups and sulfur and platinum atoms away from the intermolecular region are unaffected upon binding. Upon dimerization, the platinum atom 9 of the MM moiety becomes electron richer, whereas the platinum atom 7 in XMMX loses electron density. In addition, the central sulfur atoms of MM become electron poorer but an opposite trend is predicted for the central sulfur atoms in MMX. Meanwhile, the central iodine 8 donates electronic charge to the MM platinum atom 9 as the XMMX interacts with the MM unit. Thus, XMMX can be considered to be an electron donor to the acceptor MM molecule in the dimer formation.

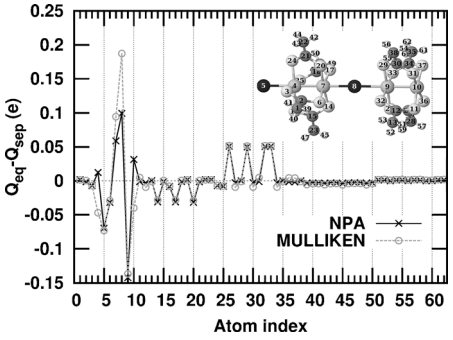

Figure 10. Computed charge differentials $Q_{eq}-Q_{sep}$ according to the Mulliken and NPA definitions. The subscripts "eq" and "sep" denote the equilibrium and separated configurations of the XMMX-MM complex in gas phase, respectively. In the inset, the atomic indices are shown in a ball-and-stick representation of the equilibrium structure. Pt atoms are depicted as gray spheres labeled as 4, 7, 9, and 10; S atoms are light-gray spheres labeled as 3, 6, 11, 14, 16, 17, 20, 24, 25, 26, 29, 31, 32, 33, 36, and 37; I atoms are black spheres labeled as 5 and 8; C atoms are dark-gray spheres labeled as 1, 2, 12, 13, 15, 18, 19, 21, 22, 23, 27, 28, 30, 34, 35, and 38; H atoms are small white spheres.

A depiction of the charge redistribution that occurs upon dimer formation is summarized in Scheme 4. The following scenario is found: The Pt atoms of the XMMX and MM isolated monomers initially have a symmetrical charge distribution. Upon binding, a charge asymmetry is induced in these atoms. In fact, the Pt(III) center in XMMX that is closer to the MM fragment acts as electron donor toward the sulfur atoms and the central iodine atom, which also donates electron density to the MM moiety. Regarding the acceptor nature of the Pt(II) center in MM, closer to the XMMX moiety, the NPA calculation reveals that Pt 6p atomic orbitals accommodate electronic charge from the central iodine atom and the adjacent sulfur atoms.

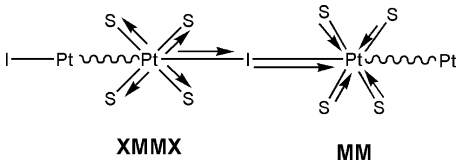

Scheme 4. Charge distribution that occurs when XMMX and MM interact. The arrows indicate the flow of the electronic charge when the dimerization (XMMX + MM → XMMX-MM) takes place.

Overall, the driving force for the Pt-Pt···I-Pt-Pt-I interaction arises from the interaction between the empty (acceptor) $6p_z$ orbitals of the platinum atom in MM with the occupied $5p_z$ atomic orbitals (donor) of the iodine atom. This claim is based on the hybridization of the $6p_z$ orbital of the platinum atom (which is unoccupied in the isolated atom) in the occupied molecular orbitals of the complex. Such a donor–acceptor interaction is much weaker than the regular metal–ligand bonding, and, in fact, falls in the range of supramolecular interactions such as hydrogen bonding. Thus, our theoretical analysis suggests that we may regard MMX compounds as molecular aggregates rather than coordination polymers. Such an interpretation is fully consistent with the experimental behavior observed.

Optical spectra of small XMMX···MM oligomers from TDDFT calculations: To validate our interpretation of UV/Vis spectroscopic data, we calculated the spectra of $[Pt_2(RCS_2)_4I]_n$ oligomers (named as $[MMX]_n$ for brevity) by using time-dependent density functional theory (TDDFT). Figure 11 shows the computed TDDFT optical spectra of XMMX and various $[MM\text{-}MMX]_n$ oligomers. Experimental

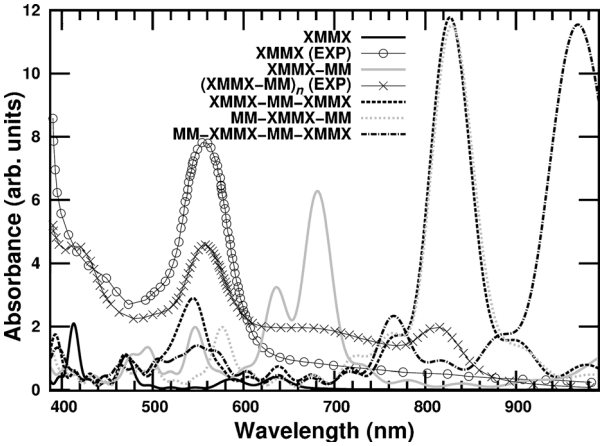

Figure 11. Calculated TDDFT spectra of XMMX and its different oligomers with MM in the gas phase at the PBE level by using the OCTOPUS code.[22] The computed spectra were normalized by the number of monomers. Only the polarization along the molecular chain was considered. The experimental spectra measured at −60 °C in CH_2Cl_2 for **2** (line with x) and the related XMMX monomer (line with empty circles) are also shown (EXP, in legend) for comparison.

spectra measured in CH_2Cl_2 at −60 °C for **2** and the related XMMX monomer have been also included for comparison. All the calculated spectra are dominated by the axial polarization (i.e., the molecular axis), whereas the contribution from the perpendicular directions is much weaker (not shown). For the XMMX monomer, we found a fair agreement between the experimental and our calculated spectra. Discrepancies found could be due to TDDFT limitations and/or to the lack of solvent in our gas-phase optical calculations. In any case, reasonable agreement exists between the calculated and experimental spectra of the XMMX compound, which validates the use of TDDFT calculations to perform a qualitative theoretical spectroscopic analysis of MMX oligomers.

The experimental spectrum of MMX in solution at low temperature shown in Figure 11 features a prominent band at $\lambda = 820$ nm that is not present in the experimental spectrum of XMMX. This finding immediately suggests that this band should be related to transitions involving the Pt···I interaction between the XMMX and MM monomers. This conjecture is confirmed by our TDDFT calculations, in which we see a prominent band at around $\lambda = 830$ nm characteristic of the trimers MM-XMMX-MM and XMMX-MM-XMMX. Thus, considering that spectra calculated for the dimer and tetramer significantly differ from the experimental observations, the TDDFT calculations suggest the formation of trimers in solution. This calculated peak at $\lambda =$ 830 nm involves mostly electronic transitions from a MO delocalized over the Pt-Pt-I backbone; namely, HOMO→ LUMO (32.6%), HOMO→LUMO+12 (31.3%), and HOMO−1→LUMO+1 (19.1%). The tetramer MM-XMMX-MM-XMMX shows a similar intense peak but is red-shifted to $\lambda = 968$ nm. The dimer XMMX-MM, on the other hand, does not exhibit such low-energy bands and instead features a double peak at $\lambda = 623$ and 680 nm attributed to transitions from HOMO→LUMO+6 (41.1%) and from HOMO−1→LUMO+7 (42.2%). As argued in the Experimental Section, the self-association of MM contributes to the broadening of the signal between the main experimental peaks (i.e., $\lambda = 550$ and 820 nm). Deep in the near-IR region ($\lambda > 1000$ nm; data not shown), computed spectra feature broad bands starting at $\lambda = 1000$ nm for the dimer and extending up to $\lambda = 1600$ nm for the tetramer. Such bands are due to transitions that originate from the HOMO to mostly LUMO (48.4%) with a smaller contribution of other higher orbitals such as LUMO+8 (20.7%) and LUMO+9 (24.9%) for XMMX-MM.

Figure 12 shows the main MOs involved in the electronic transitions described above. The Kohn–Sham dimer HOMO consists of a mixture of σ* combinations of the different platinum $5d_{z2}$ and 5 d_{x2-y2} and iodine $5p_z$ atomic orbitals, except for a σ combination found in the XMM-X bond in the central region. We found a pair of degenerate MOs (i.e., HOMO−1 and HOMO−2) localized on the XMMX moiety at about 0.62 eV below the HOMO. These MOs feature a purely π* combination between the $5p_{x/y}$ atomic orbital of distal iodine atom with the $5d_{xz/yz}$ atomic orbital of the terminal platinum atom, all away from the intermolecular region. Because these MOs are localized on the XMMX part, we anticipated (and confirmed) that their energies remain unaffected regardless of the distance between the XMMX and MM units. The LUMO of the dimer is delocalized over the Pt-Pt-I molecular backbone and resembles the HOMO, except that is 1 eV higher in energy and that the sign of the iodine $5p_z$ orbital is reverse, which results in a purely σ* combination between all the platinum $5d_{z2}$ and 5 d_{x2-y2} and iodine $5p_z$ atomic orbitals.

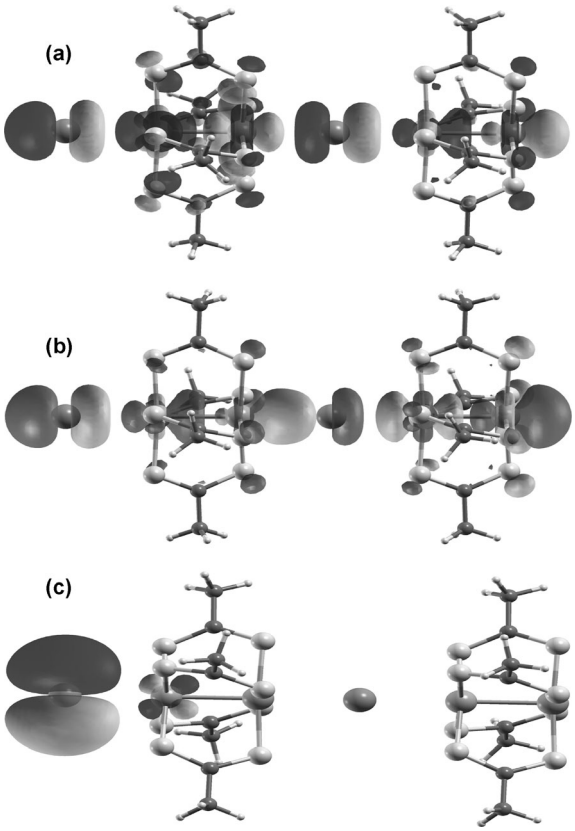

Figure 12. Selected Kohn–Sham molecular orbitals for the MMX-MM complex in the gas phase calculated at the PBE level by using the OCTOPUS code. The isosurface contours correspond to a value of +0.06 (gray) and −0.06 (black) $(e\,Å^{-3})^{1/2}$. The following orbitals are depicted: a) LUMO, b) HOMO, and c) HOMO−1. The latter MO is degenerate.

Electronic and optical properties of the periodic MMX system: Due to their high computational cost, oligomers $[MMX]_n$ with $n = 5$ or higher were not calculated. Nonetheless, to get an idea of the spectroscopic signals that could be expected for long MMX chains, we present herein the computed spectra of a periodic one-dimensional MMX system, which could be also useful to interpret the spectra of the MMX compound in the solid state.

The electronic properties of MMX are summarized in Figure 13, which displays the calculated band structure and projected density of states (PDOS) along the chain direction. Figure 13 (left) features a nearly constant LUMO and HOMO−1 levels and a highly dispersive metallic half-filled

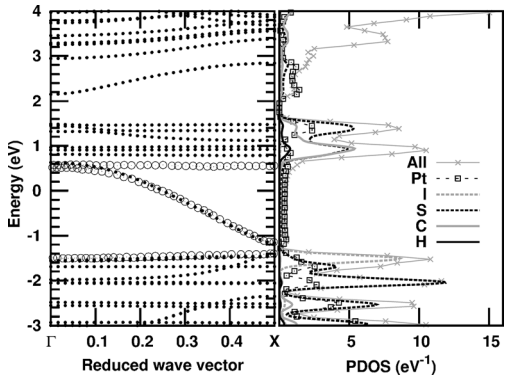

Figure 13. Calculated band structure (left) and projected density of states (PDOS; right) of an isolated infinite chain of MMXs in vacuum computed at the PBE level with the GPAW code.[26] The reduced wave vector is in units of $2\pi/L_x$ ($L_x = 8.63$ Å) is the length of the unit cell along the periodic dimension. HOMO−1, HOMO, and LUMO bands from ref. [25] are shown by the empty circles on the left. All energies are given with respect to the Fermi level.

HOMO band. The difference in energy of the HOMO between the Γ point and the edge of the Brillouin Zone (BZ), the so-called bandwidth, is 1.789 eV, which is in good agreement with the PBE value of 1.70 eV computed by Di Felice and co-workers.[25] The difference in energy between the HOMO and HOMO−1 at the edge of the BZ is 0.251 eV, which is also in good agreement with the value of 0.20 eV reported by Di Felice and co-workers.[25] In contrast, our band gap at the Γ point is 0.186 eV is somewhat far from the PBE value of 0.06 eV reported in Di Felice and co-workers,[25] in which HOMO and HOMO−1 become nearly degenerate at the Γ point.

The absorption spectrum calculated within the random-phase approximation (RPA) level is shown in Figure 14. As expected for 1D systems, the response in the parallel direction (par, in the legend) is much stronger than in the perpendicular (y, z) directions (per, in the legend). The RPA spectra for light polarized in the x direction features two prominent peaks at around $\lambda = 405$ and 500 nm, and a progression of bands up to $\lambda = 1000$ nm. Inclusion of local field effects improves the spectrum significantly by causing a general reduction in intensity and a shift of the first peaks to higher energies, thus reflecting the strong anisotropy of the MMX chain. Although we have neglected many-body effects at the GW/Bethe-Salpeter level, we do not expect any qualitative change in the conclusions reported herein at the RPA level. Finally, we note that the spectrum of the infinite system resembles the computed spectrum for the tetramer. The peak observed at $\lambda = 1000$ nm in both cases is related to a previously measured band in crystalline samples.[27]

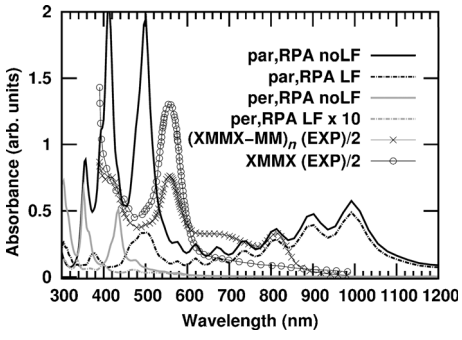

Figure 14. Optical absorption spectra of an isolated infinite chain of MMX in vacuum calculated at the PBE level by using the GPAW code.[26] In legend, RPA stands for the random phase approximation, (no)LF means that local field effects are (not) included, par (per) indicates parallel (perpendicular) directions of electric field with respect to the chain axis, and EXP denotes the experimental spectra in solution.

Conclusion

We have experimentally and computationally investigated the assembly of $[Pt_2(S_2CR)_4I]$ subunits in solution and the factors that affect this aggregation. We have analyzed the influence of the solvent, temperature, and concentration, thus finding suitable parameters for the initial building-block associations. The overall body of data presented herein suggests a new way to look at such linear structures. Interestingly, both the experimental and computational results indicate that the thermodynamic difference between the polymeric structure and the molecular building blocks (i.e., MM and XMMX) found separately is of few kcal mol^{-1}. By understanding the factors that govern this process, we have been able to isolate single/few MMX chains on mica. Although the formation of MMX nanostructures by direct sublimation of MMX crystals is a model system to understand MMX growing on the nanoscale, the formation of these nanostructures from solution has a much higher potential toward applications of MMX chains as molecular wires.

Experimental Section

Materials and methods: All the reagents were purchased from Sigma-Aldrich and used as received. The solvent CS_2 (purity: >99.9%) was also purchased from Sigma-Aldrich and used without further purification. The synthesis of the dithicarboxylic acids (RCS(SH)), $[Pt_2(RCS_2)_4]$, $[Pt_2(RCS_2)_4I_2]$ precursors, and $[Pt_2(RCS_2)_4I]_n$ compounds was carried out following previously reported procedures.[12] ^{1}H NMR spectra were recorded on a Bruker AMX-300 spectrometer. C, H, S elemental analyses were performed on a Perkin–Elmer 240-B microanalyzer. Electronic absorption spectra were recorded on an Agilent 8452 diode array spectrophotometer over a range of $\lambda = 190$–1100 nm in 0.1, 0.2, and 1 cm quartz cuvettes thermostatted by a Unisoku cryostat.

AFM images were acquired in dynamic mode by using a Nanotec Electronica system operating at room temperature under ambient air conditions. For the AFM measurements, Olympus cantilevers were used with a nominal force constant of 0.75 N m^{-1}. The images were processed using WS×M. The surface used for AFM was Muscovite mica (EMS Company) cleaved with adhesive tape just before deposition.

Iodine titration of $[Pt_2(RCS_2)_4]$ ($R = (CH_2)_4CH_3$): The titration of the $[Pt_2(RCS_2)_4]$ compound was performed by adding aliquots (30 μL) of solutions of I_2 in CH_2Cl_2 (10 mM) to a sample (3 mL) of solutions of $[Pt_2(RCS_2)_4]$ ($R = (CH_2)_4CH_3$) in CH_2Cl_2 (1 mM). Additions of iodine were made at room temperature and the mixture was stirred for 10 min.

Thereafter, the mixtures were cooled down to −90 °C to carry out low-temperature UV/Vis spectroscopic measurements.

Photo-induced reassembly of MMX structures in THF: Light/dark cycles were essayed for a 1 mM solution of compound $[Pt_2(RCS_2)_4]$ (R = $(CH_2)_4CH_3$) in THF at −90 °C. In the light phase, the shutter of the UV/Vis instrument was left open to irradiate over the range $\lambda = 200$–1100 nm. During this period of evolution, spectra were recorded over 2500 seconds. After this time, during the dark phase, the lamp in the instrument was switched off for a dark period of 60 min with the sample left in the instrument at −90 °C.

AFM sample preparation: $[Pt_2(S_2CCH_3)_4I]_n$ was diluted in dichloromethane to a concentration of 0.1 mg mL^{-1}, and deposited on mica (15 μL) by drop casting at room or low temperature until complete evaporation of the solvent was achieved.

For the low-temperature experiments, three different deposition temperatures were studied: −50, −25, and 0 °C. In these cases, the mica substrates were previously cooled in an argon atmosphere in a septum sealed flask. To this end, the system was firstly introduced in a low-temperature bath over 15 min until the deposition temperature was reached. An aliquot (15 μL) of the diluted solution was deposited by drop casting in the system cooled by using a Hamilton syringe. The surface was incubated until complete evaporation of the solvent (approximately 15 min) was achieved. For each experiment, we prepared control samples according to the procedure described above. The control samples did not show one-dimensional structures.

Computational details: In all the calculations, we used the Perdew-Burke-Ernzerhof (PBE) exchange correlation functional.[29] After comparing a few DFT exchange correlation functionals, we found that PBE represents a good compromise between accuracy and computational cost.

Optimized structures for the MMX clusters were computed with the program Gaussian 09[23] by using DFT[28] and atom-centered basis sets. We described the Pt, S, and I atoms with the Los Alamos National Laboratory double-zeta (LANL2DZ)[30] basis set (core electrons were described by an effective core potential), whereas the rest of the atoms (C and H) were represented by the Pople 6–31G* basis set. First, the hydrogen atoms were added because their positions were not resolved in the X-ray diffraction data. The structure of the entire system was relaxed without constraints. The resulting optimized geometries in the gas phase are quite similar to the experimental one, with deviations in bond lengths of around or less than 0.1 Å. For the isolated XMMX-MM complex, some optimized geometrical parameters were 2.74, 2.91, 2.44 Å for the bond distances between Pt–Pt, Pt–I, and Pt–S, respectively.

For accurate calculation of the dissociation energies, we used the OCTOPUS code,[22] which enables us to reach the complete basis set limit easily. Within this code, all the quantities are discretized on the real space by using a numerical mesh. A simulation box consists of atom-centered spheres of radii of 6.0 Å. The grid spacing between the points in the mesh was set to 0.15 Å. These parameters were carefully converged to yield errors in relative energies of less than 0.01 eV (0.23 kcal mol^{-1}). Norm-conserving Troullier–Martins pseudopotentials[31] (of the Fritz-Haber-Institut type)[32] were used to describe the interaction between the core and valence electrons. The optimized geometries generated previously with the Gaussian 09 package were used without further modification for the energetics calculation with the OCTOPUS program.

All NPA and Mulliken charges were calculated by using the Gaussian 09 package.[23] The charges were computed on the optimized XMMX-MM complex and the dissociated form in the gas phase. The calculations were done at the PBE level with the LANL2DZ basis set (for Pt, S, and I atoms) and 6–31G* on the rest.

TDDFT calculations (using the real-time propagation) were performed on isolated MMX clusters by using the OCTOPUS code.[22] This calculation starts with the optimized ground-state Kohn–Sham orbitals,[28] which are then perturbed by a weak electric field along the molecular Pt-Pt-I axis (z). The optical spectrum is then proportional to the Fourier transform of the time-varying electric dipole moment of the system. For stable propagation of the Kohn–Sham orbitals, the time step and total propagation time was 0.001 and 60 $\hbar$ eV^{-1} units (0.000658 and 39.4927 fs), respectively, in all the TDDFT calculations. We used the PBE exchange-correlation functional. All the calculations were performed in the gas phase. To make the optical calculations more manageable, we slightly relaxed the grid spacing and box-size requirements used to prepare Scheme 3, while the rest of parameters remained identical. A simulation box of atom-centered spheres with radii of 5.0 Å and a grid spacing of 0.18 Å were found sufficient for the optical calculations. With these more relaxed parameters, we checked that the HOMO–LUMO gap was converged up to meV accuracy and that the impact on the final spectra was minimal.

The electronic and optical properties of the infinite MMX chain were computed with the GPAW DFT code,[26] which is based on a real-space grid implementation of the projector augmented wave (PAW) method.[33] All the calculations were also performed with the exchange-correlation functional approximation of PBE.[29] The grid spacing was set to 0.25 Å, and a Fermi temperature of 0.025 eV was used in all the periodic calculations. A total of 175 bands were found sufficient to converge the lower energy part of the optical spectrum. A single monomer of MMX at the experimental crystalline geometry was placed in an orthorhombic cell of $8.63 \times 20 \times 20$ Å^3. With these box dimensions, a vacuum layer of 10 Å was used to prevent the interaction between adjacent replicas along the lateral (nonperiodic) directions. A total of 16 irreducible k points were used to sample the Brillouin Zone (BZ) along the periodic direction (x), while the perpendicular directions (y, z) were considered to be isolated. For the optical spectra calculations, local-field effects were converged with reciprocal lattice vectors up to a cutoff of 2 Hartrees for the dimensions of the response matrix. In total, the unit cell contained 119 electrons and 31 atoms with Pt···Pt and Pt···I distances of 2.682 and 2.976 Å, respectively.

Acknowledgements

We acknowledge the financial support from the European Research Council Advanced Grant DYNamo (ERC-2010-AdG, Proposal No. 267374), Spanish Grants (FIS2011-65702-C02-01, PIB2010US-00652, CTQ2012-37420-C02-02 and MAT2010-20843-C02-01), ACI-Promociona (ACI2009-1036 and ACI2009-0969), Grupos Consolidados UPV/EHU del Gobierno Vasco (IT-319-07 and IT-578-13), European Commission projects CRONOS (Grant number 280879-2 CRONOS CP-FP7), Comunidad de Madrid (S-0505/MAT/0303), and Consolider nano THERM (Grant No. CSD2010-00044). We are thankful for the computational time granted by the Barcelona Supercomputing Center, "Red Española de Supercomputación" throughout the project QCM-2011-3-0029 and the technical and human support provided by IZO-SGI, SGIker (UPV/EHU, MICINN, GV/EJ, ERDF and ESF). A.P.P. thanks Dr. Duncan J. Mowbray for useful discussions.

[1] a) J. M. Lehn, *Supramolecular Chemistry*, VCH, Weinheim, **1995**; b) J. M. Lehn, *Science* **2002**, *295*, 2400–2403.

[2] J. Simon, P. Bassoul, *Design of molecular materials: supramolecular engineering*, Wiley-VCH, **2001**.

[3] a) J. V. Barth, G. Costantini, K. Kern, *Nature* **2005**, *437*, 671–679; b) N. Lin, S. Stepanow, M. Ruben, J. V. Barth, *Top. Curr. Chem.* **2008**, *287*, 1–44.

[4] J. A. Theobald, N. S. Oxtoby, M. A. Phillips, N. R. Champness, P. H. Beton, *Nature* **2003**, *424*, 1029–1031.

[5] D. J. L. Tranchemontagne, Z. Ni, M. O'Keeffe, O. M. Yaghi, *Angew. Chem.* **2008**, *120*, 5214–5225; *Angew. Chem. Int. Ed.* **2008**, *47*, 5136–5147.

[6] H. K. Chae, D. Y. Siberio-Perez, J. Kim, Y. Go, M. Eddaoudi, A. J. Matzger, M. O'Keeffe, O. M. Yaghi, *Nature* **2004**, *427*, 523–527.

[7] Y. You, H. Yang, J. W. Chung, J. H. Kim, Y. Jung, S. Y. Park, *Angew. Chem.* **2010**, *122*, 3845–3849; *Angew. Chem. Int. Ed.* **2010**, *49*, 3757–3761.

[8] a) T. Uemura, N. Yanai, S. Kitagawa, *Chem. Soc. Rev.* **2009**, *38*, 1228–1236; b) L. Ma, C. Abney, W. Lin, *Chem. Soc. Rev.* **2009**, *38*,

1248–1256; c) L. J. Murray, M. Dinca, J. R. Long, *Chem. Soc. Rev.* **2009**, *38*, 1294–1314; d) J. Lee, O. K. Farha, J. Roberts, K. A. Scheidt, S. T. Nguyen, J. T. Hupp, *Chem. Soc. Rev.* **2009**, *38*, 1450–1459; e) D. A. Serban, P. Greco, S. Melinte, A. Vlad, C. A. Dutu, S. Zacchini, M. C. Iapalucci, F. Biscarini, M. Cavallini, *Small* **2009**, *5*, 1117–1122.

[9] a) C. Janiak, *Dalton Trans.* **2003**, 2781–2804; b) S. Kitagawa, S. Noro in *Comprehensive Coordination Chemistry II, Vol. 7*, Elsevier, Amsterdam, **2004**; c) G. Givaja, P. Amo-Ochoa, C. J. Gómez-García, F. Zamora, *Chem. Soc. Rev.* **2012**, *41*, 115–147.

[10] R. Mas-Ballesté, J. Gomez-Herrero, F. Zamora, *Chem. Soc. Rev.* **2010**, *39*, 4220–4233.

[11] M. Yamashita, H. e. Okamoto, *Material Designs and New Physical Properties in MX- and MMX-Chain Compounds*, Springer, Wien, **2013**.

[12] C. Bellitto, A. Flamini, L. Gastaldi, L. Scaramuzza, *Inorg. Chem.* **1983**, *22*, 444–449.

[13] J. Gómez-Herrero, F. Zamora, *Adv. Mater.* **2011**, *23*, 5311–5317.

[14] L. Welte, A. Calzolari, R. di Felice, F. Zamora, J. Gómez-Herrero, *Nat. Nanotechnol.* **2010**, *5*, 110–115.

[15] A. Guijarro, O. Castillo, L. Welte, A. Calzolari, P. J. S. Miguel, C. J. Gomez-Garcia, D. Olea, R. di Felice, J. Gomez-Herrero, F. Zamora, *Adv. Funct. Mater.* **2010**, *20*, 1451–1457.

[16] L. Welte, U. García-Couceiro, O. Castillo, D. Olea, C. Polop, A. Guijarro, A. Luque, J. M. Gómez-Rodríguez, J. Gómez-Herrero, F. Zamora, *Adv. Mater.* **2009**, *21*, 2025–2028.

[17] M. Cavallini, *J. Mater. Chem.* **2009**, *19*, 6085–6092.

[18] M. Mitsumi, K. Kitamura, A. Morinaga, Y. Ozawa, M. Kobayashi, K. Toriumi, Y. Iso, H. Kitagawa, T. Mitani, *Angew. Chem.* **2002**, *114*, 2891–2895; *Angew. Chem. Int. Ed.* **2002**, *41*, 2767–2771.

[19] R. Mas-Ballesté, R. Gonzalez-Prieto, A. Guijarro, M. A. Fernandez-Vindel, F. Zamora, *Dalton Trans.* **2009**, 7341–7343.

[20] C. Hermosa, J. V. Álvarez, M. R. Azani, C. J. Gómez-García, M. Fritz, J. M. Soler, J. Gómez-Herrero, C. Gómez-Navarro, F. Zamora, *Nat. Commun.* **2013**, *4*, 1709.

[21] a) L. Welte, R. González-Prieto, D. Olea, M. Rosario Torres, J. L. Priego, R. Jiménez-Aparicio, J. Gómez-Herrero, F. Zamora, *ACS Nano* **2008**, *2*, 2051–2056; b) D. Gentili, G. Givaja, R. Mas-Ballesté, M.-R. Azani, A. Shehu, F. Leonardi, E. Mateo-Martí, P. Greco, F. Zamora, M. Cavallini, *Chem. Sci.* **2012**, *3*, 2047–2051.

[22] A. Castro, H. Appel, M. Oliveira, C. A. Rozzi, X. Andrade, F. Lorenzen, M. A. L. Marques, E. K. U. Gross, A. Rubio, *Phys. Status Solidi B* **2006**, *243*, 2465–2488.

[23] Gaussian 09, Revision A.01, M. J. Frisch, G. W. Trucks, H. B. Schlegel, G. E. Scuseria, M. A. Robb, J. R. Cheeseman, G. Scalmani, V. Barone, B. Mennucci, G. A. Petersson, H. Nakatsuji, M. Caricato, X. Li, H. P. Hratchian, A. F. Izmaylov, J. Bloino, G. Zheng, J. L. Sonnenberg, M. Hada, M. Ehara, K. Toyota, R. Fukuda, J. Hasegawa, M. Ishida, T. Nakajima, Y. Honda, O. Kitao, H. Nakai, T. Vreven, J. A. Montgomery, Jr., J. E. Peralta, F. Ogliaro, M. Bearpark, J. J. Heyd, E. Brothers, K. N. Kudin, V. N. Staroverov, R. Kobayashi, J. Normand, K. Raghavachari, A. Rendell, J. C. Burant, S. S. Iyengar, J. Tomasi, M. Cossi, N. Rega, J. M. Millam, M. Klene, J. E. Knox, J. B. Cross, V. Bakken, C. Adamo, J. Jaramillo, R. Gomperts, R. E. Stratmann, O. Yazyev, A. J. Austin, R. Cammi, C. Pomelli, J. W. Ochterski, R. L. Martin, K. Morokuma, V. G. Zakrzewski, G. A. Voth, P. Salvador, J. J. Dannenberg, S. Dapprich, A. D. Daniels, Ö. Farkas, J. B. Foresman, J. V. Ortiz, J. Cioslowski, D. J. Fox, Gaussian, Inc. Wallingford CT, **2009**.

[24] A. P. Paz, L. A. Espinosa Leal, M. R. Azani, A. Guijarro, P. J. S. Miguel, G. Givaja, O. Castillo, R. Mas-Balleste, F. Zamora, A. Rubio, *Chem. Eur. J.* **2012**, *18*, 13787–13799.

[25] A. Calzolari, S. S. Alexandre, F. Zamora, R. Di Felice, *J. Am. Chem. Soc.* **2008**, *130*, 5552–5562.

[26] a) J. J. Mortensen, L. B. Hansen, K. W. Jacobsen, *Phys. Rev. B* **2005**, *71*; b) J. Enkovaara, C. Rostgaard, J. J. Mortensen, J. Chen, M. Dulak, L. Ferrighi, J. Gavnholt, C. Glinsvad, V. Haikola, H. A. Hansen, H. H. Kristoffersen, M. Kuisma, A. H. Larsen, L. Lehtovaara, M. Ljungberg, O. Lopez-Acevedo, P. G. Moses, J. Ojanen, T. Olsen, V. Petzold, N. A. Romero, J. Stausholm-Moller, M. Strange, G. A. Tritsaris, M. Vanin, M. Walter, B. Hammer, H. Hakkinen, G. K. H. Madsen, R. M. Nieminen, J. Norskov, M. Puska, T. T. Rantala, J. Schiotz, K. S. Thygesen, K. W. Jacobsen, *J. Phys. Condens. Matter* **2010**, *22*; c) J. Yan, J. J. Mortensen, K. W. Jacobsen, K. S. Thygesen, *Phys. Rev. B* **2011**, *83*.

[27] a) M. Mitsumi, T. Murase, H. Kishida, T. Yoshinari, Y. Ozawa, K. Toriumi, T. Sonoyama, H. Kitagawa, T. Mitani, *J. Am. Chem. Soc.* **2001**, *123*, 11179–11192; b) M. Mitsumi, T. Yamashita, Y. Aiga, K. Toriumi, H. Kitagawa, T. Mitani, M. Kurmoo, *Inorg. Chem.* **2011**, *50*, 4368–4377.

[28] W. Kohn, L. J. Sham, *Phys. Rev.* **1965**, *140*, A1133.

[29] J. P. Perdew, K. Burke, M. Ernzerhof, *Phys. Rev. Lett.* **1996**, *77*, 3865–3868.

[30] P. J. Hay, W. R. Wadt, *J. Chem. Phys.* **1985**, *82*, 270–283.

[31] N. Troullier, J. L. Martins, *Phys. Rev. B* **1991**, *43*, 1993–2006.

[32] M. Fuchs, M. Scheffler, *Comp. Phys. Commun.* **1999**, *119*, 67–98.

[33] P. E. Blöchl, *Phys. Rev. B* **1994**, *50*, 17953–17979.

Received: April 16, 2013
Published online: September 24, 2013

CHEMISTRY
A EUROPEAN JOURNAL

Supporting Information

The Isolation of Single MMX Chains from Solution: Unravelling the Assembly–Disassembly Process**

Mohammad-Reza Azani,[a] Alejandro Pérez Paz,[b] Cristina Hermosa,[a] Gonzalo Givaja,[a] Julio Gómez-Herrero,[c, d] Rubén Mas-Ballesté,*[a] Felix Zamora,*[a, d] and Angel Rubio*[b]

chem_201301450_sm_miscellaneous_information.pdf

Supporting Information

Isolating single MMX chains from solution: unravelling the assembly-disassembly process

Mohammad-Reza Azani, Alejandro Pérez Paz, Cristina Hermosa, Gonzalo Givaja, Julio Gómez-Herrero, Rubén Mas-Ballesté,* Felix Zamora,* Angel Rubio*

Additional theoretical data

All geometries were fully relaxed in gas phase with the Gaussian 09 code using the PBE exchange correlation functional and the LANL2DZ basis set on Pt, S, and I and 6-31G* on the rest. All binding energies are given in kcal/mol units and were corrected for the basis set superposition error (BSSE). Unrestricted calculations were used whenever radicals were involved. See main text for more details.

molecule/cleavage mode	Asymmetric	Symmetric
MM-XMMX	5.74356	17.5477
MM-XMMX-MM	4.021	15.077
XMMX-MM-XMMX	6.233	15.639

An implicit solvent PCM calculation (CH_2Cl_2) with Gaussian 09 yielded 9.6 and 19.6 kcal/mol (no BSSE corrected values), for the asymmetric and symmetric dissociation of MM-XMMX, respectively, using the same basis set as above.

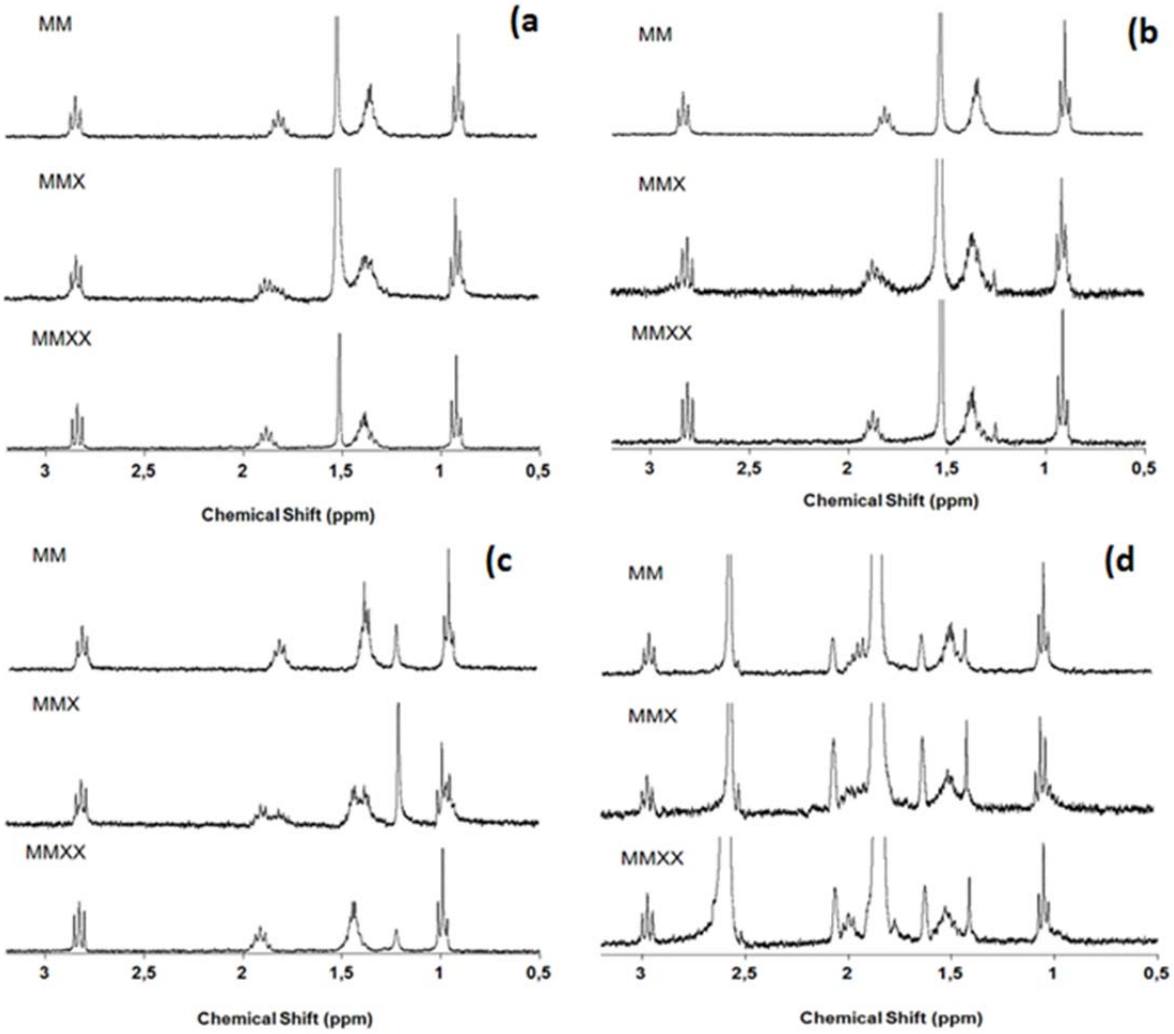

Figure S1. ^{1}H NMR spectra of compound **1** in: a) CD_2Cl_2, b) $CDCl_3$, c) $CS_2/CHCl_3$ (9:1), d) THF-d_8 and its comparison with the spectra of its precursors $[Pt_2(RCS_2)_4I_2]$ and $[Pt_2(RCS_2)_4]$ (R = $(CH_2)_4CH_3$) in the same solvents.

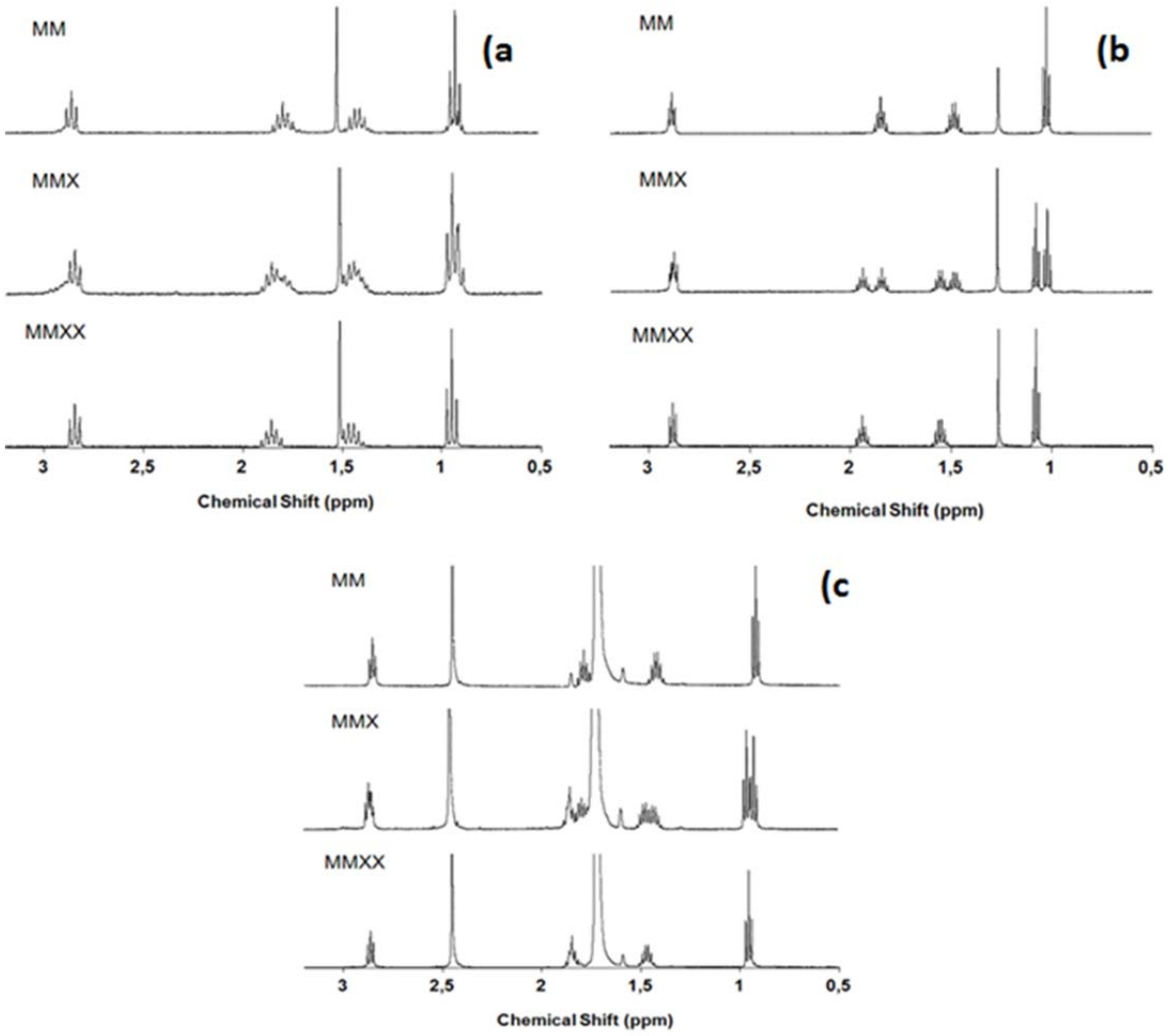

Figure S2. ^{1}H NMR spectra of compound **2** in: a) CD_2Cl_2, b) $CDCl_3$, c) $CS_2/CHCl_3$ (9:1), d) THF-d_8 and its comparison with the spectra of its precursors $[Pt_2(RCS_2)_4I_2]$ and $[Pt_2(RCS_2)_4]$ (R = $(CH_2)_3CH_3$) in the same solvents.

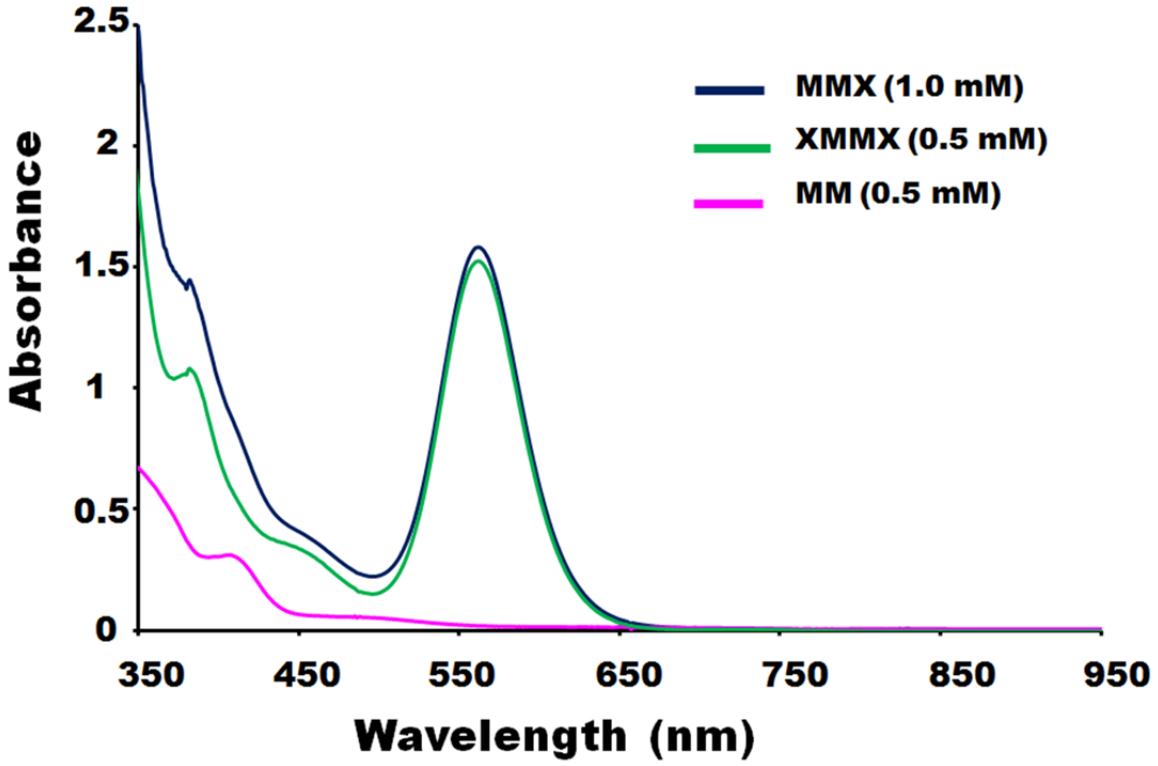

Figure S3. Comparison of the UV-vis spectra obtained solutions 0.5 mM of $[Pt_2(RCS_2)_4I_2]$ and $[Pt_2(RCS_2)_4]$ (R = $(CH_2)_3CH_3$) and data obtained for a 1 mM solution of compound **2**. All spectra **were** measured at room temperature in CH_2Cl_2 using a 2 mm cell.

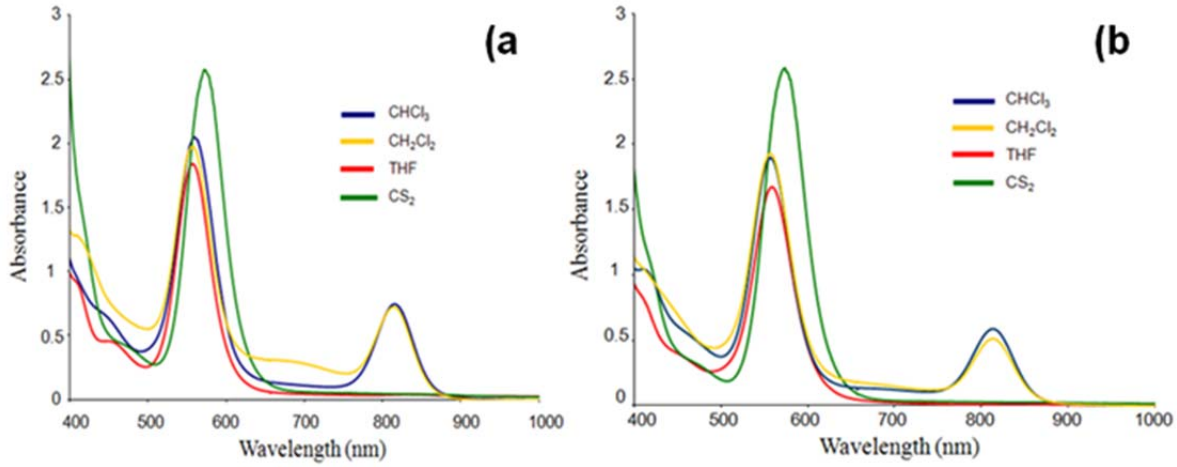

Figure S4. UV-vis spectra measured for 1 mM solutions of a) **2** and b) **3** (2 mm cell at -60 ^oC) in $CHCl_3$, CH_2Cl_2, THF and CS_2.

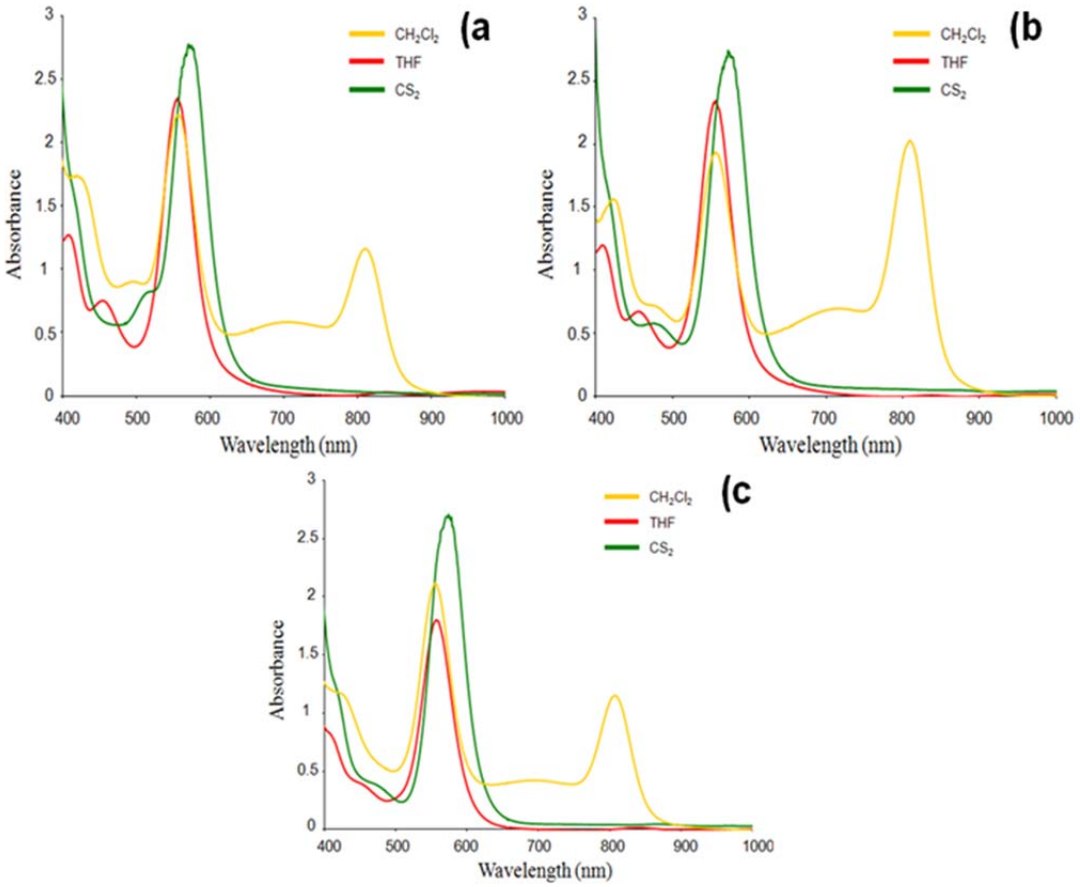

Figure S5. UV-vis spectra measured for 1 mM solutions of a) **1,** b) **2** and c) **3** (2 mm cell at -90 ºC) in CH_2Cl_2, CS_2 and THF.

Article 4

Title: Patterned conductive nanostructures from reversible self-assembly of 1D coordination polymer

Autors: Denis Gentili, Gonzalo Givaja, Ruben Mas-Ballesté, Mohammad-Reza Azani, Arian Shehu, Francesca Leonardi, Eva Mateo-Martí, Pierpaolo Greco, Félix Zamora and Massimiliano Cavallini*

Journal: Chemical Science

Year: 2012

Volume / Pages: 3 / 2047-2051.

Chemical Science

Cite this: DOI: 10.1039/c2sc00029f

www.rsc.org/chemicalscience

EDGE ARTICLE

Patterned conductive nanostructures from reversible self-assembly of 1D coordination polymer†‡

Denis Gentili,[a] Gonzalo Givaja,[b] Rubén Mas-Ballesté,[b] Mohammad-Reza Azani,[b] Arian Shehu,[a] Francesca Leonardi,[a] Eva Mateo-Martí,[c] Pierpaolo Greco,[d] Félix Zamora*[b] and Massimiliano Cavallini*[a]

Received 9th January 2012, Accepted 7th March 2012
DOI: 10.1039/c2sc00029f

In this study, the outstanding ability of the coordination polymer $[Pt_2(n\text{BuCS}_2)_4I]_n$ (*n*Bu = *n*-butyl) (**1**) to reversibly self-organize from solution was demonstrated. This feature allowed us to generate highly electrical conductive structures located upon demand on technologically relevant surfaces, by easy-to-handle and low cost micromolding in capillaries (MIMIC) and lithographically controlled wetting (LCW). Electrical characterization reveals a near Ohmic behaviour and a high stability of the stripes (in air). Electrodes produced by the MIMIC technique from a solution of compound **1** demonstrated that this material can be efficiently used as electrodes for organic field-effect transistors (OFETs).

Introduction

The assembly of molecules, biological materials and nanoparticles in ordered superstructures on solid surfaces is of great interest in many areas of science and technology.[1,2] Supramolecular chemistry,[3] exploring self-assembly beyond single molecular entities, has provided remarkable results, but in order to embed these supramolecular structures in real applications it is necessary to gain control over their intimate spatial architecture, from the molecular scale to the macro scale. The exploitation of self-assembly properties in bottom-up nanofabrication has been demonstrated as a successful strategy towards these aims.[3,4] A major challenge in miniaturized device fabrication is to enhance performance by taking advantage of selected features of materials. Therefore, the application of advanced techniques able to exploit self-organizing properties of materials is essential for the construction of devices based on supramolecular constituents.[4–6]

Self-organizations promoted by non-covalent interactions have been extensively studied in solution, in the solid state and on surfaces, leading to a large variety of supramolecules with different architectures.[7] Some of these supramolecules have been designed using coordinative bonds.[8] By means of coordinative bonds, infinite associations between two simple building blocks, metal entities and organic or inorganic ligands have led to the formation of a large number of architectures of different dimensionalities,[9] which are known as coordination polymers (CPs). The kinetic lability of metal–ligand bonds[10] supports the reproducible construction of functional, highly ordered superstructures for a wide range of technological applications (*i.e.* catalysis, reaction confinement, gas storage and separation).[6,11–14]

Coordination polymers show interesting chemical[14] and physical[15] properties, including high electrical conductivity.[16] Current interest in the development of highly conductive CPs is also motivated by their potential technological impact.[17]

A relevant example concerning the electrical conductivity of CPs is the so-called MMX chains. The structure of an MMX chain can be described as a *pseudo*-one-dimensional arrangement of halides (X) bridging dimetallic subunits, in which metal ions are connected by four ligands (*e.g.* pyrophosphates or dithiocarboxylates). The MMX chains based on platinum, dithiocarboxylate and iodine have shown metallic conductivity at room temperature. They are promising candidates for nanoelectronic applications, where molecular wires capable of transporting electrical charges across long distances are required.[17] Furthermore, the relatively low work function (~3.7 eV)[18] and the fact that thin films of MMX are almost transparent in thickness, <50 nm, make this class of CPs extremely appealing for molecular electronics and optoelectronics. Recently, Zamora *et al.* showed the outstanding electrical properties of randomly deposited MMX nanoribbons and nanocrystals ($[Pt_2(RCS_2)_4I]_n$, R = methyl or *n*-penthyl) on mica.[18,19] However, the conductive nanoribbons were formed on mica by direct sublimation from crystals of $[Pt_2(\text{methyl-CS}_2)_4I]_n$ under a high vacuum.[20] This method does not allow spatial control of the deposition of nanoribbons on surfaces. Once the conductivity of nanostructures of such CPs has been demonstrated, the next frontier is to fabricate a functional device based on this polymer. To

[a]*Consiglio Nazionale delle Ricerche - Istituto per lo Studio dei Materiali Nanostrutturati (CNR-ISMN), Via Gobetti 101, 40129 Bologna, Italy. E-mail: mcavalli@bo.ismn.cnr.it*
[b]*Departamento de Química Inorgánica, Universidad Autónoma de Madrid, 28049 Madrid, Spain. E-mail: felix.zamora@uam.es*
[c]*Centro de Astrobiología (CSIC-INTA), Ctra. Ajalvir, Km. 4, 28850 Torrejon de Ardoz, Madrid, Spain*
[d]*SCRIBA Nanotecnologie S.r.l, Via P. Gobetti 52/3, 40129 Bologna, Italy*
† This work is dedicated to Fabio Biscarini on the occasion of his 50th birthday.
‡ Electronic supplementary information (ESI) available: Material and methods section and extra figures. See DOI: 10.1039/c2sc00029f

address this challenge, we evaluated the processability of such a polymer. Being demonstrated an outstanding ability for reversible depolymerization/repolymerization, we envisioned the possibility of integrating a CP self-assembly in a spatially confined environment by unconventional wet lithography,[21] exploiting its depolymerization/repolymerization ability.[10]

Results and discussion

A significant feature of $[Pt_2(n\text{BuCS}_2)_4I]_n$ (nBu = n-buthyl) (**1**) is its processability. Indeed, it is very uncommon that a coordination polymer can be dissolved and recrystallized conserving its structural integrity.[16] However, this characteristic is what allowed us to design devices based on local crystallization of polymer **1** from CH_2Cl_2 solutions. In fact, this uncommon behaviour raises the questions of which species are present in solution and which factors have an effect on their subsequent reassembly. In order to address these important unknown factors, we analysed the spectroscopic features of **1** dissolved in CH_2Cl_2 and compared them with those of the $[Pt_2(n\text{BuCS}_2)_4]$ (**2**) and $[Pt_2(n\text{BuCS}_2)_4I_2]$ (**3**) precursors. The data shows that, at room temperature, **1** dissolved in an equimolar mixture of **2** and **3**. The UV-vis spectrum of a 1 mM solution of **1** can be seen as the result of overlapping the UV-vis spectra separately measured from 0.5 mM CH_2Cl_2 solutions of precursors **2** and **3** (Fig. 1a). Consistently, the ^{1}H NMR spectrum of **1** in CD_2Cl_2 shows an overlapping of the spectra of species **2** and **3** (Fig. 1b). The spectroscopic data indicate an asymmetric rupture of **1**, which formed two different diamagnetic dimetallic compounds containing two Pt(II) centres (in the case of **2**) or two Pt(III) centres (**3**) (Scheme 1).

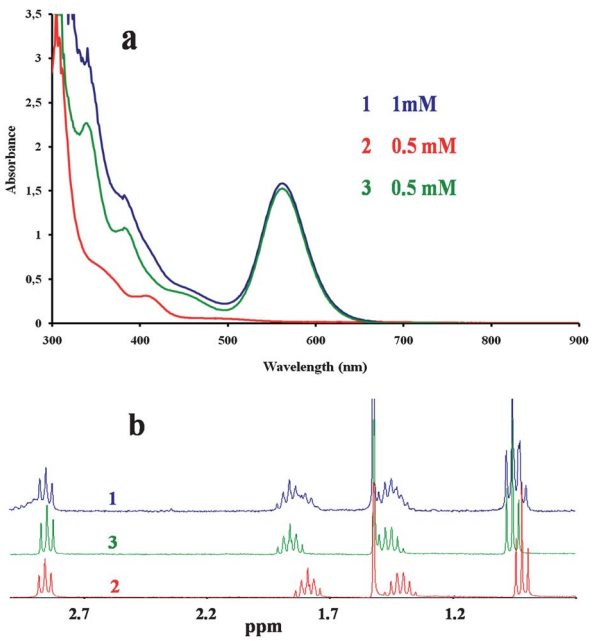

Fig. 1 Spectroscopic studies of $[Pt_2(n\text{BuCS}_2)_4I]_n$ (**1**) in CH_2Cl_2. UV-vis (a) and ^{1}H NMR (b) spectra at room temperature of a 1 mM solution of **1** in CH_2Cl_2, compared with spectra of 0.5 mM solutions of **2** and **3**. The spectroscopic features observed for **1** correspond to the addition of those observed for **2** and **3**.

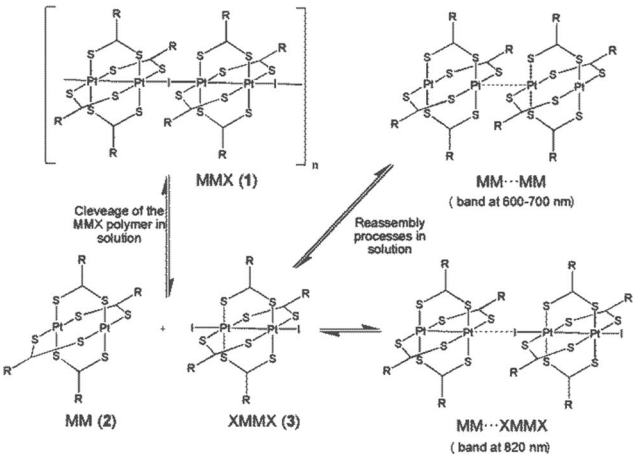

Scheme 1 A schematic representation of the behaviour observed for the solutions of $[Pt_2(n\text{BuCS}_2)_4I]_n$ in CH_2Cl_2.

Concerning the (re)assembly of **2** and **3**, as previously observed for analogous species,[22] precursor **2** associated in solution *via* reversible weak $d^8\cdots d^8$ interactions, which can be observed by the appearance at low temperature of an adsorption band at 600–700 nm. Similar behaviour was observed for the solutions of **1**. In addition, a new band at 820 nm appeared in the spectrum of **1** in CH_2Cl_2 at −50 °C (Fig. S1†). Considering that this feature was not observed for the solutions of pure precursors **2** or **3**, this new band indicates the assembly of molecules **2** and **3**, generating oligomers of polymer **1**. Interestingly, the ratio between the **2**···**2** and the **2**···**3** association was affected by the overall concentration of dissolved **1**, in that the **2**···**2** assembly was less favoured at lower concentrations (Fig. S2†). Despite the fact that local deposition occurred at room temperature, the low temperature experiments offer valuable insights that help to understand the process of MMX polymer formation from solution.

A rather uncommon feature was shown for compound **1**: it can be dissolved and repolymerized, conserving its structural integrity, enabling its processability and the formation of organized structures on surfaces. The key factor for the processability and the successful application of MMX as an electrode is its excellent reversibility in the depolymerization/repolymerization process. Thus, micromolding in capillaries (MIMIC)[23] and lithographically controlled wetting (LCW)[24] (see the schemes in Fig. 2 and a detailed description in the ESI†) were used to fabricate ordered patterns of parallel sub-micrometric wires (μ-wires) and interdigitated electrodes for field-effect transistors (FETs). Noticeably, both methods were able to deliver a solution at spatially controlled positions, exploiting the self-organization properties of the solute at the later stages of shrinking, leading to the formation of patterned superstructures.[25] Fig. 3 shows an optical micrograph of the interdigitated electrodes of an FET printed by LCW (Fig. 3a) and parallel μ-wires (width 900 nm, height 124 nm, periodicity 1.5 μm) on pre-fabricated gold electrodes (Fig. 3b) that were printed by MIMIC (see the morphological characterization in the ESI, Figs S3–S5†). Detailed characterization by XPS, PM-RAIRS and SEM is reported in the ESI†. The electrical characterization was performed by measuring the current flowing in the μ-wires as a function of bias voltage, ranging from +50 to −50 V. The I–V curve (Fig. 3c) reveals

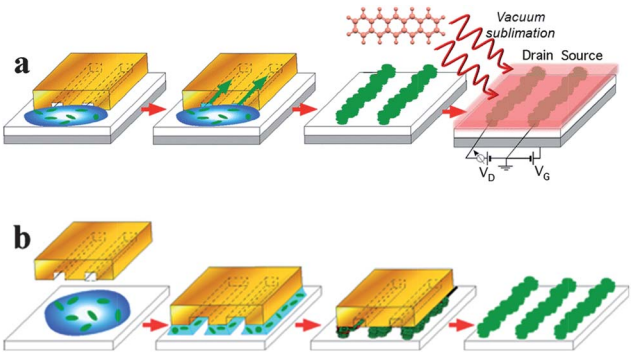

Fig. 2 (a) A schematic representation of micromolding in capillaries (MIMIC). After vacuum sublimation (right in upper row) of pentacene this procedure allowed us to form the microstructure and electrodes of a field effect transistor. (b) A schematic representation of lithographically controlled wetting (LCW).

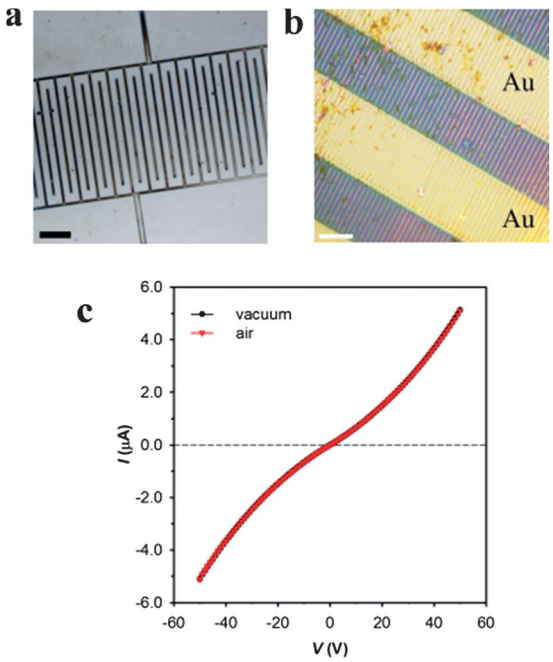

Fig. 3 Microfabrication by unconventional wet lithography. (a) An optical micrograph (scale bar = 100 μm) of interdigitated comb-like electrodes of $[Pt_2(n\text{BuCS}_2)_4I]_n$ printed on silicon oxide by LCW. (b) An optical image (scale bar = 10 μm) of parallel μ-wires printed onto Au electrodes. (c) Current *vs.* voltage characteristics of the wires in (b).

a near Ohmic behaviour within the range explored. It is important to note that the time stability of the wires (we tested our devices for more than 6 months, in air at room temperature and in high humidity), in terms of their electrical behaviour, was not influenced by air and was consistently reproduced in ten voltage-sweeping cycles (Fig. S6†).

Indeed, the data points acquired in both the vacuum and air fell on top of each other, showing no sign of hysteresis or any other electrical deterioration. This is a very important issue for electronic applications. Assuming that the current spreads across the entire section of the wires of **1**, we estimated a high current density of *ca.* 5 A cm^{-2} at 50 V, which for sub-micrometric wires is comparable to and, in some cases, even better than corresponding metallic wires.[6,26]

Under a polarized optical microscope (POM) the stripes exhibit birefringence (Fig. 4). This means that the stripes are made of large crystalline domains of $[Pt_2(n\text{BuCS}_2)_4I]_n$. The occurrence of complete light extinction at the same orientations for all of the stripes indicates that they were grown with the same orientation. This means that the confined deposition has induced a coherent, long-range order along the direction of the stripes. The printed structures on the surfaces were also characterized by several methods in order to assess their chemical integrity. A room temperature X-ray photoelectron spectroscopy (XPS) study of both bulk and patterned **1** on gold surfaces revealed that the characteristic binding energies for C, S, I and Pt were in good agreement with the proposed chemical composition. The data summarized in Table S1† and pictured in Fig. S7† undoubtedly reveal the mixed valence nature of the polymer on the XPS, and, as such, the Pt 4f core levels could be deconvoluted into Pt^{2+} $4f_{7/2,5/2}$ and Pt^{3+} $4f_{7/2,5/2}$ doublets by a Gaussian–Lorentzian line shape fit. It has been previously proposed that X-ray irradiation can promote the reduction of Pt^{3+} to Pt^{2+} on MMX species and this might account for the observed weak intensity of the Pt^{3+} $4f_{7/2,5/2}$ doublet,[27] both in bulk and on the surface.

While XPS provides information about the inorganic part of **1**, a polarization modulation reflection absorption infrared spectroscopy (PM-RAIRS) analysis was required to gather further information related to the organic moiety of the compound. The RAIRS spectrum of compound **1** was produced in order to analyse its adsorption from solution to the gold surface. The infrared spectra contained intense absorptive features indicating that **1** was successfully adsorbed onto the gold surface. The spectrum shows bands in the region 3000–2850 cm^{-1}, which corresponds to CH_2 and CH_3 asymmetric and symmetric stretching modes, which show that CH_2 and CH_3 groups were present on **1**. A very intense band at 1111 cm^{-1} assignable to the symmetric C–S stretching vibrations of the dithiocarboxylate ligands can also be observed (Fig. S8†). It is worth mentioning that theoretical calculations on $[Pt_2(\text{MeCS}_2)_4]$ have recently shown that the chemical structure of this polymer adsorbed on gold is retained upon interaction with the substrate.[18] Therefore, the spectroscopic data and the structural analogies between both polymers suggest that the structural integrity of **1** is retained

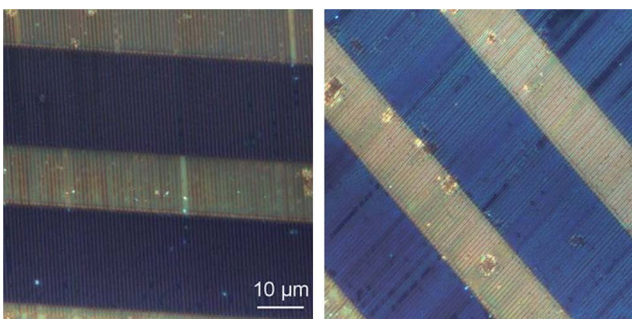

Fig. 4 An optical image taken under cross-polarized conditions of parallel μ-wires of $[Pt_2(n\text{BuCS}_2)_4I]_n$ printed onto Au electrodes. The sample rotation shows the complete light extinction at the same orientations for all of the stripes.

upon adsorption on gold. The interactions of related coordination compounds and polymers with substrates have shown similar behaviour.[10,28,29]

As an example of the direct application of **1**, we tested the use of this material as electrodes in organic field-effect transistor (OFET) devices.[30] Different OFETs were built in a bottom-gate, bottom-contact architecture. Highly n-type doped Si wafers covered by 200 nm of thermally grown SiO_2 were used as both substrates and gate terminals. As shown in Fig. 5a, the drain and source electrodes of **1** were fabricated by MIMIC (2 mg mL^{-1} in THF, 10 μL), then a layer of 30 nm-high pentacene[31] was thermally sublimed onto them in an ultra-high vacuum chamber (growth rate 0.75 nm min^{-1}). Four different types of devices were built with a channel length of 70 μm and widths ranging 700–3500 μm. The optical image shows the well-defined geometry of the electrodes of **1**, whilst the AFM studies in the OFET channel reveal the interconnected island morphology of the pentacene thin film (Fig. 5a,b).

The electrical transfer and output characteristics of a typical p-type pentacene-based FET are displayed in Fig. 5c,d. The OFET devices showed a field-effect performance with charge mobility, μ_{sat}, up to 5.2×10^{-3} cm^2 V^{-1} s^{-1} (for comparison the corresponding devices built with Au electrodes exhibit a charge mobility of $\mu_{sat} = 1.1 \times 10^{-2}$ cm^2 V^{-1} s^{-1}), with on/off ratios around 10^6 and an excellent stability under ambient conditions (after six months from fabrication the device remains almost unaltered).

The small banding in the transfer characteristic (Fig. 3c) suggests that a high contact resistance, which limits the absolute value of the charge mobility, is present in our devices. This can be partially ascribed to the unoptimised thin films of pentacene, as confirmed by the correlation length measured in our thin film (~200 nm), which is 5 times less than in films exhibiting state-of-the-art charge mobility (~1 μm).[32] Despite this limit, which could be improved by a further thin-film growth optimization and by the chemical functionalization of the substrate,[33] both the on/off ratio, threshold voltage and switching rate are comparable to state-of-the-art values.[32]

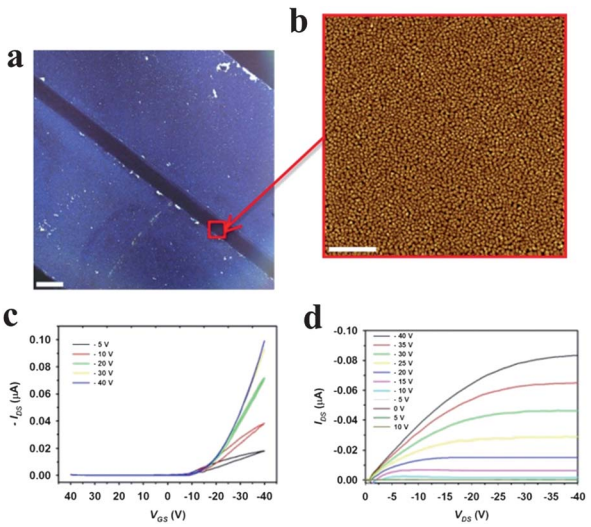

Fig. 5 (a) An optical image (scale bar = 100 μm) taken under cross-polarized conditions of drain and source $[Pt_2(n\text{BuCS}_2)_4I]_n$ electrodes. (b) The AFM morphology (scale bar = 2 μm) of pentacene thin film grown in the OFET channel. (c) Transfer at various drain biases and (d) output at various gate biases measured in the air of the OFET.

Conclusions

The data presented herein demonstrates the unusual ability of $[Pt_2(\text{alkyl-CS}_2)_4I]_n$ chains to reversibly assemble and disassemble in solution into their structural building blocks, $[Pt_2(\text{alkyl-CS}_2)_4]$ and $[Pt_2(\text{alkyl-CS}_2)_4I_2]$. The outstanding features of polymer **1** in solution enable its processability by unconventional lithography. Thus, solutions of **1** were used to fabricate reliable sub-micrometric patterns for designing working electronic devices. The patterning of homogeneous structures from the sub-micrometric to the macro scale is a breakthrough, since CP properties critically depend on the uniformity at different length scales. In this respect, our work represents an important advance in view of the application of CPs in molecular devices and in organic electronics in general as molecular wires or as electrodes. As a consequence of the wet processability and excellent conductance of the MMX polymer, they can be considered a possible alternative to the traditional Au electrode in organic/hybrid devices, which can lead to the development of a new generation of devices based on CPs.

Acknowledgements

This work was supported by the MICINN (MAT2007-66476-C02-01/02, MAT-2010-17720 and ACI2009-0969, and PLE2009-0065), Comunidad de Madrid (CAM2009-S2009-MAT-1467), GHJ-PLE2009-0065. MC and DG are supported by ESF-EURYI DYMOT. We are grateful to Dr C. M. Pradier for help with infrared measurements and to J. Sobrado for technical support during XPS measurements at CAB.

Notes and references

1 Z. Nie, A. Petukhova and E. Kumacheva, *Nat. Nanotechnol.*, 2010, **5**, 15–25.
2 A. Martinez-Otero, E. Evangelio, R. Alibes, J. L. Bourdelande, D. Ruiz-Molina, F. Busque and J. Hernando, *Langmuir*, 2008, **24**, 2963–2966.
3 J.-M. Lehn, *Supramolecular Chemistry*, VCH, Weinheim, 1995.
4 M. Cavallini, *J. Mater. Chem.*, 2009, **19**, 6085–6092.
5 M. Cavallini, I. Bergenti, S. Milita, J. C. Kengne, D. Gentili, G. Ruani, I. Salitros, V. Meded and M. Ruben, *Langmuir*, 2011, **27**, 4076–4081.
6 D. A. Serban, P. Greco, S. Melinte, A. Vlad, C. A. Dutu, S. Zacchini, M. C. Iapalucci, F. Biscarini and M. Cavallini, *Small*, 2009, **5**, 1117–1122.
7 J. A. Theobald, N. S. Oxtoby, M. A. Phillips, N. R. Champness and P. H. Beton, *Nature*, 2003, **424**, 1029–1031.
8 D. J. L. Tranchemontagne, Z. Ni, M. O'Keeffe and O. M. Yaghi, *Angew. Chem., Int. Ed.*, 2008, **47**, 5136–5147.
9 H. K. Chae, D. Y. Siberio-Perez, J. Kim, Y. Go, M. Eddaoudi, A. J. Matzger, M. O'Keeffe and O. M. Yaghi, *Nature*, 2004, **427**, 523–527.
10 Y. You, H. Yang, J. W. Chung, J. H. Kim, Y. Jung and S. Y. Park, *Angew. Chem., Int. Ed.*, 2010, **49**, 3757–3761.
11 T. Uemura, N. Yanai and S. Kitagawa, *Chem. Soc. Rev.*, 2009, **38**, 1228–1236.
12 L. Ma, C. Abney and W. Lin, *Chem. Soc. Rev.*, 2009, **38**, 1248–1256.
13 L. J. Murray, M. Dinca and J. R. Long, *Chem. Soc. Rev.*, 2009, **38**, 1294–1314.

14 J. Lee, O. K. Farha, J. Roberts, K. A. Scheidt, S. T. Nguyen and J. T. Hupp, *Chem. Soc. Rev.*, 2009, **38**, 1450–1459.
15 S. Kitagawa, R. Kitaura and S. Noro, *Angew. Chem., Int. Ed.*, 2004, **43**, 2334–2375.
16 C. Janiak, *Dalton Trans.*, 2003, 2781–2804.
17 R. Mas-Balleste, J. Gomez-Herrero and F. Zamora, *Chem. Soc. Rev.*, 2010, **39**, 4220–4233.
18 L. Welte, A. Calzolari, R. Di Felice, F. Zamora and J. Gomez-Herrero, *Nat. Nanotechnol.*, 2010, **5**, 110–115.
19 A. Guijarro, O. Castillo, L. Welte, A. Calzolari, P. J. S. Miguel, C. J. Gómez-García, D. Olea, R. di Felice, J. Gómez-Herrero and F. Zamora, *Adv. Funct. Mater.*, 2010, **20**, 1451–1457.
20 L. Welte, U. García-Couceiro, O. Castillo, D. Olea, C. Polop, A. Guijarro, A. Luque, J. M. Gómez-Rodríguez, J. Gómez-Herrero and F. Zamora, *Adv. Mater.*, 2009, **21**, 2025–2028.
21 M. Cavallini, C. Albonetti and F. Biscarini, *Adv. Mater.*, 2009, **21**, 1043–1053.
22 R. Mas-Balleste, R. Gonzalez-Prieto, A. Guijarro, M. A. Fernandez-Vindel and F. Zamora, *Dalton Trans.*, 2009, 7341–7343.
23 E. Kim, Y. N. Xia and G. M. Whitesides, *Nature*, 1995, **376**, 581–584.
24 M. Cavallini and F. Biscarini, *Nano Lett.*, 2003, **3**, 1269–1271.
25 M. Cavallini, P. D'Angelo, V. Vendrell Criado, D. Gentili, A. Shehu, F. Leonardi, S. Milita, F. Liscio and F. Biscarini, *Adv. Mater.*, 2011, **23**, 5091–5097.
26 P. Greco, M. Cavallini, P. Stoliar, S. D. Quiroga, S. Dutta, S. Zachini, M. C. Lapalucci, V. Morandi, S. Milita, P. G. Merli and F. Biscarini, *J. Am. Chem. Soc.*, 2008, **130**, 1177–1182.
27 M. Mitsumi, K. Kitamura, A. Morinaga, Y. Ozawa, M. Kobayashi, K. Toriumi, Y. Iso, H. Kitagawa and T. Mitani, *Angew. Chem., Int. Ed.*, 2002, **41**, 2767–2771.
28 S. L. Tait, A. Langner, N. Lin, S. Stepanow, C. Rajadurai, M. Ruben and K. Kern, *J. Phys. Chem. C*, 2007, **111**, 10982–10987.
29 M. Cavallini, I. Bergenti, S. Milita, G. Ruani, I. Salitros, Z. R. Qu, R. Chandrasekar and M. Ruben, *Angew. Chem., Int. Ed.*, 2008, **47**, 8596–8600.
30 H. B. Akkerman, P. W. M. Blom, D. M. de Leeuw and B. de Boer, *Nature*, 2006, **441**, 69–72.
31 A. Shehu, S. D. Quiroga, P. D'Angelo, C. Albonetti, F. Borgatti, M. Murgia, A. Scorzoni, P. Stoliar and F. Biscarini, *Phys. Rev. Lett.*, 2010, **104**, 246602.
32 D. Braga and G. Horowitz, *Adv. Mater.*, 2009, **21**, 1473–1486.
33 M. H. Yoon, C. Kim, A. Facchetti and T. J. Marks, *J. Am. Chem. Soc.*, 2006, **128**, 12851–12869.

SUPLEMENTARY INFORMATION

Patterned conductive nanostructures from reversible self-assemble of 1D coordination polymer

Denis Gentili, Gonzalo Givaja, Rubén Mas-Ballesté, Mohamad R. Azani, Arian Shehu, Francesca Leonardi, Eva Mateo-Martí, Pierpaolo Greco, Félix Zamora* and Massimiliano Cavallini*

Materials and Methods

$[Pt_2(n\text{BuCS}_2)_4I]_n$ polymer and its precursors were synthesized according to methods published elsewhere.[1] All reagents were purchased from Aldrich and used as received. Electronic absorption spectra were recorded on an Agilent 8452 diode array spectrophotometer over a 190–1100 nm range in 0.2 cm quartz cuvettes thermostatted by a Unisoku cryostat. ^{1}H NMR spectra in CD_2Cl_2 were recorded on a Bruker AMX-300 spectrometer, using TMS as external reference.

Lithographic methods

Solvents: The solutions were prepared using dichloromethane (Aldrich, anhydrous, ≥99.8%) and tetrahydrofuran (Aldrich, anhydrous, ≥99.9%).

Stamps: The elastomeric polydimethylsiloxane stamps (PDMS, Sylgard 184, Dow Corning) stamps were prepared by replica molding of a blank Compact Disk for parallel lines (periodicity of 1.5 μm, width at half height 500 nm and 220 nm deep), a photolithographic master for interdigitated comb-like microstructures and for OFET microelectrodes (two parallel lines with width at half height 500 μm and distance of 70 μm, provided by SCRIBA Nanotecnologie S.r.l.). PDMS stamps were cured for 6 h at 60°C, then peeled off and washed in pure ethanol for one hour.

Substrates: Si wafers (n-type doped) with 200 nm thermally grown SiO_2 layer, borosilicate glass with 250 nm gold layer (Arrandee™, Germany), and microscope glass slides. All substrates were sonicated in electronic-grade water (milli-pure quality, 2 min), in acetone (Aldrich chromatography quality, 2 min), then in 2-propanol (Aldrich spectroscopic grade quality, 2 min), and blown dry in N_2.

MIMIC: the stamp grooves placed in contact with the substrate (silicon oxide, glass, and gold surfaces) form capillary channels and $[Pt_2(n\text{BuCS}_2)_4I]_n$ solution, poured at the open end of the stamp, flows into microchannels by capillary forces (Figure 1a). After the complete evaporation of the solvent, the stamp is gently removed leaving the micro and nanostructures on the surface.

LCW: the stamp is gently placed in contact with a film of $[Pt_2(n\text{BuCS}_2)_4I]_n$ solution spread on the substrate and the capillary forces pin the solution to the stamp protrusions, giving rise to an array of

menisci (Figure 1b). After the complete evaporation of the solvent, the stamp is gently removed leaving the micro and nanostructures on the surface.

Characterization: Optical micrographs were recorded with a Nikon i-80 microscope equipped with epi-illuminator, dark-field and cross polars using 50X objective. AFM images were recorded with a commercial AFM (NT-MDT, Moscow, Russia) operating in semi-contact mode in ambient condition. Si_3N_4 cantilevers, with typical curvature radius of a tip 10 nm were used. Image analysis was done using the open source SPM software Gwyddion-www.gwyddion.net. SEM images were collected using an S-4000 (Hitachi) instrument.

Scanning Electron Microscopy: The Scanning Electron Microscopy (SEM) images were obtained with a ZEISS 1530 SEM equipped with a Schottky emitter and operating at 10 keV. The instrument was equipped with an Energy Dispersive X-Ray Spectrometer (EDX) for X-Ray microanalysis, and two different Secondary Electrons (SE) detectors, the InLens (IL) and the Everhart-Thornley detectors (ETD). The IL detector collected a secondary electrons component (the so-called SE1) generated by the primary incident beam in a small region around the beam impinging point, and for this reason it shows an higher sensibility to surface morphology. The ETD collects the complete SE spectrum, the SE1 component, but also the SE generated by the back scattered electrons (BSE) emitted by the specimen (SE2) and the SE generated by the BSE colliding with the chamber of the instrument (SE3). In addition ETD acts also as a BSE detector with a rather low efficiency. Therefore the detected signal shows a reduced sensitivity to the local surface morphology, but a higher sensitivity to the density and/or compositional variations.

***Electrical characterization*:** The mobility in the saturation regime (μ_{sat}) was calculated using the equation $I_{DS} = (W/2L)C_i\mu_{sat}(V_G–V_{th})^2$, where C_i is the capacitance of the insulating SiO_2 layer and V_{th} is the threshold voltage extracted from the square root of the drain current ($I_{DS}^{0.5}$) *versus* gate voltage (V_G) characteristics for a fixed drain voltage (V_{DS}). The OFET devices were measured in atmospheric conditions.

X-ray Photoelectron Spectroscopy (XPS)

XPS analyses of the samples were carried out in an ultrahigh vacuum chamber equipped with a hemispherical electron analyzer, and using an Al Kα X-ray source (1486.6 eV). The base pressure in the

chamber was $5x10^{-10}$ mbar, and the experiments were performed at room temperature. The following core level peaks were recorded under the same experimental conditions: O(1s), C(1s), S(2p), I(3d), Pt(4f) and Au(4f). The pass energy applied for taking the overview sample was 30 eV, while 20 eV pass energy was applied for the fine analysis of the core level spectra. The core-level binding energies were calibrated against the binding energy of the Au($4f_{7/2}$) peak set to 84.0 eV for gold surface sample; with this calibration, the carbon peak attributed to hydrocarbon contamination was measured at 284.6 eV. The peak deconvolution in different components was shaped, after background subtraction, as a convolution of Lorenztian and Gaussian curves. Lorenztian and Gaussian widths of 0.1 and 1 eV, respectively, common for all the components, were used.

XPS analysis has been performed in order to obtain chemical information related to the $[Pt_2(n\text{BuCS}_2)_4I]_n$ before and after surface deposition. In a wide scan XPS overview spectra of a compacted $[Pt_2(n\text{BuCS}_2)_4I]_n$ pellet, the following atomic species can be identified: C, S, I and Pt. The same atomic species have been identified after the adsorption of $[Pt_2(n\text{BuCS}_2)_4I]_n$ on gold surface. Therefore, there is a good agreement between solid compound and after adsorption on gold surface (Table S1).

In order to obtain the chemical state of Pt element in the $[Pt_2(n\text{BuCS}_2)_4I]_n$ compound, selected Pt(4f) energy region from 66 to 82 eV was individually scanned. Figure S6 shows the core-level spectra of the Pt(4f). The binding energy of Pt ($4f_{7/2}$) peak shows two components at 72.7 and 74.2 eV assigned to Pt^{2+} and to Pt^{3+}, respectively[2]. In both cases (pellet and adsorption on gold surface of the $[Pt_2(n\text{BuCS}_2)_4I]_n$) the Pt(4f) peak shows two components and the percentage of the two components are Pt^{2+} (76%) and to Pt^{3+} (24%).

Table S1. Binding energies (eV) and with of the peaks[a], [b] from the XPS data of $[Pt_2(n\text{BuCS}_2)_4I]_n$ on bulk and patterned on gold surfaces.

	Pt^{2+} $4f_{7/2}$	Pt^{3+} $4f_{7/2}$	Pt^{2+} $4f_{5/2}$	Pt^{3+} $4f_{5/2}$
Bulk	72.32 (1.9)	74.17 (2.0)	75.66	77.51
Stripes	72.68 (1.8)	74.22 (1.3)	76.02	77.56

[a] Full width at half-maximum values for peaks are given in parentheses. [b] Values corrected against the Au $4f_{7/2}$ peak set at 84.0 eV.

Polarization Modulation Reflection Absorption Infrared Spectroscopy (PM-RAIRS)

The PM-RAIRS spectra were recorded on a commercial NICOLET Nexus spectrometer. The external beam was focused on the sample, with a mirror, at an optimal incident angle of 80º. The incident beam was modulated between p and s polarizations with a ZnSe grid polarizer and a ZnSe photoelastic modulator (HINDS Instruments, PEM 90, modulation frequency = 37 kHz). The light reflected at the sample was then focused on a nitrogen-cooled mercury-cadmium-telluride detector. All spectra were recorded at 8 cm^{-1} resolution by co-adding 128 scans. The PM-RAIRS signal is given by the differential reflectivity ($\Delta R/R$) (Rp - Rs)/(Rp + Rs).[3,4]

Figure S7 shows RAIRS spectra of MMX compound immobilized on gold surface from solution. The infrared spectra contain intense absorptive features indicative that MMX compound has been successfully adsorbed on the gold surface.

A RAIR spectrum shows several bands in the region from 3000 to 2850 cm^{-1}, which corresponds to CH_2 and CH_3 asymmetric and symmetric stretching modes, which identify that CH_2 and CH_3 groups are present in the $[Pt_2(n\text{BuCS}_2)_4I]_n$ compound. Other vibrations related with these functional groups appear in the spectra as: the $\delta(CH_2)$ scissoring vibration band at 1457 cm^{-1}, CH_3 deformation modes $\delta(CH_3)_{sym}$ (symmetrical bending) at 1361 cm^{-1} and $\delta(CH_3)_{asym}$ at 1450 cm^{-1}.

Usually, the stretching frequencies of dithiocarboxylate complexes of Ni(II) and Zn(II) are observed between 900 and 1100 cm^{-1}.[5,6] In our case the most intense broad band in the spectra appears at 1111-1043 cm^{-1}. This intense absorption in the 1050–1100 cm^{-1} region has been previously assigned to the CS_2^- group asymmetric stretching vibration, the corresponding symmetric stretching vibration is located below 850 cm^{-1}, it is not possible to identify in our spectra range. The presence of CS_2^- group means that the ligand bridges two metal atoms (Pt) through two sulfur atoms, each sulfur atom coordinates to one of two metal atoms in this case, respectively and the two C–S bonds are completely delocalized.

RAIRS comparisons spectra between dust compound and after compound adsorption on gold surface have been performed in order to further understand MMX interaction on the surface. While dust infrared spectra shows only vibration band at 1080 cm^{-1} region previously assigned to the CS_2^- group, in good agreement with the crystallographic data for the MMX compound, that indicate almost coincident C-S bond lengths, confirming the equivalency of both sulphur atoms. On the other hand, once $[Pt_2(n\text{BuCS}_2)_4I]_n$ has been adsorbed on the gold surface RAIRS spectra shows two extra intense bands at 1264 and 1043 cm^{-1}, which cannot be assigned to any other infrared vibration than C=S and C-S stretching vibrations respectively, meaning that adsorption process on the surface could take place via the sulphur atom, this suggestion is in a good agreement with the well-known S-Au affinity, therefore interaction through the CS_2^- group on the gold surface make the two sulphur in-equivalence (C=S and C-S).

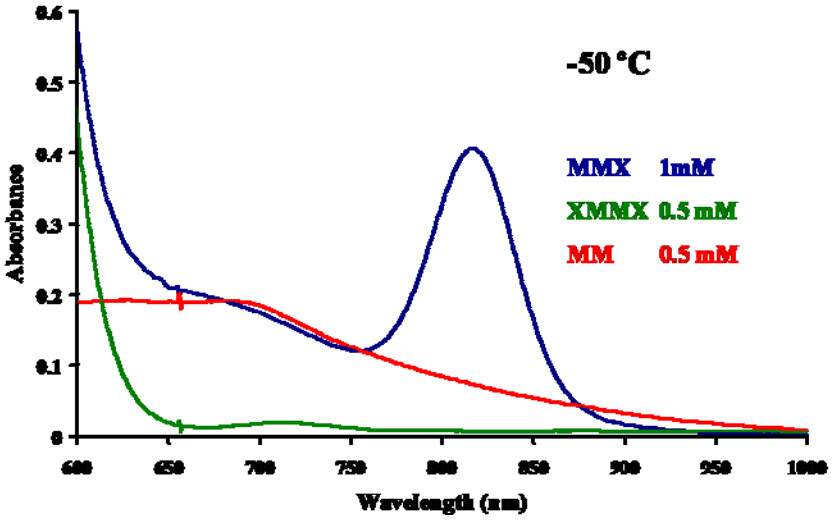

Figure S1. UV-vis spectrum of a 1 mM solution of $[Pt_2(n\text{BuCS}_2)_4I]_n$ in CH_2Cl_2, compared with UV-vis spectra of 0.5 mM solutions of $[Pt_2(n\text{BuCS}_2)_4]$ and $[Pt_2(n\text{BuCS}_2)_4I_2]$ in CH_2Cl_2. All data was taken at -50 ºC. Spectrum of $[Pt_2(n\text{BuCS}_2)_4I_2]$ does not show significant variations with respect to the data observed at room temperature. $[Pt_2(n\text{BuCS}_2)_4]$ solution at low temperature presents the appearance of a new absorption in the range of 600-700 nm due to MM···MM association. In the MMX spectrum at -50 ºC two new absorptions appear: One at 600-700 nm attributed to MM···MM assembly and another one at 820 nm assigned to MM···XMMX association. Absorption at 600-700 nm in the 1 mM MMX solution is lower than the observed in 0.5 mM solution of MM because part of the MM present in solution goes to MM···XMMX assemblies.

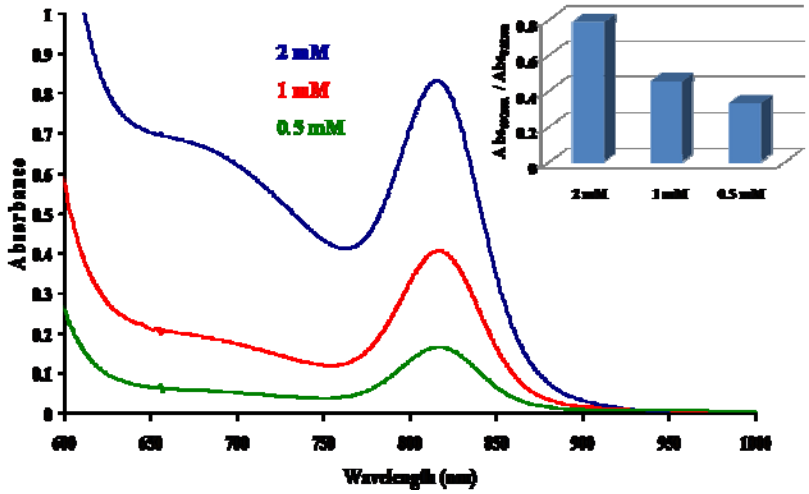

Figure S2. UV-vis spectra of 2 mM, 1 mM and 0.5 mM solutions of $[Pt_2(n\text{BuCS}_2)_4I]_n$ in CH_2Cl_2 measured at -50 ºC. The ratio between MM···MM and MM···XMMX assemblies depends on the concentration. At higher concentrations the relative amount of MM···MM suprastructures increases.

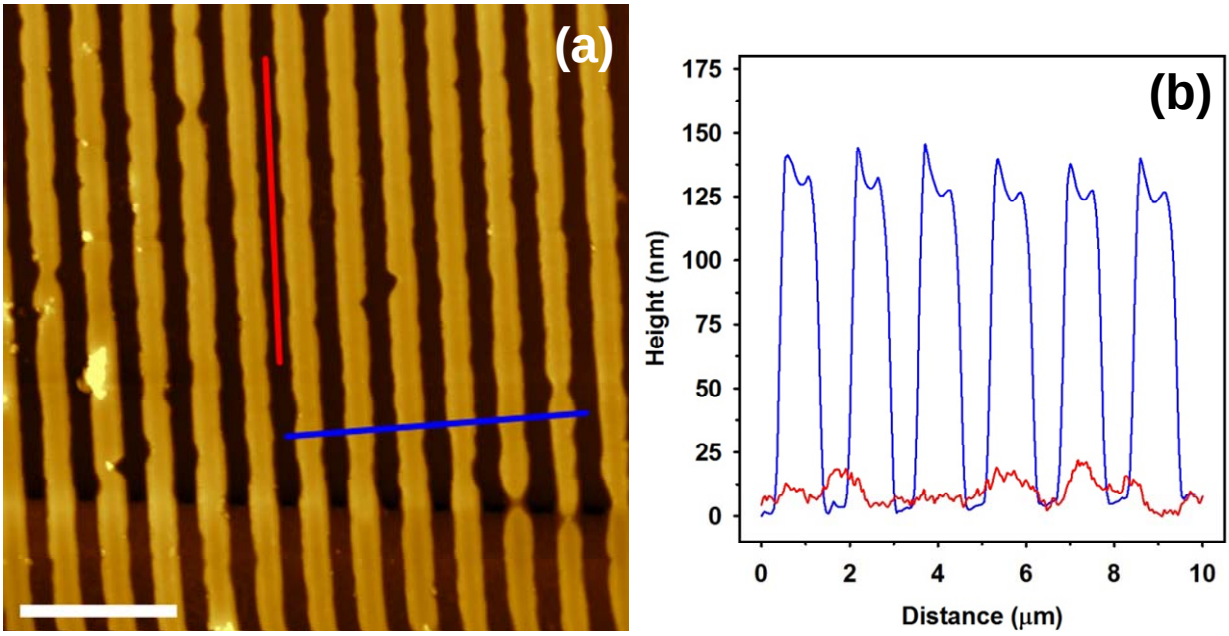

Figure S3. a) AFM morphology (scale bar = 5 μm), and b) AFM profiles of $[Pt_2(nBuCS_2)_4I]_n$ wires patterned on gold electrodes (LCW, parallel lines, 2 mg/mL in CH_2Cl_2).

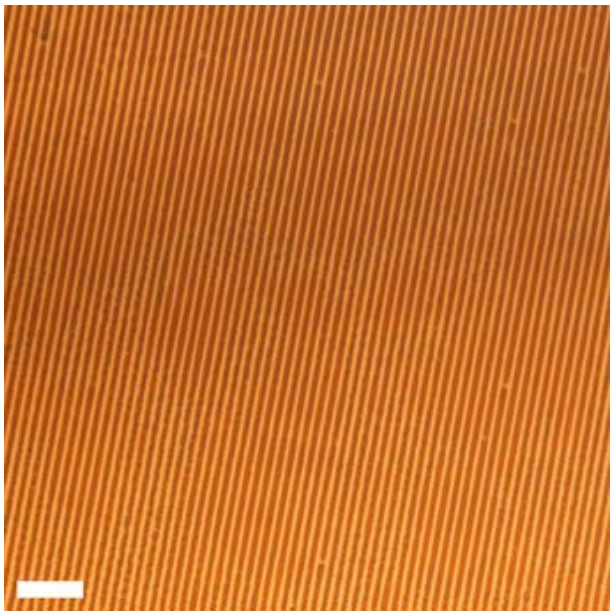

Figure S4. Optical microscopy (scale bar = 10 μm) of $[Pt_2(nBuCS_2)_4I]_n$ wires patterned on gold surface (LCW, parallel lines, 1 mg/mL in CH_2Cl_2).

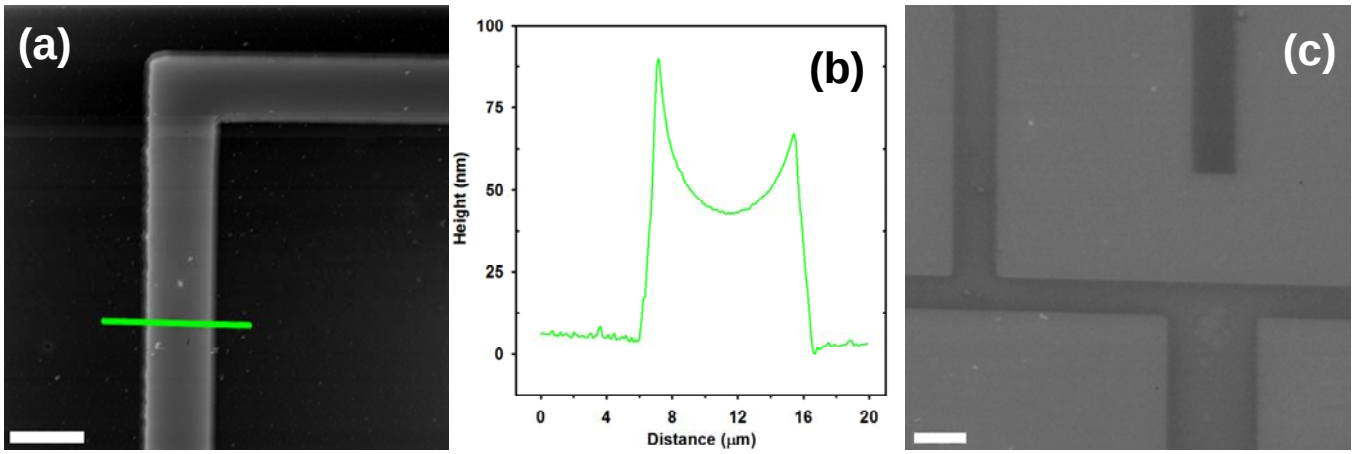

Figure S5. a) AFM image (scale bar = 10 μm), b) AFM profile, and c) SEM (scale bar = 10 μm) of $[Pt_2(n\text{BuCS}_2)_4I]_n$ pattern on silicon oxide (LCW, interdigitated comb-like, 2 mg/mL in CH_2Cl_2).

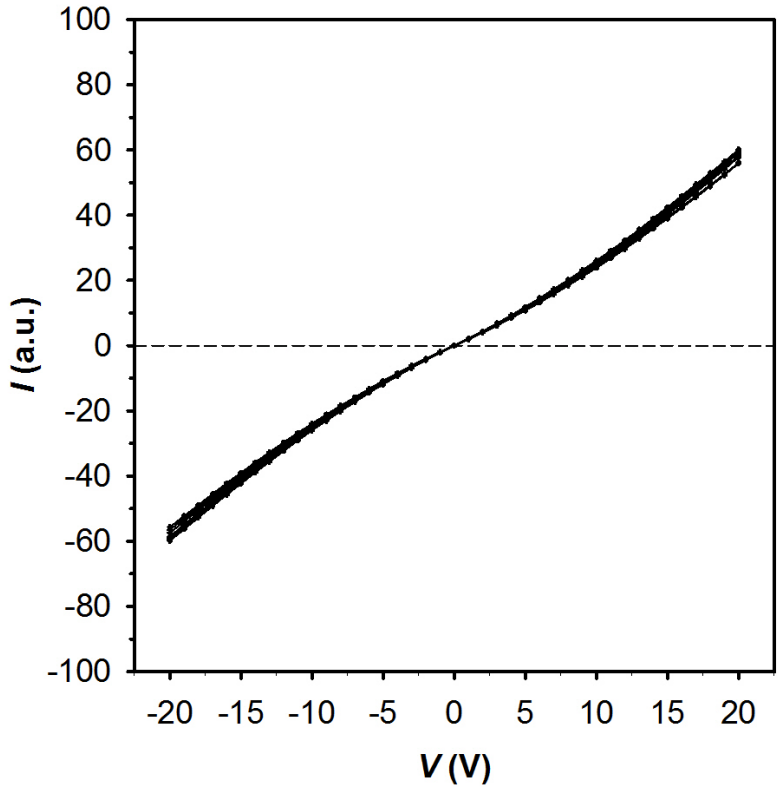

Figure S6. Current *vs* voltage characteristic upon the application of 10 cycles on wires patterned on gold electrodes.

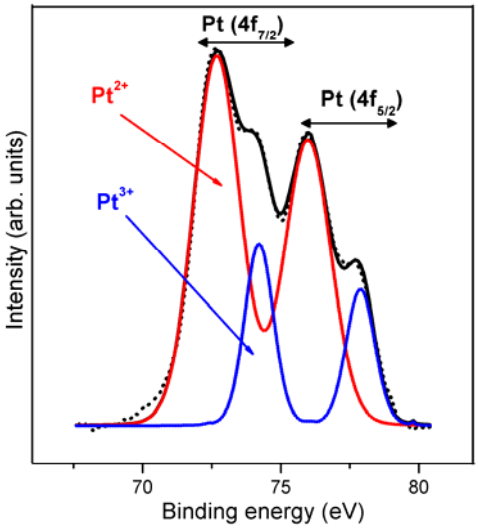

Figure S7. XPS core-level peak of Pt ($4f_{7/2}$ and $4f_{5/2}$) from $[Pt_2(n BuCS_2)_4I]_n$ on gold surface. The binding energies values of the two components of the Pt $4f_{7/2}$ peak are 72.7 eV (red line) and 74.2 eV (blue line) assigned to Pt^{2+} and Pt^{3+}, respectively.

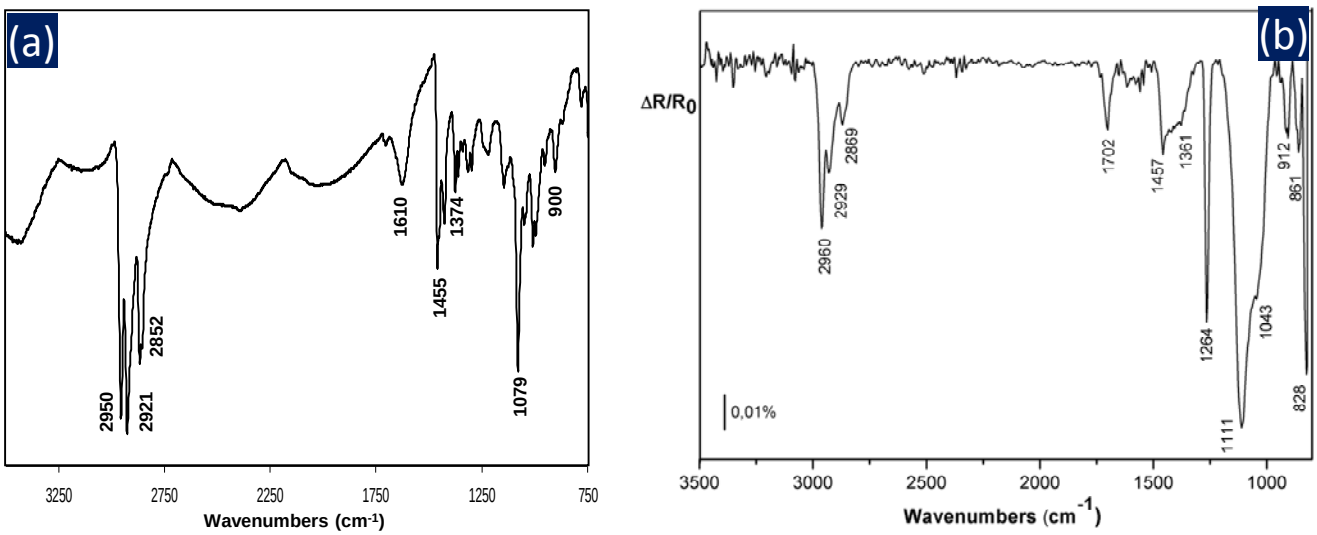

Figure S8. FTIR (a) in PM-RAIRS spectra after adsorption of $[Pt_2(n BuCS_2)_4I]_n$ on gold surfaces from solution.

References

1. Mitsumi, M. *et al.*, Valence-ordering structures and magnetic behavior of metallic MMX chain compounds, *Angew. Chem. Int. Ed.* **41**, 2767-2771 (2002).
2. Mitsumi, M. *et al.*, Metallic behavior and periodical valence ordering in a MMX chain compound, Pt-2(EtCS2)(4)I, *J. Am. Chem. Soc.* **123**, 11179-11192 (2001).
3. Barner, B.J., Green, M.J., Saez, E.I., and Corn, R.M., Polarization Modulation Fourier-Transform Infrared Reflectance Measurements of Thin-Films and Monolayers at Metal-Surfaces Utilizing Real-Time Sampling Electronics, *Anal. Chem.* **63**, 55-60 (1991).
4. Buffeteau, T., Desbat, B., and Turlet, J.M., Polarization Modulation Ft-Ir Spectroscopy of Surfaces and Ultra-Thin Films - Experimental Procedure and Quantitative-Analysis, *Appl. Spectrosc.* **45** (3), 380-389 (1991).
5. Shankaranarayana, M. and Patel, C.C., Infrared Spectra and Structures of Xanthates and Dixanthogens, *Can. J. Chem. Rev. Can. Chim.* **39**, 1633-1636 (1961).
6. Burke, J.M. and Fackler, J.P., Vibrational-Spectra of Dithioaryl Acid Complexes of Nickel(Ii), Palladium(Ii), Platinum(Ii), and Zinc(Ii), and Their Sulfur Addition Products - X-Ray Crystal-Structure of Dimer of Bis(Dithiocumato)Platinum(Ii)-a Material with a 2.87ure of Dimer of Bis(Dithiocumato)Plaa Metal-Metal Bond, *Inorg. Chem.* **11**, 3000-3008 (1972).

Chapter 4

IV. Conclusions

3.1. Gold(I)···Gold(I) Interaction:

The results on Au(I)…Au(I) interaction were demonstrated that aurophilic assemblies are considerably dependent on subtle changes on the ligands that hold together the gold centers in bimetallic molecules of the general formula [Au_2L_2]. It was observed that compounds with dithiocarboxylate ligands can reversibly aggregate in solution through supramolecular interactions, whereas xanthate compounds with the same steric hindrance do not show this phenomenon. These behavior of different ligands should be understood as a delicate balance of diverse subtle weak interactions that concur at the same time, not only Au···Au, Au···S, or S···S, but probably also solvation forces or interactions between the CH_2R or OR groups. Luminescence studies suggested that the intramolecular interactions play a more relevant role in the luminescent properties than the intermolecular ones because all the compounds present emission at similar wavelengths in the solid state. The origin of the emissions was ligand to metal-metal charge transfer (LMMCT) transitions in all compounds.

The computational studies indicate that not only Au···Au interactions, but also Au···S and S···S have effects on the structure. In fact, it was observed that for compounds with xanthate ligands, bimetallic molecules connected through Au···Au interactions to form a chain (compound **5**), or through weaker Au···S interactions to form layers (compounds **4** and **6**). Additionally, the dithiocarboxylate analogues may appear as oligonuclear molecules.

In overall, these results can open new door to design new complex structures with different nuclearity and Au-Au distances which can have potential interest for the engineering of molecular conductive devices.

3.2. Platinum(II)···Platinum(II) Interaction:

The results on Pt(II)…Pt(II) interaction were shown that the aggregation of $[Pt_2L_4]$ to form supramolecular one dimensional chains can be extended to a family of compounds containing dithiocarboxylate ligands. This aggregation occurs through Pt···Pt interactions and several variables such as high concentration and low temperatures can amplify it to form $[Pt_2L_4]_n$. In contrast, decreasing the initial monomer concentration can results in a narrower distribution of polymeric species. The nature of the ligand is also play key role on this aggregation. In fact, bulkier ligands (branched ligands) because of their steric hindrance inhibit the formation of oligomeric species in the solution and increase the metal-metal distance in crystal structures. In linear ligands, the length of ligand has an important impact in solution, although, does not affect on the intermolecular interactions in the crystal phase

Also the solvent can also affect on the supramolecular aggregation of the diplatinum complexes. In fact the coordinative ability of CS_2 and THF hamper the aggregation by coordinate to the Pt metal centre throw weak interaction. Different behavior in non-coordinative solvent (CH_2Cl_2 and $CHCl_3$) can be due to their different polarity.

Theoretical simulations confirm that $[Pt_2L_4]$ species binds through weak intermolecular Pt···Pt interactions and in spite of Au(I) aggregation, the intermolecular Pt···S and S···S interactions between monomers show repulsive behavior at all levels of calculations.

Theoretical simulations were demonstrated that this weak metal–metal attraction is mediated by the interaction between the platinum $5d_z^2$ and $6p_z$ atomic orbitals. Theoretical calculations of the optical spectra were revealed the nature of the low-energy transitions that appear at low temperature. In fact, theoretical investigations of the spectroscopic properties clearly was shown that the appearance bands in visible region is due to oligomeric species that keep their cohesion through Pt···Pt interactions. Additionally, further increasing the nuclearity of $[Pt_2L_4]_n$ decreases the energy of these optical transitions.

In overall, these results can useful to understand more about the assembly of diplatinum species into 1D conductive polymer. Also they can offer noticeable hints to design new molecular electronic devices based on supramolecular assembly.

3.3. MMX:

In MMX part, the assembly of $[Pt_2(RCS_2)_4I]$ subunits in solution and the factors that affect this aggregation was investigated experimentally and computationally. The influence of the solvent, temperature, and concentration were analyzed to find the suitable parameters for the initial building-block associations. Both the experimental and computational results indicate that thermodynamic difference is of few $kcalmol^{-1}$ between the polymeric structure and the molecular building blocks (MM and XMMX). By understanding the factors that govern this process, single/few MMX chains on mica were isolated. Additionally, unconventional lithography was used to fabricate reliable sub-micrometric patterns for designing working electronic devices. In fact, the wet process ability and excellent conductance of the MMX polymer that were shown in this thesis can lead to the development of a new generation of devices based on coordination polymers (CPs). In overall, these results represent an important advance in view of the application of CPs as molecular wires or as electrodes in molecular devices and in organic electronics.

Chapter 5

V. Collaborated Publications

(Not included in this thesis)

Article 1

Title: Intrinsic electrical conductivity of nanostructured metal-organic polymer chains

Autors: Cristina Hermosa, Jose Vicente Álvarez, Mohammad-Reza Azani, Carlos J. Gómez-García, Michelle Fritz, Jose M. Soler, Julio Gómez-Herrero, Cristina Gómez-Navarro and Félix Zamora

Journal: Nature Communications

Year: 2013

Volume / Number: 4 / 1709.

Article 2

Title: Electrochemically generated nanoparticles of MMX chain

Autors: Emiliano Martínez-Periñan, Mohammad-Reza Azani, Jose M. Abad, Eva Mateo-Martí, Félix Pariente, Rubén Mas-Ballesté, Félix Zamora and Encarnacion Lorenzo.

Journal: Chemistry - A European Journal

Year: 2014

Volume / Number: --- / ---